Processing of All Cellulose Composites *via* an Ionic Liquid Route

A thesis submitted in partial fulfilment of the requirements for the Degree of Doctor of Philosophy in Mechanical Engineering in the University of Canterbury by

Tim Huber

Dept of Mechanical Engineering, University of Canterbury, Christchurch, New Zealand

July 2012

ACKNOWLEDGEMENTS

I would like to thank the New Zealand Foundation for Research, Science, and Technology and the Department of Mechanical Engineering of the University of Canterbury for the financial support. I am very grateful to my main supervisor Dr Mark Staiger for giving me the opportunity to be part of his research group and his support, supervision and trust in me through the years. Many thanks as well to the other members of my supervision team, Dr Shusheng Pang, Dr Owen Curnow and Dr Ken Marsh for offering support and helpful discussion whenever needed. A special thanks to my supervisor Dr Simon Bickerton for inviting me to the CACM during the difficult times we had in Christchurch and all his help and support. A very special 'thank you' to Dr Jörg Müssig for being a great friend, supervisor and inspiration throughout the most part of my academic career and especially during my PhD. Furthermore, many thanks to all members of the Materials Research group at the University of Canterbury.

I would like to thank all the administrative staff in department for all their help with the necessary and not so necessary paperwork. Many thanks to Kevin Stobbs for his support with the laboratory work and to Mike Flaws for his help with the microscopes. The help of Helen Devereux with the AFM and of Manfred Ingerfeld with the confocal microscope is very kindly acknowledged. Many thanks to Lidia Motoi and Nick Tucker at Plant and Food for their help with the rheometer and to Roger Newman and Stefan Hill at Scion for their help with the solid-state NMR measurements. I thank Benoît Duchemin for his general support and helpful comments and especially for his help with the WAXD measurements. Many thanks to Nina Graupner for all her help with my experiments at the University of Applied Sciences in Bremen and to Dr Dieter Veit,

Thorsten Deichmann, Britta Kuckhoff and the other members at the ITA, Aachen for their help with and usage of their 3D-braiding equipment. I'd also like to thank my intern students Christophe Fournier, Sebastian Kalka and Julius Steinberg for being a great help during their time here.

I don't think I can thank all my friends here at UC enough for all their support and help with everything work-related and even more important all things not work related. Many, many thanks to Dr Nick, Jay, Karl, Jeri and all the other great guys in the Materials Research group. Thanks to Rob for sacrificing his skateboard to science and his time to extracurricular activities at the Volstead bar. Many thanks to Paddy and all the other guys of the spectacularly unsuccessful and yet great Burnside football team for all the necessary distractions from work and many thanks to all my others friends in New Zealand and the Smith family for making me feel at home as far from home as possible.

Last, but most certainly not least, I thank my family and friends back home for all their wonderful support in those years. Vielen, vielen Dank an meine Eltern und meine groβartigen Geschwister für all die Unterstützung und eurer Vertrauen in mich. Ohne euch wäre das alles niemals möglich gewesen.

TABLE OF CONTENTS

List of Figures

List of Tables

Nomenclature

2D: Two Dimensional

3D: Three Dimensional

ACC: All Cellulose Composite

BC: Bacterial Cellulose

$BF4^-$: Tetrafluoroborate

BmimAc: 1-Butyl-3-Methylimidazolium Acetate

BmimCl: 1-Butyl-3-methylimidazolium Chloride

Br^-: Bromide

C: Carbon

c: Concentration

$CH3COO^-$: Acetate

Cl^-: Chlorine

CrI: Crystallinity index

DmimDMP: Dimethylimidazolium Dimethylphosphate

DMSO: Dimethylsulfoxide

DS: Degree of substitution

DSC: Differential Scanning Calorimetry

E': Storage modulus

E'': Loss modulus

EmimAc: 1-Ethyl-3-Methylimidazolium Acetate

FE-SEM: Field-Emission Scanning Electron Microscopy

HDPE: High Density Polyethylene

HDR: High Draw Ratio

HIPS: High Impact Polystyrene

hr: Hours

IL: Ionic Liquid

ISO: Isotropic

LDR: Low Draw Ratio

LOI: Limiting Oxygen Index

MAPP: Maleic Anhydride grafted Polypropylene

mass%: Mass Percentage

MCC: Microcrystalline Cellulose

Mw: Molecular Weight

NaOH: Sodium Hydroxide

NMR: Nuclear Magnetic Resonance

NO_3: Nitrate

n.r.: Not Reported

NR_4: Tetraalkylammonium

OH: Hydroxyl

PBS: Polybutylene succinate

PCL: Polycaprolactone

PE: Polyethylene

PEG: Poly (ethylene glycol)

PF_6: Hexafluorophosphate

PHB: Poly-3-hydroxybutyrate

PLA: Poly(lactic) acid

PO: Propylene Oxide

PP: Polypropylene

ppm: Parts Per Million

PR_4: Tetraalkylphosphonium

RH: Relative Humidity

R_1R_2IM: Alkylimidazolium

RTIL: Room Temperature Ionic Liquid

SCN: Thyocynate

SCRIMP: Seeman Composites Resin Infusion Moulding Process

SD: Standard Deviation

SIP: Solvent Infusion Process

SMC: Sheet Moulding Compound

STM: Solvent Transfer Moulding

TGA: Thermogravimetric Analysis

TMA: Thermomechanical Analysis

UD: Unidirectional

UTS: Ultimate Tensile Strength

VARTM: Vacuum Assisted Resin Transfer Moulding

V_f: Fibre Volume Fraction

vol%: Volume Percentage

WAXD: Wide Angle X-Ray Diffraction

WAXS: Wide Angle X-Ray Scattering

WF: Wood Fibre

ε_f: Strain to Failure

η: Viscosity

ABSTRACT

Newly developed all-cellulose composites (ACCs) can overcome the chemical incoherence between cellulose and other polymers by dissolution and regeneration of a portion of cellulose to create a chemically identical matrix phase. New "close to industry"-processing ways for ACCs were developed to create "thick" ACCs (>1 mm thickness) based on composite processes already used in the composite industry.

The ionic liquid (IL) 1-Butyl-3-Methylimidazolium Acetate (BmimAc) is a strong solvent for both, native cellulose and cellulose II. The dissolution process is strongly depended on the temperature and viscosity of the IL-cellulose solution. Next to complete dissolution, rayon fibre can be dissolved partially to achieve the formation of a matrix phase *in situ*. The highly hydrophilic cellulose based materials show different amounts of shrinkage after composite processing when the coagulant necessary to regenerate the dissolved cellulose is removed by evaporative drying.

Multilayered, "thick" composite laminates could be produced by a simple hand-impregnation of rayon and linen textiles with the solvent and partial dissolution of the cellulosic textiles. A solvent infusion process (SIP) based on vacuum assisted resin infusion was successfully developed to process ACCs. The application of pressure during SIP is crucial to achieve good interlaminar adhesion. The SIP based laminates showed improved tensile strength and stiffness compared to the hand impregnation process.

An analysis of the processing parameters showed that the drying process used to remove the coagulant is important to achieve good fibre-matrix-bonding as harsh

evaporative drying causes shrinkage induced cracks in the created matrix phase. Using ethanol as a coagulant instead of water reduced composite swelling and corresponding shrinkage, but leads to a strong reduction in crystallinity of the regenerated cellulose, as shown X-ray diffraction and solid state NMR measurements. Regeneration in distilled water, followed by drying at room temperature produced the best ACC laminate.

The SIP based laminates showed high flexural and impact strength compared to other biocomposites. The composites were also found to be easily compostable especially compared to a PLA-rayon composite.

The rayon fibre was processed on an ITA 3D rotary braiding machine, generally used for the processing of stronger and stiffer glass and carbon fibres. A rectangular profile was produced and analysed. The fibre strength and Young's modulus were unaffected by the braiding process. The braid could be processed into an ACC by immersion in IL for 60 min at 100 °C. The so produced ACCs showed further improvements in tensile and impact strength due to improved through the thickness strength.

I. LITERATURE REVIEW

1. BIO- AND GREEN COMPOSITES

1.1 DEFINITIONS AND GENERAL BACKGROUND INFORMATION

1.1.1 Definitions

Biocomposites are generally understood to be the combination of a petroleum-based polymer matrix phase (e.g. polyethylene, polypropylene, epoxy resin) and reinforcing phase derived from a natural resource such as natural or synthetic cellulose fibres or wood particles. In addition to biocomposites, "green" (bio) composites have been developed in recent years, using not only a natural reinforcement but also a naturally-derived or biopolymer (e.g. polylactides, palm oil based resins, starch) as a matrix phase. Apart from removing any dependence on crude oil, the aims of green composites are to be completely biodegradable, sustainable and CO_2 neutral, while providing a high strength and stiffness [1, 2].

Henry Ford can be seen as one of the pioneers in the area of biocomposites, experimenting with car parts based on compressed soy beans in the early 1940ies [1]. However, due to low priced petroleum based polymers, biocomposites offered no economical advantage. Non-surprisingly further reports on the use of natural fibres in composites date back until the early 1970's and 80's [3, 4]. Since then modern advances in the development of cellulose fibre-reinforced polymer composites have created an increasing interest, especially in the last decade (Figure 1).

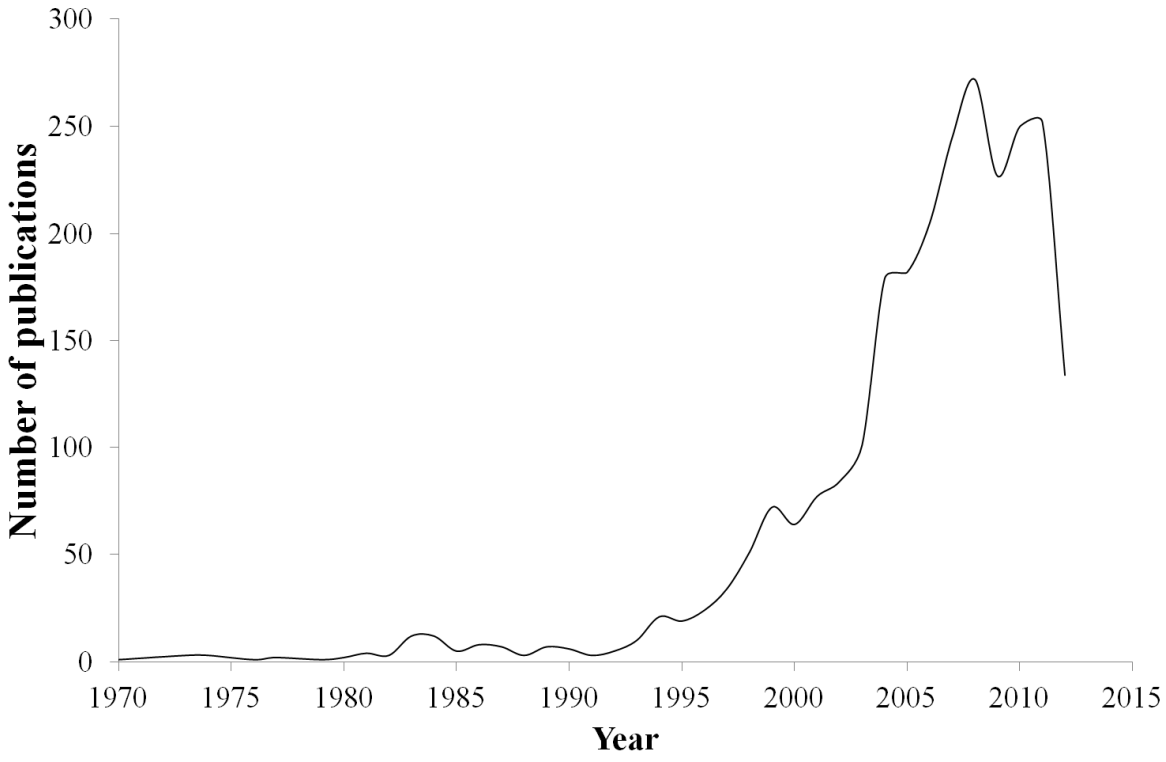

Figure 1: Development of publications on "natural fibre composites" in the last 40 years. Data generated with Scopus® (31/05/2012).

One of the main driving forces behind bio-and green composites is the desire to create more eco-friendly materials. In recent years the necessity to develop sustainable, environmental friendly or bio-derived materials has been acknowledged by governments worldwide. For example, the U.S. Department of Energy sponsored a research project that aimed to provide pathways that allow that at least 10 % of basic chemical building blocks to be derived from plant or other renewable resources by 2020 with an incentive to increase this value to 50 % by 2050 [1]. The European Union and Japan have introduced regulations for vehicles to be made from at least 95 % recyclable materials within the next decade [5]. Another EU regulation on reducing carbon dioxide emissions of passenger vehicles has led to the motivation to create more lightweight structures to decrease fuel consumption [6]. As a result, biocomposites, due to their reduced dependency on crude oil, lower density, improved CO_2-balance, greater recyclability, and

ease of disposal of cellulose-containing composites compared with conventional petrochemical polymer composites, have generated great interest especially within the European automotive industry [7-15].

Thus, biocomposites are now applied in many applications, in particular in the automotive industry. Figure 2 shows an exemplary display of natural fibre based components in the Mercedes E class.

Figure 2: Components of the Mercedes E class containing natural fibres [16].

Natural fibres usually require a lot less energy for processing and manufacture compared to glass or petrochemical based fibres, which contributes to general lower energy requirements in a product life cycle assessment considering greenhouse gas emissions and non-renewable energy use [17]. It was reported in a review by Joshi *et al.*, that natural fibre composites are environmentally superior to glass fibre composites when analysed with a comparative life cycle assessment [18].

Apart from the automotive industry, bio- and green composites are also finding applications in a wide range of products from structural to biomedical [2, 19-23].

1.2 NATURAL AND SYNTETHTIC CELLULOSE FIBRES

1.2.1 Natural Fibres

In general, natural fibres can be divided into two main groups; organic and inorganic fibres. Plant and animal based fibres are organic fibres, whereas mineral fibres are classified as inorganic. While both, animal fibres such as wool or silk and mineral fibres (e.g. asbestos, basalt) are also of technical importance, this review will focus exclusively on plant based fibres.

Plant based fibres can be further divided depending on their origin within the plant. Cotton fibres, for example, are classified as seed fibres, while flax and hemp are termed stem or bast fibres [24]. An overview of different natural fibres and their classification can be seen in Figure 3.

The most commonly used natural fibres for composite applications are wood, jute, flax, sisal and hemp, although many others are also suitable for biocomposites [2, 25-28]. Natural fibres have a lower density than glass fibres or mineral fillers resulting in a high specific tensile strength and stiffness, making them a lightweight, biodegradable alternative to more traditional reinforcements. The fibres themselves also sequestrate carbon dioxide during their life cycle [1]. Furthermore, natural fibres have advantages in processing as they are less hazardous to handle and generally cause almost no abrasion to the processing equipment [29]. However, silicate containing reinforcements such as bamboo fibres or rice hulls can cause abrasive damage.

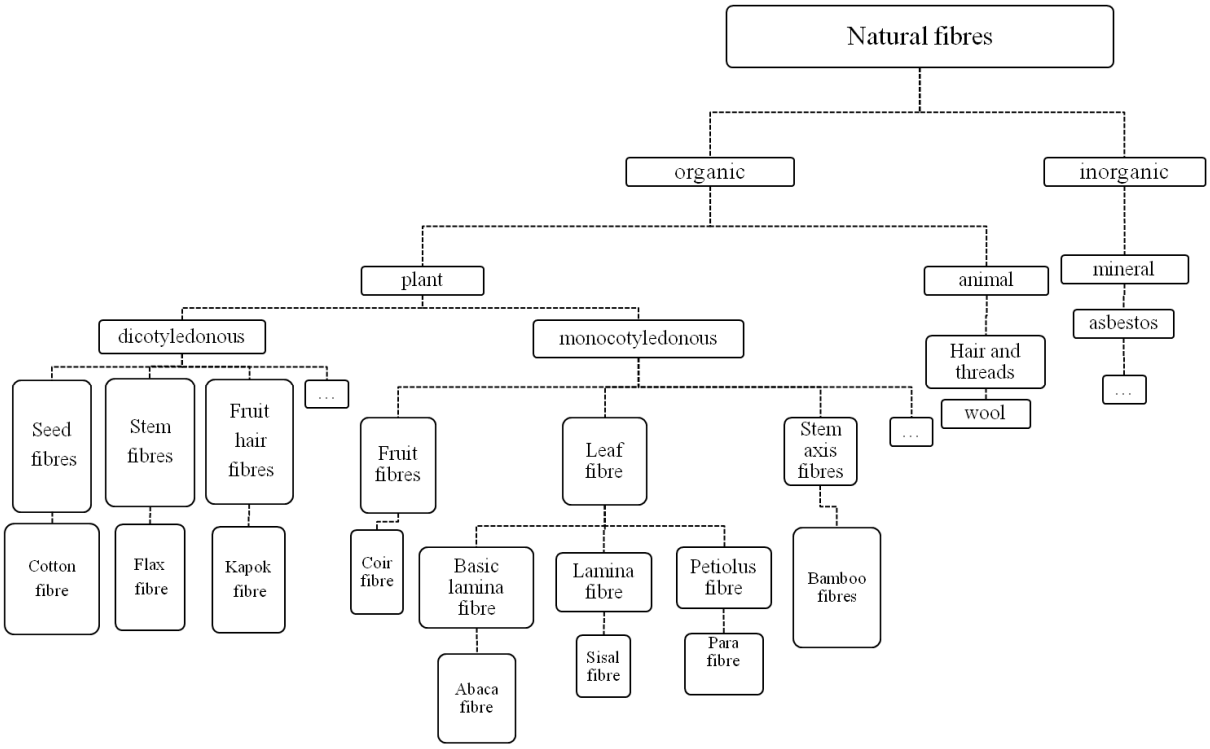

Figure 3: An overview of the classification of natural fibres. Adapted from Müssig 2001 [30].

Natural fibres usually show a large scatter of properties compared to industrially made fibres, due to different growing and processing conditions [31]. This can often lead to an overall decrease in composite properties and therefore limits the application potential. A tight quality control during fibre harvesting and processing and precise property evaluation are necessary to generate constant quality and predictable materials and to accurately quantify the mechanical properties of a batch of fibres, respectively [32, 33].

Nowadays, several traditional processing methods for thermosetting and thermoplastic polymers such as compression and injection moulding or extrusion have been modified to allow the use of natural fibres for composite processing. New processing routes have also been developed that allow more rapid fabrication of biocomposite components at production rates demanded by industry [34].

1.2.2 Synthetic Cellulose Fibres

In contrast to natural fibres, synthetic cellulose fibres are industrially processed fibres, but made from natural resources. Probably the most known synthetic cellulose fibre is viscose. The expression “Viscose” originates from the highly “viscous cellulose” solution obtained during the dissolution process, that was later contracted to “Viscose” [35].

Viscose yarns are based on a continuous regenerated synthetic cellulose fibre first developed in the late 19th century. The viscose process was discovered by the British chemists Charles Cross, Edward Bevan and Clayton Beadle in 1891 and made commercially available around 1905. Sales began to increase after 1910 with further improvements in the process. However, in the 1920s after the expiry of the original viscose patents, production of the yarns ceased. At that time, mainly in the United States, the name rayon was adopted for the yarns since the term viscose was being used for the viscous organic liquid used to make rayon and cellophane. However, the name viscose is still widely used for the fabrics in Europe. Further developments over the next few decades led to stronger yarns and when combined with the demand for staple fibre, led to further increased sales. Originally rayon was only produced for polyfill (consisting of several hundred continuous fibres). In the 1930s it was discovered that waste rayon discarded during the process was useful as a staple fibre [35].

The viscose process involves a derivatisation of a cellulosic raw material to create wet-spinnable cellulose solution. Regeneration of the dissolved cellulose in a water bath results in non-derivatised cellulose fibres. A major drawback of the rayon process is the contamination of wastewater by carbon disulfide and other polluting sulphur by-products of the cellulose derivatisation step. For this reason several companies invested into more

direct processing ways, while avoiding the use of carbon disulfide, which resulted in the Lyocell process, using *N*-methylmorpholine-*N*-oxide (NMMO) as a solvent. While other direct and more eco-friendly processing pathways are still being investigated, viscose rayon and the Lyocell fibre have evolved to be the main fibres of industrial importance [36].

Many improvements have been made to the viscose process and the resulting products such as rayon fibre in the last century to increase fibre quality and reduce the environmental impact [35]. The so-called synthetic cellulose fibres have shown a steady rate of production in the range of 2,500 to 3,000 kt/year in the last decades with the main application being textile fibres [37].

1.2.3 Fibre Structure

1.2.3.1 Natural Fibres

Natural fibres are made up from different components; cellulose, hemicellulose and lignin are the main elements, but many natural fibres also contain pectin, small amounts of ash and may exhibit a thin wax layer on the surface [38].

The main component, the cellulose molecule is usually present in its native form also called cellulose I arranged as microfibrils. Those fibrils consist of long chains of so-called cellobiose units, one unit being made up from two glucose molecules. The high number of hydroxyl groups in those cellulose chains do not only cause strong inter- and intramolecular hydrogen bonding but also hydrogen bonding with atmospheric hydroxyl groups. As a result of this, all cellulosic fibres are hydrophilic in nature and show a moisture content between 8-12.6 % [38]. Detailed information on cellulose structure will be presented in Section I.2.

The microfibrils are helically wound along the longitudinal fibre axis. The angle between these microfibrils and the fibre axis (known as the microfibrillar angle), the cellulose content and degree of polymerization (DP) of the cellulose chains each influence the mechanical properties of the fibre [39]. The cellulose fibrils in a natural fibre are usually embedded in a matrix of hemicellulose and lignin. A typical stem or bast fibre can be seen in Figure 4 showing a scanning electron micrograph (SEM) of flax (*Linum usitatissimum L.*) fibres. The rough fibre surface is the result of partially removed non-cellulosic components.

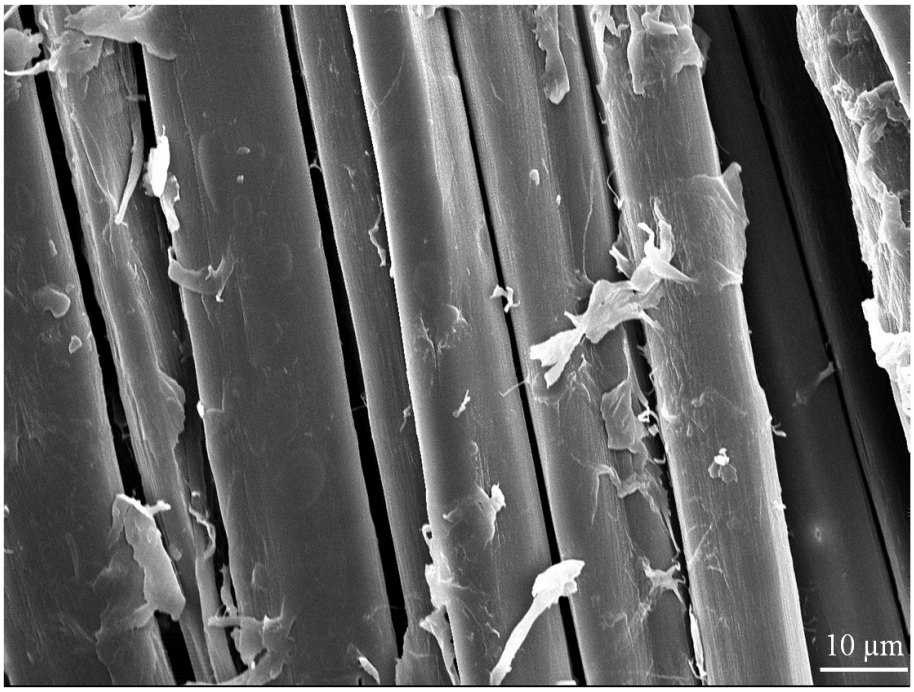

Figure 4: SEM micrograph of flax fibres/ fibre bundles in a bleached linen household fabric showing variation in fibre diameter and remaining non-cellulosic components.

Hemicellulose

Hemicellulose is another form of a sugar based polymer but in contrast to the highly linear chains of the cellulose molecule, hemicellulose consists of short and highly branched polymer chains. Typical sugar units in hemicellulose are galactose, glucose, mannose, xylose and arabinose. The structure of hemicellulose is considered amorphous,

being randomly orientated and exhibiting low mechanical properties. Hemicellulose has been identified as the main contributor to fibre swelling when natural fibres are exposed to aqueous environmental conditions [40].

Lignin

Lignin is a three-dimensional, heavily cross-linked copolymer with aliphatic and aromatic structures. The aromatic structures are formed by the removal of water from a sugar unit. Several monomers can form lignin and the types and properties depend on the source material. In contrast to cellulose and hemicellulose, lignin is hydrophobic in nature. Together with the hemicellulose it provides matrix for the strong cellulose fibrils. Lignin also resists most microorganisms and its aerobic breakdown is slow, and therefore it protects the load bearing cellulose from a premature degradation [40, 41]. Different types of lignin can be found in different plants and even within different plant structures. This can have a strong effect on not only biodegradation but also susceptibility to microbial activity and therefore fibre-retting during fibre processing [42].

Like cellulose, lignin is considered one of the most abundant biopolymers of the world. However, to date, most of the industrially processed lignin is mainly used as an energy source for the paper industry and finds only few industrial applications [43].

Average values of the above mentioned components, moisture content and microfibrillar angle can be seen in Table 1 for various natural fibres.

Table 1: Average amounts of structural components, moisture content and microfibrillar angle of different natural fibres. Table adapted in modified form from [38].

Fibre	Cellulose content in mass%	Hemi-cellulose content in mass%	Lignin content in mass%	Other components (pectin, wax, ash) in mass%	Moisture content in mass%	Micro-fibrillar angle in °
Flax	71	18.6-20.6	2.2	4	10	10
Cotton	82.7	5.7	n.r.	0.6	n.r.	n.r.
Ramie	68.6-76.2	13.1-16.7	0.6-0.7	2.2	8	7.5
Coir	36-43	0.15-0.25	41-45	3-4	8	41-45
Sisal	67-78	10-14.2	8-11	12	11	20

1.2.3.2 Synthetic Cellulose Fibres

Other than natural fibres, synthetic cellulose fibres consist entirely of cellulose. The cellulose crystalline structure changes from the native form, cellulose I, to another allomorph called cellulose II as a result of the manufacturing process.

Synthetic cellulose fibres can be generally divided between non-derivatised and derivatised cellulose fibres. Such cellulose fibres can be produced in many different ways, although only a few are of industrial importance. The most used cellulose fibres are viscose, modal, Lyocell, Cupro and rayon tirecord fibre. The fabrication of those fibres either involve the (a) production of a cellulose derivative, which in a follow-up step, is converted back to pure cellulose (e.g. viscose) or (b) dissolution of the cellulose raw material in a non-derivatising solvent (e.g. Lyocell) [35].

The most industrially important derivatised cellulose fibres are cellulose acetate and cellulose triacetate fibres [44].

The main differences in the synthetic cellulose fibres are a result of different raw materials, different fibre forming processes and applied post forming treatment, resulting in different fibre shapes, structures and properties [45]. However, all synthetic cellulose fibres consist of crystalline microfibrils embedded in amorphous cellulose. The crystallinity of those fibres can vary from 38 % up to 62 %, depending on the manufacturing process [36]. Viscose fibres often show an uneven cross-section with lobulated structures. Furthermore, distinct skin and core and regions can often be determined. In contrast, Lyocell fibres are usually circular in cross-section with a uniform structure [46]. The microfibrils in Lyocell fibres have been reported to be longer and thinner, showing a higher degree of orientation than their viscose counterparts [45]. Figure 5 shows the typical cross-section and microfibrillar structures of a Lyocell and textile viscose fibre.

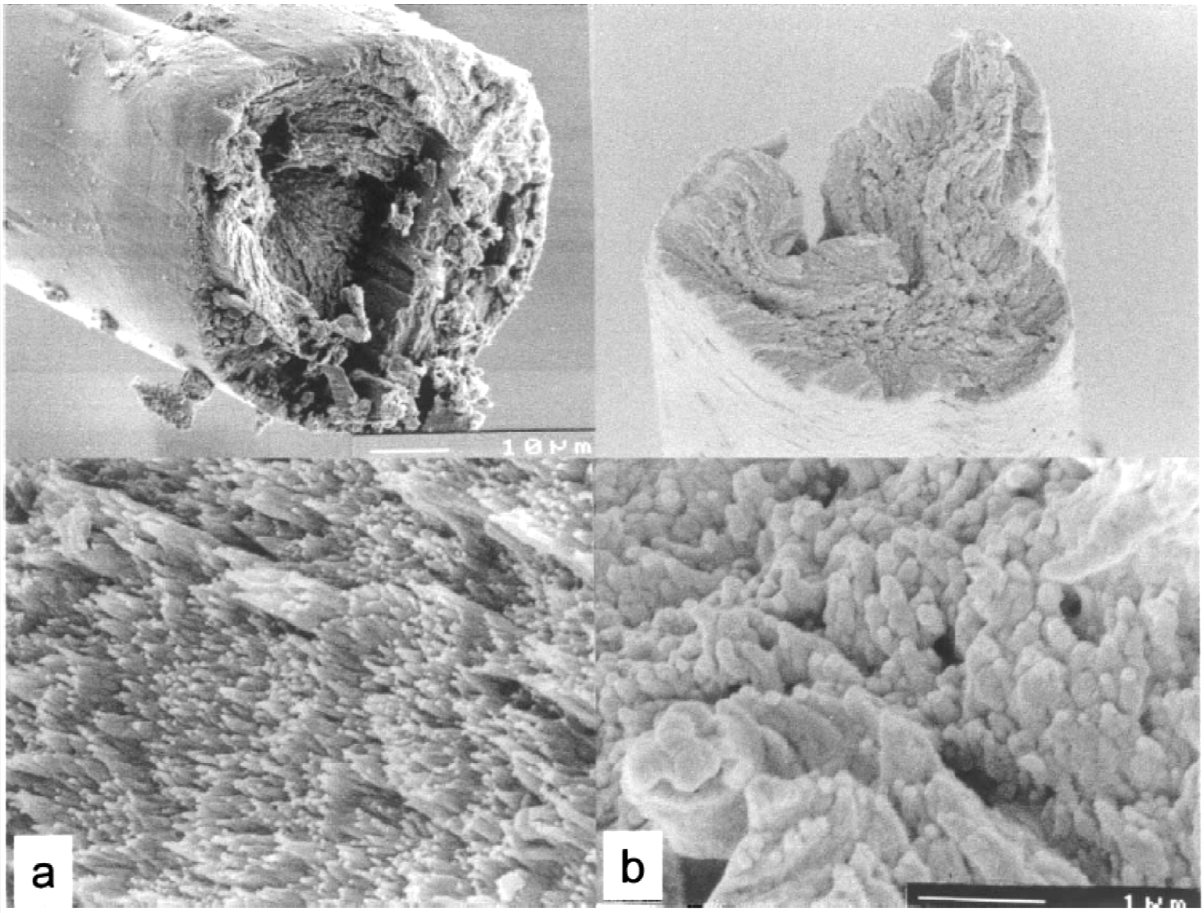

Figure 5: SEM micrographs of fracture surfaces of a (a) Lycoell fibre and (b) Viscose fibre, showing the differences in cross-sectional shape and microfibrillar structures. Taken from [46].

1.2.4 Fibre Properties

1.2.4.1 Natural Fibres

As mentioned, the properties of natural fibres differ not only between different fibre types but also depend on fibre growing and harvesting conditions. Additionally, many natural fibres show a large scatter of properties, within a single batch, often the result of uneven cross-sections and fibre defects [47]. Hence, reported properties of natural fibres often merely represent the group of tested fibres rather than an average of the fibre type. The difference in property scatter of a flax fibre compared to synthetic cellulose fibres is highlighted in Figure 6.

Due to the wide range of different natural fibres, a broad spectrum of fibre properties is available, ranging from low strength but high strain fibres such as coir and cotton to very stiff and strong fibres with a very low strain such as flax and ramie. Average values including the very high variation of some natural fibres can be seen in Table 2. The low density (<1.9 g/m^3) is typical characteristic of all natural fibres [1].

Table 2: Average mechanical properties and densities of various natural fibres

Fibre	Density in g/m^3	Tensile strength in MPa	Young's modulus in GPa	Elongation at break in %	Source
Flax	1.5	345-1035	27.6	2.7-3.2	
Cotton	1.5-1.6	287-597	5.5-12.6	7-8	
Ramie	n.r.	400-938	61.4-128	3.6-3.8	[48]
Coir	1.2	175	4-6	30	
Sisal	1.5	511-635	9.4-22	2-2.5	

1.2.4.2 Synthetic Cellulose Fibres

In contrast to the wide scatter of properties of natural fibres, synthetic cellulose fibres can be processed to tailor the properties in a much narrower range. In general, synthetic cellulose fibres exhibit a higher strain (>10 %) than many natural fibres. However, synthetic cellulose fibres tend to have a significantly lower strength and stiffness. In spite of these differences, the high variability of natural fibre such as flax results in its properties lying within the vicinity of synthetic fibres such as rayon tirecord and Lyocell fibres (Figure 6) [49].

Lyocell fibres primarily consist of monoclinic cellulose type-II crystallites [46, 50]. Crystallites with a length, width and thickness of 12-14 nm, 8-10 nm and 3-4 nm, respectively accumulate into strand-shaped bundles with lengths of 150-550 nm, partly assembled into aggregates of 30-60 nm in diameter [50].

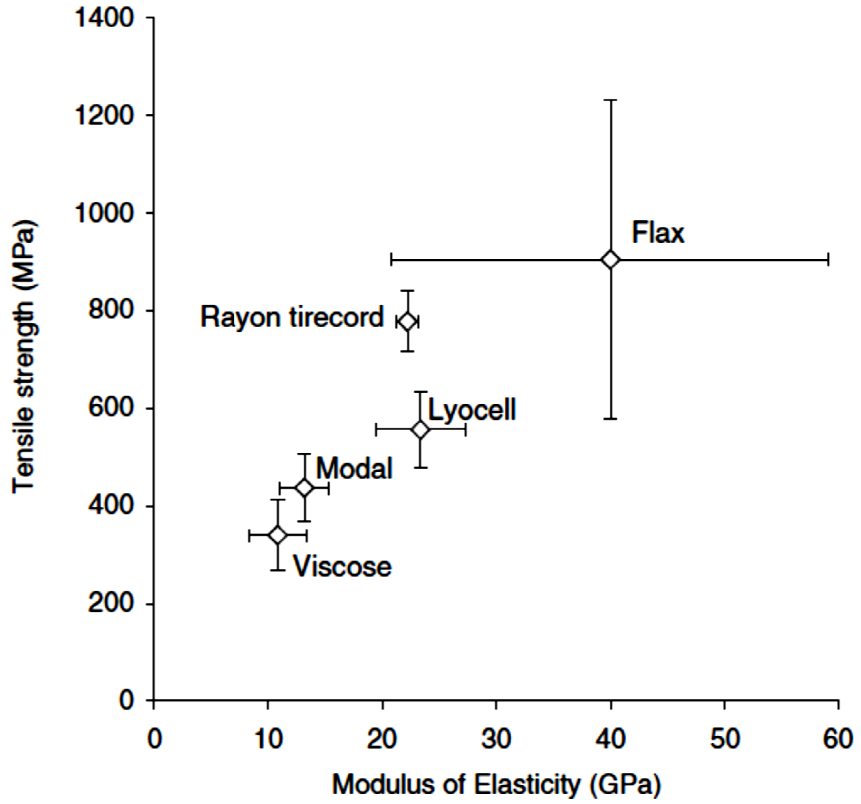

Figure 6: Tensile strength and Young's modulus of several synthetic cellulose fibres compared to flax. Taken from [49].

1.3 BIO- AND BIO-BASED POLYMERS

Bio-based polymers, meaning a polymer which is derived from natural resources and/or biodegradable, as well biopolymers, meaning a naturally occurring polymer, have been an important focus of several research groups within the last decade. Many different combinations of bio-based polymers and biopolymers and natural fibres have been analysed to find strong and truly green composites such that the resulting composite material is completely biodegradable and sustainable. To cover all of the recent

developments in the field of biopolymers and resulting green composite is beyond the scope of this Chapter, and the interested reader is referred to several excellent review articles in this area by Goda and Cao, Jacob John and Thomas, and La Mantia and Morreale [2, 51, 52].

In general, bio-based polymers can be classified according to their source, dividing between agro based polymers (cellulose), microbially synthesised (poly(hydroxyalkanoate)), chemically synthesised from fermented agro based resource monomers (poly(lactic acid)) and chemically synthesised from conventionally synthesised monomers [53]. An overview of the biobased polymer family is provided in Figure 7.

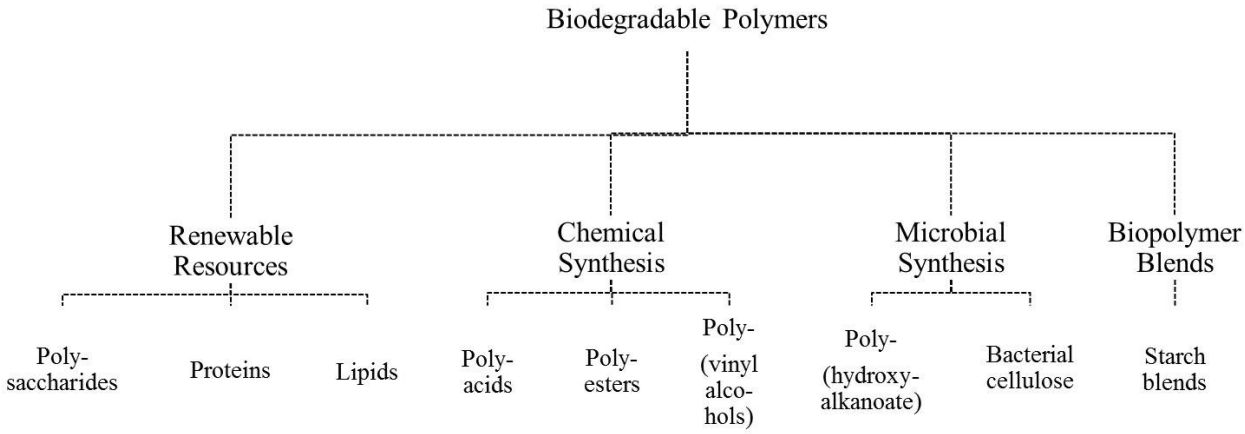

Figure 7: Classification of bio-based polymers. Adapted from [53].

In the following two of the most commonly materials, a biopolymer (starch) and a bio-based polymer (poly (lactic acid)) will be briefly introduced in comparison to the cellulose polymer.

The starch molecule consists of D-glucose units, called homoglucan or glucopyranose. It is built from amylose and amylopectin, the amounts of which strongly depend on the plant

origin. Typical sources for starch are wheat, maize or potatoes. Native starch show values ranging from 25 to 39 %. For most applications, the starch structure is physically and/or chemically disrupted, typically by a heat-water treatment. Depending on the level of destructurisation, different starch materials can be produced, such as starch foam that is mostly used in packaging. Another option is plasticised or "thermoplastic" starch, a material used as polymeric matrix phase in green composites [54].

Plasticised starch has a much lower crystallinity compared to native starch and a major drawback is its high sensitivity to moisture and its low mechanical properties [55]. To improve this, plasticised starch is often mixed with other either synthetic or bio-based polymers [56].

The poly (lactic acid) (PLA) monomer is lactic acid, which is mostly produced by bacterial fermentation of a carbohydrate using a certain strain of *Lactobacilli*. The source of carbohydrate depends on the strain of bacteria, but many simple sugar units like glucose, dextrose, sucrose or maltose all present in agricultural plants such as maize or sugar cane can be used [57]. Two different routes can be used to produce PLA from lactic acid; either a solvent based condensation reaction or a coagulant removal of water. Both are used by major manufactures of PLA [58].

PLA has been used for medical applications for decades, but only recently PLA has attracted interest as a biodegradable material not only for several disposable products in the packaging sector but also as a textile fabric [56]. However, PLA needs industrial composting conditions to degrade and is not cold compostable as experimentally shown in Section VI.4. PLA is also suitable as a thermoplastic matrix for bio- and green composites several of which have produced successful in everyday consumer products

such as a mobile phone housing made by NEC and UNITIKA LTD [59] from a PLA-kenaf composite or biodegradable urns made PLA and flax [60].

While the low glass transition temperature of PLA of 50-60 °C can be a problem in some applications, it has been shown that the addition of natural fibres can clearly improve its thermomechanical behaviour [61]. Furthermore, the addition of microfibrillated cellulose to PLA can improve its crystallisation and increase its tensile strength [62].

1.4 BIOCOMPOSITES AND THEIR CHALLENGES

The combinations of different natural fibres and bio-based polymers to create green composites are numerous, and the resulting materials show a wide range of mechanical properties [63]. While some of those composites are still in an experimental stage, several have found their way to industrial applications.

However, substituting traditional reinforcements such as glass fibre and carbon fibre with cellulosic fibres creates new challenges for engineers and scientists.

The strong hydrogen bond network that is responsible for the high mechanical properties of cellulose containing fibres is unfortunately also the cause of some difficulties in the use of cellulosic reinforcements.

The hydrophilicity of natural fibres requires an additional drying or conditioning step during processing to control their moisture content as well as rapid processing as the fibres reabsorb moisture quickly [64].

If stored or processed incorrectly natural fibres can start to biodegrade due to their relatively high moisture content, causing a drastic reduction in composite properties, the development of unpleasant odours and low dimensional stability [65].

Moreover, one of the major problems limiting the application potential of cellulose based composites is the inherent chemical incompatibility between a hydrophobic polymer matrix and hydrophilic cellulose [66, 67]. This causes interfacial bonding between the cellulosic and bio-based polymer components to be often weak, particularly in the case of thermoplastic bio-based polymers [68]. This leads to an inefficient transfer of stress under load, thus lowering mechanical strength and stiffness of the composite [7, 66, 69, 70].

The chemical compatibility can be improved by a chemical treatment of the fibre or matrix. Silane, alkaline, acetylation, chemical grafting and corona discharge treatments provide widely varying degrees of improvement [25, 39, 68, 71-75]. Interfacial bonding can also be increased by applying nanosized forms of cellulose such as bacterial cellulose [76, 77], microfibrillated cellulose [78, 79] and cellulose whiskers [80-83] that provide an increased surface area per volume to the surface of the natural fibres. While significant improvements in mechanical properties can be obtained, the above methods also add cost and complexity to the formulation of biocomposites.

Examples of other problems that can arise are the inherently low flame-retardant properties of cellulosic materials and the relatively low degradation temperature compared to glass and carbon fibres [84].

1.5 CONCLUSIONS

Green composites are a promising class of materials as they offer solutions to several problems mankind will face in the oncoming decades such as a shortage of non-sustainable resources and increasing pressure to reduce the ecological impact of polymer based materials. However, the ecological aspects of green composites alone are not likely to increase their industrial application range and attract large composite manufactures. Good mechanical properties and easy-to-adapt processing ways need to be established to make green composites a true alternative to traditional petroleum-based composites.

The scatter of material properties is a major disadvantage of natural fibres and corresponding composites. Therefore ways need to be found to produce green composites with good mechanical properties of constant quality. Alternatively, synthetic cellulose fibres could be used as their properties are easier to predict due to their industrial manufacture.

Although many natural fibres exhibit impressive mechanical properties due to their structural backbone, the cellulose molecule, green and biocomposites often struggle to achieve mechanical properties that would make them a viable alternative to traditional composites such as glass fibre reinforced composites (GFRC). The reason for this is often a weak interface between the fibre and matrix phase, resulting in a poor load transfer and premature failure.

As shall be discussed in detail in Section I.3, monocomponent composites made from a green polymer such as cellulose could overcome those problems by utilising chemically

identical phases, thereby enabling improved adhesion between fibre and matrix phases. As result, high mechanical properties can be achieved for completely green composites taking full advantage of the high specific mechanical properties of cellulose containing fibres.

2. CELLULOSE

2.1 INTRODUCTION

Natural fibres show a wide range of properties and resulting application range and potential that are mostly determined by their chemical composition. The composition of natural fibres is typically composed of various macromolecules including cellulose, hemicellulose, lignin, pectin and waxes. Not all natural fibres will have all of these components, but cellulose is common to all such plant structures in varying amounts [85].

Therefore, cellulose is one of the most abundant biopolymers on earth with approximately 1.5 x 10^{12} tons of cellulose produced each year. Thus, it represents an enormous amount of a renewable and biodegradable resource for raw materials [85, 86]. Cellulose fibres are widely recognised for their applicability in ecofriendly composite materials, although unlocking their full potential remains a challenge for load-bearing engineering applications.

2.1.1 Cellulose History

The molecular composition of cellulose, isolated from plant cell walls, was first discovered and determined by Anselme Payen (1795-1871) [85]. Payen believed that cellulose was a chemically uniform carbohydrate based on glucose. He stated that cellulose was a more highly aggregated isomer than starch but in other ways very similar. Edmond Frémy (1814-1894) on the other hand suggested that differences in cellulose and starch arise from different isomeric states. Interestingly, the term “cellulose” as defined by Payen in 1838 meant purified plant tissue still containing other carbohydrates, a material that, by nowadays definition, is referred to as “pulp”. As cotton fibre consists almost entirely of cellulose, it became a standard in the early days of cellulose research and therefore the

term “cellulose” was reserved for the portion of a plant cell wall resembling the physical and chemical properties of cotton cellulose [87]. Cellulose today is defined as non-branched chain of glucose units of variable length.

The cellulose molecule has been the subject of many discussions since it was described. Various models have been developed to describe and refine its structure, crystallinity and transformations and although a widely agreed-upon definition seems to be established, many of the older models still persist in the scientific literature and haven’t been completely discarded [88].

2.2 CHEMISTRY AND PHASES OF CELLULOSE

Cellulose is a linear polymer composed from aldehyde sugars, so-called D-anhydroglucopyranose units ($C_6H_{11}O_5$/ IUPAC nomenclature: (3R,4S,5S,6R)-6-(hydroxymethyl) oxane-2,3,4,5-tetrol), often simply referred to as glucose units, assembled into groups of two as “cellobiose” units (Figure 8). A single glucose unit is a hexose that takes on one of two forms (α or β), depending on the position of the hydroxyl groups. Individual cellulose chains are highly hydrophilic due to the large numbers of hydroxyl groups present. Consequently, single cellulose chains have a strong tendency to form inter- and intra-molecular bonds which are responsible for the crystalline, strong and rigid nature of cellulose. Several different packaging systems of the cellulose molecules exist; native cellulose, present in plant fibres, algae and produced by bacteria is called cellulose I. The most common other allomorphs of cellulose are cellulose II, III and IV. Cellulose II can be formed by mercerization or regeneration of cellulose I [85, 89-91]. Cellulose III can be formed from either, cellulose I or cellulose II by a treatment with liquid ammonia, resulting in either cellulose III_1 or cellulose III_2 depending on the original

cellulose allomorph. Cellulose IV_1 and Cellulose IV_2 can be prepared by the corresponding form of cellulose III by heating in glycerol [92]. What all those allomorphs seem to have in common is that the cellulose chains resemble flat ribbons allowing a dense and crystalline packing. In the above mentioned allomorphs, cellulose has a twofold screw-axis symetry. Non-crystalline or unordered cellulose systems are generally referred to as amorphous cellulose [93].

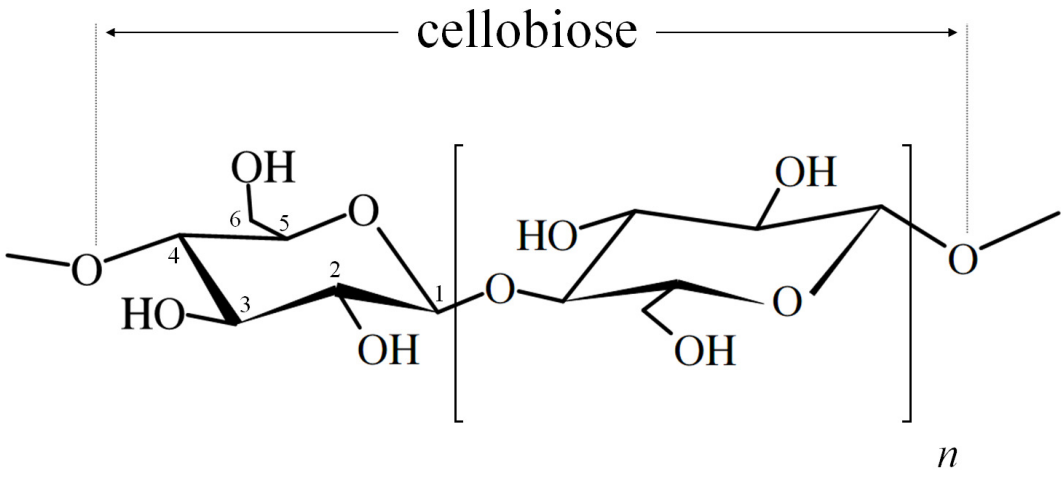

Figure 8: Molecular structure of a cellobiose unit with numbered carbon atoms.

2.2.1 Cellulose I

Native cellulose or cellulose I is the most crystalline type of which there are two forms: I_α and I_β. While the cellulose I_α crystal has a triclinic unit cell, the cellulose $I_ß$ crystal has a monoclinic unit cell. Both, cellulose I_α and I_β are present in native cellulose structures but their ratio depends on the source of cellulose. Cellulose from algae and bacteria is usually rich in cellulose I_α, while cellulose I_β is predominant in wood and other natural fibres [87, 88, 92, 94, 95].

The cellulose I crystal structure has been widely investigated in the last century and several models have been applied to explain its structure. By today's standards the

cellulosic chains are assumed to be aligned in a parallel manner meaning that the reducing ends of the cellulose chains are at the same end in one unit cell. Intramolecular hydrogen bonds exist between O-3'-H and O-5', and between O-2'-H and O-6', while intermolecular bonds are established between O-6'-H and O-3' as shown in Figure 9 [96].

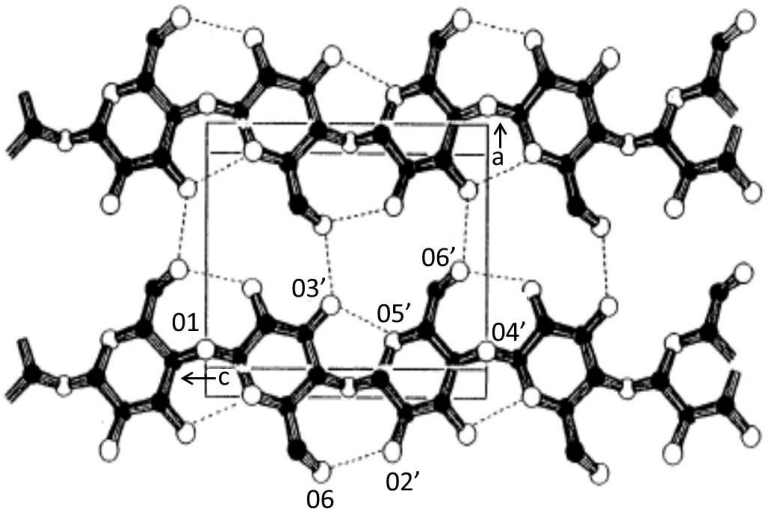

Figure 9: Inter-and intramolecular hydrogen bonds in the cellulose molecule. Adapted from [97].

The main difference between cellulose I_α and I_β as determined by X-ray diffraction is the stacking sequence of the aforementioned planes [87]. I_α hydrogen bonds are aligned on a constant inclined axis while the I_β bonds are stacked with an alternating "offset" of half a glucose monomer length [98] (Figure 10). Analysis of the two unit cells via infrared spectroscopy also indicates differences in hydrogen bonding as detected in Solid State Nuclear Magnetic Resonance (solid state NMR) experiments [87]. The strong hydrogen bonding of the cellulose molecules cannot be easily broken down and therefore do require solution processing if they are supposed to be used as a matrix phase as described in more in detail in Chapter III.

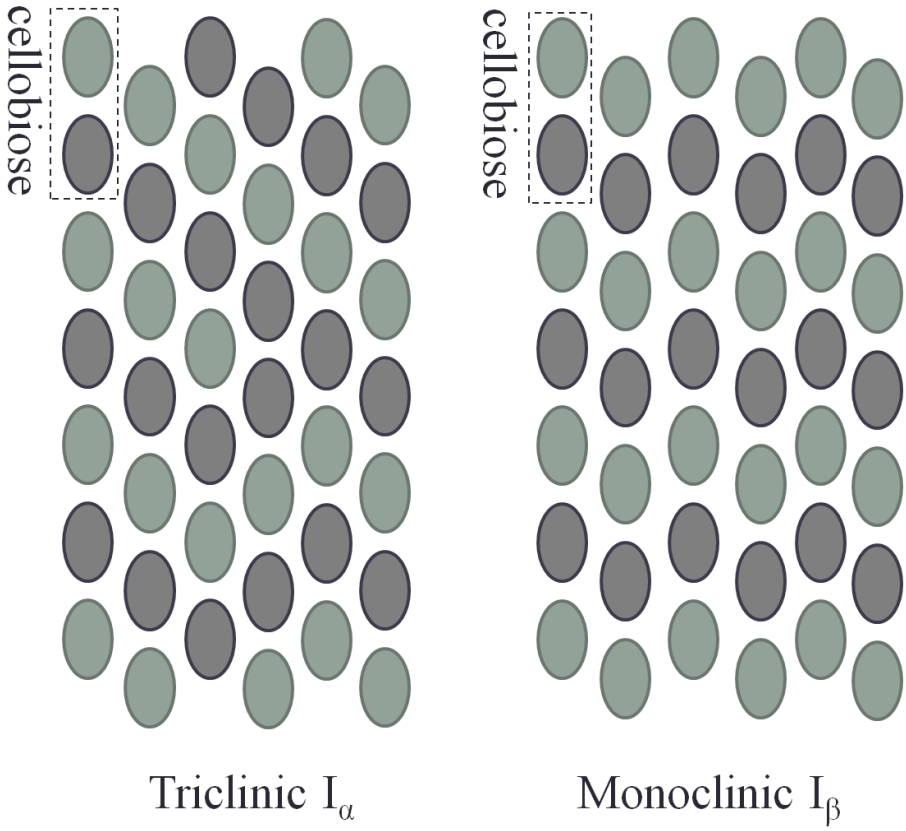

Figure 10: Schematic of the two different orientations of cellulose I. One unit in the schematic resembles one glucose molecule. The two different stacking sequences, triclinic and monoclinic, are displayed. Adapted from [99].

2.2.2 Cellulose II

The first conclusive models of the cellulose II molecular structure were proposed by Kolpak and Blackwell [89] and Stipanovic and Sarko in 1976 [100]. Cellulose II is considered the most stable form of the cellulose allomorphs. It can be created by either a treatment with NaOH, a process called "mercerization", or by dissolution and regeneration of cellulose I. Both processes result in an almost identical unit cell [92]. As cellulose II is formed from a cellulose solution, it is the main component of synthetic cellulose fibres such as rayon and Lyocell.

In contrast to cellulose I, cellulose II shows an anti-parallel packing of the cellulose chains, meaning half of the reducing ends of the cellulose chain can be found on both ends of the crystal [93].

While the general structural model of cellulose II has been widely accepted, several refinements have been made to describe the hydrogen bonding network and determine the position of the hydroxymethyl group [87, 101, 102].

2.2.3 Other Allomorphs and Transitions

As mentioned earlier, Cellulose III can be formed from, cellulose I and cellulose II, resulting in either cellulose III_1 or cellulose III_2. The structural change is usually caused by a treatment with liquid ammonia or amines [93].

The unit cells of cellulose III_1 and III_2 show a high amount of similarity; however cellulose III_I shows a parallel arrangement while cellulose III_2 is anti-parallel. Both forms can be transformed to their original structures by a mild heat treatment [92]. Little is known about the exact structure of the unit cell of cellulose III_2 but cellulose III_1 was reported to have a one-chain unit cell, with some similarities to cellulose II [87].

Similar to cellulose III, cellulose IV can be produced by a heat treatment with temperatures higher than 240 °C from either cellulose III_1 or cellulose III_2 [93]. The conversion however has often been characterized as incomplete [91]. It was recently suggested that no distinction should be made between cellulose IV_1 and cellulose I_β or it should be referred to as cellulose I_β with lateral distortions, since the unit cells of cellulose IV_1 and cellulose I_β are very similar [103].

An overview of the different allomorphs and possible transformations can be seen in Figure 11.

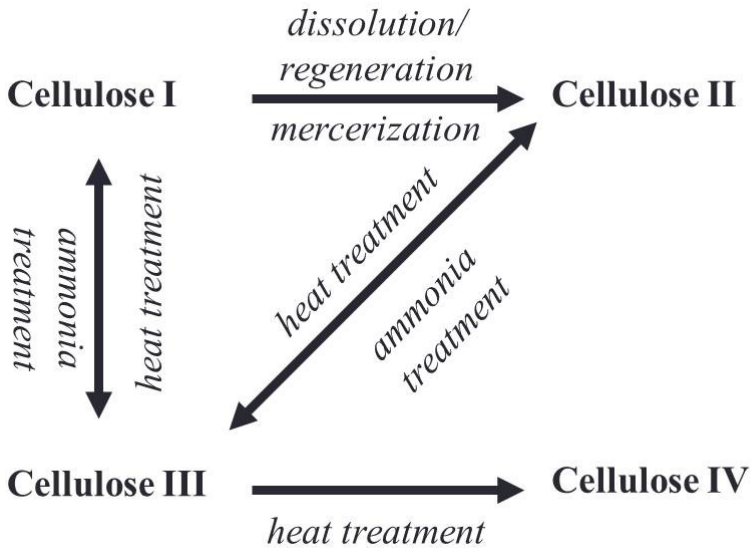

Figure 11: Possible transformations between the different cellulose allomorphs.

2.2.4 Amorphous Cellulose

Amorphous cellulose is characterized as having a very low order of the cellulose molecules [104]. The amorphous regions of cellulose microfibrils are described to lie as a thin layer between single microfibrils aligned to the fibre axis [87]. This model is often called the micellar model or fringe fibrillar model [96].

The amorphous portion of cellulose in natural fibres can be usually found in the outer regions of the fibre, while the highly crystalline fractions are localized in the fibre core [105]. Interestingly, the crystalline regions are often found evenly distributed over the fibre cross-section or concentrated in the outer regions in synthetic cellulose fibres, if the earlier described sleeve-core regions (see Section III.3.2) are present [46, 106].

A transition from the crystalline forms to amorphous cellulose can, for example, be achieved by ball-milling but can also be the product of a dissolution and regeneration process depending on the applied processing conditions [107, 108].

Amorphous cellulose can be recrystallised into a semi-crystalline form of cellulose II when brought in contact with water. At high humidities, near 100 %, the water acts as a plasticiser, allowing a reorientation of the cellulose molecules. While this effect was attributed to the hydrogen bonding ability of the water molecules, similar processes could not be achieved when using alcohols (methanol, ethanol, propanol) instead of water [104, 109].

2.2.5 Mechanical Properties of Cellulose

The mechanical properties of cellulose differ quite widely between the different allomorphs. An average Young's modulus of 10.3 GPa was calculated for amorphous cellulose using a force-field model [110]. In 1962, using X-ray diffraction, Sakurada *et al.*, determined the Young's modulus of elementary cellulose fibril of bleached ramie fibre to be 134 GPa [111]. Using a similar experimental set-up, Nishino *et al.* measured the elastic modulus of several cellulose polymorphs. Cellulose I was found to have a modulus of 138 GPa whereas cellulose IV exhibited a lower value of 75 GPa [112]. Ishikawa *et al.* published a similar ranking for those polymorphs sourced from ramie fibre [113]. This variation in tensile properties is due to differences in the molecular structure of the different allomorphs. Deformation mechanisms involve complex stretching and re-organisation of the hydrogen bonds, which differs greatly for crystalline and amorphous phases.

The mechanical properties of cellulose compete well with other engineering materials such as aluminium (~70 GPa) or glass fibres (~70-90 GPa) [114]. As a result of the low density of 1.58-1.59 g/cm^3 Wegst *et al.* ranked the specific stiffness of native cellulose of 67 GPa cm^3 g^{-1} as among the highest of all natural materials [91, 115, 116].

Cellulose I is the strongest allomorph with a theoretical ultimate tensile strength of about 13-17 GPa. Cellulose II and amorphous cellulose are less strong with tensile strengths of approximately 9 and 0.8 GPa, respectively [117]. The high tensile strength and low density of the native cellulose crystal results in the highest specific tensile strength of any known natural polymers for cellulose I (667 MPa cm^3 g^{-1})[115].

While these theoretically calculated properties show the potential of utilising the cellulose molecule as a composite raw material, the experimentally determined properties of cellulose present in fibres fall short compared to those theoretical values. Reasons for this can include defects in the molecular structure or a low crystallinity in case of regenerated cellulose. Furthermore difficulties in fibre separation or removal of the cellulose molecules from the other components present in natural fibres can reduce the mechanical properties [117].

2.3 CONCLUSIONS

Cellulose is a very complex biopolymer that is inherently different from traditional crude oil based polymers due its strong hydrogen bonds, their interaction and resulting different crystalline conformations.

However, cellulose demonstrates superior mechanical properties compared to other biomaterials. Monocomponent composites made entirely from cellulose could overcome

the fibre-matrix-bonding problem by chemical similarity. Combined with the already existing knowledge in cellulosic fibre composite processing, those monocomponent or all-cellulose, composites could represent an interesting and promising alternative to existing green composites.

As a result of the present strong hydrogen bond network, cellulose needs to be dissolved and regenerated to be used as a polymer in composite processing. This means an inevitable disruption or even a complete disintegration and reforming of the crystalline structure and the processing will therefore have a strong influence on the physical properties of any cellulose-based composite. Hence, different cellulose allomorphs and structural reorganisation of the cellulose molecule during processing could have a decisive influence on a composite made entirely from cellulose. Especially the interface between a cellulosic matrix and cellulosic fibre could depend on the hydrogen bonding mechanism of the cellulose molecule.

As the cellulose molecule are strongly hydrophilic, atmospheric moisture, water as a processing material and corresponding drying conditions will have a strong effect on all-cellulose composite and needs to be investigated in detail.

3. ALL-CELLULOSE COMPOSITES

3.1 NON-DERIVATIZED ALL-CELLULOSE COMPOSITES

3.1.1 Introduction

The commonly accepted definition of a composite is a material that consists of two or more distinct materials to improve, for example, mechanical properties such as the stiffness, strength and/or toughness over the individual constituents or other relevant properties such as shrinkage or thermal expansion. However, in a monocomponent or single polymer composite, reinforcing and matrix phases are based on the same material. Theoretically, this would lead to a composite where boundaries between reinforcement and matrix are almost indistinct in the presence of ideal chemical bonding, a state described as "interfaceless" by Nishino *et al.* [118]. Therefore, the need for energy intensive fibre treatments or coupling agents for improving interfacial bonding could be drastically reduced or even completely eliminated.

While the reinforcement and matrix of monocomponent composites are necessarily of the same chemical composition, physical morphology and/or structural phases of the two components may differ in reality. The performance of a monocomponent or single-polymer composite is best illustrated with an example of the concept as put forward by Capiati and Porter in 1975 [119]. In this work, high-density polyethylene (HDPE) composites were produced with a gradient of changing morphology between the reinforcing fibres and the matrix material resulting in an improved interfacial shear strength in the range between glass fibre reinforced polyester and epoxy resins. The different melting temperatures of conventionally crystallised HDPE used as matrix phase and highly orientated HDPE reinforcements with extended molecular chains were utilised to fabricate a HDPE monocomposite by thermoforming [119].

The main challenge in processing single-polymer composites has been identified as retaining the properties of the orientated polymer reinforcement during processing. In case of thermal processing, temperature based molecular relaxations need to be avoided [120]. Similarly, in case of the less common solvent-based processing used for example for all-cellulose composites [63] or all-aramide composites [121], an "over-dissolution" of the fibre needs to be to circumvented to achieve good mechanical properties of the composite.

Processing methods for single-polymer composites include (I) melt (solution) or powder impregnation used for example for all-polypropylene (PP) and all polyethylene (PE) composites. For this process, the reinforcement simply gets impregnated with a highly viscous polymer resin. (II) Forming the matrix phase from the fibres by hot compaction processing used for example for PP, PE, nylon 6,6 and PMMA. The polymer fibres get compacted into an orientated polymer sheet using suitable processing temperatures and pressures. However, problems can arise from choosing an adequate processing temperature that allows the formations of a consistent matrix phase but does not melt the fibres. (III) film-stacking, meaning a textile is sandwiched between two sheets of matrix phase and compacted by hot pressing was successfully used for PP and PLA. (IV) co-extrusion has also been used successfully for example to process highly orientated all-PP composites [122].

In addition to the enhanced bonding at the reinforcement-matrix interface, monocomponent composites can also provide a more straightforward path for recycling as the fibre and matrix do not require separating [123-126].

The concept of an all-cellulose composite (ACC) was first discussed by Nishino *et al.* in 2003 [114]. ACCs can be considered as bio-derived monocomponent composites; although strictly speaking, the same source of cellulosic materials would need to be used for the reinforcing and matrix phases. While the ease of recycling is an important advantage for thermoplastic-based monocomponent composites, the main driver for the development of ACCs is to improve chemical bonding at the reinforcement-matrix interface. During the processing of ACCs, it is quite possible to have two or more different allomorphs present. In theory, cellulose molecules strongly interact through hydrogen bonding, although the interaction between different cellulose allomorphs has not been quantified. Thus, the details of chemical bonding at allomorph boundaries in ACCs remain elusive. The morphological characteristics of the interface have only been observed qualitatively using for example scanning [118] or transmission electron microscopy [127].

3.1.2 Preparation and Synthesis of ACCs

3.1.2.1 Processing Routes

There are two distinctly different processing strategies in the literature for the preparation of ACCs (Figure 12). The first of these methods (2-step method) involves firstly a complete dissolution of a portion of cellulose in a solvent which is then regenerated in the presence of undissolved cellulose. An example of this method was first given by Nishino *et al.* in which Kraft fibre was fully dissolved and then regenerated in the presence of ramie fibres [118].

A second route (1-step method) involves partial dissolution of the surface of cellulosic fibres which is then regenerated *in situ* to form a matrix around the undissolved portion.

An example of this method was first given by Gindl *et al*. in which they partially dissolved microcrystalline cellulose, resulting in volume fractions of up to 90% of the original fibre and 10% of newly regenerated cellulose matrix [128]. This method has also been described as "surface selective dissolution" [105]. In these processing routes, the dissolution step is followed by solvent removal and cellulose regeneration using water or other coagulants, after which the composites usually have to be dried.

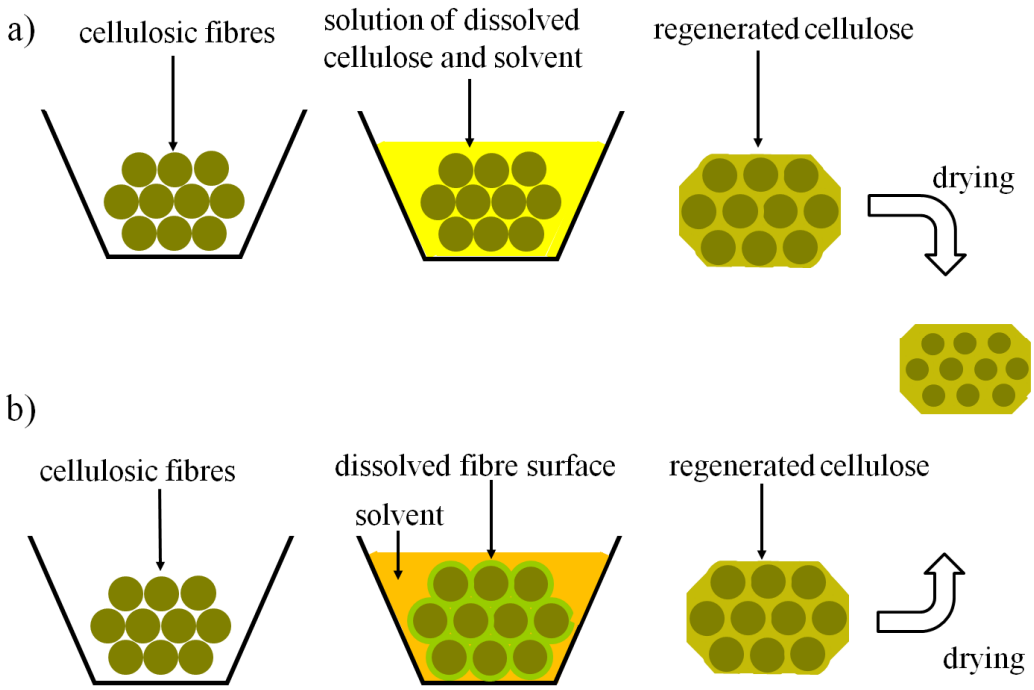

Figure 12: Schematic of two-step (a) and one-step (b) all-cellulose composite preparation. The schematic of the one-step process is adapted from Nishino and Arimoto [129].

3.1.2.2 Cellulose Dissolution

Known non-derivatising solvents for cellulose include lithium chloride/*N,N*-dimethylacetamide (LiCl/DMAc), dinitrogen tetroxide/dimethylformamide (N_2O_4/DMF), *N*-methylmorpholine-*N*-oxide (NMMO), mineral acids, sodium hydroxide (NaOH), dimethylsulfoxide/tetrabutylammonium fluoride (DMSO/TBAF), dimethylimidazolone/lithium chloride, and various molten salt hydrates and ionic liquids (ILs). Of these, LiCl/DMAc, NMMO, NaOH (often in the in mixture with urea or thiourea)

and the ionic liquid 1-butyl-3-methylimidazolium chloride (BmimCl) have been used mostly in the processing of ACCs (Table 3). However, limited dissolution capacity, slow dissolution rates, toxicity and non-recyclability are the reasons that prevent some of these solvents from being used in large industrial scales. It has been observed that some ILs offer high cellulose dissolution rates. The low vapour pressure of ILs also makes them easy to reuse and safer to handle, and has led to the term "green solvents" [130-134].

Table 3: Cellulose solvents used for the production of all-cellulose composites and the year their functionality was reported.

Solvent	Year	Reference
Ionic liquids	1934	Graenacher, C.[135]
NMMO	1969	Johnson D.L., [136]
LiCl/DMAc	1981	McCormick C., [137]
NaOH-urea	1995	Isogai A. & Antalla R., [138]

N-methylmorpholine-N-oxide (NMMO)

NMMO belongs to the family of cyclic, aliphatic, tertiary amine oxides, where the nitrogen carries the cyclic and aliphatic groups, and oxygen (Figure 13) [139]. The highly polar N-O group is responsible for the high hydrophilicity of NMMO and its complete miscibility with water, as it readily forms hydrogen bonds. NMMO is a powerful cellulose solvent due to the high polarity and weakness of the N-O bond [139].

NMMO is used industrially in the Lyocell process for producing regenerated cellulose fibres. The main steps of this process are the preparation of a slurry by dissolution of

cellulose (usually pulp or cotton) in a mixture of water, NMMO, stabilizers and additives. The cellulose solubility depends on the mixing ratio of cellulose, water and NMMO. A more detailed description of the dissolution process and the influencing factors can be found in the review of Fink *et al.* [46]. The dissolution is followed by an extrusion of the viscous dope at elevated temperatures (generally 90-120 °C) through an air gap. The fibres are then coagulated into a precipitation bath, washed and dried. Around 99% of the NMMO can be recovered from the precipitation and washing baths [140].

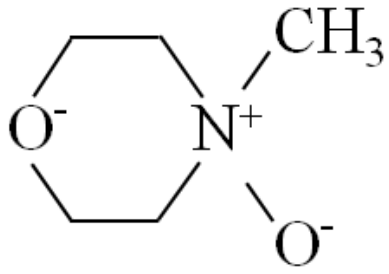

Figure 13: Structural formula of the NMMO molecule.

Lithium chloride/N,N-dimethylacetamide (LiCl/DMAc)

Another solvent for the preparation of ACCs is DMAc mixed with LiCl (Figure 14). Cellulose needs to undergo a so-called "activation procedure" during which the fibre is penetrated with a polar medium [141]. Without activation, it can take several months for the dissolution to proceed regardless of the crystallinity of the cellulose. Thus, even amorphous cellulose obtained by ball-milling proves difficult to dissolve in the absence of the activation procedure [142]. Interestingly, the activation step before the actual dissolution does not affect cellulose crystallinity [143].

There are two different ways to prepare the mixture: (I) the LiCl/DMAc solution is prepared first and then the cellulose is added, or (II) cellulose and DMAc are mixed together followed by addition of LiCl [144]. Stirring is also critically important for the

dissolution to proceed due to the heterogeneous fibre-solvent mixture. It has been reported that the solubility of cellulose increases with LiCl content [145].

Many studies on ACCs report the use of LiCl/DMAc [105, 106, 114, 118, 128, 129, 146-151], which may be due to its ability to completely dissolve high molecular mass cellulose [143]. In those studies a concentration of 8 mass% LiCl was used for the dissolution of cellulose.

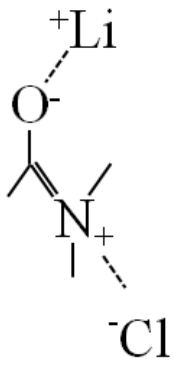

Figure 14: Structural formula of the LiCl/DMAc molecule.

Sodium Hydroxide (NaOH)

A more eco-friendly non-derivatising solvent for cellulose is based on NaOH [152] or aqueous NaOH solutions with additions of urea and/or thiourea used at sub ambient temperatures or other additives such as poly(ethylene glycol) (PEG) or zinc oxide [21, 153]. NaOH-urea-thiourea dissolution is a simple, safe process requiring minimal energy input. The addition of urea ($(NH_2)_2CO$) and/or thiourea ($(NH_2)_2CS$) to aqueous NaOH greatly enhances the dissolution, while NaOH can only partially dissolve celluloses of low DP [154-157]. The alkaline solvent is cooled to subzero temperatures. Once the subzero temperature is attained, the mixture is often stirred under thawing, resulting in cellulose dissolution [154, 158]. The solution can be centrifuged to separate the undissolved portion from the truly dissolved cellulose [159, 160]. The dissolved cellulose is then

transformed into a gel by a thermal path, precipitated in an acidic medium or coagulated otherwise. Depending on the process, different microstructures can be obtained [161]. Coagulation was used to produce cellulose membranes with varying pore geometries and mechanical properties according to the coagulant type, concentration and coagulation time [162-164]. NaOH-urea and NaOH-thiourea can also be used to process the cellulose into textile fibres with mechanical properties close to commercially-available rayon fibre [154, 155].

Ionic Liquids (ILs)

In 1934, Charles Graenacher was the first to discover an IL solvent system for cellulose, but this was thought to be of little practical value at the time [135]. Much more recently the use of ILs as a solvent for cellulose has been reported by Swatloski *et al.* [130]. Ionic liquids are molten salts with melting points below 100 °C. There is a wide range of possible cations (e.g. Alkylimidazolium ($[R1R2IM]^+$), Tetraalkylammonium ($[NR_4]^+$) and Tetraalkylphosphonium ($[PR_4]^+$) and anions (e.g. Hexafluorophosphate ($[PF_6]^-$), nitrate ($[NO_3]$-) or chloride, bromide and iodide salts [165]. Only some of them are able to dissolve cellulose, but the number of possible ion combinations is said to be as high as one trillion which leaves much scope for the development of new types of cellulose solvents [166]. Their ability to dissolve cellulose originates from their high effective polarity, due to their ionic character. The most successful ILs in cellulose dissolution reported so far, are hydrophilic and consist of the cations methylimidazoloium and methylpyridinium cores with allyl-, ethyl- or butyl side chains with chloride, acetate or formate anions [167, 168]. Recently, Pinkert *et al.* provided a detailed review of cellulose dissolution by ionic liquids [169]. ILs combine all of the desirable characteristics of the previous solvents including low volatility, potential low cost due to ease of recycling, capacity for rapid and

complete dissolution of a broad range of cellulose sources and with no requirement for pre-treatment or activation. More information on cellulose dissolution in an ionic liquid will be provided in Chapter III.

3.1.2.3 Influence of Cellulose Sources on Dissolution Behaviour

Various cellulosic materials including wood pulps, ramie, sisal and regenerated cellulose fibres, microcrystalline cellulose powder, bacterial cellulose and filter paper have been used to process ACCs (Table 4). The time required for cellulose dissolution depends strongly on the fibre structure, especially the degree of orientation and crystallinity in the outer part of the fibre. Thus, the dissolution conditions need to be tailored to different sources of cellulose for the processing of ACCs. Soykeabkaew *et al.* compared immersion times necessary to form a matrix phase of highly-orientated cellulose structures present in Bocell fibres to less ordered cellulose configurations in the outer regions of Lyocell fibres. They reported that the Bocell fibres needed more than one hour immersion time in LiCl/DMAc to form a matrix phase while for the Lyocell fibres less than 20 min were sufficient. Longer immersion times also lead to a reduction in fibre diameter as the fibre surface dissolution increases [105, 106].

3.1.2.4 Cellulose Regeneration

The steps involved in the regeneration of the dissolved cellulose are (I) removal of the solvent by a coagulant (water, alcohol or acetone are commonly used) and then (II) removal of the coagulant through evaporative drying. Cellulose regeneration is an important step in the processing of ACCs as it controls the precipitation of the final cellulose phases. Duchemin *et al.* suggested that the regeneration rate controls the phase composition, which in turn will dictate the physical properties of the ACC. Cellulose

phases of higher crystallinity are observed as the rate of regeneration is decreased. This is thought to be due to the cellulose chains in solution having greater time to order themselves into a lower energy configuration. Thus, the rate of application of the coagulant for removal of the solvent and then subsequent drying rate can be manipulated to given varying properties in the final ACC [127].

Contact of the coagulant with the cellulose will lead to swelling, especially if water is used. Distortion of the sample due to warping is even more apparent in thicker samples as a diffusion gradient of the coagulant from the surface to the interior of the solution results in differential shrinkage and subsequent delamination and void formation. Furthermore, the dissolved and undissolved portions of cellulose will swell by different amounts which upon regeneration again can cause differential shrinkage during regeneration, leading to the formation of voids at the fibre-matrix interface [127].

3.1.3 Phase Characterisation

Identification and characterisation of cellulose phases present in ACCs has been mainly carried out with wide-angle X-ray scattering (WAXS) [105, 118, 128, 129, 147, 167] and to a lesser extent solid state nuclear magnetic resonance (NMR) [170].

The treatment of cellulose with LiCl/DMAc leads to a decrease in crystallinity depending on the immersion time. Longer dissolution times lead to a reduction of cellulose I crystallites resulting in a change of crystallinity after regeneration of the cellulose. Nishino *et al.* [118, 129] and Soykeabkaew *et al.* [105] reported that after dissolution with LiCl/DMAc the regenerated phase was non-crystalline or amorphous based on WAXS. On the contrary, Duchemin *et al.* [170] obtained results from WAXS and NMR that suggest that exposure of crystalline cellulose to LiCl/DMAc results in peeling away of thin layers

from the original crystallites which retain some molecular ordering. After solvent removal, these thin layers can form a paracrystalline phase that is distinct from typical amorphous cellulose and closer in structure to cellulose I. They also suggested that the presence of a paracrystalline matrix phase is one of the underlying reasons for the high mechanical properties of ACCs. Zhao *et al.* observed that dissolution of cellulose I using the IL BmimCl results in a matrix phase consisting of cellulose II [167]. Gindl and Keckes also identify the regenerated phase of dissolved cellulose I as cellulose II [128].

3.1.4 Mechanical Properties

The mechanical properties of anisotropic composites strongly depend on the dissolution and regeneration conditions. The longitudinal tensile strength decreases with increasing dissolution time due to a decreasing cross-sectional area of the load-bearing cellulose fibres and therefore a reduction in fibre volume fraction. The transverse tensile strength follows an opposite trend as the matrix phase increased and the interface becomes more homogenous. Soykeabkaew *et al*. [105] reported that assumption based on their experiments with unidirectional ramie fibre composites. An immersion time in LiCl/DMAc of 12 hr lead to a decrease in longitudinal tensile strength of about 60 % compared to an immersion time of 6 hr. Simultaneously, the transversal tensile strength is increased by about 33 %. However, there are very few publications stating transversal strength and stiffness of unidirectional composites to verify this assumption. Extending the dissolution time can lead to over-dissolution of the fibres, resulting in a rapid decrease in tensile properties for either isotropic or anisotropic ACCs [118, 151]. The application of the solvent can also affect the composition of the reinforcing fibres. Gindl *et al.* observed that the hardness of the fibres changes when treated with LiCl/DMAc, presumably due to partial dissolution of cellulose within the cell walls [148].

The inherent properties of the reinforcement will also affect the properties and processing of ACCs. Many different combinations of fibre, matrix and solvent systems have been studied in the literature, giving a large range of properties for ACCs. Table 4 lists the tensile properties of ACCs made using different materials and solvents, demonstrating the large variability possible with formulation and processing. Thus, judging and comparing the influence of various parameters and properties between different studies of ACCs is difficult. However, it is of interest to compare the family of ACCs with other biocomposites. In general, the tensile strength of ACCs is significantly higher compared with the more traditional isotropic and unidirectional biocomposites (Figure 16, Figure 17, Table 4 and Table 5).

Interestingly, a comparison of unidirectional ACCs with traditional biocomposites does not reveal dramatic differences in the Young's modulus. The underlying reasons may be complex given the variable formulations but may be due to either (I) the cellulose solvent decreasing the modulus of the reinforcing fibres in ACCs or (II) the modulus of biocomposites being dominated by the modulus of the fibres, with the fibre-matrix interfacial strength being less important. In contrast, significant increases in modulus are observed for isotropic ACCs compared with traditional biocomposites in which it could be envisaged that the strong matrix properties of ACCs dominate this behaviour.

The strain to failure of ACCs (ε_{fACC}) is largely dominated by the type of reinforcement used. For example, ACCs reinforced with low strain ramie fibre (ε_f = 1.2-3.8 %, [38]), show lower values of ε_{fACC} (3.7-4.8 %) when compared with reinforcement made from high strain Lyocell fibre (ε_f = 9.4-27.9 %, [106]) resulting in a higher ε_{fACC} (10-24%) (Table 4). However, ACCs based on hemp fibre reported by Quajai *et al.* [171] achieved values of 20

% for ε_{fACC}. This is unexpected as ε_f of hemp fibres is only 1.6 % [38], yet was not commented on by the authors. In fact, this last example emphasises the difficulty in comparing different ACCs in the literature due to differences in processing that can greatly influence the final properties.

Other chemical or mechanical processing steps have been used to influence ACC properties (Table 4). The positive effect of a "mercerization" on lignocellulosic fibres, namely an improvement of tensile properties and absorption characteristics, is well known [172, 173]. When applied to the ACCs, a non-reversible swelling of the fibres occurs that fills in voids and cracks significantly improving the interface and, therefore, the tensile properties of the composite. SEM pictures of an untreated (a) and mercerized (b) composite can be seen in Figure 15 [151].

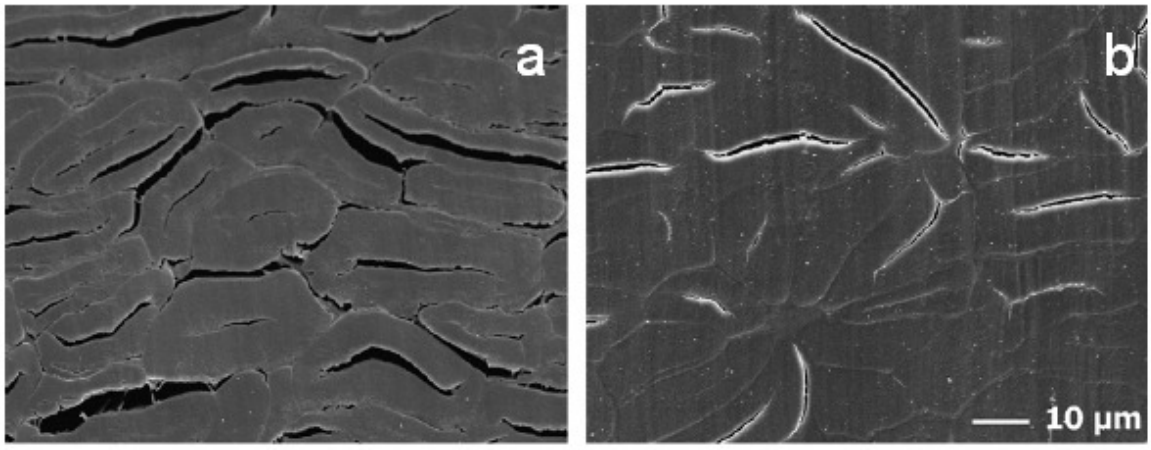

Figure 15: SEM pictures of ramie fibre reinforced cellulose composite made with 4 % cellulose concentration solution in an untreated (a) and mercerized (b) state. Reprinted from [151].

Furthermore, Gindl *et al*. reported that wet drawing of the composites after regeneration of the dissolved cellulose could change the orientation of the cellulose crystals within the composite towards a unidirectional direction according to the direction of the applied load. The wet state changes the molecule mobility as the water

adsorption weakens the inter- and intramolecular hydrogen bonds. By drawing the composites, the crystal orientation changes linearly with the draw ratio (the ratio between specimen length after and before stretching) whereas the overall crystallinity of the composite stays unaffected. Drying the samples afterwards causes the molecule chains to keep their positions resulting in anisotropy of the specimens with an improved tensile strength in longitudinal direction [146, 147].

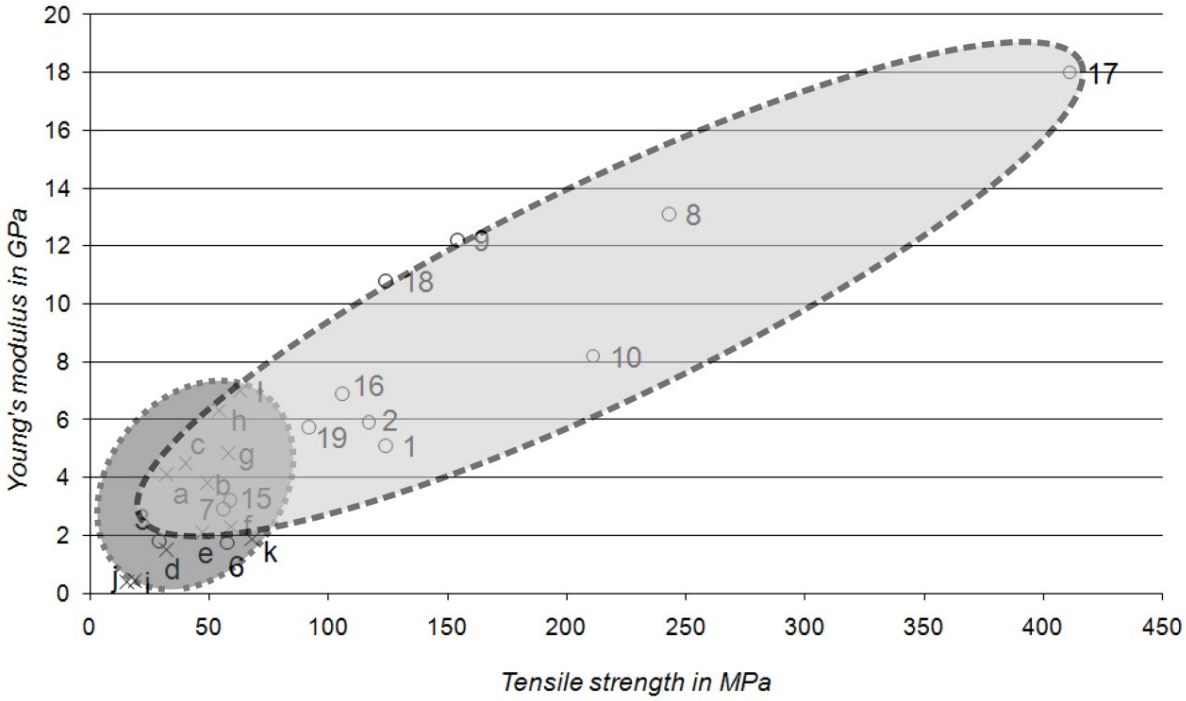

Figure 16: Ranges of tensile strengths and Young's moduli of isotropic ACCs (dashed line) compared with traditional isotropic biocomposites (dotted line). The numbers and letters of the references are found in Table 4 and Table 5, respectively.

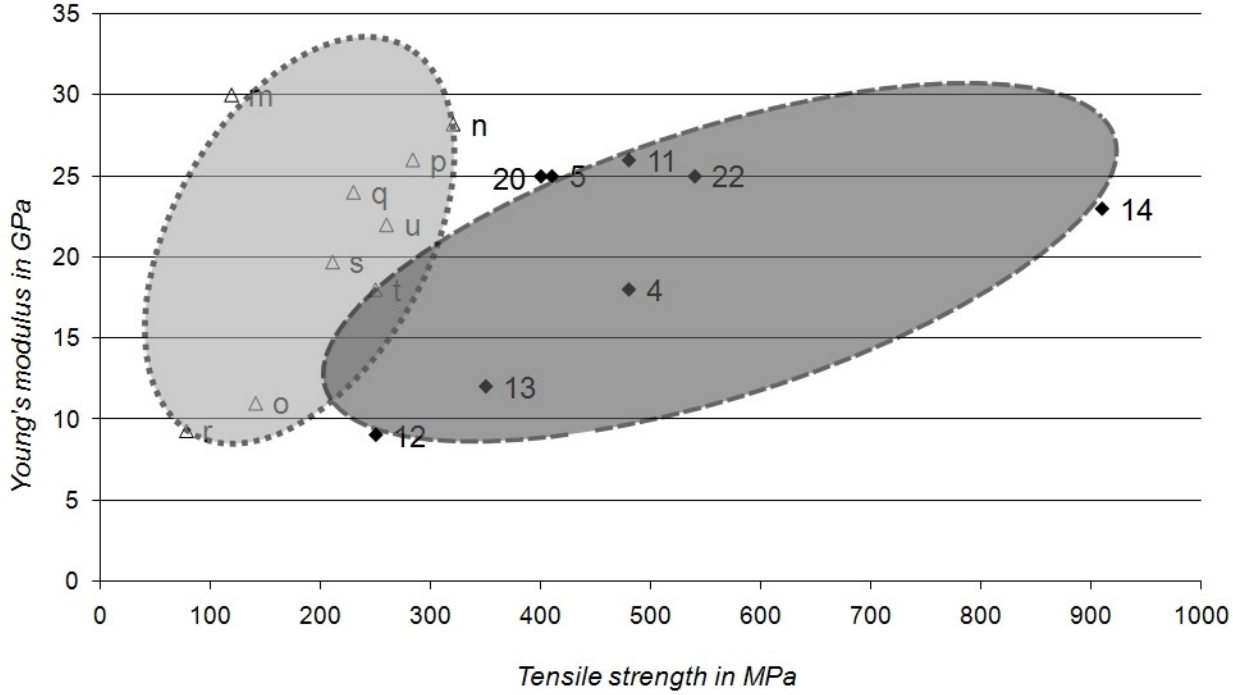

Figure 17: Ranges of tensile strengths and Young's moduli of unidirectional ACCs (dashed line) compared with traditional unidirectional biocomposites (dotted line). The numbers and letters of the references are found in Table 4 and Table 5, respectively.

Table 4: Overview over isotropic (ISO) and unidirectional (UD) all-cellulose composites produced by one and two step processes and after additional fibre or composite treatment. Included are the types of cellulose source, reinforcement, solvent and fibre fraction used. Both Tensile properties parallel (↑) and transverse (→) to the fibre direction are given where available. MCC = microcrystalline cellulose, BC = bacterial cellulose, LDR = low draw ratio, HDR = high draw ratio.

Two Step Process											
No.	Cellulose source for matrix	Cellulose source for reinforcement	Solvent	Fibre volume fraction in %	Tensile strength ↑ in MPa	Tensile strength → in MPa	Young's modulus ↑ in GPa	Strain to failure ↑ in %	Strain to failure → in %	thickness in mm	Reference
1	Cotton linter pulps	Cellulose whiskers (ISO)	NaOH/urea	10	124	n.r.	5.1	n.r.	n.r.	0.04	Qi *et al*., 2009,[174]
2	Cotton linter pulps	Cellulose whiskers (ISO)	NaOH/urea	20	117	n.r.	5.9	n.r.	n.r.	0.04	Qi *et al*., 2009, [174]
3	Cellulose powder	Hemp fibre (ISO)	NMMO	40	28.9	n.r.	1.8	20.8	n.r.	0.2	Quajai & Shanks, 2009, [171]
4	Wood pulp	Ramie fibre (UD)	LiCl/DMAc	80	480	12	n.r.	4	5	1	Nishino *et al*., 2004, [118]

5	Ramie fibre	Ramie fibre (UD)	LiCl/DMAc	85	410	n.r.	25	4.8	n.r.	n.r.	Qin *et al.*, 2008, [175]
6	Filter paper	Rice husks (ISO)	Ionic liquid (BmimCl)	40	57.5	n.r.	1.74	5.67	n.r.	0.3	Zhao *et al.*, 2009, [167]
7	Filter paper	Rice husks (ISO)	Ionic liquid (BmimCl)	60	56	n.r.	2.92	2.76	n.r.	0.3	Zhao *et al.*, 2009, [167]
8	Cotton linter pulps	Ramie fibre (ISO)	NaOH/urea	20	108	n.r.	5.6	4	n.r.	0.3	Yang *et al.,* 2010, [176]
9	MCC	Cellulose nanowhiskers (ISO)	LiCl/DMAc	1	128.4	n.r.	4.8	3	n.r.	0.3	Pullawan *et al.,* 2010,[177]
10	MCC	Nano crystalline cellulose (ISO)	HemimCl	3.68	49.24	n.r.	3.96	2.11	n.r.	0.04	Ma *et al.,* 2010,[178]
One Step Process											

No.	Cellulose source for matrix and reinforce-ment	Reinforcement type	Solvent	Fibre volume fraction in %	Tensile strength ↑ in MPa	Tensile strength → in MPa	Young's modulus ↑ in GPa	Strain to failure ↑ in %	Strain to failure → in %	thicknes s in mm	Reference
11	MCC	(ISO)	LiCl/DMAc	n.r.	242.8	n.r.	13.1	8.6	n.r.	0.35	Gindl & Keckes, 2005, [128]
12	Beech pulp	(ISO)	LiCl/DMAc	80	154	n.r.	12.2	0.023	n.r.	1	Gindl *et al.*, 2006, [148]
13	Filter paper	(ISO)	LiCl/DMAc	16	211	n.r.	8.2	3.8	n.r.	0.2	Nishino & Arimoto, 2007, [129]
14	Ramie fibre	(UD)	LiCl/DMAc	85	480	29	26	3.7	4.5	n.r.	Soykeabkaew *et al.*, 2008, [105]
15	LDR-Lyocell fibre	(UD)	LiCl/DMAc	72	250	n.r.	9	24	n.r.	n.r.	Soykeabkaew *et al.*, 2009, [106]
16	HDR-Lyocell fibre	(UD)	LiCl/DMAc	73	350	n.r.	12	10	n.r.	n.r.	Soykeabkaew *et al.*, 2009, [106]

17	Bocell fibre	(UD)	LiCl/DMAc	88	910	n.r.	23	8.2	n.r.	n.r.	Soykeabkaew *et al.*, 2009, [106]
18	MCC	(ISO)	LiCl/DMAc	n.r.	58.7	n.r.	3.2	2.5	n.r.	0.2	Duchemin *et al.*, 2009, [127]
19	MCC	(ISO)	LiCl/DMAc	n.r.	105.7	n.r.	6.9	3.3	n.r.	0.2	Duchemin *et al.*, 2009, [127]
20	BC	(ISO)	LiCl/DMAc	n.r.	411	n.r.	18	4.3	n.r.	0.035	Soykeabkaew *et al.*, 2009, [179]
21	MCC	(ISO)	Ionic liquid (BmimCl)	n.r.	91.8	n.r.	5.75	3.76	n.r.	0.017	Duchemin *et al.*, 2009, [180]
22	Filter paper	(ISO)	Ionic liquid (BmimCl)	n.r.	124	n.r.	10.8	2	n.r.	0.017	Duchemin *et al.*, 2009, [180]
23	Cotton fibre	(ISO)	LiCl/DMAc	n.r.	144.9	n.r.	5.5	19.3	n.r.	n.r.	Arévalo *et al.*, 2010,

											[181]
24	Filter paper	(ISO)	PEG/NaOH	n.r.	74.7	n.r.	7.9	9.42	n.r.	0.2	Han & Yang, 2010, [182]
All-cellulose Composites Prepared with further Fibre or Composite Processing											
No.	Cellulose source for matrix	Cellulose source for reinforce-ment	Solvent	Additional processing step	Fibre volume fraction in %	Tensile strength ↑ in MPa	Tensile strength → in MPa	Young's modulus ↑ in GPa	Strain to failure ↑ in %	Strain to failure → in %	thickness in mm	Reference
25	Wood pulp	Ramie fibre (UD)	LiCl/DMAc	Immersing in water, acetone, DMAc	80	400	17	25	3	21	1	Nishino *et al*., 2004, [118]
26	MCC	(ISO)	LiCl/DMAc	wet drawing to align cellulose fibrils	n.r.	428	95	33.5	2.3	n.r.	0.11	Gindl & Keckes, 2006, [147]
27	Ramie fibre	Ramie fibre (UD)	LiCl/DMAc	mercerization	85	540	n.r.	25	4.8	n.r.	n.r.	Qin *et al*., 2008, [175]

Table 5: Overview over the tensile properties of different isotropic and unidirectional biocomposites.

Isotropic Composites						
Matrix	Fibre type	Fibre fraction in (vol % or mass%)	Tensile strength in MPa	Young's Modulus in GPa	Strain to failure in %	Reference
PBAT	Flax	30 (vol %)	32	4.1	2	Bodros *et al.*, 2007, [12], (a)
PBS	Flax	30 (vol %)	49	3.8	2.5	Bodros *et al.*, 2007, [12], (b)
PHB	Flax	30 (vol %)	40	4.5	1.8	Bodros *et al.*, 2007, [12],(c)
PLA	MCC	5 (mass%)	31.9	1.5	>100	Petersson & Oksman, 2006, [183], (d)
PLA	Cellulose whiskers	5 (mass%)	47	2.1	5.4	Mathew *et al.*, 2006, [184], (e)
PLA	Cellulose microfibres	5 (mass%)	59	2.3	3.3	Mathew *et al.*, 2006, [184], (f)
PLA	Rayon	40 (vol %)	57.97	4.85	n.r.	Bax & Müssig, 2008, [185], (g)
PLA	Flax	40 (vol %)	54.15	6.31	n.r.	Bax & Müssig, 2008, [185], (h)
PCL	Starch nano-crystals	50 (mass%)	15.5	0.384	5.0	Habibi & Dufresne, 2008, [21], (I)
PCL	Cellulose	50 (mass%)	18.7	0.442	8.6	Habibi & Dufresne,

	nano-crystals					2008,[21], (j)
Poly-ester	Banana	40 (vol %)	68	1.87	6	Sreekuma *et al.*, 2008, [186], (k)
PTP	Hemp	21 (mass%)	63	7	n.r.	Müssig *et al.*, 2006, [23], (l)
Unidirectional Composites						
Matrix	Fibre	Fibre fraction in (vol % or wt %)	Tensile strength in MPa	Young's Modulus in GPa	Strain to failure in %	Reference
Epoxy	Flax	50 (mass%)	119	30	n.r.	Bos, 2004, [25], (m)
PP	Flax	55 (vol %)	320.7	28.2	n.r.	Madsen & Liholt, 2003, [187], (n)
PP	Jute	21.2 (vol %)	141	11	n.r.	Khondker *et al.*, 2006, [188], (o)
Epoxy	Flax	49 (vol %)	284	26	n.r.	van de Weyenberg *et al.*, 2006, [189], (p)
PLA	Kenaf	70 (vol %)	230	24	n.r.	Ochi 2008, [190], (q)
Starch	Flax	60 (mass%)	78	9.3	n.r.	Romhany *et al.*, 2003, [67], (r)
Epoxy	Sisal	46 (vol %)	211	19.7	1.9	Oksman *et al.*, 2002, [28], (s)

3.1.5 Viscoelastic Properties of All Cellulose Composites

The viscoelastic properties of ACCs are determined by the viscoelastic properties of the cellulose chains and corresponding allomorphs. Amorphous cellulose exhibits a viscoelastic behaviour involving different molecular motions depending on temperature [191, 192]. Due to its high content of hydroxyl groups, hydrogen bonds are formed with neighbouring units of the same molecule, with neighbouring chains and any water that is present. Intra- and intermolecular hydrogen bonds are responsible for the thermal stability of the cellulose molecule. Intramolecular hydrogen bonds increase the stiffness of the polymer while the intermolecular hydrogen bonds and van der Waals interactions are responsible for single chains arranging into a 2D sheet [94]. The stable structure of the cellulose molecule is the result of a dense network of hydrogen bonds and their different bonding patterns within a single cellulose structure and their dependency on different temperatures [193].

At low temperatures, the molecular mobility is considered as localized at the molecular level, giving rise to secondary relaxations [194]. Two secondary relaxations of amorphous cellulose are reported, occasionally referred to as γ_{cell} and β_{cell} [195, 196]. The γ-relaxation is reported to appear at a constant temperature of -123 °C. It has been shown by the analysis of other polysaccharides such as dextran, that the γ-relaxation is mainly associated with a rotation of the CH_2OH groups of the cellulose molecule rather than the rotation of its OH groups [195]. The β_{cell} –relaxation is associated with cooperative but localized motion of segments of the main chain of the cellulose molecule depending on the water content [194]. The temperature range for the β_{cell} –relaxation was reported as -83.15 to 43.15 °C [195, 196]. At higher temperatures, cellulose exhibits three further transitions, designated α_1, α_2 and α_3 by Manabe *et al.* and measured for regenerated

cellulose [197]. The α_3 transition is very closely related to the water content and therefore not associated with the inherent molecular motion but with the cooperative motion of cellulose chain segments and absorbed water molecules. The α_2 transition can be separated into two distinct relaxations ($\alpha_{2,\ 1}$ and $\alpha_{2,\ 2}$) that are caused by micro-Brownian motions of amorphous chain segments [197-199]. The α_1 transition is associated with motions in the non-crystalline regions as the crystalline segments are constrained. However, as the α_1 transition also coincides with the onset chemical decomposition of the molecule due to the high temperature, it is possible that released chain segments from the crystalline regions also contribute to the relaxation [200, 201].

The viscoelastic properties of ACCs have been investigated using dynamic mechanical analysis (DMA) [105, 106, 112, 118, 129]. The storage modulus (E') of the composites formed with LiCl/DMAc as solvent system are reported to be higher than 20 GPa between temperatures of -150 and 0 °C. E' only gradually decreases with increasing temperature as a consequence of strong hydrogen bonding in cellulose I [105, 106, 129]. At temperatures above 250 °C, the cellulose composites start do degrade, resulting in severe drop in E'. The decrease in E' at higher temperatures than 250 °C of those composites goes in hand with the reported α_2 transition of regenerated cellulose.

3.1.6 Optical Properties of All Cellulose Composites

Optically transparent cellulose-containing composites based on bacterial cellulose, epoxy and acrylic resins have been produced; according to Nogi *et al*. [202] the optical transparency is due to the dimensions of the bacterial cellulose ribbons lying in the nanometre range. However, ACCs have also been observed to be optically transparent under certain conditions as first reported by Gindl *et al.* [128] and attributed to the lateral

dimension of the used microcrystalline crystals of 1-3.5 nm. ACC films based on the LiCl/DMAc solvent system show variations in optical transparency as a function of the dissolution time, with increased dissolution time resulting in greater transparency (Figure 18). As the dimensions of the used cellulosic materials in other studies exceed the nanometre range, the transparency of those ACCs has been attributed to the good adhesion between reinforcement and matrix phase and closure of internal pores in the cell wall [105, 129].

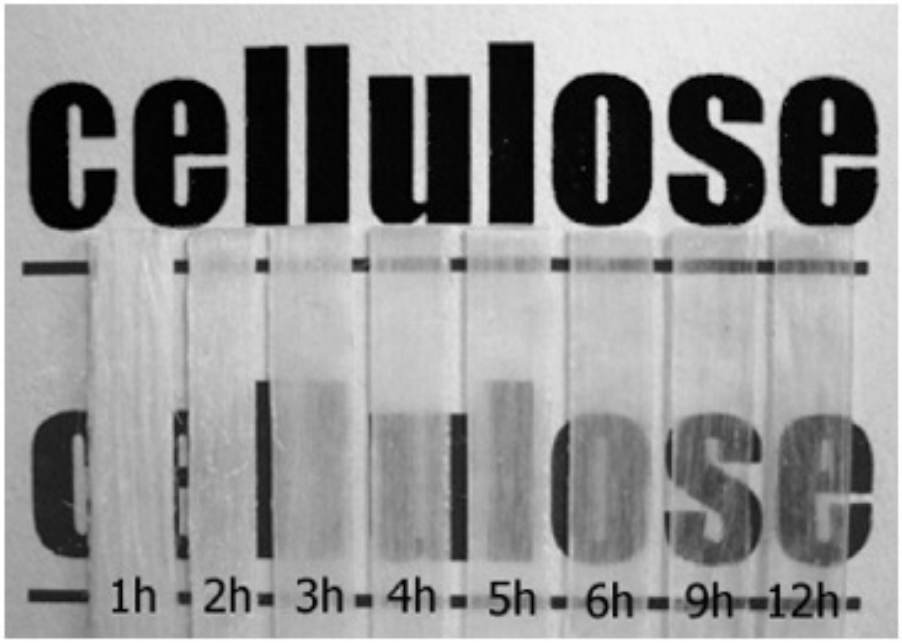

Figure 18: Optical transparency of ACCs as a function of dissolution time in DMAc/LiCl. Reprinted from [105].

3.2 COMPOSITES BASED ON CELLUOSE DERIVATIVES

3.2.1 Introduction

The field of derivatised cellulose, of which much is beyond the scope of this subchapter, has been reviewed elsewhere [203-208]. Thus, only three of the most recent approaches for the production of thermoplastic “all-plant fibre composites”, self-reinforced cellulose

composites and cellulosic nanocomposites via benzylation, oxypropylation and esterification, respectively are presented exemplarily.

3.2.2 Benzylated, Oxypropylated and Esterified Cellulose

3.2.2.1 Composite Processing

In the last decade, alternative approaches to form all-cellulosic structures using cellulose derivatives have been undertaken and these materials should be termed 'derivatised ACCs'. The first approach described involves the production of all-plant or all-wood fibre composites by a benzylation treatment of the cellulose source [209, 210]. This is based on a Williamson synthesis reaction involving nucleophilic substitution of an oxide or a phenoxide ion for a halide ion

$$\begin{aligned} &\text{Wood}-\text{OH}+\text{NaOH}\rightarrow\text{Wood}-\text{O}^{-}\text{Na}^{+}+\text{H}_2\text{O} \\ &\text{Wood}-\text{ONa}+\text{ClCH}_2-\text{C}_6\text{H}_6\rightarrow\text{Wood}-\text{O}-\text{CH}_2-\text{C}_6\text{H}_6+\text{NaCl} \end{aligned} \quad (1)$$

where, Wood-OH represents the hydroxyl groups mainly present in cellulose [211, 212]. The matrix material is swollen in NaOH and afterwards transferred to the benzyl chloride. The solution is stirred for several hours at temperatures above 100 °C. It is then washed to remove inorganic salts, benzyl chloride and its by-products to yield a liquid matrix phase consisting of the used cellulosic material. Due to the complexity of wood and its macromolecules, the extent of benzylation is measured indirectly by observing the mass gain as the modification proceeds. Benzylated fibres show the formation of a thermoplastic region surrounding the fibre core [211-214]. The composites can then be simply formed by hot-pressing [211-214]. Fibre volume fractions of up to 40% have been achieved using this method. Lu *et al.* reported that the rate of benzylation is hardly

affected by the wood source, but depends strongly on the amounts of NaOH and benzyl chloride ($C_6H_5CH_2Cl$) as well as the processing temperatures and reaction times [211-213, 215]. Increasing the degree of benzylation of cellulosic material leads to a decrease in crystallization due to a disruption of the hydrogen bonds within the cellulose molecules, reducing the final mechanical properties. This is explained by the larger benzyl molecule introducing a larger free volume and causing a change in the supramolecular structure of the molecule [211-213].

It has been shown that it is also possible to produce "all-plant fibre composites" by an oxypropylation treatment of cellulosic fibres as first reported by Gandini *et al.* in 2005. This is done by using a Brønsted base to activate the hydroxyl groups of the cellulose followed by an anionic polymerization of the propylene oxide (PO) in a "grafting from" process. The fibres are first immersed in a solution of ethanol and potassium hydroxide for several hours. After the alcohol has evaporated, the fibres are then mixed with PO under nitrogen atmosphere in an autoclave at temperatures of 130-150°C. The PO homopolymer created by chain-transfer reactions can be removed by a Soxhlet extraction using hexane. This effectively grafts a thermoplastic polymer matrix onto the outer surfaces of the fibres, with the amount measured indirectly by mass gain [216-218]. In this reaction, cellulose I is converted to an oxypropylated amorphous derivative. de Menezes *et al.* report that the amorphous regions of the cellulosic materials are more prone to modification than crystalline regions, while the degree of modification is dependent on the amount of PO used [217]. With increasing amounts of PO, the crystalline regions will also take part in the reaction although increased degradation of the cellulose structure and reduction in mechanical properties can occur. As for

benzylated cellulose, oxypropylated cellulose can be hot-pressed to form a composite film, with fibre fractions ranging from 10 vol. % to 40 vol. % [211-214, 216-218].

Matsumura *et al.* produced cellulose nanocomposites by partial esterification of wood pulp by a treatment with a p-toluene sulfonic/hexanoic anhydride system using a cyclohexane based reaction medium that caused no swelling of the cellulose fibres. To produce the composites, pulp fibres were exposed to a hexanoylation reaction to receive heterogeneously hexanoylated pulp fibres. The hexanoylation was assumed to start from both, the surface of individual microfibrils and unordered regions within the fibre followed by hexanoylation of the microfibril core. Those fibres were mixed with water or methanol and filtered afterwards to receive a uniform fibre mat in disc shape. The discs were compression moulded at both, 155-170 °C and at room temperature. The so produced thermoplastic composites of unmodified cellulose I and esterified cellulose were semitransparent [219, 220].

3.2.2.2 Mechanical Properties

The degree of benzylation is decisive for the composites' properties. A higher presence of benzyl groups is reported to increase the viscosity of the material. This can lead to insufficient wetting of the fibres and at a fibre volume share of 40 % the fibres are not completely surrounded by the matrix phase. These results in a weakened interface that reducing the flexural and tensile strength [212, 214]. An overview of the tensile properties of benzylated and oxypropylated ACCs is given in Table 6.

.

The thermomechanical and viscoelastic properties of benzylated ACCs have been analysed with thermomechanical analysis (TMA) [212, 213]. Benzylated ACCs exhibit thermoplastic behaviour due to the benzylated cellulosic material with a softening temperature in the range of about 90 °C to 120 °C depending on the source of cellulose and degree of benzylation. Lu *et al.* suggested that, as the plastification does not change the chemical backbone of the cellulose molecule chains, that softening should not be attributed to the α_1 transition of the cellulose but could rather be caused by inter-molecular slips [213].

Analogous, for oxypropylated cellulose, the amount of PO used is a determining factor for the tensile properties, as the use of higher amounts leads to a decrease in strength and stiffness but an increase in elongation to break. Those changes are likely to be caused by an increase of the thermoplastic amorphous phase [216].

For the esterified composites, the degree of substitution (DS) during the hexanoylation reaction is the decisive factor for the mechanical performance. Similar to oxypropylated cellulose, elongation increased with DS, while strength and stiffness decrease at highest tested DS of 2.0 [220].

Comparing the reported tensile properties of non-derivatised ACCs (Table 4) with those of benzylated, oxypropylated and esterified ACCs (Table 6) shows that the biggest differences seem to be in tensile strength. The strongest non-derivatised ACCs are about five to ten times stronger than their derivatised counterparts, while the Young's moduli and strain at failure are in a similar range. Based on the reported values of filter paper in Table 4 and Table 6 one can assume that the non-derivatised formation of the composite using LiCl/DMAc leads to better tensile properties than oxypropylation, but

without a comparative study the influence of processing on composite properties are not evaluable. Therefore the biggest difference seems to be the thermoformability of the derivatised ACCs.

Table 6: Overview of isotropic (ISO) and unidirectional (UD) ACCs based on cellulose derivatives produced by benzylation, oxypropylation and esterification. The cellulose sources, reinforcements, fibre volume fractions and tensile properties are shown.

Cellulose source	Reinforcement	Treatment	Fibre volume fraction in %	Tensile strength in MPa	Young's modulus in GPa	Strain at failure in %	Reference
Wood sawdust	Sisal fibre (UD)	benzylation	30	90	15	4.8	Lu *et al.*, 2002 [212]
Wood sawdust	sisal fibre (UD)	benzylation	40	68	20	4.2	Lu *et al.*, 2002 [212]
wood sawdust	sisal fibre (ISO)	benzylation	15	32	2.35	2.1	Zhang *et al.*, 2005 [214]
Sisal fibre	UD	benzylation	n.r.	43	3	n.r.	Lu *et al.* , 2003 [213]
Filter paper	ISO	oxypropylation	n.r.	18.7	1.18	2.7	de Menezes *et al.*, 2009 [216]
Filter paper	ISO	oxypropylation	n.r.	25.7	1.31	4.91	de Menezes *et al.*, 2009 [216]
Wood pulp	ISO	esterification	n.r.	25	0.8	6	Matsumura & Glasser, 2000 [219]
Wood pulp	ISO	esterification	n.r.	20	1.3	5	Matsumura & Glasser, 2000 [219]

3.3 CONCLUSIONS

Cellulose reinforced cellulosic structures have been reported decades ago and have found many applications. However, growing environmental awareness and increasing interest in sustainable material concepts have only recently led to the development of bio- and green composites for structural composite applications. The newly developed all-cellulose composites described above represent an approach to formulating green composites that aim to eliminate the chemical incompatibilities between reinforcement and matrix phases by utilising cellulose for both components and therefore an improvement in mechanical properties.

While the concept seems to be a promising approach and the reported results show attractive properties, more analysis from an engineering point of view is necessary to access the true potential of this new class of green composites. To attract a true interest from potential industrial partners, relevant parameters for the production of those composite have to be established. Those include adaptability to already existing composite processing techniques, a possibility to upscale the production volume, the potential to automate involved processes and quality control and management to name but a few.

As the scatter of the reported mechanical properties for ACCs is very high, a better understanding of the interaction of solvent and raw materials seems necessary to improve the predictability of the composites. Furthermore, it will be necessary to analyse the influence of moisture on the highly hydrophilic ACCs, to judge their economic potential.

4. RESEARCH OBJECTIVES

So far developed all-cellulose composites have indicated the great potential of this new class of green composites due to their improved interfacial adhesion and resulting impressive mechanical properties. However, certain points need to be addressed to further promote the development and application of all-cellulose composites.

Most processing of all-cellulose composites has been carried out using traditional cellulose solvents such as LiCl/DMAc, NMMO and NaOH-urea. Ionic liquids have been reported to be an excellent solvent for cellulosic materials but most reported scientific literature only describes the use of one ionic liquid, BmimCl, for the processing of all-cellulose composites. Therefore the first objective of this research work is to understand the dissolution behaviour of different cellulosic materials and their use for the processing of ACCs using a different ionic liquid, BmimAc that has been reported to be a potential good solvent for cellulose.

Cellulose is well known for its hydrophilicity, hence establishing a better understanding of the effects of moisture uptake and loss on ACCs and especially their microstructure, especially during composite processing, is the second research objective.

Up to this point all ACCs reported in literature have been in the form of thin films. Based on the findings of cellulose dissolution in the used IL the main research focus of this work will be to develop new or ideally adapt already existing composite processing routes for the development of "thick" (>1 mm) ACCs in complex shapes. While the application potential of ACCs has been indicated in the scientific literature this research objective

appears to be of high importance to truly enable ACCs to compete with other composite materials.

While some conclusions have been drawn on the fibre-matrix-bonding in ACCs, the scientific literature is missing a detailed analysis on the factors influencing the fibre-matrix interphase. Therefore, the produced composites will be analysed thoroughly regarding the connections of microstructure, fibre-matrix interface and the resulting mechanical properties. Furthermore, this work aims to improve the basic understanding of how ACCs could be used in real-life, everyday applications. Thus, other relevant aspects such as biodegradability and flammability will be analysed.

The use of three-dimensional textiles is a recent development in composite processing and no work has been carried on using cellulose fibres for producing those textiles. To complete the processing analysis, the feasibility of producing three-dimensional textile preforms for ACC processing and their effect on the composite properties will be analysed.

II. MATERIALS AND EXPERIMENTAL PROCEDURES

Materials and experimental methods used throughout all experimental procedures will be described in detail in this chapter. Materials and experimental methods specific to individual chapters will be presented in the corresponding chapter.

1. MATERIALS

The used ionic liquid is 1-Butyl-3-methylimidazolium acetate (BASIONIC BC 02) purchased from Sigma-Aldrich (St. Louis, MO, USA). The IL is dried in a vacuum oven at 80 ˚C (Binder VD 23, Binder GmbH, Tutlingen, Germany) for 5 days to remove the absorbed moisture before processing.

The used rayon fibre was supplied by Cordenka GmbH (Obernburg, Germany) in the form of a Cordenka 700 yarn. The yarn count was given as 1000 and the fibre diameter was 12 µm. The degree of polymerisation of the cellulose was not supplied but the DP of viscose rayon fibres generally ranges from 300-1200 [35]. A single fibre of the rayon fibre is reported to have a tensile strength of 830 MPa, a Young's modulus of 20 GPa and a strain to failure of 13 % [221]. A technical rayon textile made from the Cordenka 700 yarn was also provided by Cordenka GmbH (Obernburg, Germany) in the form of a K2/2 twill weave (surface mass of 450 g/m^2).

Microcrystalline cellulose (MCC) was purchased from Merck Chemicals (Darmstadt, Germany). The average degree of polymerisation of the MCC was 150-250 and the crystallinity was 70-80 %. The particle size and distribution of the MCC was given as <20 µm ≤ 20 %, 20-160 µm ≥ 80 % and >160 µm ≤ 2 %.

All cellulose materials were dried for at least 48 h in a vacuum oven at 80 ˚C before processing.

Ethanol was (97 % purity) was purchased from Thermo Fisher (Waltham, MA, USA) and was used without further treatment.

Dimethylsulfoxide (DMSO) was purchased from Sigma Aldrich and used as received.

2. EXPERIMENTAL PROCEDURES

2.1 MICROSCOPY

2.1.1 Sample Preparation for Microscopy

To examine the cross-section of different untested samples they were mounted Epofix cold-setting embedding resin (Electron Microscopy Sciences, Hatfield, PA, USA) and polished according to ASTM E3 [222] to a final grain size of 1 μm. The mounted samples were grinded using a Buehler Phoenix-Beta grinder-polisher (Illinois Tool Work Inc., Lake Bluff, IL, USA) with Buehler Carbi-Met2 silicon carbide taps with the ANSI/CAMI grit numbers 180, 240, 320, 400 and 600 used in consecutive order. The sample was grinded for about 60 s per grit number. Tap water was used as a lubricant. The rotational speed of the grinding disc was 250-300 rpm.

The grinded sample was then polished using the Buehler Phoenix-Beta grinder-polisher with Buehler trident polishing cloth PLA 8" polishing pads. Buehler MetaDi polycrystalline diamond suspension with particles sizes of 9, 3 and 1 μm were used as a polishing agent. The sample was polished for 60-90 s per polishing step. The rotational speed of the polishing disc was 300-350 rpm. The sample surface was cleaned using an industrial detergent and tap water between each polishing step. After the final polishing

step, the sample was cleaned in a Cole-Parmer 8853 ultrasonic bath (Cole-Parmer, Vernon Hills, IL, USA) for 20 min and dried at atmospheric conditions afterwards.

2.1.2 Optical Microscopy

Optical microscopy was carried out using an Olympus U-PMTVC stereo microscope (Olympus Corp., Tokyo, Japan). Images were recorded using a SPOT Insight QE digital camera (SPOT Imaging solutions, Sterling Heights, MI, USA).

Reflected light microscopy was also performed using a Leica DR IRM microscope (Leica, Wetzlar, Germany). Micrographs of the cross-section were taken using a NIKON Digital Sight DS-Fi1 camera (Nikon Imaging Japan Inc., Tokyo, Japan) with the software NIKON NIS Elements F 3.2 (Nikon Imaging Japan Inc., Tokyo, Japan).

Samples were conditioned at room temperature (23 ± 1 ˚C) and 50% RH before optical analysis.

2.1.3 Field Emission Scanning Electron Microscopy

Field emission scanning electron microscopy (FE-SEM) was performed with a JEOL 7000F FE-SEM (JEOL Ltd, Tokyo, Japan) with a probe current of 7 mA. The used acceleration voltage ranged from 5 to 15 kV. Specific values are stated in the micrograph captions. Samples for FE-SEM were gold-coated for 120-180 s at 25 mA using an Emitech K975X coater (Quorum Technologies Ltd, East Grinstead, United Kingdom).

2.2 MASS CHANGES

Sample mass changes were recorded using a Mettler Toledo XP Analytical balance, (Mettler-Toledo Inc., Columbus, OH, USA, accuracy 0.001 mg).

2.3 TENSILE TESTING

If not stated otherwise, all tensile testing was carried out on an MTS858 Table Top System (MTS, Eden Prairie, MN, USA) using a 2.5 kN load cell in displacement control with a crosshead speed of 2 mm/min. The used gauge lengths were 40 and 60 mm. Pneumatically-controlled grips with an applied pressure of 0.3-0.4 MPa were used to hold the sample. Load and displacement were recorded until specimen failure using the MTS Testware software MTS 793. Displacement measurements were taken by measuring the cross-head displacement. Before testing, the sample dimensions were accurately measured using a Fowler Pro-Max digital vernier calliper (Fred V. Fowler Co., Inc., Newton, MA, USA).

2.4 FLEXURAL TESTING

3-point bending tests were conducted on a MTS 581 tabletop system with a 2.5 kN load cell according to ASTM D790 [223]. A crosshead speed of 2 mm/min was used. A span of 35 mm was used between the sample supports. Before testing, the sample dimensions were accurately measured using a Fowler Pro-Max digital vernier calliper.

2.5 HOT PRESSING

A hot press (Gibitre Instruments, Bergamo, Italy) was used for processing ACCs at elevated temperatures and pressures.

III. CELLULOSE DISSOLUTION IN AN IONIC LIQUID

1. INTRODUCTION

1.1 IONIC LIQUIDS

Ionic liquids (ILs) are loosely defined as liquid forming salts at temperatures lower than the boiling point of water. If the salt is liquid at room temperature the term "room temperature ionic liquid" (RTIL) is often used to make a distinction. Other terms for ionic liquids include molten salts, ionic fluids or liquid organic salts [166].

Generally, large cations are combined with small anions. The most common cations and anions used for ionic liquids for cellulose dissolutions can be seen in Figure 19. However, up to a trillion combinations are said to be possible, making ILs are very versatile group of materials and allowing the synthesis of task-specific ILs [224].

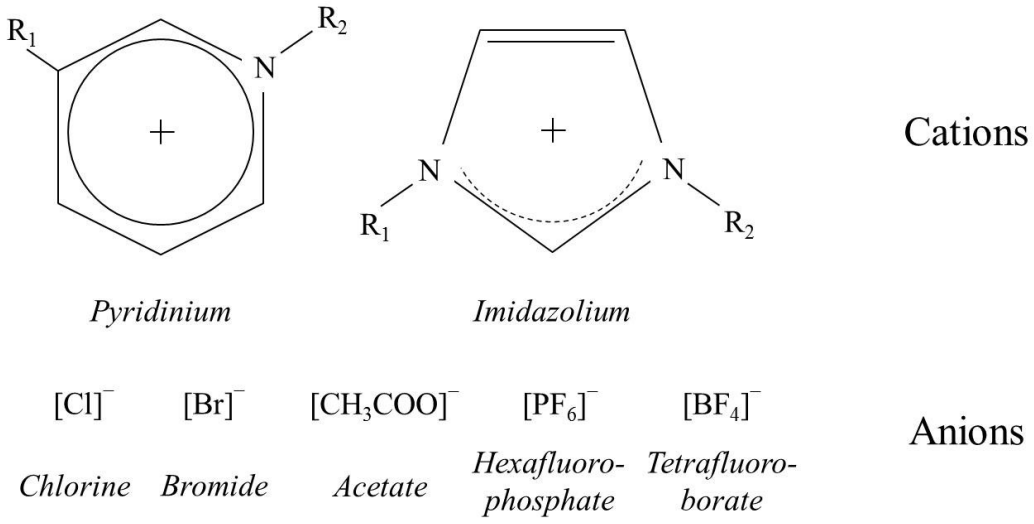

Figure 19: Typical cations and anions used for ionic liquids for cellulose dissolution.

ILs have attracted the interest of many research groups due to their assigned qualities of chemical and thermal stability, high conductivity, non-flammability, the ability to dissolve organic and inorganic compounds, combined with a very low vapour pressure,

often identified as negligible [166, 224]. Ils have been identified as “green(er) solvents” due to the lack of volatility and resultant easier handling compared to other solvents. However, recent studies on toxicity contradict that green image and in fact some ILs have been identified to be an environmental hazard [225, 226].

A major drawback of ionic liquids is their high price compared to other organic solvents. However, recently, it was suggested that the costs of ILs will decrease in the future, due to higher production levels, making ILs economically competitive with other solvents [227].

The recyclability of ILs is a much discussed topic in the research community due to their relatively high cost. The removal of contaminants by distillation is facilitated by low vapour pressure of ILs, suggesting a strong potential for recycling [228] [229]. However, such a broad sweeping assumption regarding the recyclability of ILs is not valid since the recovery rate is found to vary significantly across different ILs [230].

In addition to distillation, extraction with supercritical carbon dioxide or membrane-technology have been analysed as potential recycling path ways, with varying success depending on the exact method and used ILs [231].

Several ionic liquids have successfully been used to dissolve cellulosic materials and to produce all-cellulose composites [169]. The “green” characteristics bestowed upon ILs should contribute to the overall image of green and sustainable composites. Although cellulose dissolution *via* ionic liquids appears promising, a greater understanding of the processing parameters that affect the dissolution process is necessary from an industrial point of view.

1.2 CELLULOSE DISSOLUTION

1.2.1 Introduction

Interestingly, the ability of certain ionic liquids to dissolve cellulosic material has been reported as early as 1934 by Charles Graenacher [135]. However, his idea generated little interest until 2002, when Swatloski *et al.* reported the ability of several cation and anion combinations to dissolve cellulose at elevated temperatures in the range of 70 to 100 °C. The IL utilised was a methyl-imidazolium cation with variation in the alkyl-substituent, and in combination with the anions Cl^-, Br^- and thyocynate (SCN). The most successful combination was Butyl-imidazolium chloride (BmimCl) that was observed to dissolve up 25 mass% of cellulose when heated to 100 °C by microwave irradiation, resulting in a clear, highly viscous solution [130].

The dissolution reaction is primarily based on the breaking of the intermolecular hydrogen bonds. The reacting parts of the cellulose molecule are the oxygen and hydrogen atoms of cellulose-OH. The cellulose atoms are the electron pair donors, while the hydrogen atoms act as electron acceptors. The cation and anion in the IL act as the electron acceptor and donor, respectively. A close local proximity of the cellulose and IL is necessary for the reaction to take place. The cellulose chains become separated by the reaction and the cellulose is then in solution [232]. It was reported that dissolved and regenerated cellulose exhibit almost the same degree of polymerisation, indicating that the dissolution reaction mainly attacks the intermolecular rather than intramolecular hydrogen bonds of the cellulose [233]. A schematic of the process can be seen in Figure 20.

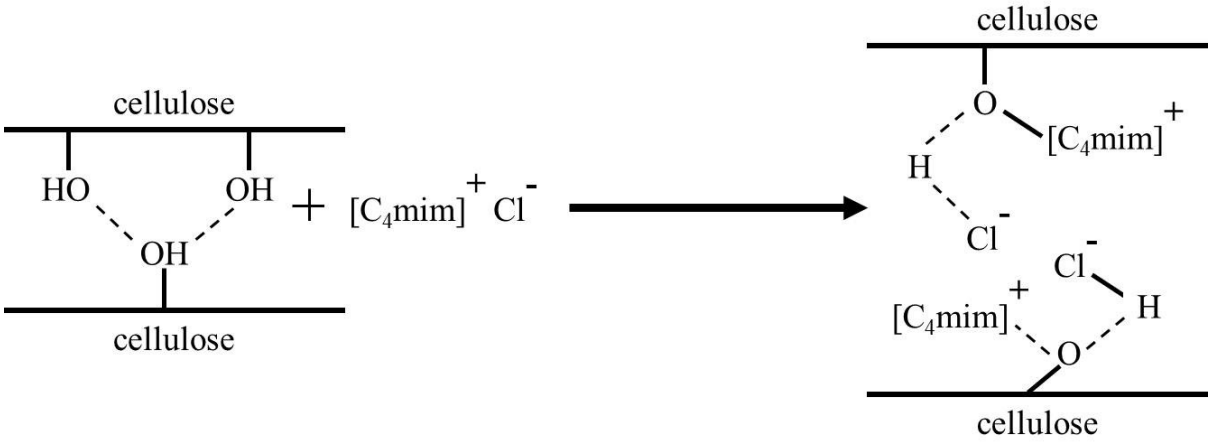

Figure 20: The reaction between an ionic liquid and cellulose, exemplarily shown for BmimCl. Redrawn from [232].

The detailed interaction of cation and anion with the cellulose molecule has not been completely elucidated. Although many researchers agree that the anion plays a major role in the dissolution reaction, the cation is still considered important [234]. For instance, it has been reported that the length of the alkyl chain in the alkyl-imidazolium cation is related to the dissolution capacity. Even numbered alkyl chains lead to more efficient cellulose dissolution than odd numbered chains [234].

While BmimCl has been successfully tested to dissolve comparatively high amounts of cellulose, BmimCl has a relatively high melting point of ~65 °C and high viscosity, leading several research groups to investigate alternative anions. Advantageous alternatives to BmimCl are Ethyl-imidazolium acetate (EmimAc) and Butyl-imidazolium acetate (BmimAc) that both exhibit lower viscosities than BmimCl [235]. Furthermore the acetate anion is less corrosive than the chlorine anion [236].

The cellulose-IL solution is brought into contact with a coagulant such as water, alcohol or acetone to regenerate the dissolved cellulose. Extended immersion in the coagulant is necessary to completely wash the ionic liquid from the newly regenerated cellulose,

resulting in a completely transparent cellulose gel in the case of complete dissolution [169, 237].

Cellulose solutions based on ionic liquids have been used for the formation of cellulose fibres [235, 238-240] and to a lesser extent for the manufacturing of all-cellulose composites [167, 180, 241] and cellulose aerogels [242-244].

1.2.2 Factors Affecting the Dissolution

Temperature, viscosity and water content have been identified as having a major influence on the cellulose dissolution capacity of an IL.

1.2.2.1 Temperature

As expected, the dissolution temperature is of major importance to the dissolution kinetics of ILs. Swatloski *et al.* reported no visible change in cellulose structure when mixed with different ILs at ambient temperatures and it was observed that cellulose dissolution required temperatures of around 100 °C and above [130]. However, degradation processes were reported for certain ionic liquids and high cellulose concentrations at temperatures of 140 and 160 °C, when using microwave heating [245]. Although detailed studies on the correlation between cellulose dissolution and temperature have not been performed, it is clear there are minimum and maximum temperatures for optimising the dissolution reaction. Most investigations on the dissolution of cellulose in different ionic liquids have been carried out in a rather narrow window of 90 to 130 °C [169].

1.2.2.2 Viscosity

The viscosity of the IL and of the cellulose-IL solution also influences cellulose dissolution kinetics. Most ionic liquids have viscosities comparable to oil, being two or three orders of magnitude higher than of many other solvents [246]. Ils are reported to behave as Newtonian fluids and it is known that their viscosity decreases with increasing temperature [245]. However, with increasing cellulose content the cellulose-IL solution becomes increasingly viscous [130]. This might be expected to lead to a reduction in the dissolution capacity since a high viscosity will hinder the diffusion of the ionic liquid into the cellulose.

Gericke *et al.* demonstrated that the intrinsic viscosity decreases with an increase in temperature for solutions of cellulose in BmimCl and EmimAc. The authors explained this by a decrease of the solvents' thermodynamic quality. The dependency of the viscosity on the cellulose concentration varies within two distinct linear regimes. At low cellulose concentrations the relationship between viscosity and concentration was described by a power law $\eta \sim c^n$, above which is then termed the overlap concentration *C*,* meaning the point at which the slope of the linear regimes changes from one to another. This dependency was found for different types of cellulose and at different temperatures. A schematic representation showing the two regimes of the viscosity-concentration dependency is given in Figure 21 [247].

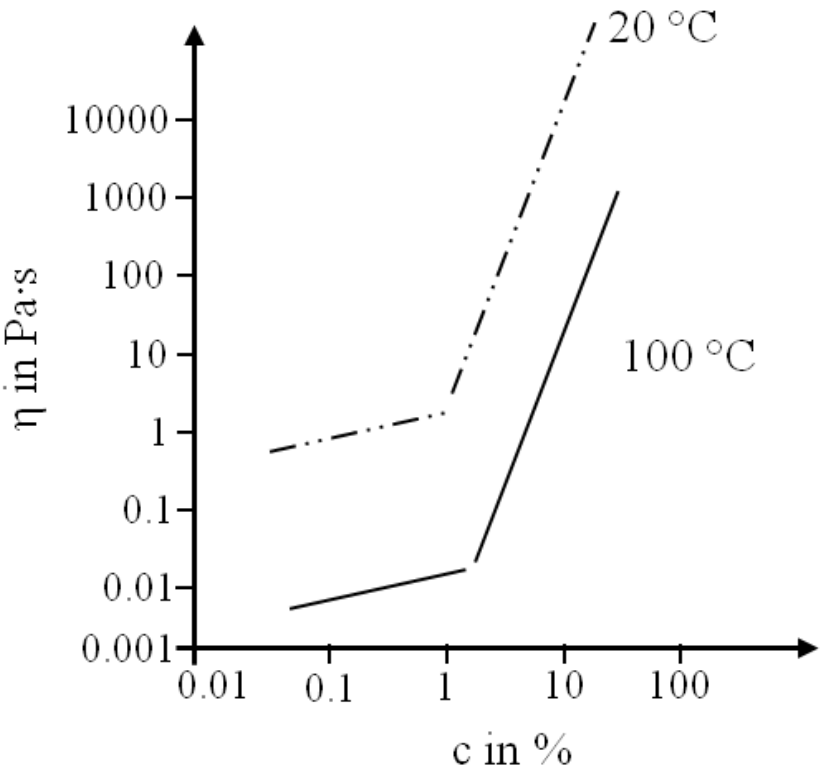

Figure 21: Viscosity (η) as a function of cellulose concentration (c) for a cellulose-EmimAc solution at two different temperatures. Schematic of the data presented by Gericke *et al.* [247].

1.2.2.3 Water Content

Water has been identified as a problematic impurity in ILs. Even in dried state the water content in BmimCl was found to be 2200 ppm by Karl-Fischer titration and even so-called hydrophobic ILs can absorb up to 1 mass% of water in 3 hr [248]. The water content of an IL seems to depend strongly on the available anions [245]. Cammarata *et al.* showed that water molecules absorbed from the atmosphere mainly exist in a free state (*i.e.* not self-associated) state in 1-Alkyl imidazolium based ILs with different anions. They are bound *via* hydrogen-bonding in symmetric 1:2 type hydrogen bond complexes in the form of anion-HOH-anion [249]. The water content also has an influence on the viscosity of the IL [245].

The presence of water has been found to greatly decrease the cellulose dissolution capacity of hydrophilic ILs [130]. The influence of hygroscopy of the IL on cellulose dissolution was studied for 12 different ILs at elevated temperatures by Mazza *et al.* but only BmimCl and Dimethylimidazolium dimethylphosphate (DmimDMP) were found to be able to dissolve cellulose at all in their experiments. Similarly, Swatloski *et al.* observed that increasing the water content in an IL decreases the solvency for cellulose up to 1 mass%, above which no cellulose could be dissolved [130, 245, 250]. DmimDMP was found to only be able to dissolve cellulose in a completely anhydrous state [250].

Clearly, an improved understanding of the aforementioned dissolution parameters of ILs is required in order to be able to reproducibly apply the processing routes of ACCs (i.e. complete or partial dissolution as described in Section I.3) in an industrial setting.

In the present Chapter, the dissolution of microcrystalline cellulose and regenerated cellulose (rayon fibre) was examined in the IL BmimAc to gain insights into the relationship between cellulose content, viscosity and temperature on the complete dissolution of the cellulose. In addition, the dissolution of rayon fibre yarn in the IL BmimAc was examined to elucidate the effect of dissolution temperature and the cellulose to IL ratio on the partial dissolution of the cellulose. This work examines these dissolution parameters with the goal of informing the pathway to the synthesis of ACCs with optimal mechanical properties.

The rheological properties of solutions of completely dissolved cellulose and IL will be determined to better understand the influence of temperature and cellulose concentration on the solution viscosity.

2. EXPERIMENTAL PROCEDURES

The dissolution behaviour of two different cellulose sources, cellulose I in the form of MCC and cellulose II in the form of a regenerated rayon fibre (Cordenka) will be analysed, to assess their potential as a starting material for the processing of ACCs. Rayon fibres exhibit lower mechanical properties compared to natural fibres (see Chapter I) and therefore do not seem to be the obvious choice for the development of ACCs. However, the fibres are consistent in quality and diameter and lend themselves as model materials for the development of processing routes for ACCs versus inconsistent chemical/surface properties of natural fibres.

The maximum amount of dissolvable cellulosic material in an ionic liquid was determined and the rheological properties of the cellulose solutions was analysed to gain more information on the processability of the cellulose sources.

Furthermore it will be assessed if a decrease in viscosity can improve the cellulose dissolution.

2.1 MATERIALS

The used IL, BmimAc is known to be strongly hydrophilic [251]. Therefore, the water content of the as-received IL was determined using Karl Fischer titration to be 416334.1 ppm using a 870 KF Titrino plus titrator (Methrom AG, Henrisau, Switzerland). The IL was dried in a vacuum oven at 80 ˚C for 5 days to remove the absorbed moisture, after which the water content reached a stable level of approximately 1620 ppm.

MCC was used in as-is state after drying. The rayon fibre was supplied as an endless, twisted filament, thus it was cut into short segments of approximately 1 mm and untwisted for the dissolution experiments.

The MCC and chopped rayon fibres were dried in a vacuum oven at 80 ˚C for 48 hr prior to use to remove any residual moisture.

2.2 CELLULOSE DISSOLUTION

2.2.1 Dissolution Capacity

20 g of BmimAc was heated using an oil bath starting at 20 ˚C and stirred using a magnetic hot plate stirrer (Henry Troemner LLC, Thorofare, NJ, USA). The IL was then mixed with 1 mass % of the dried MCC. The temperature was increased in an increment of 10 ˚C if complete dissolution was not achieved within 60 min until all of the cellulosic material was dissolved. The upper limit of temperature was restricted to 100 ˚C since higher temperatures led to discoloration of the solutions that indicated that thermal degradation of the cellulose solution was occurring. The viscosity of the cellulose-IL solution increases rapidly with increasing dissolved cellulose such that the solutions are too viscous to be mixed homogenously with a magnetic stirrer. As a result, the dissolution limits of MCC and rayon were determined by using an overhead stirrer (IKA Eurostar overhead stirrer, IKA Works GmbH & Co. KG, Staufen, Germany) to mix the cellulose in increments of 1 mass% into the BmimAc while maintaining a temperature of 100 ˚C. The experiments were stopped as soon as complete dissolution did not occur within 60 min. The last added and completely dissolved mass% was then assumed as the maximum of dissolvable cellulose.

The addition of co-solvents such as DMSO are known to reduce the viscosity of cellulose-IL solutions [252, 253]. Therefore in addition, 40 mass % of DMSO was combined with BmimAc in separate experiments to examine the effect of this solvent mixture on the solvency for MCC when compared with neat BmimAc.

2.2.2 Dissolution Behaviour

2.2.2.1 Optical Microscopy

Samples of cellulose-IL solutions were examined using the Olympus U-PMTVC microscope directly observe the extent of cellulose dissolution. Optical microscopy was also used to examine changes in fibre diameter of the rayon fibre during dissolution. Single rayon fibres were exposed to a droplet of BmimAc before being placed between two glass slides. Images of the fibres were recorded after 20 and 60 min at 70 ˚C using the SPOT Insight QE digital camera. The fibre diameter was measured using image analysis software (ImageJ, v 1.44j, Wayne Rasband, National Institutes of Health, Bethesda, MD, USA). 10 different rayon fibres were analysed for each dissolution time. 5 images were captured of each fibre and 5 diameter measurements taken from each image, giving a total of 250 measurements of the fibre diameter for each dissolution time.

2.2.2.2 Confocal Microscopy

The dissolution behaviour of the rayon multifilaments was also analysed using confocal microscopy. Short segments of the multifilament were stained using Congo Red dye. After staining, the filament segments were dried again for 24 hr at 80 ˚C.

The fibres were then soaked in IL and put in a heating stage (Linkam LTS120 heating stage, Linkam Scientific Industries, Guilford, UK) of a Leica TCS SP5 confocal microscope (Leica Microsystems, Wetzlar, Germany). Images were taken using the software LAS AF ExpressView v.1.0.1384 (Leica Microsystems, Wetzlar, Germany). The heating stage was used to heat the fibres and IL from room temperature up to 90 ˚C at 10 ˚C/minute. Images were taken at room temperature, 40, 50, 60, 70, 80 and 90 ˚C using a Leica HCPL FLUOTAR 10 x 0.3 objective with an attached digital camera. Two different light spectra were used for the confocal microscopy: 520-653 nm and 420-520 nm to detect red and green light, respectively.

2.2.2.3 Scanning Electron Microscopy

The influence of dissolution time and temperature on the rayon multifilaments were analysed by FE-SEM. The yarns were cut to a length of 150 mm and dried for 24 hr at 100 °C in a vacuum oven. The yarns were then impregnated with IL using an IL: cellulose mass ratio of 0.7: 0.3. The yarns were then placed on an aluminium plate (250 × 250 × 2 mm) and placed in an oven to partially dissolve the fibre surface. 15 yarns were dissolved for each of 60 min at 100 ˚C (experiment I), 30 min at 100 ˚C (experiment II) and 30 min at 125 ˚C (experiment III) to analyse the effect of dissolution time and temperature. The yarns were then washed in ethanol to regenerate the dissolved cellulose and remove the IL. Afterwards, the samples were dried in a vacuum oven at 50 ˚C for 24. Regeneration and drying were carried out while the yarns were secured to a steel plate with adhesive tape with no additional applied pressure.

The dried composite yarns were mounted as described in Section II.2.1.1 to obtain transverse cross-sectional images of the fibres. The mounted samples were gold-coated for 120 s.

2.3 RHEOLOGICAL MEASUREMENTS

Rheological measurements were conducted on the dried IL, a mixture of IL with 40 mass% of DMSO and solutions of 2, 6 and 10 mass% of dissolved MCC and Cordenka fibre. Cellulose-IL solutions were prepared by adding the desired mass % of cellulose to 20-21 g of IL. The IL was maintained at 100 ˚C using a hot plate stirrer and the cellulose-IL solutions were mixed using an overhead stirrer until complete dissolution was achieved. The solutions were then dried in a vacuum oven at 65 ˚C for 72 hr.

An Anton Paar Physica MCR 301 rheometer (Anton Paar GmbH, Graz, Austria), with parallel plate geometry (plate diameter 20 mm) was used for the rheology experiments. A Peltier Temperature Control System with a Peltier hood was used for heating and cooling (Peltier Systems, LLC, Athens, TX, USA). The rheometer was controlled using the software Rheoplus v3.40 by Anton Paar.

The gap between the parallel plates was set at 0.207 mm for all measurements. Oscillatory measurements were performed using a strain of 10 % over a frequency (ω) range of 0.5 to 500 rad/s. The shear storage modulus (G'), loss modulus (G'') and complex viscosity (η*) were recorded as a function of frequency and temperature. The measurements were performed at temperatures of 20, 40, 60, 80 and 100 ˚C.

3. RESULTS AND DISCUSSION

3.1 DISSOLUTION BEHAVIOUR OF MCC

Using the above described procedure, the maximum dissolvable amount of MCC in BmimAc was determined to be 20 mass%, making BmimAc a strong solvent for cellulose in comparison to other ionic liquids [169]. A dramatic increase in the viscosity was observed with an increasing concentration of cellulose that causes difficulties in achieving a homogenous mixture. Figure 22 shows maximum concentration of MCC fully dissolvable as a function of temperature.

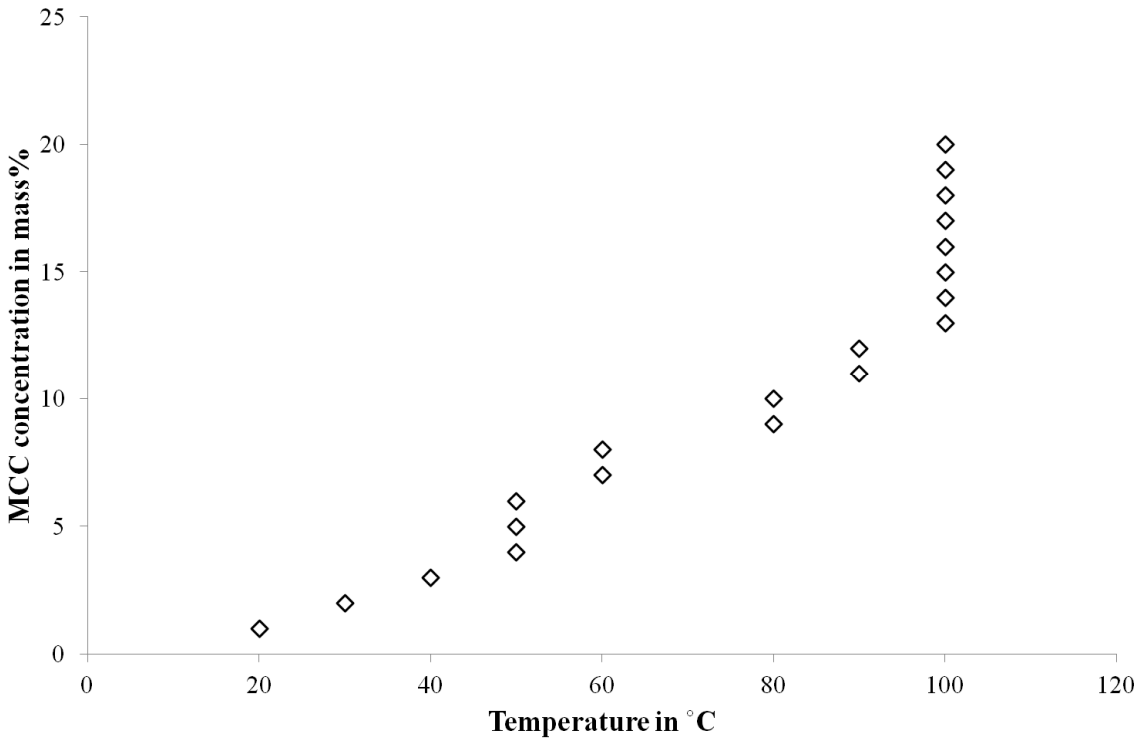

Figure 22: The amount of dissolvable MCC with increasing temperature.

Clearly, increasing the temperature results in an increased solvency of the IL. The increase in solvency is presumed to be the result of decreasing viscosity of the MCC-IL solution and increased cellulose-IL reactivity at higher temperatures [254, 255].

No further dissolution could be observed at concentrations higher than 20 mass%. An increase in temperature lead to the onset of degradation of the solution and resulted in a colour change from golden orange to dark brown as shown in Figure 23. The degraded solution could only partially be regenerated, indicating a structural damage to the cellulose chains.

Interestingly cellulose degradation is usually not expected at temperatures lower than 130 ˚C [256, 257]. The flash point of BmimAc is given as 153 ˚C and the thermal degradation of most IL has been reported as being above 150 ˚C and higher [258]. Although, the observed degradation was unexpected given the properties of the IL, it is known that cellulose-IL solution degradation may occur, particularly after extended times at elevated temperatures (>10 hr)[169].

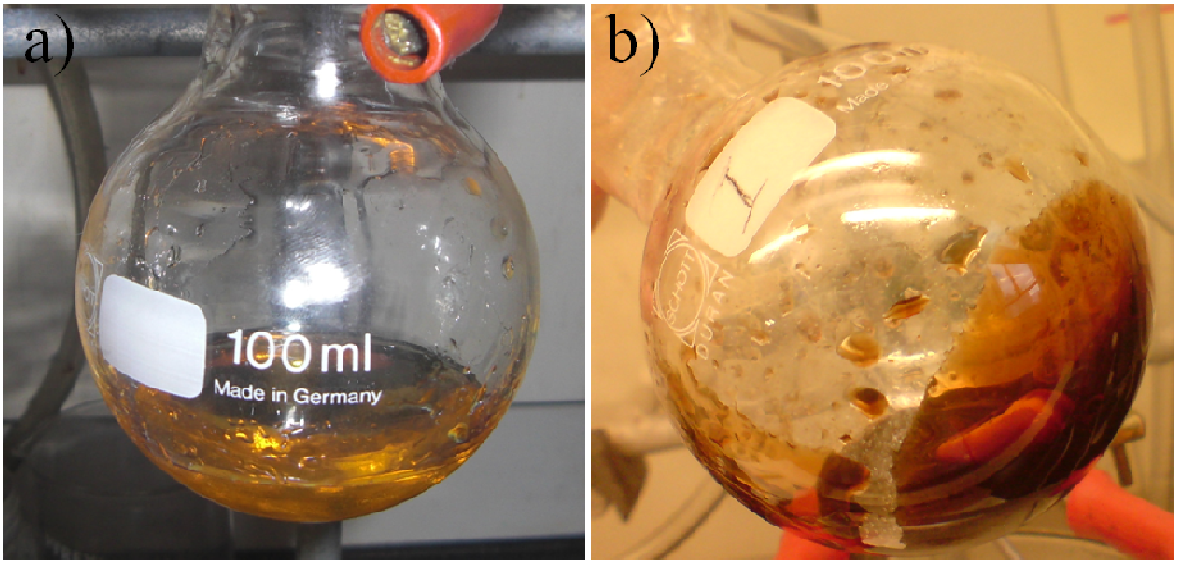

Figure 23: 5 mass% MCC-IL solution at 90 ˚C (a) and after heating to 120 ˚C (b) showing the onset of degradation.

A possible explanation for the degradation is localised heating or “hot-spots” within the cellulose-IL solution if mixing is inhomogeneous due to the high viscosity at elevated temperatures. This could lead to an inhomogeneous heat transfer within the mixture

and the formation of hot spots. The inhomogeneous heat transfer could be caused by the much higher thermal conductivity of cellulosic materials (40-45 $Wm^{-1}K^{-1}$ for regenerated cellulose and 45-53 $Wm^{-1}K^{-1}$ for cotton [259]) compared to Ils (0.200 $Wm^{-1}K^{-1}$ for 1-ethyl-3-methylimidazolium Tetrafluoroborate ($EmimBF_4$), 0.186 $Wm^{-1}K^{-1}$ for -Butyl-3-methylimidazolium Tetrafluoroborate ($BmimBF_4$)[260]). Degradation may be localised, but the discolouration spreads to the entire solution. A supporting fact is that the change in decreasing viscosity of the IL-cellulose solution with increasing temperature is diminished with further increases in temperature (Figure 24). The measured complex viscosity η*, is a combination recoverable or elastic and non-recoverable or viscous deformation.

The smaller changes in viscosity with increasing temperature indicates that a further increase in temperature has minimal influence on the viscosity and presumably cellulose dissolution [261]. Consequently, this indicates that an appropriate method for mixing needs to be developed to prevent premature thermal degradation of the cellulose solutions where in an industrial setting much greater quantities of cellulose would require dissolution.

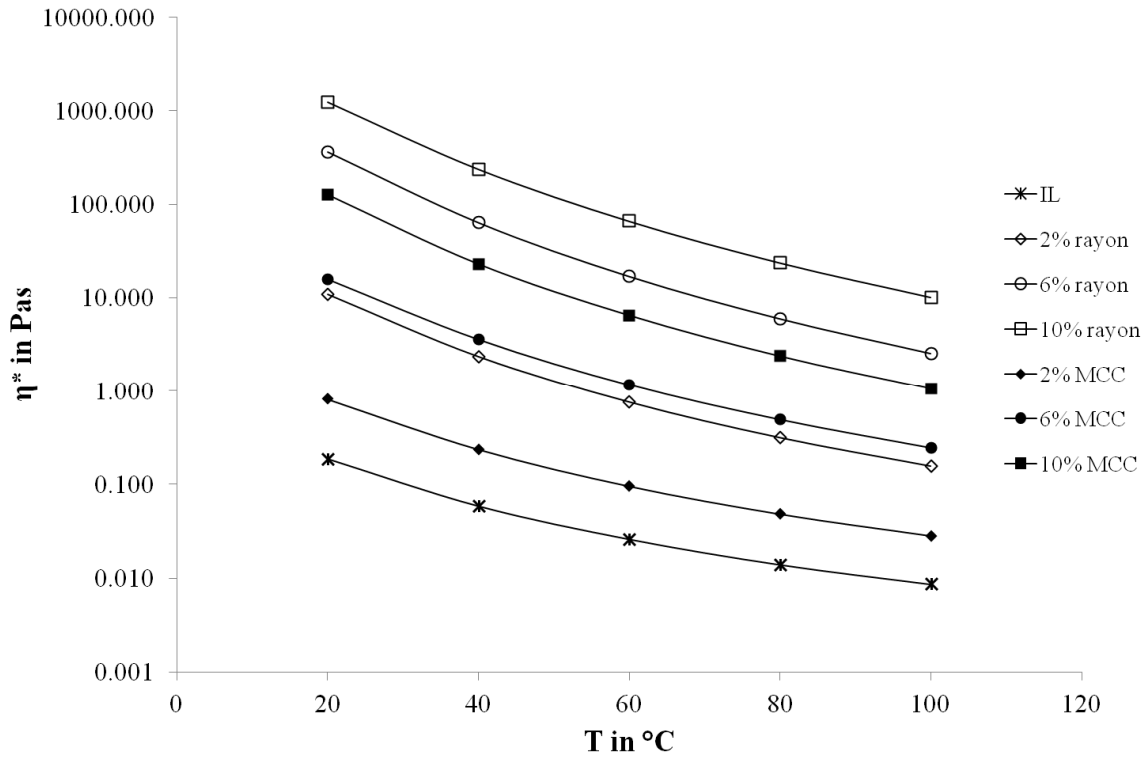

Figure 24: Complex viscosity (η*) plotted over temperature (T) for the different solutions of MCC,

40 mass% of DMSO was added to the IL, to determine its effect on the viscosity of the solution and cellulose dissolution, and the maximum concentration of MCC that is able to be dissolved by the methods described above. The 40 wt.% DMSO-IL blend resulted in a dramatic reduction in the complex viscosity by over 80% as shown in Figure 25 [262]. Consequently, the maximum in the dissolvable cellulose concentration cellulose was observed to increase from 20 to 36 mass%.

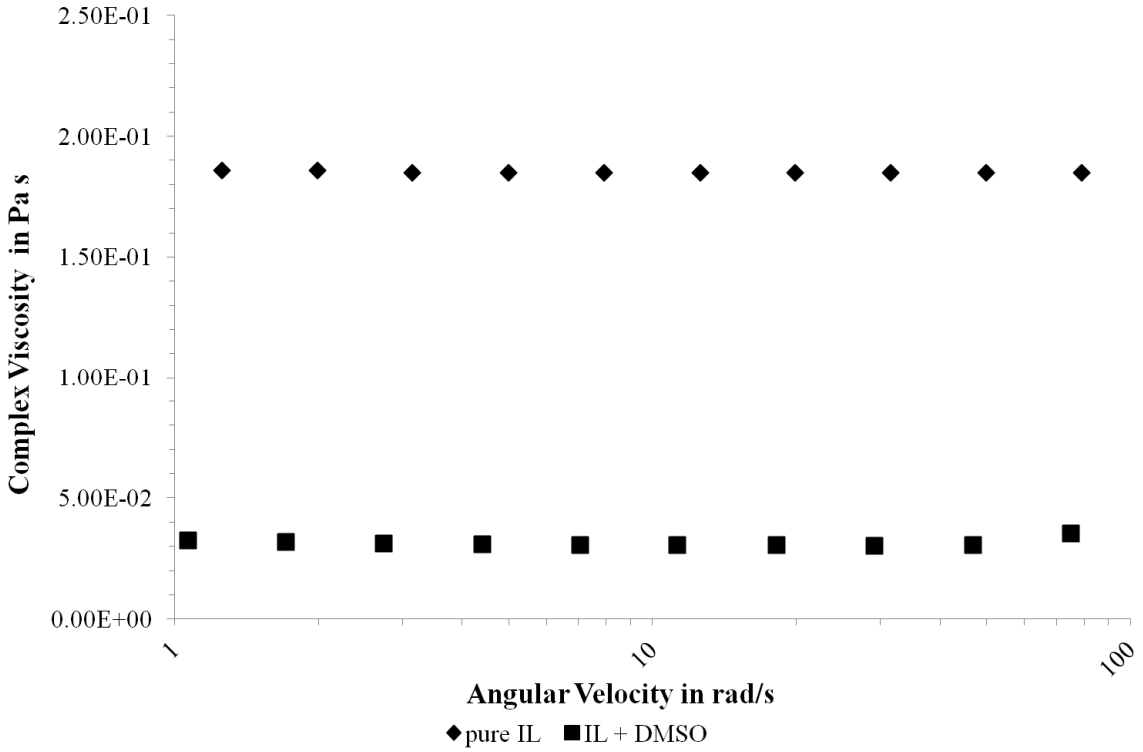

Figure 25: The complex viscosity (η*) as a function of the angular velocity (ω) for pure IL and a 40 wt.% DMSO-IL blend at a temperature of 20 °C

3.2 DISSOLUTION BEHAVIOUR OF CORDENKA FIBRE

Cellulose concentrations up to 10 mass% rayon fibre were observed to fully dissolve in BmimAc. A homogeneous mixture of fibres and IL was not possible at concentrations greater than 10 mass% due to the high viscosity of the solution. As for MCC, the inhomogeneity of mixing leads to degradation of the rayon-IL solutions.

MCC and rayon differ in terms of their aspect ratio, DP and crystallinity as pointed in Section III.2.1. MCC exhibited a higher solubility in the IL compared with rayon, indicating that the higher DP of the rayon fibres is likely a dominating factor in determining the maximum solubility of the cellulose in the IL. It is interesting to note the differences in solubility of MCC and rayon since less crystalline cellulose such as rayon are also relatively more soluble. However, ILs are capable of dissolving highly

crystalline cellulose as well [263, 264]. Although the IL mainly acts to interrupt the intermolecular hydrogen bonding in cellulose, the DP of cellulose may be slightly reduced by dissolution in an IL [265]. The higher DP of the rayon fibres will therefore increase the entanglement of the single cellulose chains causing a stronger increase in viscosity and reduce the accessibility of the hydrogen groups. Both factors contribute to a reduced dissolution capacity, as it can be seen from the lower maximal amount of dissolvable rayon cellulose compared to MCC and the higher viscosities of the rayon-IL solutions compared to the MCC-IL solutions (Figure 31).

The change of rayon fibre geometry during the dissolution has been analysed using optical and confocal microscopy. Figure 26 shows optical images of 4 single rayon fibres, before and after contact with the IL, as well as after being kept at 70 ˚C for 20 and 60 min. A change on fibre structure can be seen with increasing dissolution time as the fibres seem to increase in diameter. In fact, fibre swelling has been observed as part of the dissolution behaviour for cellulosic fibres in ionic liquids [266]. However, this was attributed to a swelling of the primary cell wall in natural fibres [267] and should therefore not occur in regenerated cellulose fibres. Thus, the underlying mechanism for fibre swelling observed during the immersion of rayon fibres in an IL requires further explanation.

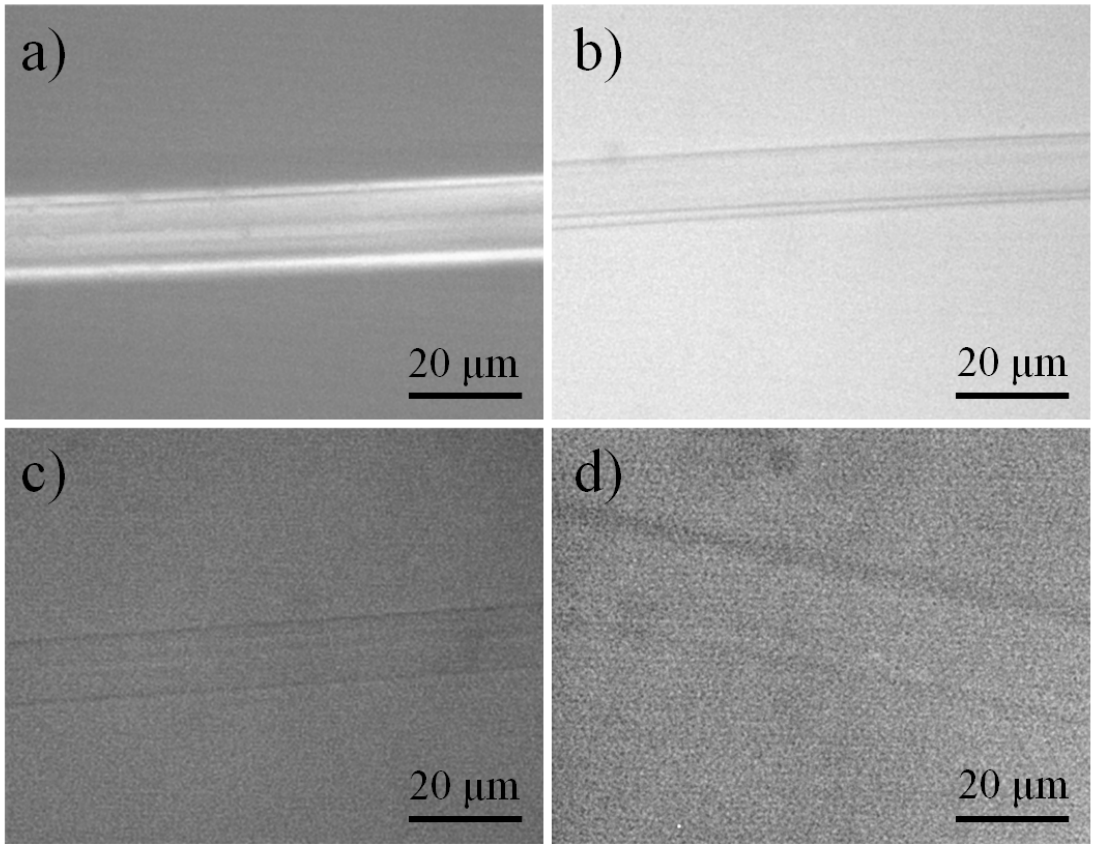

Figure 26: Transmission light micrographs of single rayon fibres (a) as-received, (b) following contact with the IL at room temperature, and for immersion times of (c) 20 min and (d) 60 min while held at a temperature of 70 ˚C.

The average diameter of the rayon fibre, as measured by image analysis of light micrographs, indicates that there is apparently no immediate change in diameter following immersion in an IL (Figure 27). However, the fibre diameter appears to increase following extended immersion times at elevated temperature. Interpretation of these observations is complicated by a high standard deviation of the results. However, a possibility is that a dissolved portion of cellulose that originates at the surface of the fibre remains in close proximity to the undissolved substrate. It is possible that this dissolved cellulose is not distinguishable from the fibre by light microscopy. Thus, the dissolved cellulose may possibly flow in a lateral direction simply under the weight of the cover slide in spite of its highly viscous state. The hypothesis for this anomalous

increase in fibre diameter is depicted schematically in Figure 28 and supported by the blurry appearance of the fibre in Figure 26d.

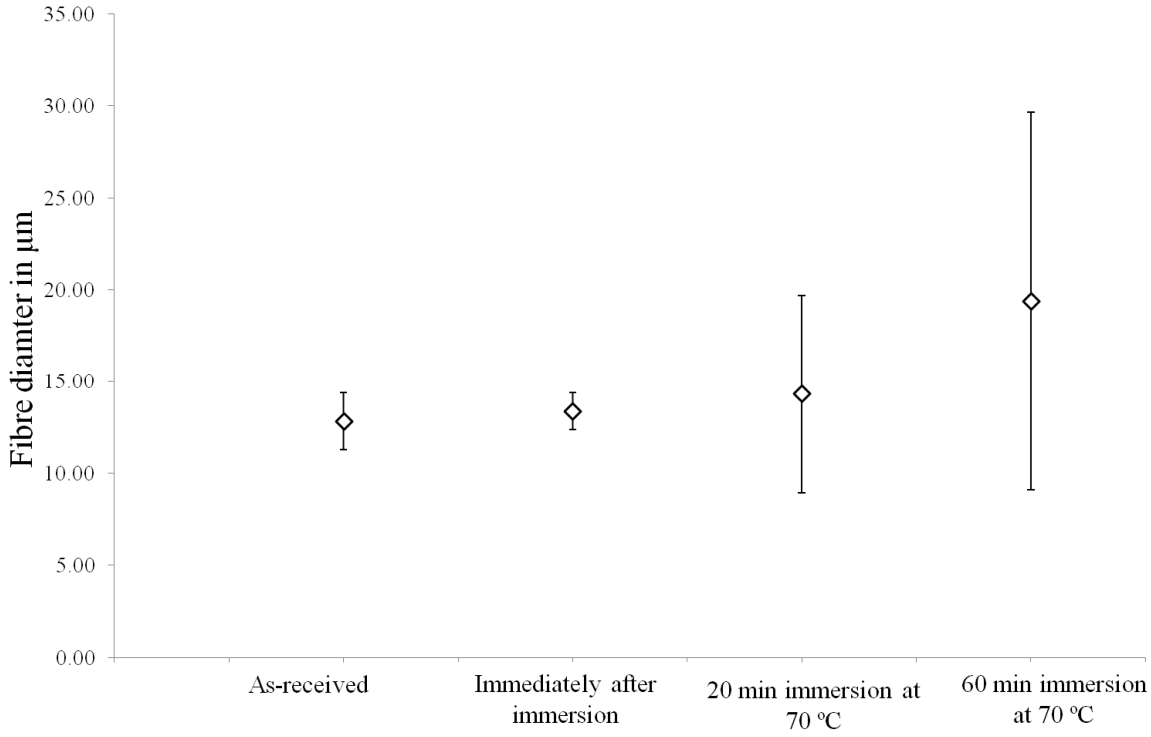

Figure 27: Average values of the measured diameters of single rayon fibres, before and after immersion in IL and after 20 min and 60 min immersion at 70 °C. The error bars resemble one standard deviation.

The dissolution behaviour of the rayon fibre was also analysed using confocal microscopy (Figure 29). The left column shows the confocal images while the right column shows images taken with light transmission.

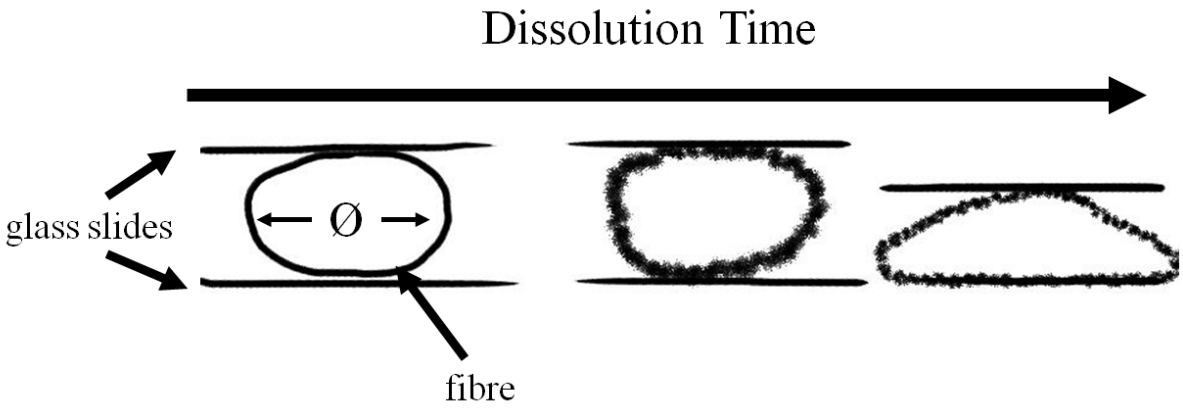

Figure 28: Sketch of the structural change of single rayon fibres with increasing dissolution time.

The edges of the fibres could be discriminated by Confocal microscopy at room temperature due to staining using the selected dye (Figure 29a). However, the edge definition of the fibres is poor at a temperature of 70 °C in the Confocal images (Figure 29c), while remaining high in transmission light microscopy (Figure 29d). It is assumed that the fibre surface is partially dissolved under these conditions with a consequent loss of the dye into the solution. The fibre structure appears to be largely unaffected by immersion in the IL according to the transmission light micrographs (Figure 29a and b). However, it is clear that the fibre edges begin to lose definition which supports the earlier assumption that the dissolved fraction of the fibre stays in close proximity to the substrate of the undissolved fibre.

The laser light spectrum was switched from 520-653 nm to 420-520 nm to pick up the "negative" image of the fibres (Figure 29e and f); this led to improved contrast in the confocal image at a temperature of 90 °C (Figure 29e). The rayon fibres were almost completely dissolved at a temperature of 90 °C according to the transmission light micrographs; only some blurry remnants of the cellulose fibres still visible (Figure 29f).

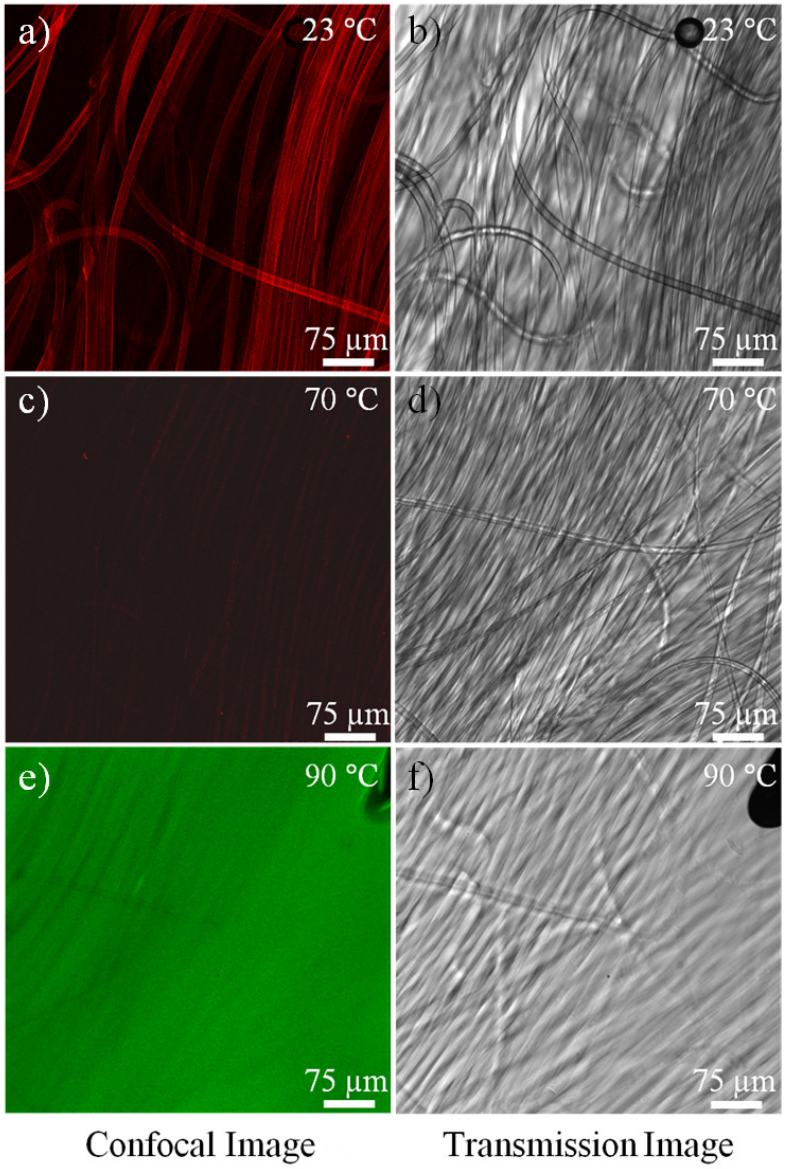

Figure 29: Confocal (left) and transmission light (right) micrographs of a rayon yarn at 23 (a & b), 70 (c & d) and 90 (e & f) °C, immersed for 1, 5 and 9 min, respectively. The change in colour is the result of a change in laser light spectrum from 520-653 nm to 420-520 nm.

Three different dissolution experiments were conducted on the filament yarns to analyse the effect of dissolution time and temperature on the yarn microstructure. The aim of this work was to elucidate the optimal dissolution conditions for partial dissolution of the rayon fibres.

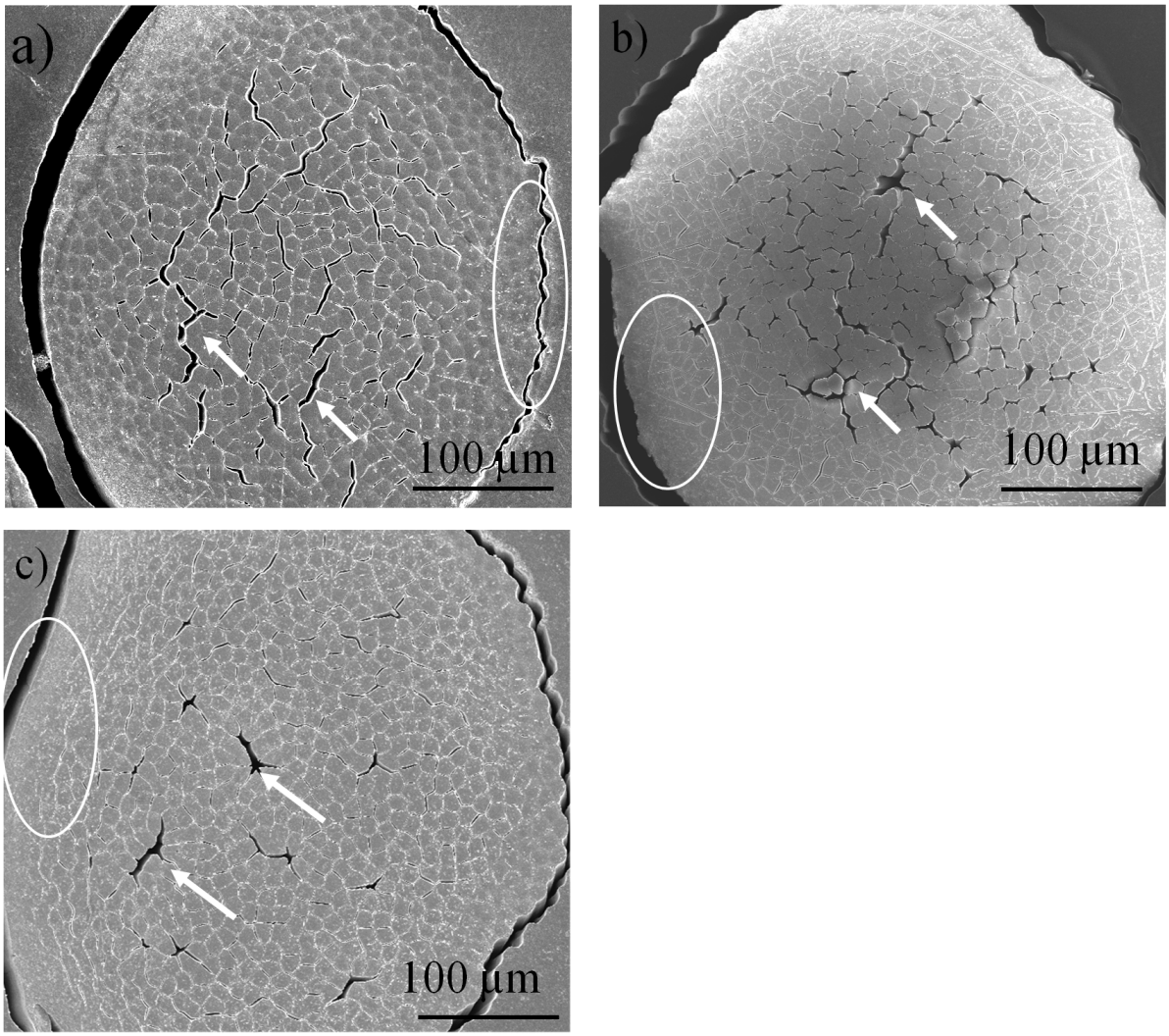

Figure 30: SEM micrographs of a rayon yarn treated with IL for 60 min at 100 °C (a), 30 min at 125 °C (b) and 30 min at 100 °C (c). Areas of completely dissolved regions are marked elliptically, voids are marked with arrows. An acceleration voltage of 5kV was used.

The fibres within each yarn were partially dissolved and subsequently bonded during the regeneration of the dissolved cellulose. However, each of the yarns exhibited a greater degree of fibre bonding in the outer regions of the yarn up to a stage of almost complete fibre dissolution (Figure 30). Typically, voids were observed in the central region of the yarn, indicating that the dissolution and/or regeneration processes were not uniform over the cross section of the yarn. The observation of non-uniform fibre bonding highlighted the need for developing methods that encourage an even distribution of the IL through textiles based on such yarns.

At a dissolution temperature of 125 °C (Figure 30-b) the yarn core was not completely dissolved, leaving some of the fibres isolated from each other. The higher dissolution temperature is likely to elevate the dissolution speed [268], leading to a strong increase in solution viscosity due to the higher amount of dissolved cellulose (Figure 31). The increased viscosity will hinder the further flow of IL to the yarn core. Thermally-induced degradation of the fibres was not observed at 125 °C. This is can be seen as unexpected as the solution degradation was observed at those temperature in the earlier described experiments (compare chapter III.2.2.2). This can be either explained by an reduced exposure time of the solution to the higher temperature or by the smaller amount of IL used. The increased dissolution temperature does not offer any advantages and increases the imhomogeneities within the yarn (Figure 30-b).

3.3 RHEOLOGICAL PROPERTIES OF IL-CELLULOSE SOLUTIONS

3.3.1 Viscosity

The amount of dissolved cellulose drastically increases the viscosity of the neat IL (Figure 31). The cellulose-IL solutions exhibit a range of rheological behaviours from Newtonian to shear thinning over 2-3 decades of frequency. Only neat IL and 2% MCC-IL solutions were almost completely Newtonian in behaviour. For all other solutions, the shear thinning is likely to be the result of shear-induced disentanglement of cellulose chains as previously reported for cellulose-IL solutions [247, 269].

The viscosity of the rayon-IL solutions is higher than that of the MCC-IL solutions for all concentrations. The higher viscosity associated with Rayon-IL solutions is due to the higher molecular weight (Mw) of the rayon fibres compared to MCC. It is well known that the viscosity of a polymer solution (or melt) is directly proportional to the Mw. The

longer polymeric chains of the rayon-IL solutions will provide a greater degree of entanglement and decrease molecular mobility. Likewise, the viscosity is observed to increase with increasing cellulose concentration due to the increasing interaction and entanglement of cellulose chains in solution [247, 261, 269].

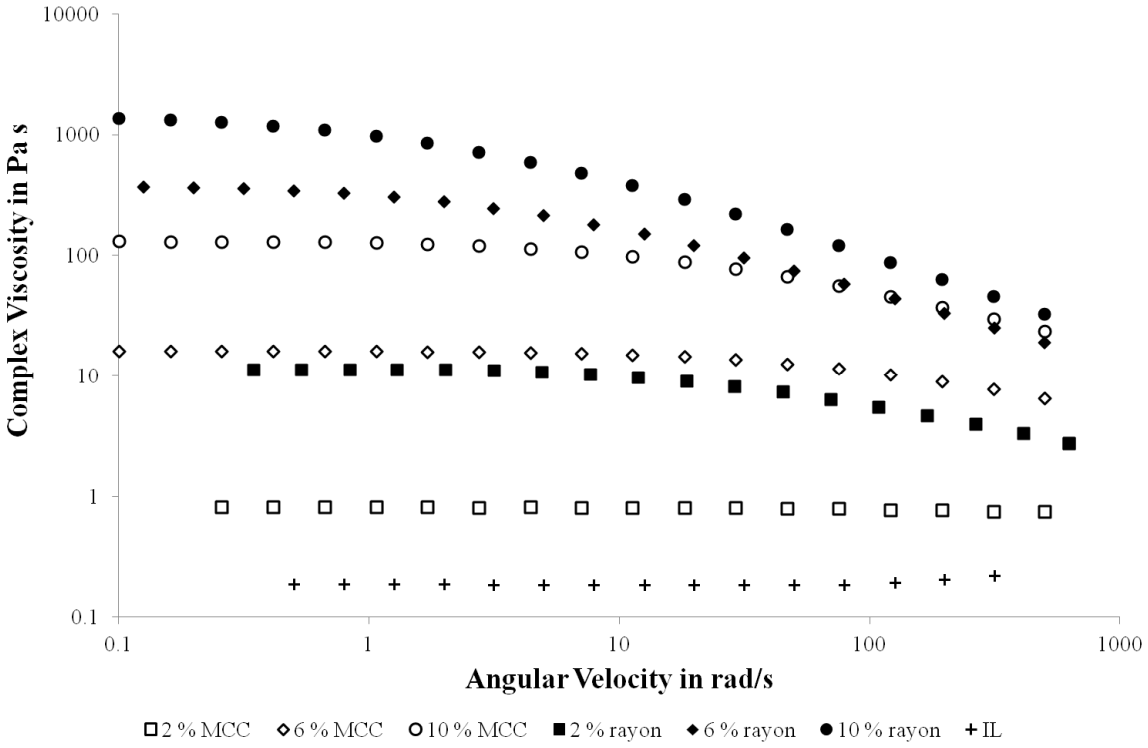

Figure 31: The complex viscosity of MCC-IL and rayon-IL solutions and pure IL at 20 °C.

As expected for polymer solutions and cellulose-NMMO solutions [247] as well as for cellulose-IL solutions [261, 269, 270], an increase in temperature clearly decreases the MCC-IL and rayon-IL solution viscosity (Figure 32). This indicates more or stronger entanglements of the polymeric chains at lower temperatures [269], although the decrease becomes less pronounced at higher temperatures (Figure 24). A similar effect was reported for wood pulp cellulose in the IL 1-allyl-3-methy-limidazolium Chloride (AmimCl), especially for higher cellulose concentrations (< 1%). This was explained by a strongly increased number of junctions caused by molecular entanglements and

interchain interactions. The authors argued that the high number of junctions leads to a strong intermolecular network that can only be partially disrupted by further heating [261].

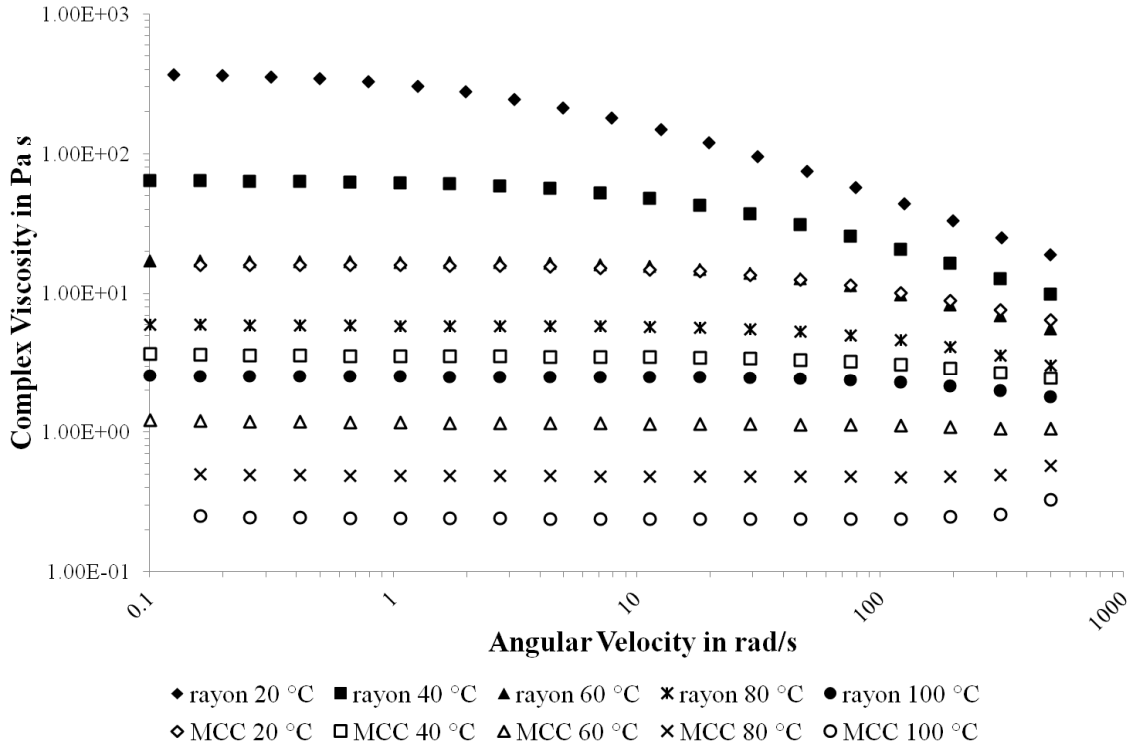

Figure 32: The complex viscosity of 6 wt. % cellulose-IL solutions as a function of temperature and shear rate.

3.3.2 Viscoelastic Properties of cellulose-IL solutions

The storage (G') and loss modulus (G'') both increase with increasing cellulose concentration (Figure 33). Furthermore, G' is observed to be higher for the rayon-IL solutions compared with the MCC-IL solutions, indicating that rayon-IL solution behaves more elastically (Figure 33). The probability of forming entangled cellulose chains is increased with increasing cellulose concentrations and higher DP [269]. The network of cellulose chains is strengthened as a result of an increased number of entanglements and reduced chain mobility [261]. This implies that the solution stores more energy under an applied load as the DP and cellulose concentration are increased.

The storage of energy within such a network structure is strongly dependent on the frequency of the applied load as this determines the time available for the dissipation of energy *via* molecular motion (*e.g.* slippage of entanglement points) [269].

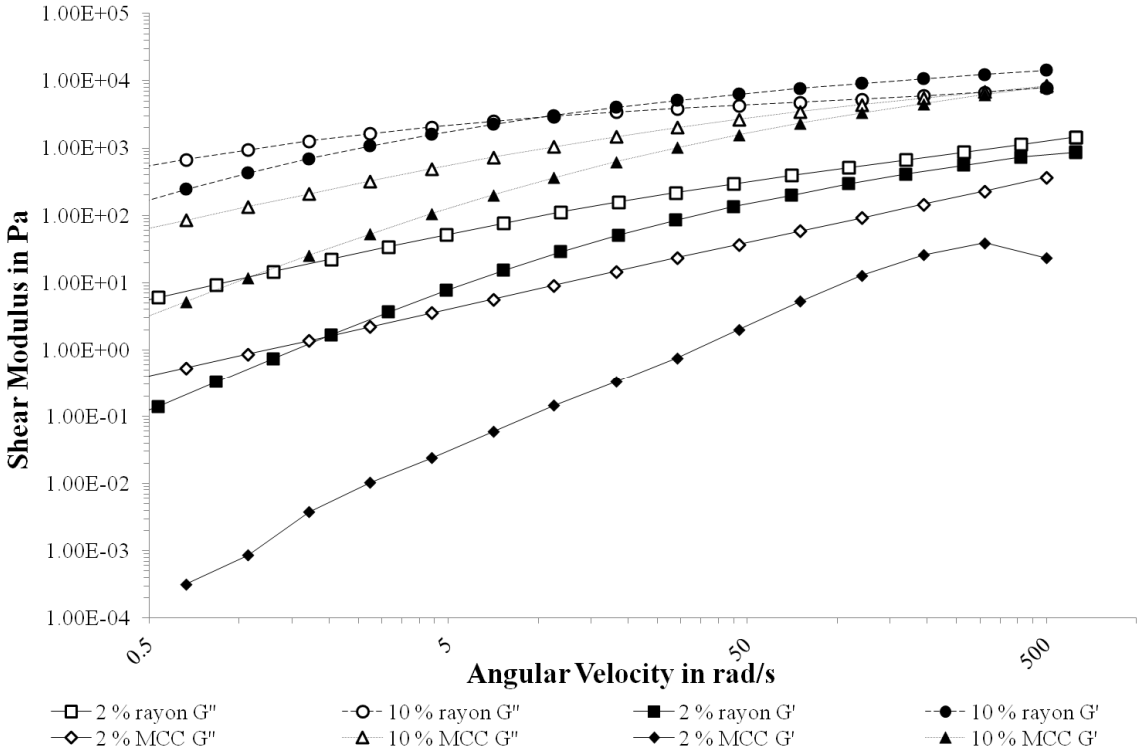

Figure 33: **Storage (G') and loss (G'') moduli of 2 and 10 mass% cellulose-IL solutions as a function of the shear rate at 20 °C.**

It is observed that the values of G' and G" are equal at a specific frequency for a concentration of 10 mass% rayon. This cross-over point signifies the frequency above which a viscoelastic solution transitions from a sol-like to a more gel-like behaviour. The inverse of the frequency of cross-over is also known as the characteristic relaxation time (λ) which is related to the Mw, polymer concentration and temperature of the solution. It was observed that λ decreased with increasing temperature, as shown for a 6 mass% and 10 mass% rayon-IL solution (Figure 34). It can also be seen that a 10 mass% MCC solution exhibits a relaxation time of only 9.7 ms at 20 °C compared to

0.125 s of the 10 mass% rayon solution, showing the higher Mw of this solution compared to MCC [271].

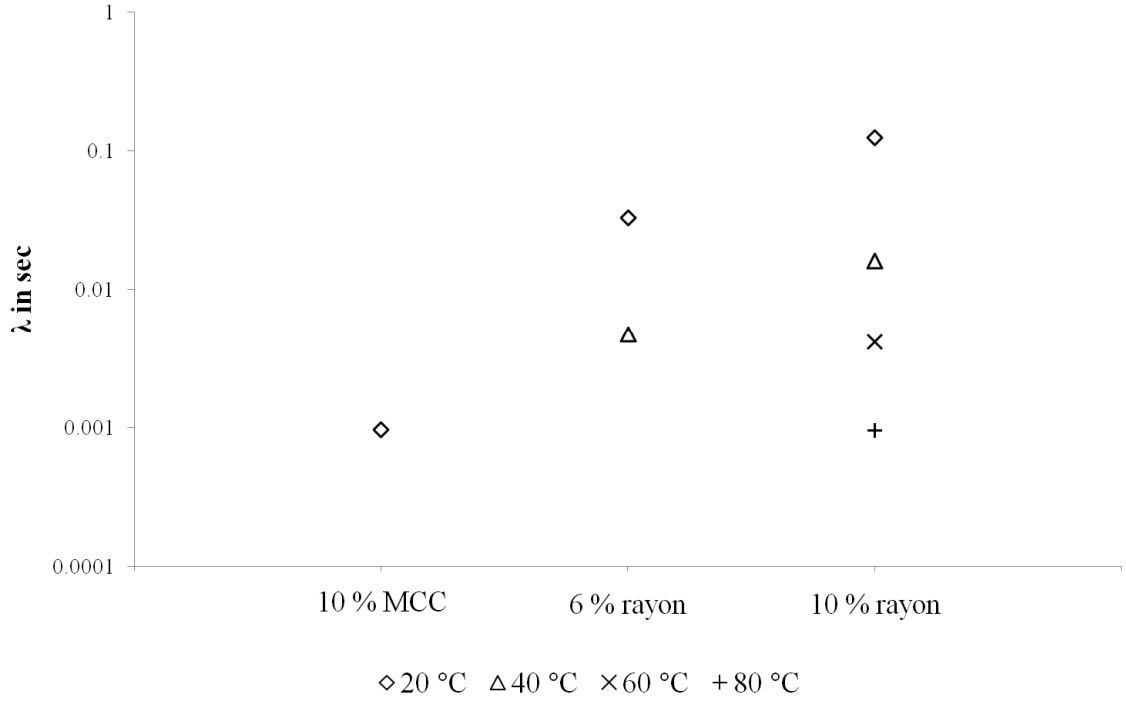

Figure 34: Relaxation time (λ) of the 10 % MCC, 6 % and 10 % rayon solutions.

Similar behaviour was observed for solutions of wood pulp in 1-allyl-3-methyl-imidazolium Chloride (AmimCl) [261] cellulose pulp with different DPs (505 and 1100) in BmimCl [269]. The G'-G" crossover would be observed at higher frequencies (ω) for solutions of MCC-IL and 2 mass% rayon-IL but this was not captured by the range of ω used in the present experiments (Figure 33).

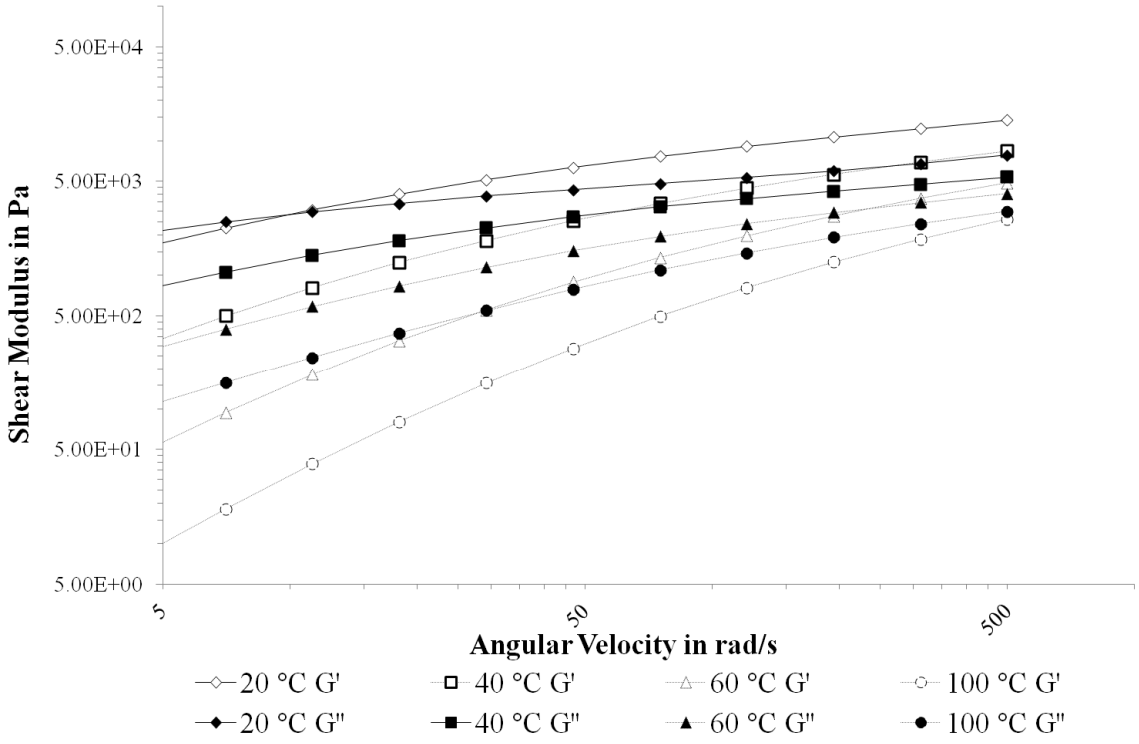

Figure 35: Crossover points of G' and G'' of a 10 mass% rayon-IL solution measured at 20, 40, 60 and 80 °C at different angular velocities.

The change in the observed dynamic behaviour of a cellulose-IL solution with increasing cellulose concentration from a viscous to a more elastic or gel-like behaviour elucidates the underlying viscoelastic mechanisms that result in poor IL distribution in rayon yarns (Figure 30) and explain the observed dissolution behaviour of the rayon fibres (Figure 27 & Figure 28). The solution in close proximity to the fibre will behave more elastically as the dissolution of the fibre surface proceeds. These results appear to suggest that pressure may be required during processing of cellulose fibre *via* partial dissolution to promote an even distribution of IL throughout an assembly of cellulosic fibres such as that found in a textile for example. It is hypothesised that an even distribution of IL also equates to the uniform regeneration of cellulose within an all-cellulose composite, providing a well distributed matrix that acts to optimise fibre-matrix adhesion.

4. CONCLUSIONS

BmimAc is an effective solvent for cellulose I in the form of MCC and cellulose II in the form of rayon fibre. The maximum solvency of BmimAc for cellulose depends strongly on the form of cellulose and the degree of polymerisation.

With increasing cellulose concentration the solution viscosity rises drastically and it could be shown that a higher DP of the cellulose source results in a higher viscosity of the solution indicating that the IL mainly dissolves intermolecular hydrogen bonds while leaving covalent intramolecular bonds intact.

Cellulose dissolution depends strongly on the solution viscosity. It could be shown that a strong reduction in IL viscosity leads to a significantly increased dissolution capacity. The dissolution temperature needs to be carefully manipulated to minimise the solution viscosity while avoiding polymer degradation. The formation of hot spots needs to be avoided to prevent degradation of the cellulose-IL solution.

Increasing the cellulose concentration and decreasing the temperature alters the mechanical response of the cellulose-IL solution from a sol-like to gel-like behaviour under an applied oscillatory stress. Thus, the cellulose-IL solution can react more like an elastic solid than a like a viscous fluid depending on the conditions of cellulose concentration and temperature.

Direct observation of the partially dissolved surface of rayon fibres does not reveal any fibre swelling. Instead, a highly viscous and localised cellulose-IL solution surrounds the fibre core as dissolution proceeds. Combined with the known change in elastic response, these observations suggest that an external stress may be necessary to

encourage the flow of the dissolved cellulose to regions beyond the immediate vicinity of the dissolving fibre. It might be appreciated that some finite flow of the dissolved cellulose through an assembly of fibres such as that found in a textile is required in order to achieve an even distribution of the final regenerated matrix phase.

The selection of MCC and rayon fibre in the processing of ACCs will be dictated by their differing morphologies (or structural form) and dissolution kinetics. For example, it could be supposed that MCC is particularly well suited as a raw material for generating the regenerated matrix in the 2-step method (see Section I.3.1.2.1) due to its ease of dissolution compared with rayon fibre. On the other hand, the particulate-type morphology of MCC is not well suited to that required for a strong and stiff composite.

In contrast, the continuous form of the rayon fibres offers superior mechanical strength and stiffness in a composite material. It might then be envisaged that the volume fraction of continuous fibre could be maximised by ACC processing *via* the 1-step partial dissolution route as the fibre surface can be selectively dissolved (see Section I.3.1.2.1). In addition, incomplete fibre-matrix wetting is a major obstacle to optimising the mechanical properties of composites. However, the observed dissolution behaviour of rayon fibre in this work indicates that cellulose that undergoes localised surface dissolution remains in close proximity to the fibres, further implying that complete fibre-matrix wetting will occur locally *in situ* provided that the fibre-solvent contact is uniform.

IV. INFLUENCE OF DIFFERENTIAL WATER UPTAKE ON THE INTERPHASE OF ALL-CELLULOSE COMPOSITES PROCESSED *VIA* A COMPLETE DISSOLUTION ROUTE

1. INTRODUCTION

Processing of ACCs *via* the 2-step route, meaning the preparation of a completely dissolved portion of cellulose and its combination with an additional cellulose source as reinforcement offers several advantages from a processing point of view. If adequate storage conditions can be provided, the cellulose solution can be prepared separately and in advance of the composite making process. Thus, the solution could be checked for impurities and/or degradation processes that can occur during cellulose dissolution (see Section III.3.1).

Theoretically, the solution can be combined with precisely determined shares of reinforcement allowing the processing of composites with predictable properties. Upon removal of the solvent the regenerated cellulose should establish strong hydrogen-bonding with the hydroxyl groups on the surface of the used cellulosic reinforcement.

However, due to those hydroxyl groups, individual cellulose chains are highly hydrophilic [85]. Consequently, the presence of water has a negative effect on the dimensional stability and mechanical properties of composites containing cellulosic reinforcements, even where the matrix is not sensitive to humidity changes [71, 272].

The moisture sensitivity of cellulosic materials is not uniform, but depending on its microstructure and therefore difficult to predict. It has been established that for pure

cellulose mainly the amorphous regions take up (and release) moisture. The crystalline regions are composed of a tightly bound structure that is less accessible to water molecules. Thus, the overall crystallinity, crystalline structure and accessibility of the amorphous regions play a major role in the moisture uptake behaviour of cellulose [273]. This could create severe problems at the interface of regenerated cellulose used as matrix phase and the cellulosic reinforcement, as those could not only show differences in overall crystallinity but also in crystalline structure, as regeneration of dissolved cellulose usually leads to the formation of a cellulose II crystal structure. Should natural fibres be used as a reinforcement, it needs to be established if strong interfacial bonding can be achieved between the cellulose II matrix phase and the cellulose I reinforcement.

Not only is crystalline configuration different for cellulose present in natural fibre, they also consist of several chemical components that will interact with moisture including hemicellulose and/or lignin (see Section I.1.2.4). Hemicelluloses are low in crystallinity and highly hydrophilic, making this constituent the main factor in the dimensional instability of natural fibres [40, 274]. In contrast, lignin is hydrophobic in spite of being completely amorphous. Lignin is found in close proximity to the cellulose microfibrils in natural fibres [2]. The varying interaction of cellulose, hemicellulose and lignin with moisture is responsible for the complex swelling behaviour of natural fibres.

The chemical similarity of matrix phase and reinforcement in ACCs has been identified as one of their key advantages in terms of mechanical properties. However, it might be anticipated that ACCs will exhibit a greater sensitivity to moisture due to its fully cellulosic composition. Furthermore, although chemically similar, the reaction of

regenerated matrix phase and native reinforcement to moisture might be different due to differences in the microstructure. Whilst ACCs show great promise in terms of their mechanical properties under ambient conditions, the effect of exposure to moisture on the microstructure of ACCs needs to be examined. Especially for ACCs processed *via* the two-step route, differences in moisture uptake could cause a reduction in interfacial bonding and therefore a drastic reduction in overall composite strength and stiffness.

In ambient conditions, water in cellulosic structures is usually present as bound water. However, if the moisture content of the cellulose is higher than the saturation point (*i.e.* ~30% at room temperature) any excess water will be present as free water [275]. As the name implies, bound water is chemically bonded to the hydroxyl groups of the cellulosic molecules, with a transition temperature lower than that of free water. Two types of bound water may be present including (a) non-freezing and (b) freezing, with non-freezing water often not being detectable in the first order transition [276].

As discussed, ACCs could be potentially exposed to environmental humidity in their final application. Similarly, the regeneration of cellulose during ACC processing commonly involves intimate contact between the cellulosic material and water. Water is an attractive coagulant as it is lower in cost, easier to handle and non-flammable when compared with other volatile organic coagulants. However, with the necessity to absorb water for regeneration also comes the need to then release this water during drying. The level of interaction between the ACC and water will strongly depend on the ratio of regenerated cellulose to cellulosic reinforcement. The two-step method is more likely to be influenced by the use of water as coagulant when compared with the partial dissolution method. The two-step method involves combining completely dissolved

cellulose with undissolved, cellulosic material. However, even the most powerful solvents for cellulose can only dissolve up to about 30-35 mass% of cellulose [169]. This in turn means that 70 mass% or more of solution will be removed during the processing by first exchanging the solvent with a coagulant to regenerate the cellulose, followed by evaporation of the coagulant to consolidate the matrix phase. In contrast, relatively small fractions of matrix (< 20 %, [105]) are created during partial dissolution of the fibre surface (*i.e.* 1-step method) that obviously results in less coagulant uptake and less shrinkage during drying.

In this Chapter, thin films of ACCs are produced from completely dissolved MCC, undissolved MCC and undissolved wood fibre to analyse the effect of moisture on the ACC microstructure by varying the humidity. The water uptake behaviour and type of water was examined for completely dissolved MCC, undissolved MCC and undissolved wood fibre. The microstructure of the ACCs was examined as a function of humidity to assess the appearance of the bonding between the regenerated cellulose and reinforcement.

2. EXPERIMENTAL PROCEDURES

2.1 MATERIALS

MCC was used as a source for both the cellulosic matrix phase and reinforcement. Wood fibre (WF) (*Pinus radiata*) was used as another form of reinforcement. WF was provided by a local sawmill (Kaiapoi, New Zealand). The average width and length of the WF was 42 ± 14 μm and 1.64 ± 0.7 mm, respectively. The exact chemical composition of the WF was not determined. However, the average cellulose, hemicellulose and lignin content of *Pinus radiata* is 40-45%, 20-25% and 25-35%, respectively [277, 278].

2.2 PREPARATION OF ACC FILMS

The MCC was dried in a vacuum furnace (Binder VD 23, Binder GmbH, Tutlingen, Germany) at 85 °C for 48 hr. The MCC was then mixed with a co-solvent system consisting of BmimAc and DMSO with the mass ratio of 0.35:0.5:1 (MCC:BmimAc:DMSO). The addition of DMSO reduces the viscosity of the solution, which in turn was found to increase the solubility limit of cellulose in BmimAc (see Chapter III,[234, 252]). The mixture was thoroughly stirred at 900 rpm at a temperature of 100 °C for 3 hr by using an overhead stirrer (IKA Eurostar). The MCC was completely dissolved by mixing and subsequently used as the matrix phase in the ACCs.

The ACCs were produced by mixing appropriate amounts of MCC solution (10 g) with undissolved MCC and wood fibre to yield compositions of 10 and 30 mass% reinforcement. The various ACC compositions are referred to as 10 % MCC, 10 % WF, 30 % MCC and 30 % WF. The reinforcement and MCC solution were mixed at room temperature with an overhead stirrer at 100 rpm for 15 min to achieve a homogeneous mixture. ACC films were formed by placing the mixtures between two flat aluminium sheets (120 mm × 120 mm × 2mm) and then consolidating the mixture in the hot press using an applied pressure of 0.2 MPa. The thickness of the mixtures was maintained uniformly at 0.3 mm using stainless steel spacer plates. The assembly was then removed from the press and placed in a bath of distilled water at room temperature to remove the solvent and thus regenerate the dissolved cellulose. The water was exchanged several times to ensure thorough removal of the solvent system. After 24 hr of washing, the gel-like film was then dried by placing it in the hot press between paper sheets under a pressure of 0.01 MPa and held at 100 °C for 6 hr. The final thickness of the films

was 0.25 mm following drying. Films of unreinforced regenerated cellulose were produced according to the above described method from 10 g of MCC solution for comparison with the ACCs.

2.3 MATERIAL CHARACTERISATION

Water uptake measurements were performed in triplicate for each of the ACCs, as-received WF and as-received MCC. Initially, the samples were conditioned at 23 ˚C and 50 % RH, and the mass of the conditioned samples was recorded. The samples were then placed in a water bath for 48 hr at room temperature. The mass of the samples was measured following the removal of excess water from the sample surface by lightly pressing the film against a paper towel. The samples were then placed in a vacuum oven at 100 ˚C and weighed every 12 hr until the mass reached equilibrium.

Short strips of approximately 4 mm in length were cut from the films and prepared for microscopical analysis. The mounted samples were conditioned at room temperature (23 ± 1 ˚C) and 20% or 50% RH before analysis of the microstructure. The cross-sections of the above samples were examined using micrographs obtained using the Leica DR IRM microscope and attached camera. The width of separation between the reinforcing phase (*i.e.* wood fire or MCC) and adjacent regenerated matrix phase was measured with image analysis software (ImageJ), to estimate the amount of fibre and matrix swelling. For each material, 10 reflected light micrographs were recorded with a minimum of 25 measurements per micrograph performed.

The cold-mounted samples were gold-coated for 120 s for SEM analysis.

Differential scanning calorimetry (DSC) was performed on a PerkinElmer DSC 8000 (PerkinElmer, Waltham, Massachusetts, USA). The saturated films were briefly pressed against a paper towel to remove any excess surface water. Samples of approximately 20 mg were prepared with a razor blade, weighed and sealed in standard PerkinElmer DSC analysis aluminium pans (40 µL). The samples were held at 30 °C for 5 min, then cooled down to -70 °C at a cooling rate of 5 °/min. Samples were held at -70 °C for 3 min and then heated up to 180 °C at a heating rate of 5 °/min. Cooling was achieved using a PerkinElmer PE intracooler 2P and nitrogen was used at a purge gas with a flow rate of 20 ml/min.

The peaks during the cooling cycle can be distinguished as free water (peak I), freezable bound water (peak II*) and non-freezable bound water (peak II) in accordance with [275]. The amount of free, non-freezing and freezing bound water within a sample is calculated according to Equation 2 (after Ping *et al.* [279]).

$$W_c = Q/\Delta H \qquad (2)$$

where W_c is the mass of water in g and Q is the heat absorbed during freezing in J which is calculated from the peak area. ΔH is the melting enthalpy of water which in this case is assumed to be that of liquid water (ΔH = 333.5 J/g). Note that this assumption does not take into account the differences in melting enthalpy of the different crystal structures of ice (I, Ic, II and III). However, the maximum error in the calculated amounts of freezable water is only 6.6 % according to Ping *et al.* [279]. Therefore, these differences are ignored in the present investigation. Since the total amount of water in a sample is known from the measurements of weight loss, the relative amounts of bound

water (freezing and non-freezing) and free water were able to be determined for the various materials.

3. RESULTS AND DISCUSSION

3.1 EFFECTS OF FILM PROCESSING AND MOSITURE UPTAKE ON THE ACC MICROSTRUCTURE

Longitudinal cracks were observed in each of the final materials (Figure 36). The presence of cracks is a consequence of the processing conditions as described in some detail by Duchemin *et al.* [127]. The formation of longitudinal cracks (as indicated by the arrows in Figure 36a, b and c) occurs within ACCs when processed with a rapid regeneration route (*e.g.* immersion in water). Furthermore, the drying procedure may contribute to void formation. In particular, the films in this work were rapidly heated to 100 ˚C that leads to differential shrinkage of the films due to a gradient in the moisture profile through the thickness of the sample.

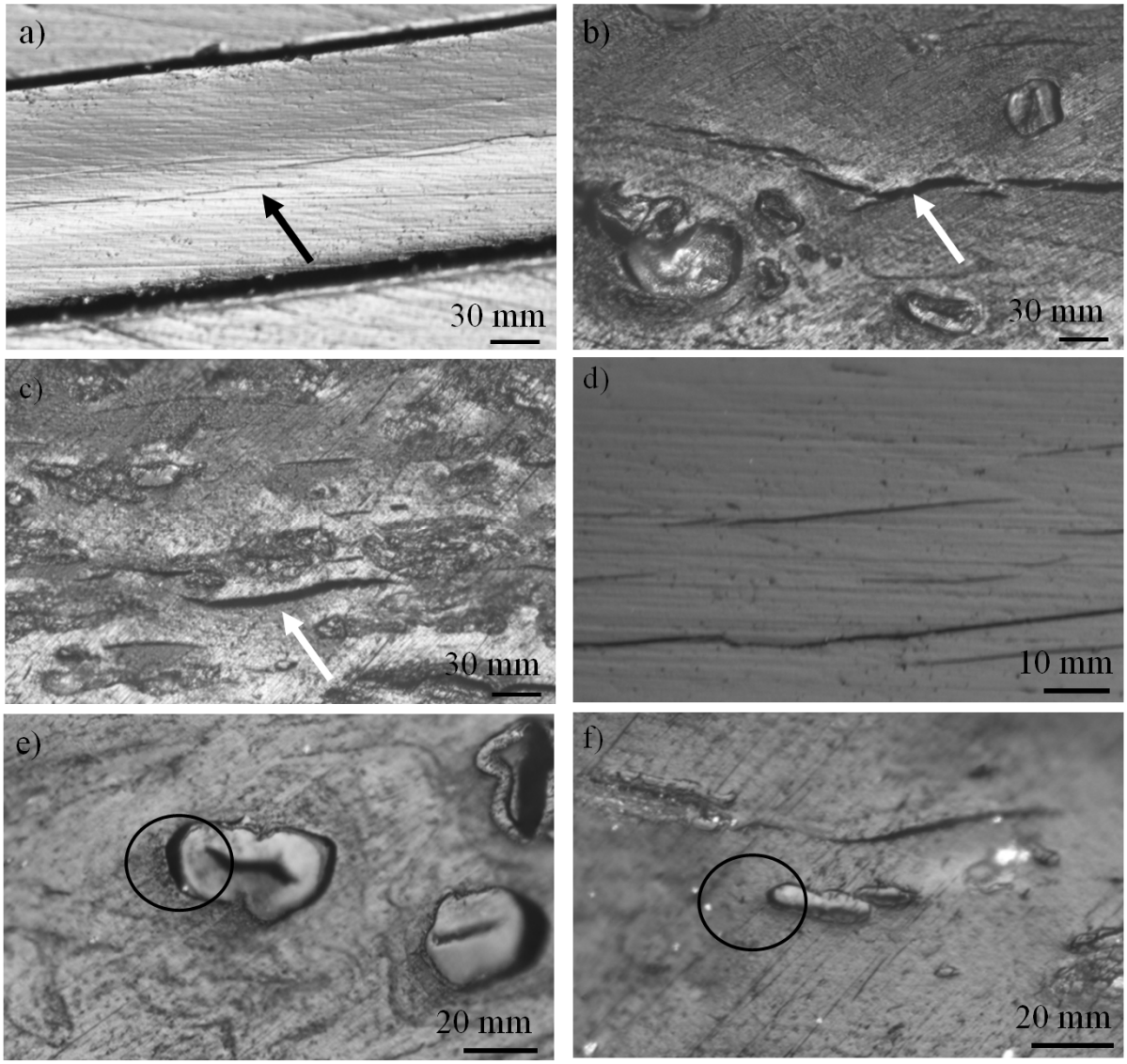

Figure 36: Reflected light micrographs of the cross-sections of unreinforced regenerated cellulose (a & d), 30 % WF (b & e) and 30 % MCC (c & f). Samples conditioned at 23 ˚C and 50 % RH for 48 hr. Longitudinal cracks, marked by arrows are visible in all three samples. Picture e) & f) show that WF and MCC have (partially) separated from the matrix phase.

The formation of longitudinal cracking is likely caused by a system of layered structures present in the films that originate from a diffusion gradient. The gradient is caused by the diffusion of water into the surface during regeneration, where the cellulose at the surface is regenerated first and undergoes shrinkage before the underlying cellulose. This sets up conditions for differential shrinkage that occurs as a function of the through-thickness distance. As the shrinkage proceeds along the direction of water diffusion due to the regeneration, this will induce lateral tensile stresses [108]. It is

plausible that the build of residual stress then results in the observed longitudinal cracking of the films upon drying. The mechanism of longitudinal crack formation in ACCs is also shown schematically in Figure 37.

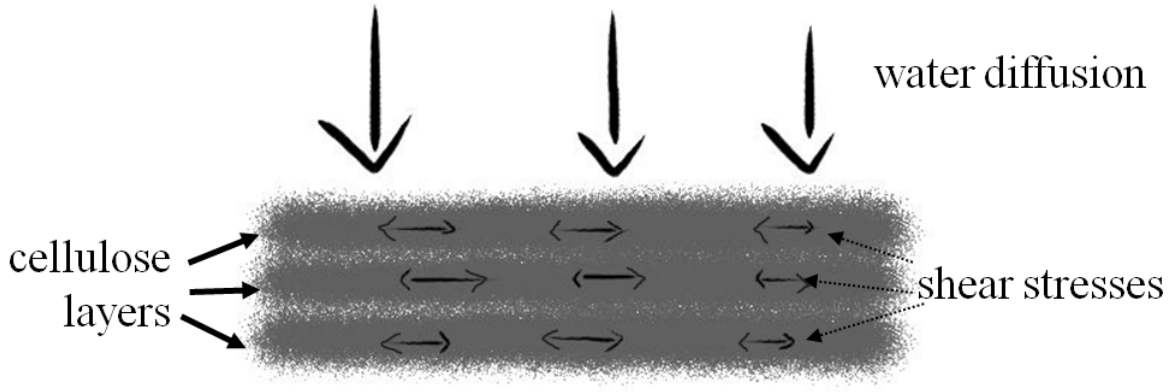

Figure 37: Schematic of the shear stresses that develop during regeneration that are thought to result in a layered composite structure; adapted from [108].

Furthermore, it is clear that the periphery of the reinforcement is only partially in contact with the matrix phase. The formation of voids was particularly extensive around the wood fibres (Figure 36c). The water uptake of a cellulosic structure is chiefly dominated by the amorphous domains which are also referred to as accessible regions within the cellulose [280]. Cellulose microfibrils in the reinforcing phases (*i.e.* WF and MCC) exhibit both crystalline and amorphous domains [281] although it is assumed here that the water uptake of the composites is dominated by the regenerated cellulose. The bonding of MCC to the regenerated cellulose was observed to have greater integrity than that of the wood fibre-regenerated cellulose combination (Figure 36e and f). An explanation for the differences in reinforcement-matrix interfacial bonding may lie with the difference in the moisture uptake behaviour of MCC, WF and regenerated cellulose.

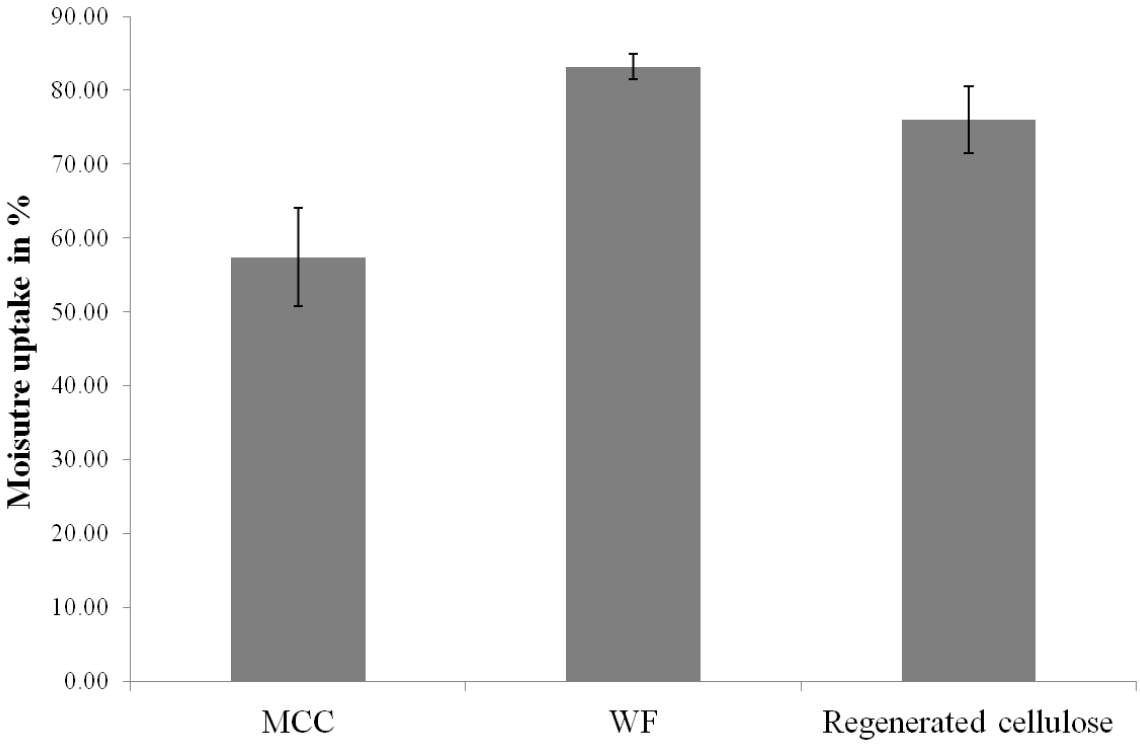

Figure 38: Moisture uptake of MCC, wood fibre and regenerated cellulose from being conditioned at 23 ˚C and 50% RH to soaking in distilled water for 48 hr. The error bars resemble one standard deviation.

Regenerated cellulose exhibited a higher moisture uptake than the as-received MCC (Figure 38). Consequently, upon drying the regenerated cellulose is most likely experiencing a higher amount of shrinkage than the MCC it is surrounding, causing a mechanical interlocking of reinforcement and matrix. This is easily explained in terms of the different structures of regenerated and microcrystalline cellulose. MCC is present in the form cellulose I, while it is known that dissolution and regeneration of cellulose I leads to a reduction in the crystallinity and change in conformation to cellulose II [118, 129, 167]. Thus, the reinforcing MCC is highly crystalline relative to the surrounding regenerated cellulose; hence, this makes the regenerated cellulose more prone to water uptake. Moreover, the cellulose II crystalline structure is more accessible to water than cellulose I [104]. Consequently, it would be reasonable to assume that the drying shrinkage of the regenerated cellulose is greater than MCC. Thus, the combination of

regenerated cellulose and MCC reinforcement would result in a mechanical interlocking of the MCC reinforcement by the surrounding cellulose matrix upon drying. The interface between MCC and regenerated cellulose was in fact at times difficult to distinguish (Figure 39-b) indicating that good adhesion is achieved between the two cellulosic materials. However, the interfacial bonding was inconsistent with some large interfacial cracks appearing (Figure 39-a), most likely the result of drying induced shrinkage that acts to separate the reinforcement and matrix.

On the contrary, the moisture uptake of the WF is slightly higher than the regenerated MCC, possibly caused by the high hydrophilicity of the hemicellulose present in wood fibres [40]. Hence, the situation is reversed such that the WF are expected to exhibit greater drying shrinkage than the regenerated cellulose matrix, leading to physical separation of the two constituents in dried state (Figure 39-c and d).

In contrast to the (partial) bonding between MCC and cellulose matrix, the wood fibre appears to be completely separated from the regenerated cellulose (Figure 39-c and d). Hence, the large voids between the wood fibre and matrix phase are at least partially attributed to the high moisture sensitivity of the wood fibre. The chemical composition of the wood fibre could also play a role in the bonding behaviour of matrix and fibre. For instance, the cellulose microfibrils present in the wood fibre are surrounded by hemicelluloses and lignin that might be hindering direct contact between the matrix phase and microfibrils. It is postulated that under these conditions, hydrogen bonding complexes can only be partially formed between the cellulose present in the wood fibre and matrix phase. Moreover, wood fibre-matrix bonding based on mechanical interlocking is not possible due to the abovementioned differential shrinkage during

drying. It is hypothesised that a pre-treatment of the wood fibre with the IL could improve the chemical bonding between reinforcing and matrix phase by partially dissolving all present constituents [254] making them more accessible to the regenerated cellulose.

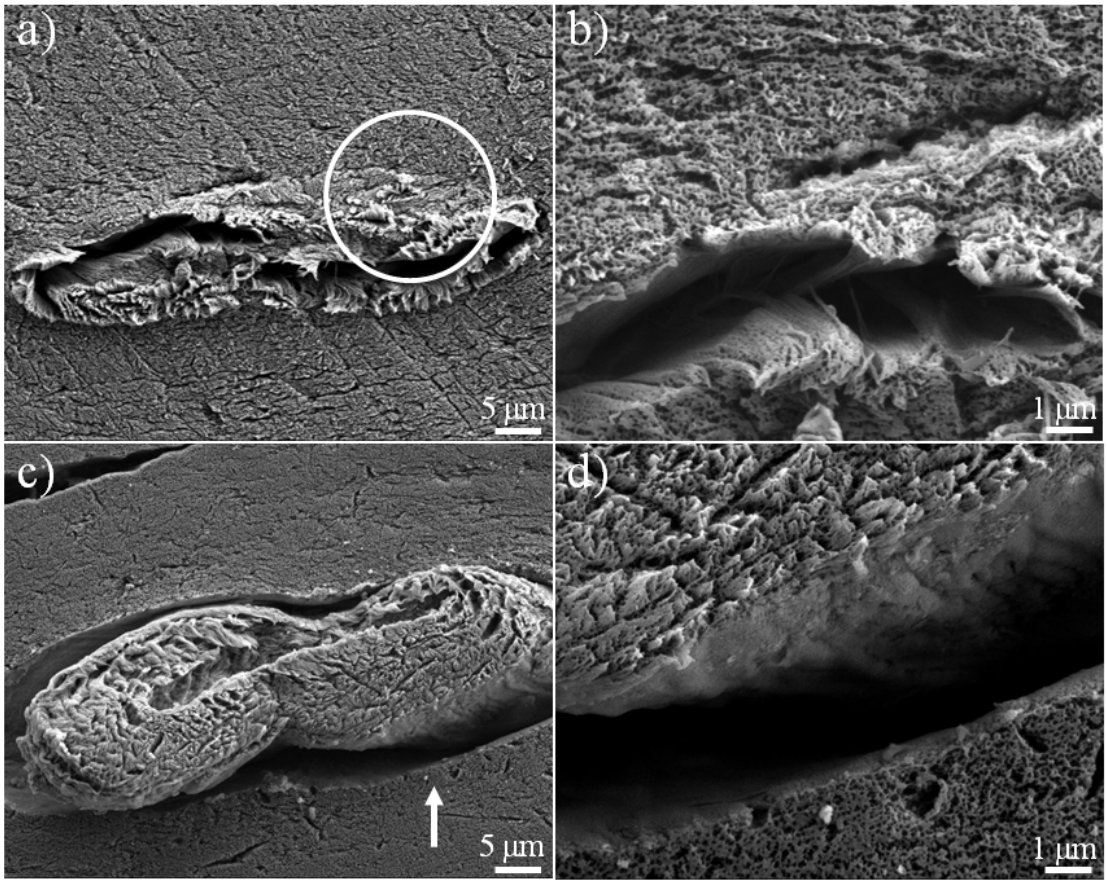

Figure 39: Scanning electron micrographs of the reinforcement-matrix interface for both an MCC particulate (a & b) and individual wood fibre (c & d) that are surrounded by a regenerated cellulose matrix. Marked are areas of very good bonding (a) and complete separation(c) between reinforcement and matrix phase. An acceleration voltage of 5 kV was used.

The width of cracks between the reinforcement and matrix phase was measured in an attempt to quantify the influence of moisture on the microstructure of the ACCs (Figure 40). Similarly, the width of longitudinal cracks in the regenerated cellulose was also examined as a function of humidity (Figure 40).

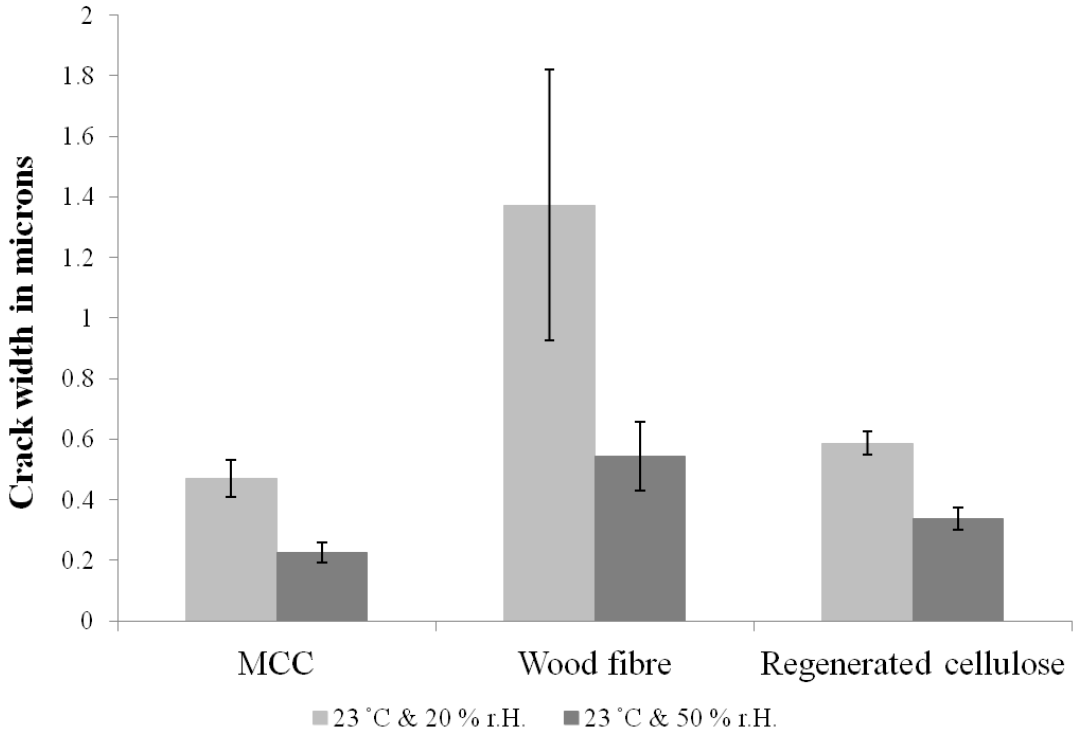

Figure 40: Average crack widths for the regenerated MCC and ACCs as a function of the humidity. Error bars indicate 1 standard deviation.

Interestingly, an increase in humidity of 30% invoked significant changes to the microstructure of all three materials. The wood fibre exhibited the largest average crack width. Additionally, the wood fibre exhibited the greatest sensitivity to humidity, with a decrease in crack width of around 60% as the RH was increased from 20 to 50%. The MCC and regenerated cellulose films exhibited less sensitivity to humidity with reductions in average crack width of 52% and 42%, respectively (Figure 40). The observed changes in the average crack width with humidity emphasises the importance of the environmental conditions on the microstructural integrity of an ACC.

3.2 ANALYSIS OF THE BOUND WATER CONTENT

DSC thermograms of the cooling cycle for the four ACC films show the presence of different types of present water. Two different peaks appeared for the two WF composites which are labelled as I (free water) and II (non-freezable bound water),

while for the MCC composites an additional peak can be seen, labelled II* (freezable bound water) (Figure 41).

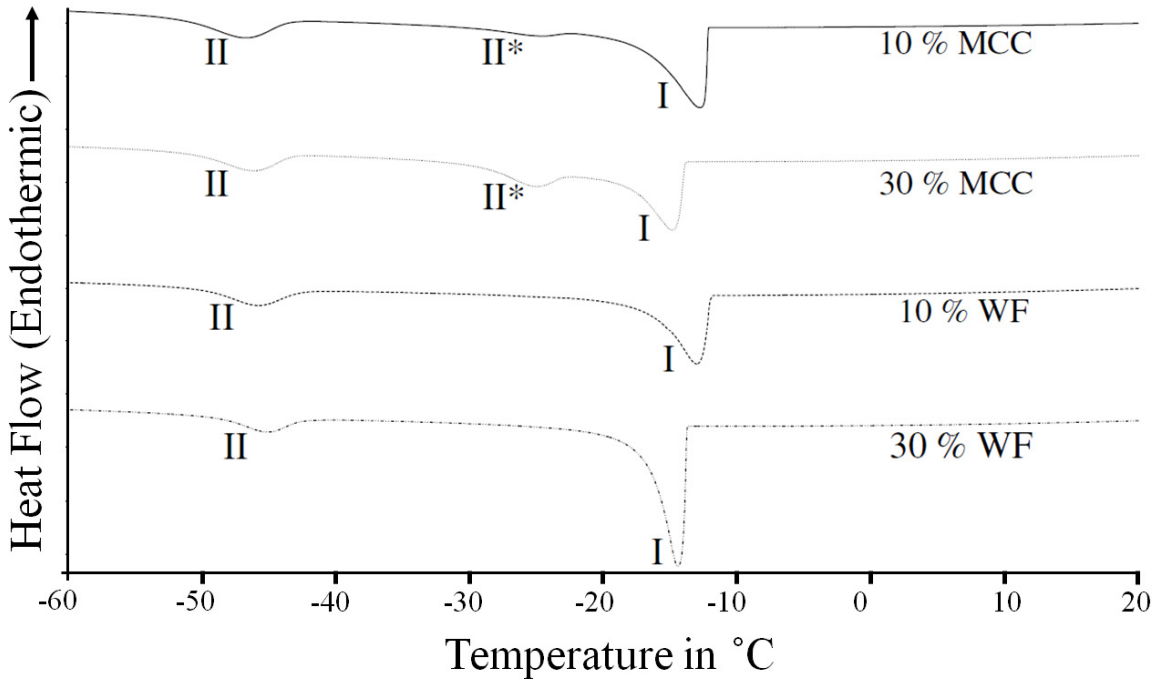

Figure 41: **DSC thermograms for heat flows of four types of ACCs (two MCC composites and two WF composites). The results were recorded while cooling from 30 ˚C to -70 ˚C at 5 ˚/min of the 4 different composite, showing the transitions of free water (I), non-freezable bound water (II) and freezable bound water (II*) in the 4 tested ACC films.**

Based on the DSC analysis results, the average peak values were calculated as given in Table 7. In the table the moisture present in the samples, free water and bound water contents are listed which were determined from the above displayed DSC results.

From Table 7, it is found that the WF composites has a higher free water content compared to the MCC composites, while more bound water is present in the MCC composites.

No recognizable amounts of freezing bound water seem to be present in the wood fibre composites. However, Hatakeyama *et al.* [282] report that the manifestation of peak II

and II* seem to merge with peak I at high water contents. It could therefore be possible that present bound water cannot be detected due to the high amount of free water present.

Table 7: Calculated peak areas, total water content and corresponding amounts of free water and bound water of the different samples.

Sample	Peak I in J	Peak II in J	Peak II* in J	Total moisture content in %	Free water content in %	Bound water content in %
10 % MCC	0.64	0.18	0.04	43.17	13.53	37.33
30 % MCC	0.46	0.16	0.11	43.54	10.54	38.95
10 % WF	0.58	0.17	-	42.04	20.79	33.30
30 %WF	0.83	0.13	-	45.06	26.13	33.29

The differences in amounts of free and bound water could give some more insight into the interaction between ACCs and moisture. The MCC composites show a slightly higher bound water content and lower free water content (Table 7) than the wood fibre composites. Water-filling voids in cellulosic structures has been referred to as “pore water” being a mixture of free and bound water [275]. As the cracks between reinforcement and regenerated cellulose are bigger for the WF composites (Figure 40), the water filling those cracks will be less closely connected to surrounding cellulose and can therefore be qualified as free water.

Bound water has proven to be difficult to remove from the composite structure [275]. It is therefore thinkable that a minimum of water will always be present even in vigorously dried composites. Water can act as a plasticiser for cellulose [109]. Thus, bound water present at the interface between reinforcement and matrix phase could lower the interfacial shear strength and therefore reduce the mechanical properties of

the ACC. On the other hand, rigorous drying of the ACC to remove any residual moisture could lead to the observed separation of matrix phase and reinforcement or longitudinal cracking due to different dimensional shrinkage. It could be shown that different reinforcement (*i.e.* MCC and wood fibre) exhibit different amounts of bound water. For ACC processing it will therefore be necessary to determine how much bound water is present in the used reinforcement and whether a critical amount exists that reduces the interfacial shear strength noticeably due to plasticising effects.

4. CONCLUSIONS

It could be shown that a low crystallinity matrix phase in the form of regenerated cellulose invokes significant moisture uptake in ACCs. As a result, microstructural damage in the form of longitudinal cracking and separation of the reinforcing and matrix phase are observed in ACCs following removal of the coagulant by drying. It is anticipated that the significant content of bound water in the composites will mean complete removal of the moisture is difficult; however, this is an important criterion for composite quality, as it could be shown that moisture influences the fibre-matrix adhesion and therefore very likely stress transfer in an ACC.

It is concluded that the two-step method for processing of ACCs *via* ionic liquids poses several challenges from an industrial perspective. Significant swelling and shrinkage occur during processing and under humid conditions due to the moisture sensitivity of the matrix phase created from completely dissolved cellulose. The sensitivity to humidity does not only cause dimensional instability but also influence the fibre-matrix bonding and inevitably, the mechanical properties of the composites.

Finally, intimate bonding between non-cellulosic components in the reinforcing phase and the cellulosic matrix phase is difficult to achieve in ACCs that are based on wood fibre and regenerated cellulose. It is concluded that a truly interfaceless composite is unlikely to be achievable using the 2-step method for the processing of ACCs.

V. NATURAL AND SYNTHETIC CELLULOSE FIBRE COMPOSITES *VIA* PARTIAL FIBRE SURFACE DISSOLUTION FORMED BY COMPRESSION MOULDING

1. INTRODUCTION

Other than the before described 2-step method for ACC manufacture, the 1-step method dissolves a portion of the reinforcement to regenerate the matrix phase *in situ*. This does offer the possibility of a very uniform matrix distribution, given that the solvent can be applied evenly. Hence, very high fibre volume fractions should be achievable and therefore minimise the negative effect of matrix shrinkage on the fibre-matrix interface observed in the 2-step method (Chapter IV).

As most ACCs produced do not exceed a thickness of 0.5 mm (see Table 4), their application potential remains limited. As dimensional shrinkage can be a problem in the 2-step method [108], it is questionable whether this method could be used to produce ACCs with a thickness above 1 mm and/or complex geometries. Using the 1-step method could therefore be a promising alternative to produce "thick" ACCs, if several layers of solvent-impregnated cellulosic textiles can be stacked and compacted. However, Duchemin *et al.* found the partial dissolution of MCC to form an ACC can lead to the creation of a skin-core structure in the composite caused by an uneven distribution of the solvent. A similar behaviour could be observed during the partial dissolution of rayon multifilament yarns (compare Section III.3.3.2). They explained this by poor penetration of used cellulosic material due to the high viscosity of the solvent [180]. Based on the finding described in Section III.3.3.2 it is possible that an increased

pressure during processing as for example used in compression could improve the solvent distribution and layer compaction.

Compression moulding is a common industrial process for the processing of thermoplastic and thermosetting matrix polymer composites. It is one of the most popular processes in the automotive industry for manufacturing 2D or simple 3D composite parts [283].

The basic principle of compression moulding involves the placement of the composite preform into a two sided rigid mould, which is then closed under pressure to give the final shape of the composite. Curing and compaction or thermoforming takes place inside the mould, often at elevated temperatures [284]. In particular, compression moulding is widely used in the German automotive industry for the production of natural fibre-thermoplastic composites (up to 61% in 2007) [285]. The most common thermoplastic matrices in Europe are based on polypropylene, while in North-America polyethylene is commonly used. Other polymers such as polystyrene and polyamide are also used as matrix materials [84]. Commonly-used natural fibres include flax and hemp, jute/kenaf, sisal, abaca and coir. A blend of fibres has proven advantageous as the fine fibres improve the adhesion between fibre and matrix due to their higher surface area, while coarser fibres provide good saturation of the felts and help avoid resin pockets [285].

Around 35% of composites used in the European automotive industry utilise a thermosetting polymer as the matrix material [285]. In general, higher mechanical properties are reported for composites based on a thermosetting matrix, although the material costs are higher and the resulting composites are difficult to recycle [286].

Commonly-used natural fibres for thermoset-matrix composites include flax, hemp or sisal, or fibre blends, usually in the form of textile preform such as non-wovens and to a lesser extend wovens. The thermosetting resin is normally applied to both sides of the textile after which the lay-up assembly is placed inside a mould typically made from steel or aluminium. The fibres are moulded into the desired shape and the resin is distributed throughout the textile and cured through the use of elevated pressure and temperature [287].

Sheet Moulding Compound (SMC) is a special form of compression moulded composite. SMC consists of fibres in the form of chopped fibre or woven textiles that have been pre-impregnated with a thermosetting resin (commonly termed a prepreg). Additional fillers or additives may also be incorporated into the prepreg. It is then placed in a mould and compacted under elevated temperatures to form a fully consolidated composite [64, 288].

SMC can be seen as a basis for the later described process to manufacture a thick or multi-layered all-cellulose composite. As the matrix phase will be created *in situ* the cellulosic fibres need to be in contact with the solvent before being processed into an ACC. This can be seen as a resemblance of the impregnation of natural fibres with thermosetting resin to prepare the prepregs used for SMC.

In this Chapter, compression moulding is adapted to the processing of ACCs that are based on synthetic and natural cellulosic fibres. Analogous to the concept of an SMC, a cellulosic fibre textile is pre-impregnated with the solvent prior to compression moulding. The concept leads to the development of thick, consolidated ACCs with the appropriate structural integrity that delivers ACCs with high mechanical properties.

2. EXPERIMENTAL PROCEDURES

2.1 MATERIALS

Two types of cellulose-based 2D textiles (unbleached flax and rayon) were trialled as precursor materials for the fabrication of ACC laminates. A typical household flax textile was purchased at a local textile store to be analysed as a low cost raw material. Flax fibre has an average cellulose I content of 70-75%, along with hemicelluloses (~ 15%), pectin (10-15%), lignin (~ 2%) and waxes (~ 2%) [289]. A single flax fibre is reported to have a tensile strength of up to 1100 MPa, Young's modulus of up to 26.5 GPa and a strain to failure of up to 3.2 % [38]. The flax textile was a simple plain weave textile with an area mass of 255 (± 3) g/m^2. Four layers were cut from each textile (120 × 120 mm) and dried in a vacuum oven at 80°C for 48 hr prior to use.

2.2 PROCESSING OF ACC LAMINATES

The individual laminae of the dried textiles were weighed after vacuum drying. The average mass of a single layer of the flax and rayon textile was 3.7 g and 4.7 g, respectively. Using a simple hand lay-up process, each lamina was hand-impregnated with a quantity of BmimAc equal to the average mass of a single layer of the textile and weighed again after impregnation to confirm the mass ratio. Four IL-impregnated laminae were stacked between two flat aluminium plates (125 × 125 mm × 2 mm). The laminate stack was then placed in a laboratory hot press at 110°C for 80 min. A pressure of 1.5 MPa was applied during the first 60 min for the initial dissolution, after which the pressure was increased to 2.5 MPa for the remaining 20 min to achieve further compaction of the laminae. Following the dissolution step, the assembly was removed from the hot press and placed in a bath of distilled water for 24 hr to remove the

BmimAc, thereby regenerating the dissolved cellulose. The laminate was then washed again in boiling distilled water for 48 hr to remove any residual IL. Finally, the laminates were vacuum-dried at 75°C for 24 hr using the hot press to simultaneously apply a constant pressure of 0.5 MPa. A schematic of the fabrication process is given in Figure 42.

2.3 MATERIALS CHARACTERISATION

Wide angle X-ray diffraction (WAXD) patterns were obtained with a Philips PW1729 diffractometer using Cu Kα radiation (λ = 1.5418 Å), voltage of 50 kV and current of 40 mA with 2θ increased in steps of 0.02°. The software PeakFIT (Systat Software Inc., Chicago, USA) was used for the data analysis. Peak assignment and Crystallinity index (CrI) calculations for cellulose I (formula 3) and cellulose II (formula 4) were carried out as described by Kljun *et al*. [290] using the formulas:

$$CrI = \frac{I_{200} - I_{am}}{I_{200}} x100 \quad (3)$$

$$CrI = \frac{I_{1\bar{1}0} - I_{am}}{I_{1\bar{1}0}} x100 \quad (4)$$

where, for cellulose I I_{200} is the maximum intensity at the 200 reflection at 2θ= 22.5° and I_{am} is the intensity at 2θ= 18°; for cellulose II $I_{1\bar{1}0}$ is the intensity of the $1\bar{1}0$ reflection at 2θ= 19.8° and I_{am} is the intensity at the diffraction of 2θ= 16°.

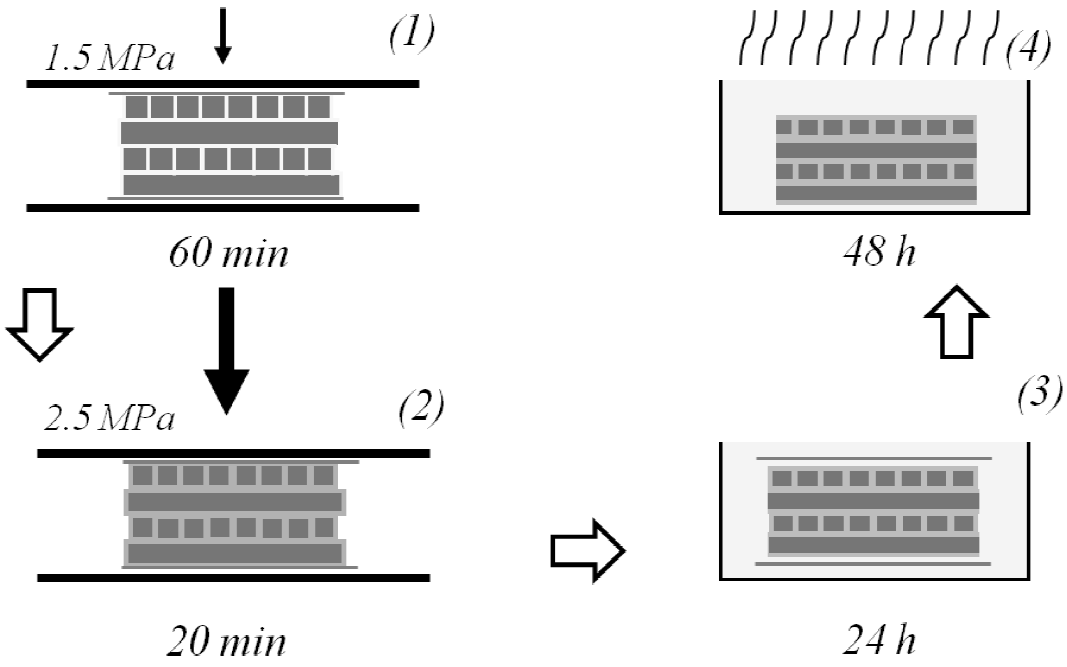

Figure 42: A schematic of the ACC laminate fabrication process. The various steps include (1) stacking of BmimAc-impregnated laminae between aluminium plates in a hot press; (2) additional compaction of the partially dissolved laminae; (3) removal of laminae from hot press and washing of the laminae in distilled water to regenerate the cellulose; and (4) removal of residual BmimAc by boiling in distilled water. The final drying step is not shown.

Samples (~3 × 5 mm) were cut from the laminates using a band saw (TOPMAQ, Christchurch, New Zealand) for observation of the cross-sections of the composites by reflected light microscopy (Leica DR IRM microscope). FE-SEM was used to observe the as-fabricated laminate surface, laminate cross-sections and fracture surfaces. Samples were cut from the laminates after testing using a diamond saw and dried in a vacuum furnace at 80°C for 24 hr. The samples were placed on carbon tabs and gold-coated for 180 s.

Five samples were cut from each laminate for tensile testing with a total length of 99 ± 2 mm and a width of 10 ± 0.5 mm. Additionally, 5 samples of the as-received flax and rayon fabric tested of the same width and length were tested. The gauge length was 40 mm. Pneumatically-controlled grips with an applied pressure of 0.4 MPa were used.

3. RESULTS AND DISCUSSION

3.1 PROCESSING-STRUCTURE CHARACTERISTICS OF ACC LAMINATES

The laminate fabrication process that was based on a simple hand layup approach was successful in compacting single sheets of cellulosic textile into a "thick" laminate composite. The final thickness of the laminates varied according to the type of textile used. The flax- and rayon-based laminates had thicknesses of 1.660 ± 0.01 and 1.98 ± 0.01 mm, respectively. The final mass of the ACC laminates after drying was compared to that of the original 4 laminae before the addition of the BmimAc. The flax- and rayon-based ACC laminates had increased in mass overall by 0.12 and 0.31 g, respectively, indicating that > 99 mass% of the BmimAc was removed during the washing procedures.

The as-received textiles could be converted into solid and stiff composite materials after processing with BmimAc, although the original weave structure was visible in the surface finish of the ACC laminates (Figure 43 b and d). It was clearly observed that there had been significant dissolution and regeneration of fibre surfaces, indicated by a smoothing of the textile surface and bonding of individual fibres within the yarn. In a recent related study, Haverhals *et al*. used the term "natural fibre welding" to describe the formation of a congealed, rigid network of fibres from a simple array of loose biopolymer fibres (silk, cotton and hemp) using the IL EmimAc as the solvent [291]. Essentially, natural fibre welding is simply chemical welding – a common industrial process that uses a solvent to permanently bond together plastic components. Haverhals *et al*. formed open networks of biopolymer fibre in their study rather than fully consolidated composites, thereby limiting improvement of the tensile strength

over the as-received fibres [291]. However, the work does demonstrate the possibility of chemical welding of individual natural fibres at the sub-macroscopic scale using an ionic liquid. The present work further demonstrates that with the addition of pressure, fully consolidated composite laminates are possible *via* chemical welding.

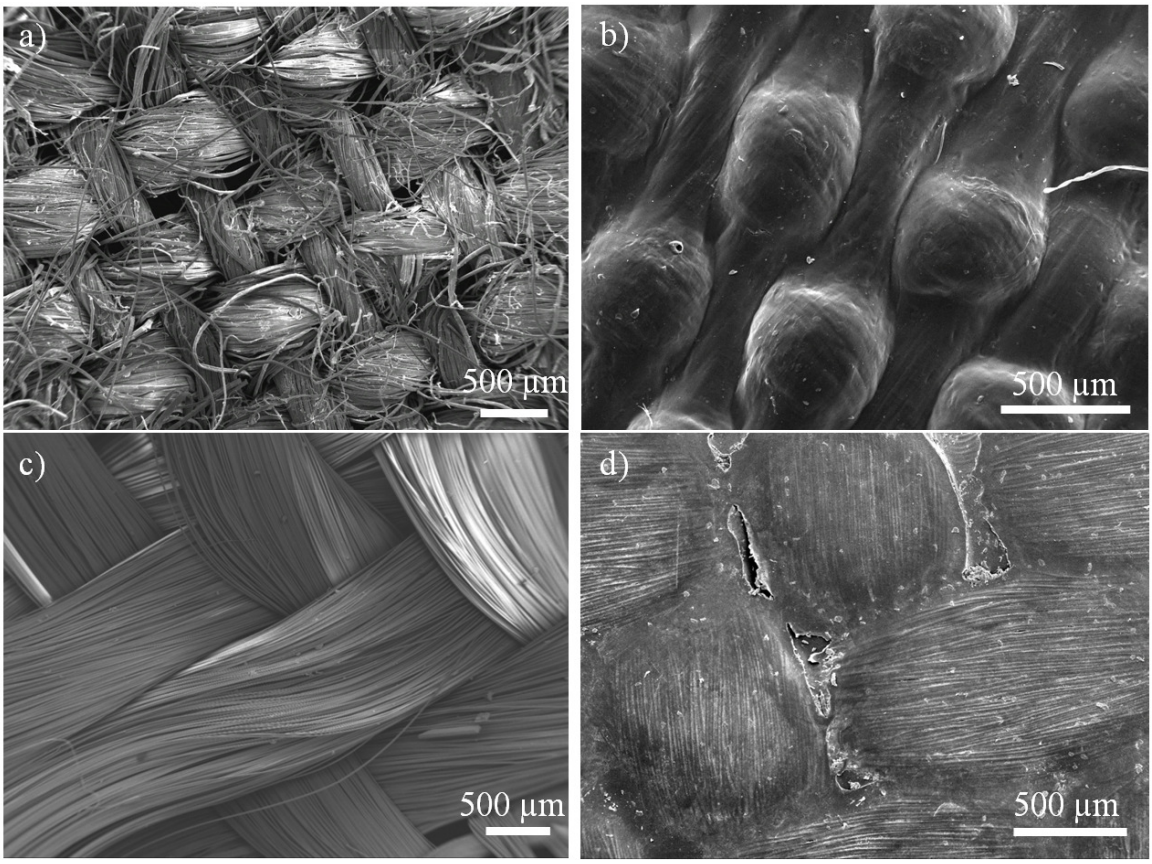

Figure 43: Scanning electron micrographs of the surfaces of the as-received (a) linen textile and (c) rayon textile, and ACCs based on (b) linen and (d) rayon. An acceleration voltage of 15 kV was used.

The examination of single yarns of flax after processing into a lamina (Figure 44b) reveals some regions of such extensive bonding of individual fibres that the outer perimeter of the fibres becomes indistinguishable. Other fibres may remain separated after processing, with large voids observed throughout the yarn (Figure 44b). A large variation in diameter and shape of the as-received, individual flax fibres is observed (Figure 44a) – a common problem of natural fibres, often making the properties of

biocomposites hard to predict [178]. Presumably, the poor uniformity of the fibre morphology restricts the even dispersion of IL through the textile, resulting in non-uniform dissolution across the yarn. Another factor affecting the dissolution behaviour and therefore the amount of created matrix phase could be the presence of lignin and hemicelluloses in the flax fibres. Sun *et al.* reported that for the complete dissolution of wood (a combination of cellulose, hemicelluloses and lignin) in EmimAc not all of the biomass could be recovered during regeneration [292]. It is thinkable that a similar process takes place during this experiment for the flax textile when dissolved by BmimAc, and non-regenerated fractions are removed from the composite during the washing stage. However, the small loss in starting materials determined from the final mass of the linen-based ACC indicates that only minuscule amounts of non-cellulosic components are washed from the material. Thus, it would appear that BmimAc has poor solvency for the non-cellulosic components at the used conditions. Interestingly, Casas *et al.* reported successful dissolution of wood in BmimAc at 140 °C under microwave irradiation. However lignin mixed with cellulose could not be regenerated in their experiments [293]. This does suggest that the herein used temperatures are not high enough to dissolve large amounts of non-cellulosic components and the small amounts that are dissolved will be washed out during regeneration.

The rayon fibres were observed to be more consistent in terms of fibre diameter and shape compared with the flax fibres (Figure 45a).

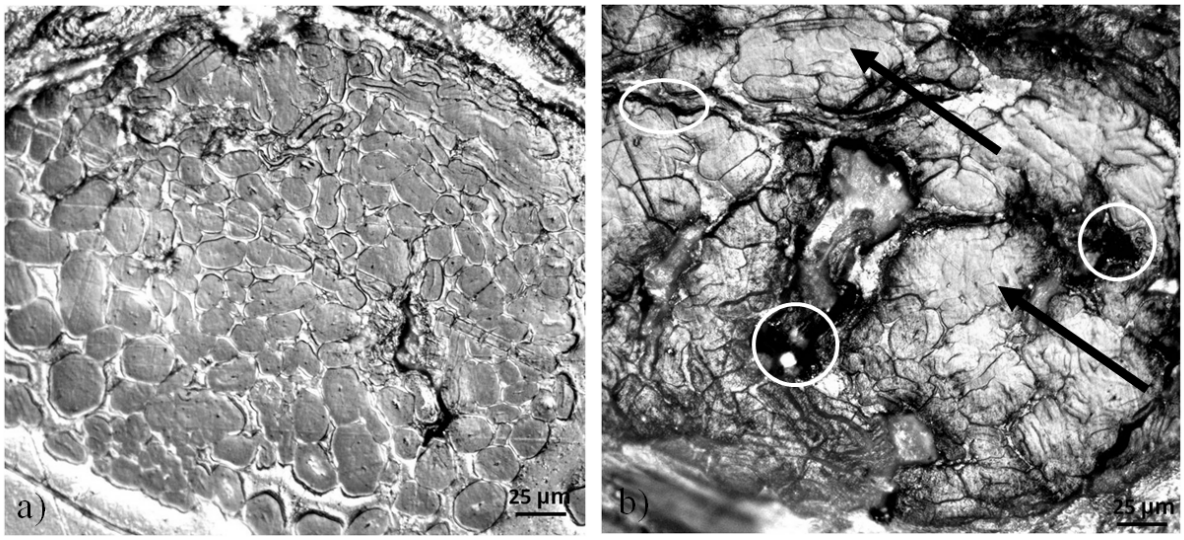

Figure 44: Reflected light micrographs of the cross-section of single yarns of flax (a) before and (b) after processing into an ACC laminate, where the black arrows indicate regions of extensive bonding of individual fibres. Intralaminar voids are marked with white circles.

The rayon-based laminates exhibited small regions between the original rayon fibres in which newly-formed matrix phase was observed (Figure 45b). Based on visual observation, the rayon-based laminates exhibited significantly less void formation in comparison with the flax-based laminates. The presence of small voids in those laminates is likely due to imhomogeneities introduced through the hand-impregnation of the textiles with BmimAc. The formation of small intralaminar voids was observed in both flax- (Figure 46 a and b) and rayon-based (Figure 46 c and d) laminates. However, interlaminar voids between 1000 and 2000 μm^2 were present in the flax-based laminates (Figure 46a) that could not be eliminated by compaction, suggesting that inadequate dissolution of the flax fibre surface of the interior laminate layers was the probable cause under these conditions.

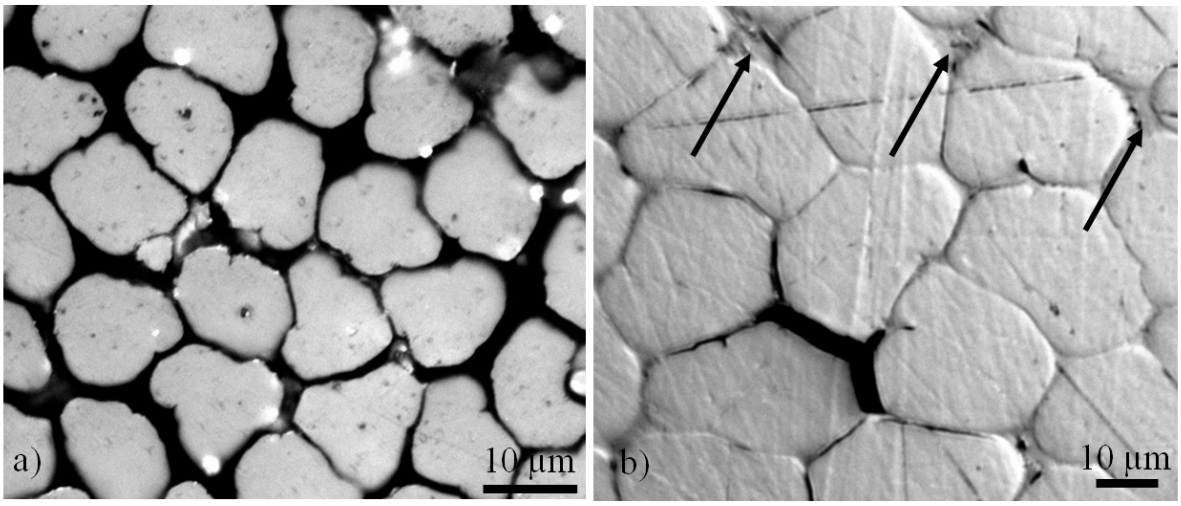

Figure 45: Reflected light micrographs of the cross-section of single fibres of rayon (a) before and (b) after processing into an ACC laminate, where the black arrows indicate regions of newly-formed matrix phase.

Cellulose is a strongly hydrophilic material [64]. Hence, the fibres and regenerated cellulose swell during the washing stage of the process (albeit at different rates) and then shrink again during the final drying step, as discussed in the previous Chapter. Duchemin *et al.* observed extensive volumetric shrinkage and warpage during regeneration and subsequent drying of an ACC processed *via* the one-step method [127]. Swelling and shrinkage will mostly affect the regenerated and therefore less crystalline fractions of cellulose [294]. Thus, shrinkage is expected in the ACCs synthesised *via* a partial dissolution route. However, it should be noted that the amount of regenerated cellulose is likely to be significantly lower via a partial dissolution route (1-step method) compared with the 2-step method. Accordingly, the shrinkage is observed to be negligible at the macroscopic scale. Nonetheless, the drying stage dramatically impacts on the matrix phase, leading to the observation of inter- and intralaminar voids (Figure 46). It is anticipated that a change in the drying rate or substitution of water with other coagulants such as alcohol or acetone could modify the propensity for void formation.

The positive effect of the applied pressure can be seen when comparing the rayon-laminate microstructure (Figure 46c and d) with the partially dissolved rayon yarns described in Section III.3.2. Partially dissolved rayon yarns (Figure 30a, b and c) showed an uneven dissolution throughout the yarn with an almost completely dissolved core region and less dissolved fibre in the yarn centre. A similar behaviour is not observed in the rayon laminates suggesting that the increased pressure improves solvent distribution during processing.

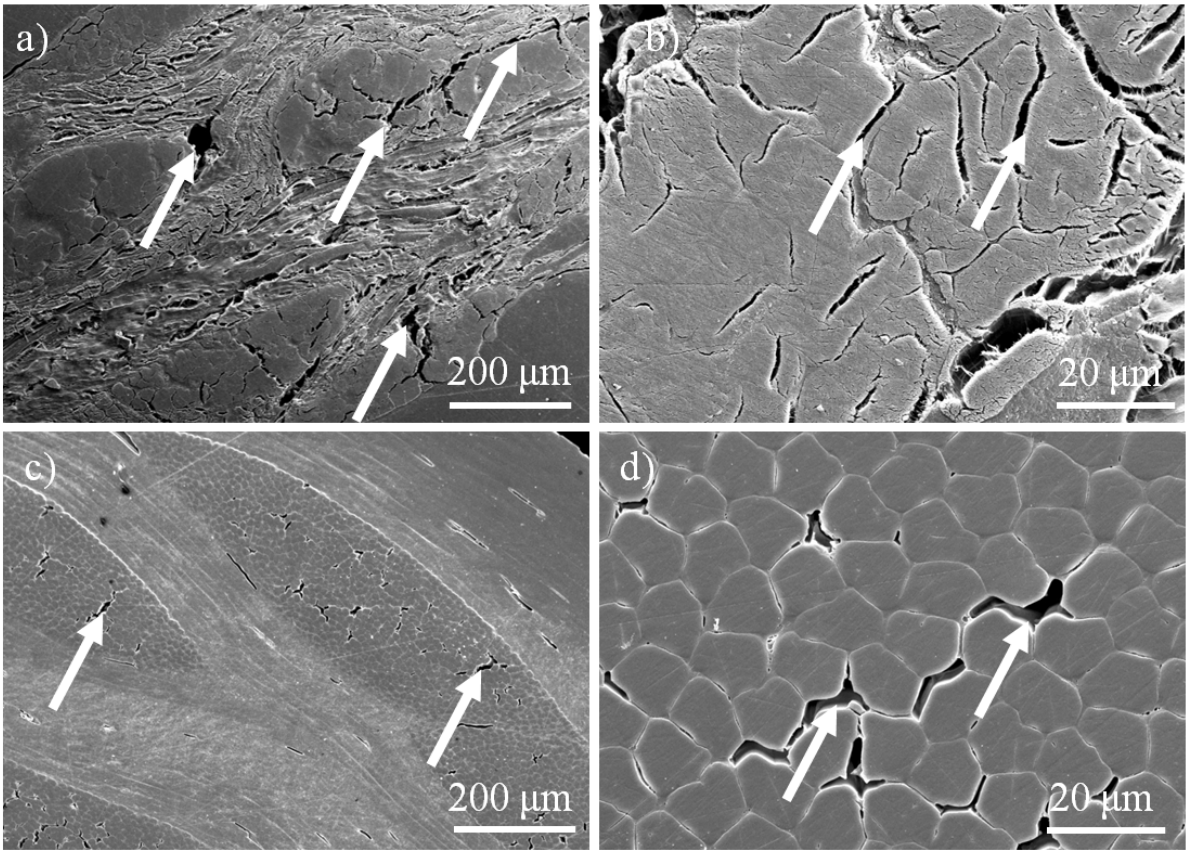

Figure 46: Scanning electron micrographs of the cross-sections of the flax (a, b) and rayon (c, d) laminates at low and high magnification. Interlaminar voids in the flax-based laminate are indicated by arrows in (a). Intralaminar voids are shown for both types of laminate as indicated by the arrows in b), c) and d). An acceleration voltage of 10 kV was used.

3.2 EFFECT OF LAMINATE PROCESSING ON PHASE COMPOSITION

Generally, dissolution and regeneration of cellulose I is believed to lead to a transformation to cellulose II, which is said to be a more stable form of cellulose due to

the anti-parallel packing of the single cellulose chains in contrast to parallel packing in cellulose I [85]. For the case of cellulose dissolution in an IL, Zhao *et al.* [167] also report the phase transformation from cellulose I to cellulose II. However, in the present study, only negligible changes in the crystallinity between the linen textiles (81 %) and the linen laminates (84 %) were observed (Figure 47). Thus, it would appear that only minimal amounts of cellulose were dissolved from the flax fibres under the experimental conditions – a fact supported by the microstructural examination (Figure 44, Figure 46). Soykeabkaew *et al.* reported limited dissolution behaviour of ramie fibres in LiCl/DMAc where only the primary cell wall was dissolved [105]. It is postulated that the modest dissolution of flax fibres results from the IL readily dissolving the less ordered S1 layer, while the highly-ordered, densely-packed S2 layer remains intact [105].

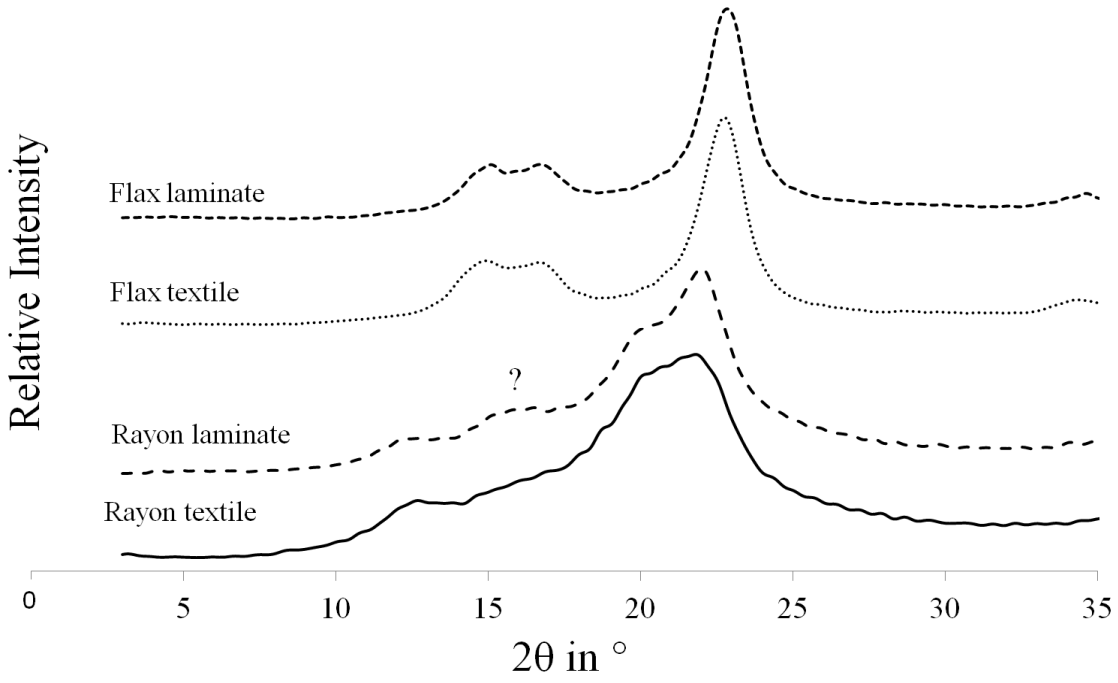

Figure 47: X-ray diffractogram of the as-received 2D textiles and final ACC laminates. The curves of the rayon laminate, flax textile and flax laminate have been offset for clarity. The question mark indicates an unidentified peak.

The rayon fibres consisted of cellulose II as indicated by peaks at 2θ = 12° for the (101) plane and 2θ = 22° for the (002) plane [295]. However, additional peaks appear at 2θ = 16.36° for the ACC laminate. Rihm reported a peak at 2θ = 15.5° after ball-milling regenerated cellulose fibres, attributing this peak to cellulose I or cellulose IV [296]. However, since cellulose II does not transform into cellulose I [101], it is possible the rayon laminate is a mixture of the two crystal lattices cellulose II and cellulose IV_2. Buleon *et al.* [297] describe the formation of such a hybrid crystal formed from cellulose II and IV by the deacetylation of cellulose triacetate in a mixture of methylamine, DMSO and water in the temperature range of 90-150°C. Furthermore, it has been reported that treatment of cellulose II in boiling water leads to the formation of cellulose IV [46]. Thus, it may be possible that either small amounts of cellulose IV or the aforementioned hybrid crystal of cellulose II and IV are formed as a result of washing the laminates in boiling water.

The crystallinity of the as-received linen textile was determined to be 81% being higher than that found for the rayon textile with 77 %. It is known that less crystalline cellulose dissolves more readily in an IL [263]. Therefore, it is also possible that the dissolution time needs to be extended to increase dissolution of the linen fibres.

3.3 TENSILE PROPERTIES OF ACC LAMINATES

The microstructural composition of the linen laminate was characterised by a low matrix phase content. As might be expected, the formation of insufficient matrix phase at the fibre interfaces is detrimental to the tensile strength and Young's modulus. The linen laminate had an ultimate tensile strength of 46 MPa which was a small improvement over a single layer of the as-received linen textile measured as 36 MPa.

Thus, the matrix does transfer load to the reinforcement in these ACCs in spite of the low levels of regenerated matrix phase. In fact, the properties of the linen-based ACCs exceed those of non-woven flax reinforced-HDPE biocomposites (fibre volume fraction: 10-30%) [298] and they are on par with other biocomposites based on flax fibre mats and mucilage polysaccharides (*e.g.* Alix *et al.* [299], fibre weight fraction: 35%) or soy protein concentrate [300] (fibre volume fraction 43 %). It is thought that another possible contribution to the improved tensile strength of the linen-based ACC over the as-received linen textile is the removal of crystallographic defects that are present in S1 *via* the abovementioned preferential dissolution of S1 with respect to S2 [110]. In contrast, woven flax-epoxy composites can have a tensile strength of 81-111 MPa (*e.g.* Goutianos *et al.* [301]), suggesting the potential for significant improvement with further manipulation of the processing parameters.

Although flax fibres are considered to be stiff [38], the laminate has a low stiffness of 0.86 GPa. This is most likely caused by the low amounts of matrix phase that could act as a support between the single fibres and the 4 lamina. The absence of a sufficient amount of matrix phase can be seen as an increase in void content, therefore reducing the overall stiffness. However, the poor interfacial adhesion will be the main contributor to the low stiffness of the flax laminate [70].

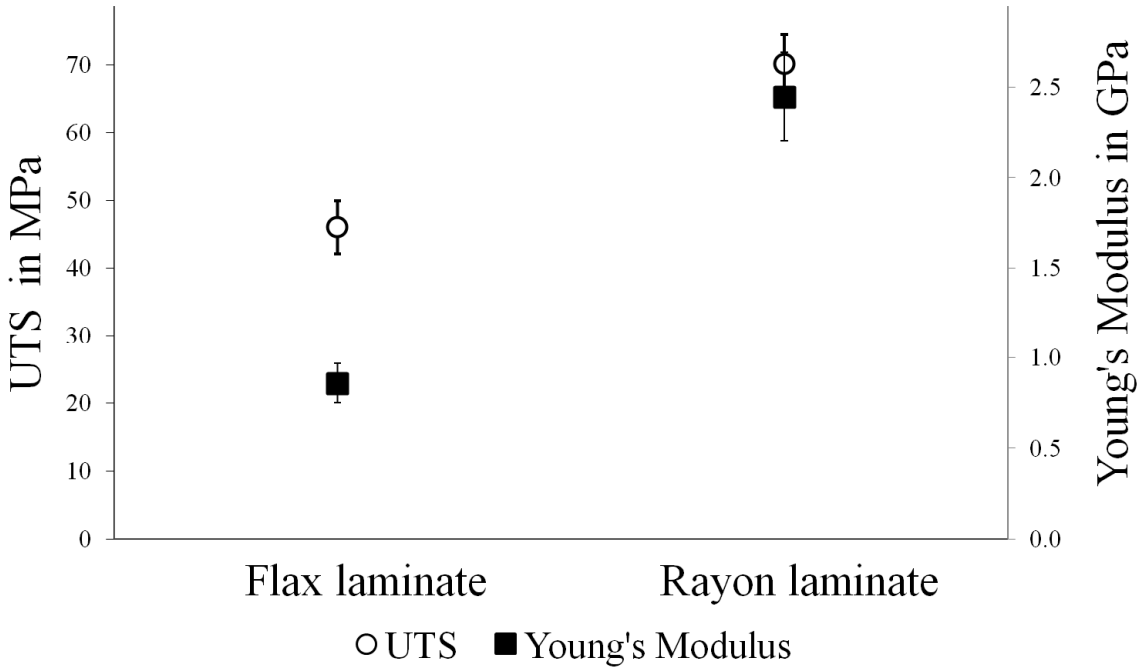

Figure 48: Tensile strength and Young's modulus of the flax and rayon laminates. One standard deviation is indicated by the error bars.

In contrast, the rayon-based ACC laminate had almost twice the tensile strength of the flax laminate with a value of 70.16 MPa. The untreated rayon textile had a tensile strength of 36.67 MPa, confirming that there is extensive fibre-matrix adhesion generated by the compression moulding process. The strong adhesion and decrease in void content are also reflected by a higher Young's modulus of 2.45 GPa. It is interesting to see that the rayon fibre, although less strong and stiff than flax can be synthesised into a stronger and stiffer composite. The reason for the higher tensile properties is an improved fibre-matrix interface that results in a better load transfer and therefore improved mechanical properties.

3.4 FRACTURE BEHAVIOUR OF ACC LAMINATES

The fracture surface of the flax laminate exhibits delamination of the laminate layers and separation of fibre bundles within a single layer (Figure 49a). Individual fibres show little or no adhesion to neighbouring fibres (Figure 49b). Again, the lack of

bonding between adjacent fibres suggests inadequate formation of a matrix phase. Additionally, the fibres appear flattened which is likely a result of the pressure applied during dissolution and regeneration.

The fracture behaviour of the rayon laminate was distinctly different to that of the flax laminate, with the textile layers remaining bonded to each other following tensile fracture (Figure 49c). The individual fibres and yarns of the rayon laminate are still identifiable, but show very little separation under load, indicating improved adhesion between the fibres (Figure 49d). This can be seen as evidence for a small amount of matrix phase being present around each fibre, created by dissolution and regeneration of fibre surfaces that connecting the single fibres to form an almost interfaceless composite.

Although the surface view of the flax fabric (Figure 43), shows a structural change of the fibres by treatment with the IL, the observations of the tested samples supports the assumptions that the reaction time the flax fabric has not been long enough to dissolve more of the fibre surface and therefore creating a sufficient matrix phase due to the aforementioned reasons. The higher crystallinity of flax fibres compared to rayon could be a reason for the slower reaction time. It is also possible that the additional components of the natural fibres such as hemicelluloses, lignin and pectin influence the dissolution reaction [169].

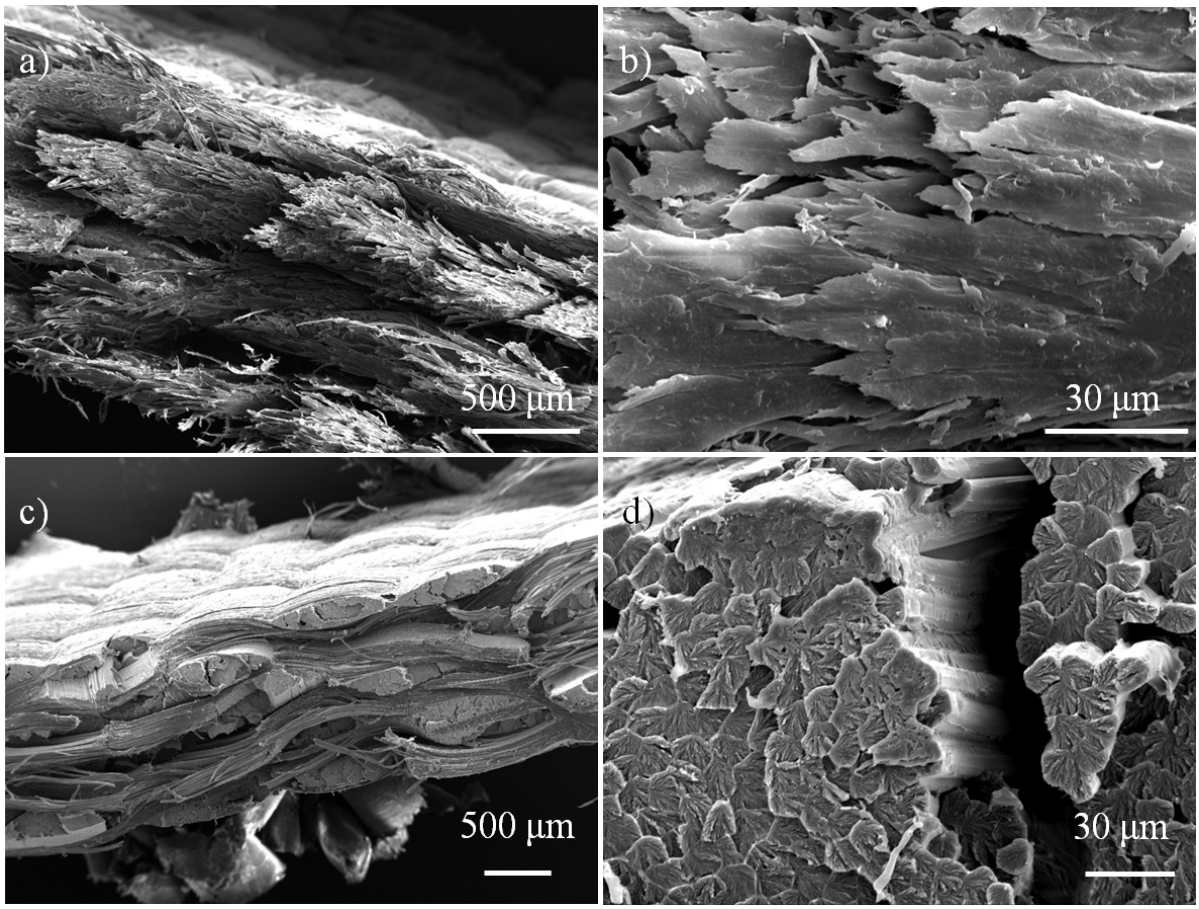

Figure 49: Scanning electron micrographs of the fracture surfaces of flax (a, b) and rayon (c, d) laminates. Images are provided at low and high magnifications to show the overall laminate fracture surface (a, c) and the individual fibres (b, d), respectively. An acceleration voltage of 10 kV was used.

4. CONCLUSIONS

It could be shown that the production of a multi-layered, "thick" ACC is possible using a simple processing route that is based on hand lay-up/compression moulding approach – a basic process still commonly used by the composites industry. The new processing route could potentially broaden the range of applications for ACCs by offering a facile method for fabricating thick ACC laminates.

This work shows that through appropriate solvent and textile selection it is possible to dissolve sufficient cellulosic material from the fibre surfaces to provide a matrix *in situ* that bonds together both the (I) yarns within a 2D textile and (II) adjacent 2D textile

layers to form a solid, “thick” and low-porosity composite laminate. Pressure during the dissolution process appears to be necessary to achieve a strong interlaminar adhesion when using multiple layers of reinforcement and improves solvent distribution.

It is clear that the rayon textile dissolved more efficiently in BmimAc compared with the flax textile. Nevertheless, it could be shown that the flax textile does dissolve in the IL, but needs longer dissolution times to form a consolidated composite. This work shows that synthetic cellulosic fibres are preferable over natural fibres for solvent-processing, as the constant fibre dimensions and more homogenous fibre composition allow better and more even fibre dissolution, resulting in a composite with improved fibre-matrix interfacial properties. Furthermore, the non-cellulosic constituents in natural fibres are thought to interfere with the dissolution process although this aspect needs further clarification. Future work will be necessary examine in more detail the differences between the dissolution behaviour of cellulose I and cellulose II, the resulting phase composition in the final ACC laminates, and the relationship between process parameters and laminate quality. However, as result of the more predictable dissolution behaviour of the rayon fibres, those will be used for all following composite processing adaptations.

A drawback of the used impregnation/hand lay-up method can be uneven solvent distribution leading to less dissolved areas within the composite. Improved solvent distribution could therefore lead to more homogenous composites.

ILs possess the advantage of an extremely low vapour pressure and therefore do not emit any hazardous fumes in contrast to some polymer resins or other solvents. However, their strongly hydrophilic character leads to moisture absorption and

potentially a reduction in solvency. Processing of ACCs in a closed, ideally air-free, cavity could therefore proof beneficial.

VI. ALL-CELLULOSE COMPOSITES PROCESSED *VIA* SOLVENT INFUSION

1. PROCESS DEVELOPMENT

1.1 INTRODUCTION

The general principle of creating an all-cellulose composite by the partial dissolution of woven textiles using an ionic liquid was successfully demonstrated *via* a hand-impregnation/compression moulding approach (Chapter V). However, the use of a hand-impregnation approach has some decisive disadvantages. The quality of traditional composites that are prepared by the hand impregnation of carbon- or glass fibre reinforcements with thermosetting resins is strongly dependent on operator skill, where poor workmanship results in void formation and/or insufficient fibre wetting [284]. Similarly, insufficient fibre wetting by the solvent during the partial dissolution of cellulose fibres will result in the inconsistent formation of the matrix phase, leading to poor fibre-matrix adhesion in the final ACC.

Likewise, the use of an ionic liquid for the dissolution of cellulose has disadvantages. In general, ionic liquids have the advantage of low volatility which makes for safe handling of the solvent. However, ILs are strongly hydrophilic and exposure to air is to be avoided during processing to avoid moisture absorption. The presence of moisture in the cellulose-IL solution dramatically reduces the solvency of certain ionic liquids for cellulose as discussed in Chapter III [130]. Indeed, both the IL and cellulose textile require protection from moisture absorption during processing to ensure that dissolution will proceed.

An alternative “clean” process to hand lay-up was developed as early as 1950 for the production of boat hulls, called the Marco method. In this method, a dry reinforcement is laid down on a solid tool and covered with a semi-flexible/splash layer to provide a seal for the application of a vacuum. The vacuum is then used to infuse a thermosetting resin into the reinforcement. The Marco method served as the basis for the development of a whole family of process methods known collectively as Vacuum Assisted Resin Transfer Moulding (VARTM) [302]. Hammami and Gebart [303] identified the key advantages of VARTM as:

- a higher fibre volume fraction (~60-70 wt.%) compared to open mould processes (~45 wt.%);
- low void content (< 1%);
- increased specific mechanical properties;
- volatile–free processing;
- low cost investment and reduced manual labour;
- high cost-efficiency for small production runs; and
- fabrication of large and highly integrated structures.

Typical applications of the VARTM process include marine, military and civil applications (*e.g.* bridges, wind turbine blades, *etc.*). The Seeman Composites Resin Infusion Molding Process (SCRIMP™) is the most common variant of VARTM (Figure 50) [304].

A new processing route conceptually based on VARTM route termed solvent infusion processing (SIP) is developed and analysed in this chapter. In a similar way to the resin infusion, it is assumed that an applied vacuum can contribute to a homogeneous solvent

distribution while at the same time minimising air contact and therefore moisture uptake. This will lead to an improved dissolution behaviour creating a more uniform matrix phase evenly throughout a textile reinforcement. Furthermore, the vacuum based infusion will lead to a minimised use of the IL, not only leading to a high fibre volume fraction by avoiding over-dissolution but also reducing processing costs. In accordance with the previously developed hand lay-up, the stacking of several layers of reinforcement will allow the production of "thick" ACC laminates. Resembling VARTM this processed could ideally be semi-automated, reducing labour-costs and allowing the production of large parts. Such a process could resemble a significant improvement to ACC processing from the current laboratory experiment style to a process that could be adapted by the composite industry.

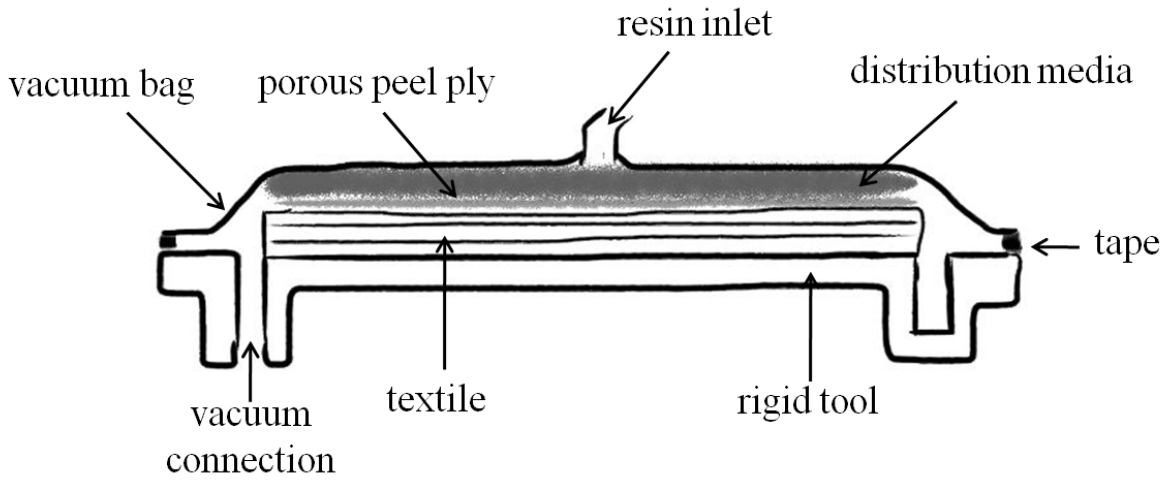

Figure 50: Sketch of the SCRIMP™ process set-up adapted from Seeman *et al.*,[305].

In this Chapter, a processing route termed solvent infusion processing (SIP) that is conceptually based on VARTM is developed to produce thick (> 1 mm) ACC laminates.

1.2 EXPERIMENTAL PROCEDURES

1.2.1 Processing Routes

The processing route for ACCs used in this work is described herein as solvent infusion processing (SIP) which is a modification of VARTM traditionally used for producing large-scale composite structures.

SIP is divided into 5 distinct stages: (I) vacuum-assisted infusion of IL (BmimAc) through the textile layers; (II) partial dissolution of the surface of the fibres at temperatures around 100 ˚C under pressure; (III) infusion of a coagulant (distilled water) that regenerates the dissolved cellulose by interfering with cellulose-IL interactions; (IV) washing to completely remove the IL; and (V) drying under applied pressure to consolidate the laminae, leading to the formation of a cellulose fibre-reinforced cellulose matrix composite, or all-cellulose composite (ACC).

SIP is based on the typical set-up for vacuum assisted resin infusion that utilises a vacuum pump to infuse an arrangement of fibre reinforcements, usually in the form of a dry textile preform, with a low viscosity thermosetting resin. The reinforcement is laid on a non-flexible mould while the other half of the mould is flexible (e.g. vacuum bag), enclosing the textile layers during VARTM. Once the infused resin has wetted the reinforcing fibres, curing of the resin takes place to form the matrix.

For the SIP experiments, 4 textile layers were placed between two sheets of perforated plastic film (~140 × 140 mm; hole diameter *ca.* 1 mm) to (I) improve the distribution of the IL and water and (II) prevent migration of the cellulose-IL solution, following the IL infusion. Sheets of 125 × 125 mm were cut from the rayon textile and dried before

composite processing. The dry thickness of the textile was approximately 0.55 mm. Distribution media was used to enhance the flow of the IL across the textile layers (Figure 51 & Figure 52). A vacuum pump delivered a constant pressure of 0.1 MPa during the solvent infusion.

The effect of the inlet and vent positioning on solvent flow during infusion, and thus the efficiency of the infusion process and corresponding cellulose dissolution, was investigated using either a radial or rectilinear infusion set-up (Figure 51). The radial and rectilinear infusion arrangements required approximately 35 g and 31 g of IL, respectively. The slightly higher amount of IL for the radial set-up is likely to be the result of the set-up geometry creating a small gap between the inlet and textile which is filled with IL during the infusion. Three variants of the infusion procedure were examined: (I) radial infusion followed by sealing the mould (inlet and vent), placing the assembly in an oven at 95°C for 60 min, and regenerating with an infusion of 500 ml of distilled water (L1); (II) as for (I) except the vacuum pressure (0.1 MPa) was reapplied every 30 min for 10 min with a total dissolution time of 90 min in the oven (L2); and (III) rectilinear infusion followed by the assembly being placed in laboratory hot press at 95 °C and 0.2 MPa for 60 min, and regenerating in a 2 l bowl of distilled water (L3). The dissolution temperature was used based on the findings of Swatloski *et al.* [130] and the experiments reported in Chapter III to allow the cellulosic fabric to be dissolved without causing any thermal degradation. After the initial regeneration had taken place all of the samples (L1, L2, L3) were washed in distilled water for 24 hr and then dried in the hot press at 60 °C and 0.02 MPa for 4 hr followed by 4 hr at 100 °C. Collection of the water-IL mixture followed by evaporation of the water allows the recovery of the used

IL. A schematic of the various steps involved in SIP (for the rectilinear set-up) is shown in Figure 52.

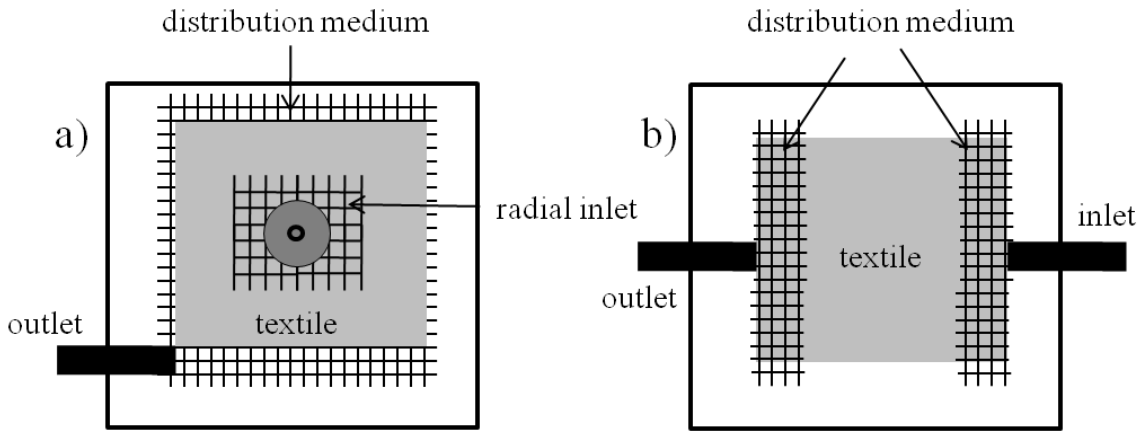

Figure 51: Schematics of (a) radial infusion and (b) rectilinear infusion set-ups used in SIP.

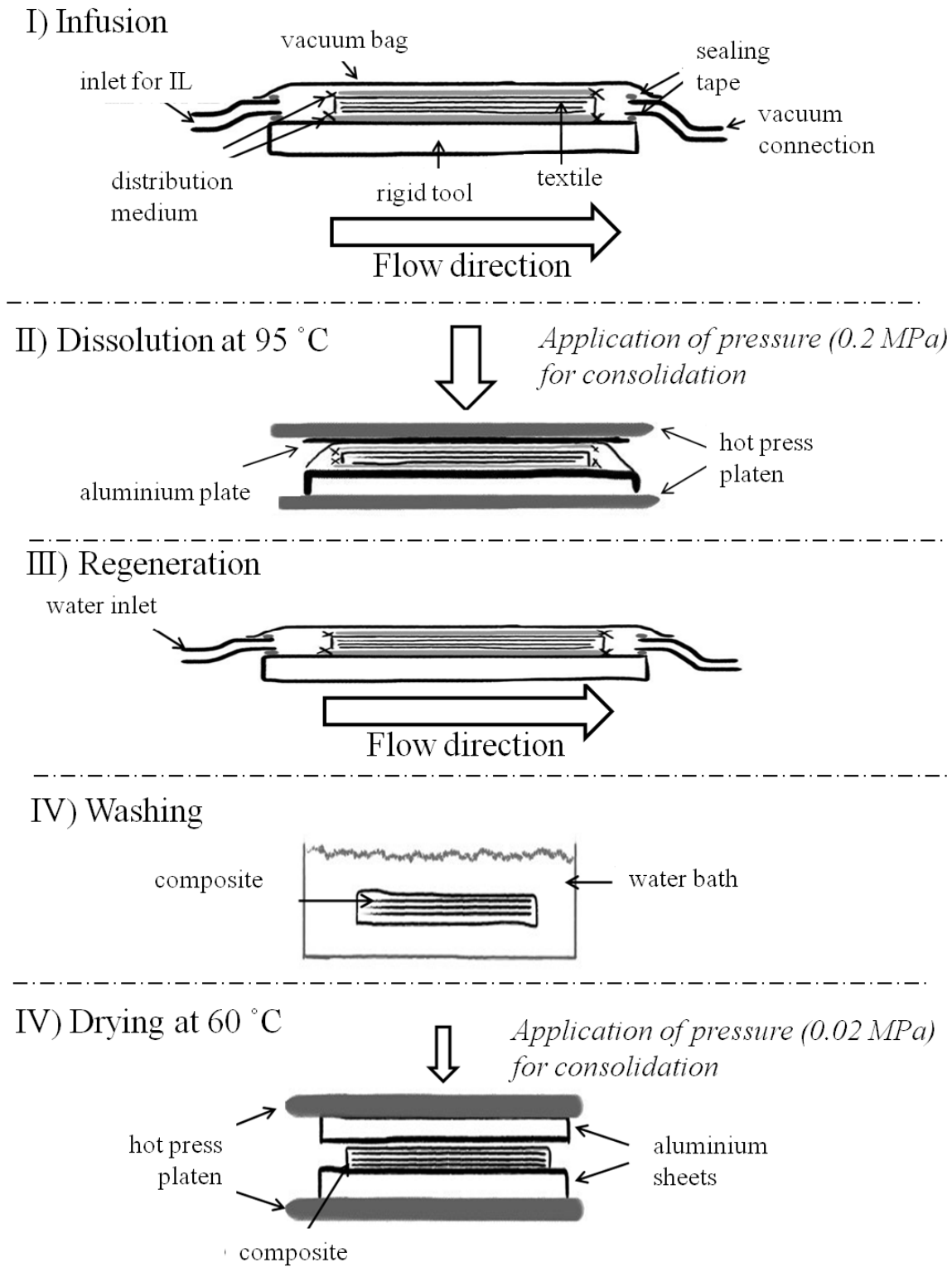

Figure 52: Schematic of SIP using the rectilinear infusion set-up.

1.2.2 Tensile Testing

Samples with dimensions of 110 mm (length) by 10 mm (width) by 1.6-2.3 mm (thickness) were cut from the laminates. The samples were conditioned at 50% RH and 23 °C for 24 hr before testing. Sample widths and thicknesses were carefully remeasured following the conditioning procedure. Pneumatic grips with a pressure of 0.3 MPa were used to clamp the samples. The gauge length was 40 mm. The presented results are the average values of 5 samples of L1, 8 samples of L2 and 7 samples of L3.

1.2.3 Scanning Electron Microscopy

SEM analysis of the microstructure of the ACC laminates was carried out on samples with dimensions of 5 mm (length) by 10 mm (width) that were cut from the laminates with a diamond saw. The cut samples were immersed in liquid paraffin wax for about 5 seconds before mounting in epoxy resin. Subsequent removal of the paraffin wax then allowed examination of the void content. SEM analysis of the fracture surfaces of the tensile samples was carried out by cutting of samples ~5 mm below the fracture face using a diamond saw.

Samples were prepared for FE-SEM by firstly drying in a vacuum furnace at 80 °C for 24 hr, then placing the samples on carbon tabs and gold coating them for 180 s at 25 mA.

1.2.4 Analysis of the solvent-fibre Interaction

To determine the effect of the solvent on the fibre geometry, the fibre cross-sectional area of 25 fibres of each laminate was measured using randomly selected areas of the SEM micrographs of the mounted untested samples. As a reference value, a sample of the original fabric was prepared in the same way as described above. The fibre area was

measured using the software ImageJ 1.42. Additionally, 5 micrographs of each composite were analysed to measure the interlaminar void size between single plies and measured using ImageJ.

1.2.5 Determination of the Fibre Volume Fraction

The precise determination of the amount of newly-formed matrix phase in ACCs is complicated by the chemical similarities of the matrix and reinforcing phases, making the detection of the fibre-matrix interface non-trivial. Therefore, to determine the fibre volume fraction (V_f), 6 SEM micrographs were analysed for each laminate using the ImageJ software. Fibre areas, non-fibre areas and total graph areas were carefully measured to calculate the according to formula 5:

$$V_f = \frac{\sum A_f - \sum A_{nf}}{A_g} \tag{5}$$

Where V_f is the fibre volume fraction, A_f is the fibre area, A_{nf} is the non-fibre area, i.e. matrix area, voids or cracks and A_g is the total area of the analysed micrograph.

1.3 RESULTS AND DISCUSSION

1.3.1 Effect of SIP on the synthesis of ACCs" for example

SIP was observed to be a facile method for producing strong and tough ACC laminates that are more than three times the thickness of ACC films reported in literature. The process can theoretically be extended to the production of ACC laminates that are several millimetres thick by increasing the number of textile layers used during SIP. As a proof of concept, a twelve layer laminate with a thickness of 4.8 ± 0.02 mm was

produced, shown in Figure 53. No dimensional shrinkage could be observed in any of the produced laminates. Hence, SIP provides a possible route for upscaled production of thick ACC laminates in a commercial setting, providing motivation to continue the development of this unique class of biocomposites.

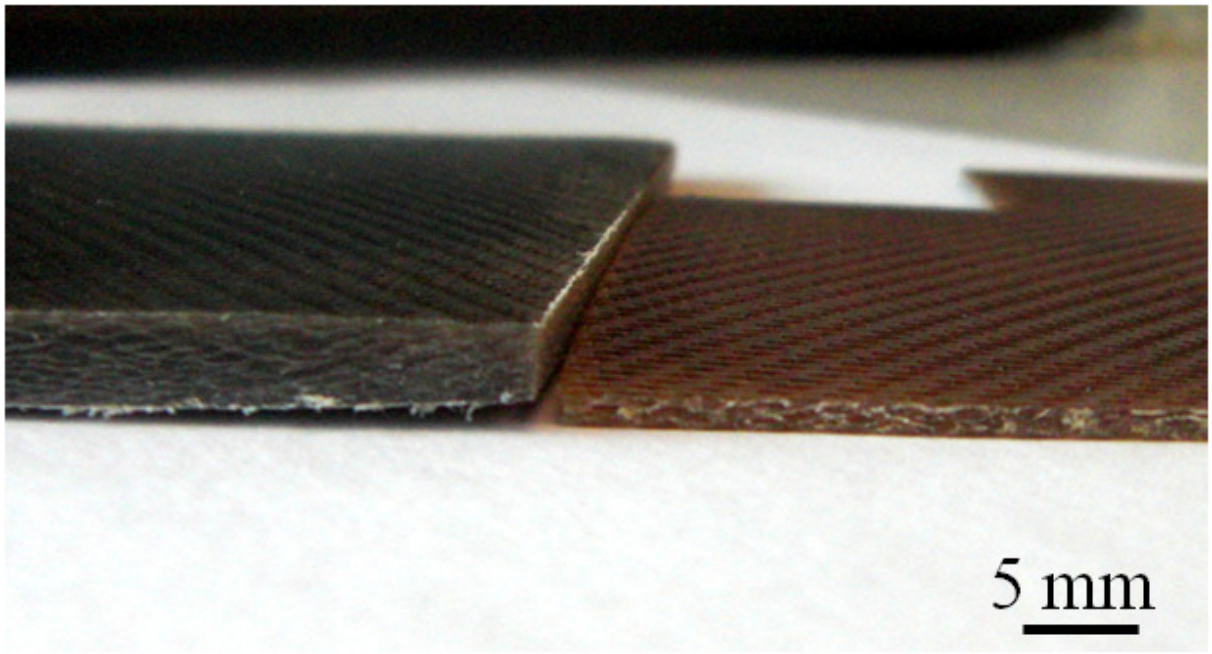

Figure 53: Photograph of a 12 layer SIP ACC rayon laminate compared to a 4 layer SIP ACC rayon laminate.

Both radial and rectilinear set-ups successfully produced consolidated laminates based on 4 layers of the textile. However, the ACC laminates exhibit significant differences in their consolidation behaviour and final thickness depending on the processing conditions. The final thickness of ACC laminates is a strong function of the applied pressure, reducing the average thickness of the laminates by 5 % to 2.28 ± 0.06 mm for L1, by 21.25 % to 1.89 ± 0.06 mm for L2 and by 31.5 % to 1.66 ± 0.04 mm for L3.

The distribution medium and inlet used in the radial set-up were pressed into the dissolved and malleable portion of the cellulosic textile during the pressure application

of L2, leaving a distinct imprint in the centre of the panel (Figure 54c). Thus, the distribution medium was placed only on the sides of the textile layers for the rectilinear infusion set-up to minimise the overlap of distribution medium and textile.

Visual differences could not be observed between the three different set-ups during wetting of the rayon layers with the IL. However, the formation of water pockets was observed after the regeneration of L1. The pockets were visible in the form of bulges on the laminate surface, indicating that the layers were partially separated during water infusion. Although the water was removed during drying, it appears to cause material inhomogeneities as indicated by discoloured regions on the laminate surface of L1 (Figure 54).

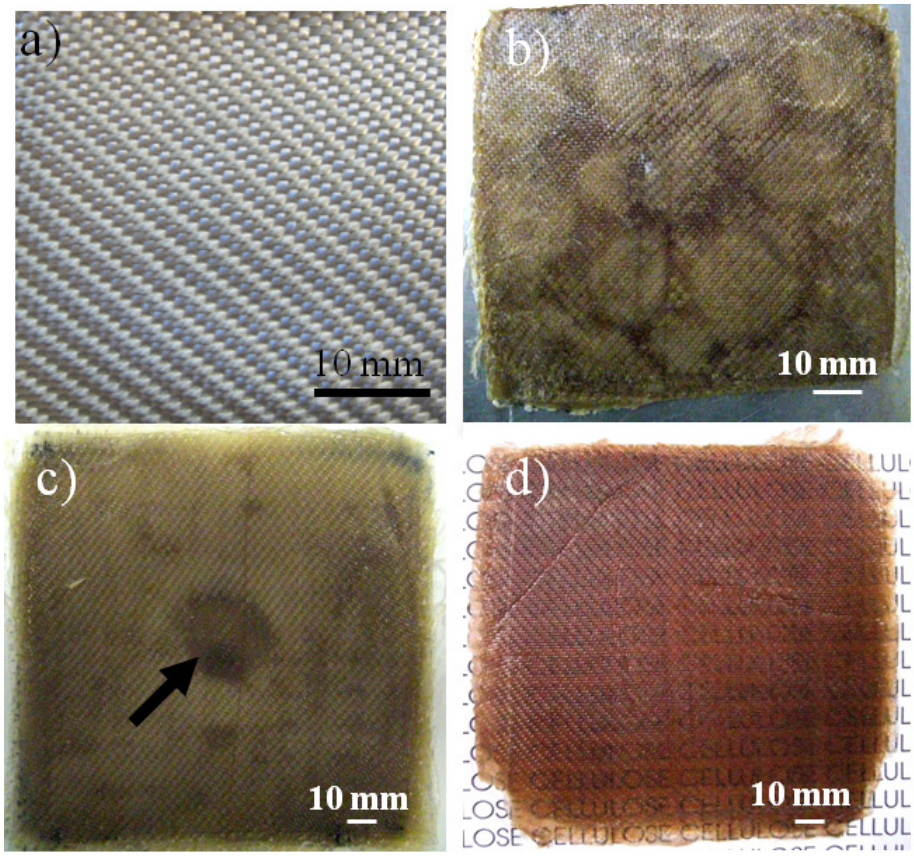

Figure 54: Photographs of the original textile (a) and laminates L1 (b), L2 (c) and L3 (d). The arrow indicates an imprint at the site of the infusion inlet for L2.

1.3.2 Microstructural Characterisation

Figure 55 presents an overview of the hierarchy of structures in the produced ACC laminates, showing a laminate (Figure 55a), one of the yarns forming a layer of the textile (Figure 55b) and single fibres within a yarn (Figure 55c). In the laminate, the 4 layers of textile are connected to each other (Figure 55), but show interlaminar voids. The yarns are compacted and the single fibres within a yarn (Figure 55) are still identifiable but are tightly bonded to each other by a thin layer of dissolved and regenerated cellulose. Those structures are visible in all three composites.

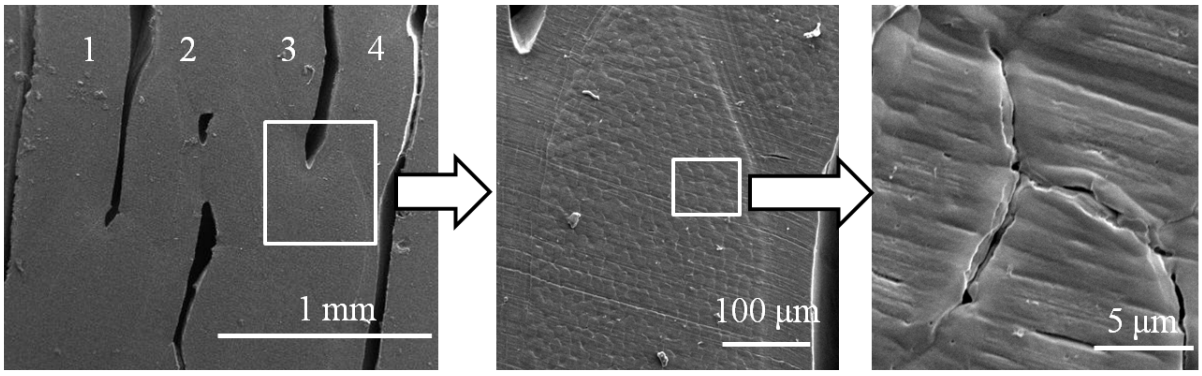

Figure 55: Scanning electron micrographs depicting the various hierarchies of structure observed in the ACC laminates for L1. The images clearly show a) 4 layers of the textile (labelled 1-4); b) an individual yarn within a single layer; and c) single fibres within a yarn. An accelerating voltage of 10 kV was used.

Conceptually, SIP was developed to produce ACC laminates with extensive inter- and intralaminar bonding and minimal void formation during regeneration and drying. All of the ACC laminates exhibited extensive inter- and intralaminar bonding. L1 exhibited large interlaminar (Figure 56a) (average area: 0.174 mm^2) and intralaminar (Figure 56d) voids, while smaller interlaminar voids were visible for L2 (Figure 56b) (average area: 0.096 mm^2). Overall L2 exhibited improved compaction and interlaminar bonding compared with L1. L3 exhibited the greatest interlaminar bonding with almost no observable voids (Figure 56c). While some intralaminar voids are present in all of the

laminates, the number and size of interlaminar voids were the greatest for L1. Interestingly, the interlaminar voids present in L1 (Figure 56d) were only observed to a small extent in L2 (Figure 56e) and were negligible in L3 (Figure 56f). Thus, increasing the applied pressure *during* dissolution appears to improve the interlaminar adhesion. The presence of interlaminar and intralaminar bonding in L1 demonstrates that the locally dissolved cellulose remains close to the fibre core in the absence of applied pressure as reported in Chapter III. On the contrary, fluctuations in the applied pressure in L2 cause a change in the capillary "ebb-and-flow" movement of the dissolved cellulose through the assembly, with backflow occurring if the pressure is released, due to the elastic character of the cellulose-IL solution (see *III*.3.3). The constant pressure applied during dissolution of L3 resulted in a more effective distribution of the dissolved cellulose to help fill voids in the structure, resulting in an almost void free composite. These simple observations clarified the critically important role of applied pressure during the dissolution and regeneration in the quality of the final ACC laminate.

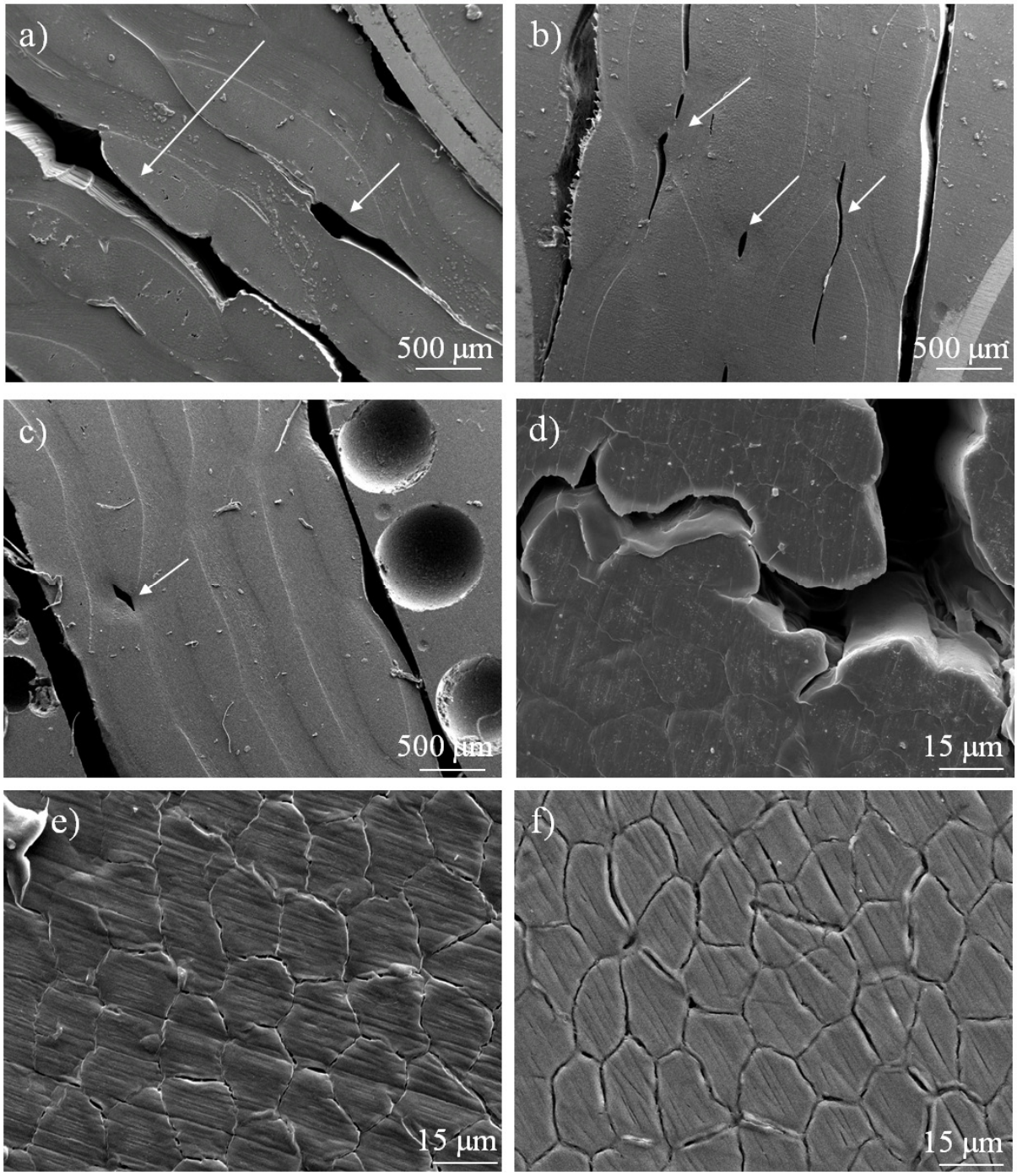

Figure 56: Scanning electron micrographs of the as-processed microstructure of ACC laminates: L1 (a and d), L2 (b and e) and L3 (c and e) at 50× (top row) and 1500× (bottom row) magnification. Arrows indicate the presence of interlaminar voids. Image d) gives an example of the large intralaminar voids present in L1. An accelerating voltage of 10 kV was used.

The cross-sectional areas of individual fibres in the three laminates and fibre in the as-received state were measured from SEM images in order to quantify the effect of SIP on the fibre shape and dimension (Table 8). The cross-sectional area of the fibres in the as-

received rayon textile was identical to that found in L1. This was somewhat surprising given that interlaminar and intralaminar bonding in L1 was observed (Figure 56). The observation of bonding between and within fibre suggests the presence of regenerated matrix phase. Therefore, it is reasonable to assume that dissolution of the rayon fibres is restricted to the very outer surface of the fibres in L1. Further, L1 does not involve the reapplication of pressure during the dissolution stage; this ensures that any dissolved cellulose remains local to the fibre core. In contrast, the variation in the vacuum pressure for L2 causes the dissolved cellulose to "ebb-and-flow" through the assembly. It is thought that a "reversible" flow occurs during pressurising and subsequent pressure relief. Finally, the above observations are consistent with the formation of the void-free ACC for L3 for which a constant pressure was applied during dissolution. The application of constant pressure is thought to cause greater redistribution of the dissolved cellulose, which in the process helps to fill any voids in the structure.

Table 8: Cross-sectional areas of the as-received fibres and fibres after SIP (L1, L2, L3).

Fibre area in μm^2	As-received	L1	L2	L3
Average	145.46	146.36	128.05	99.64
Change in %	x	0.62	-11.97	-31.5

1.3.3 Fibre Volume Fraction

As expected, L3 was determined to have the highest V_f amongst the ACC laminates as a result of the highest compaction during dissolution (Figure 57). This observation correlates with the observations of the laminate microstructure as discussed (Figure

56). The rectilinear infusion set-up appears to produce the most uniform solvent distribution as evidenced by the lowest standard deviation amongst the laminates (Figure 57). In contrast to L3, L1 shows a comparatively low V_f, most likely a result of the large voids in the laminates.

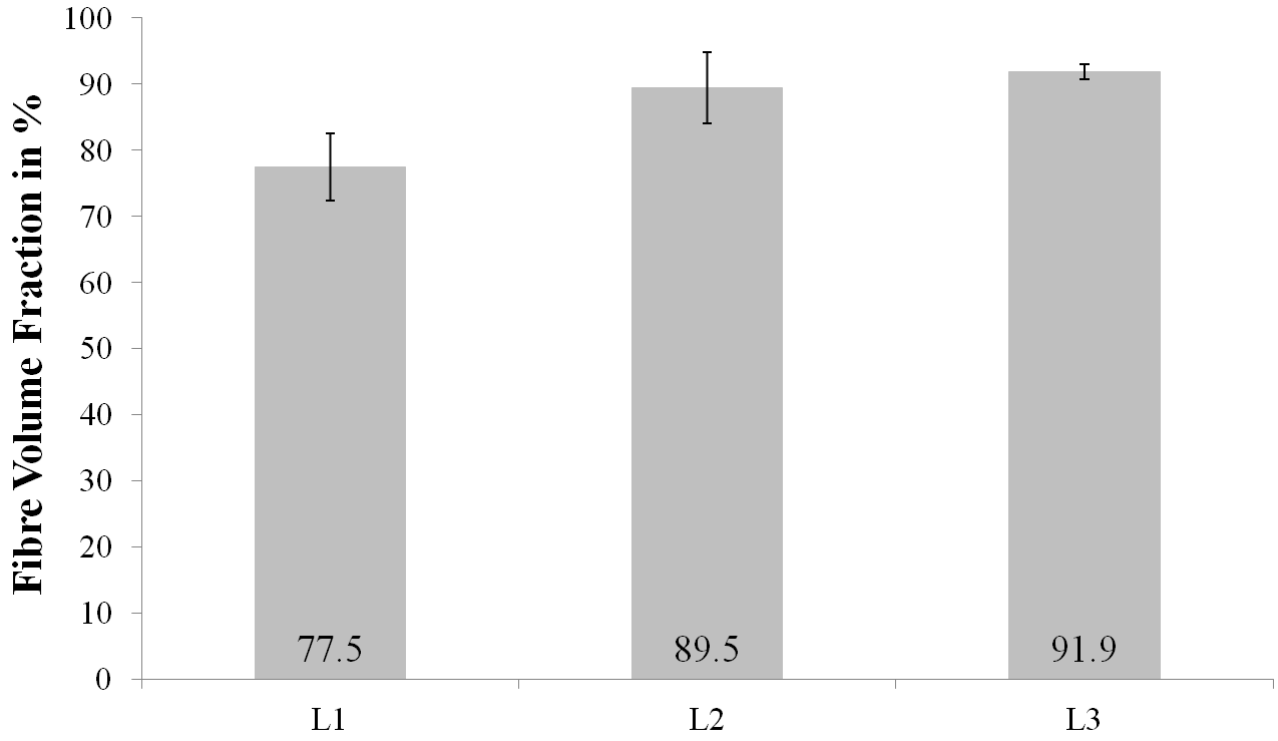

Figure 57: Average values of calculated fibre volume fraction for the three different laminates. The error bars indicate 1 standard deviation.

1.3.4 Tensile Properties in Dependence of Processing

The tensile strength of the laminates in this work is 57.76 MPa for L1, 80.32 MPa for L2 and 93.62 MPa for L3, which are significantly higher than the rayon textile (36.67 MPa)(Figure 58). All data have a pattern of normal distribution according to the David *et al.* test, [306] and significant differences could be found (α=5%) between the presented values using the Student-t-Test [306].

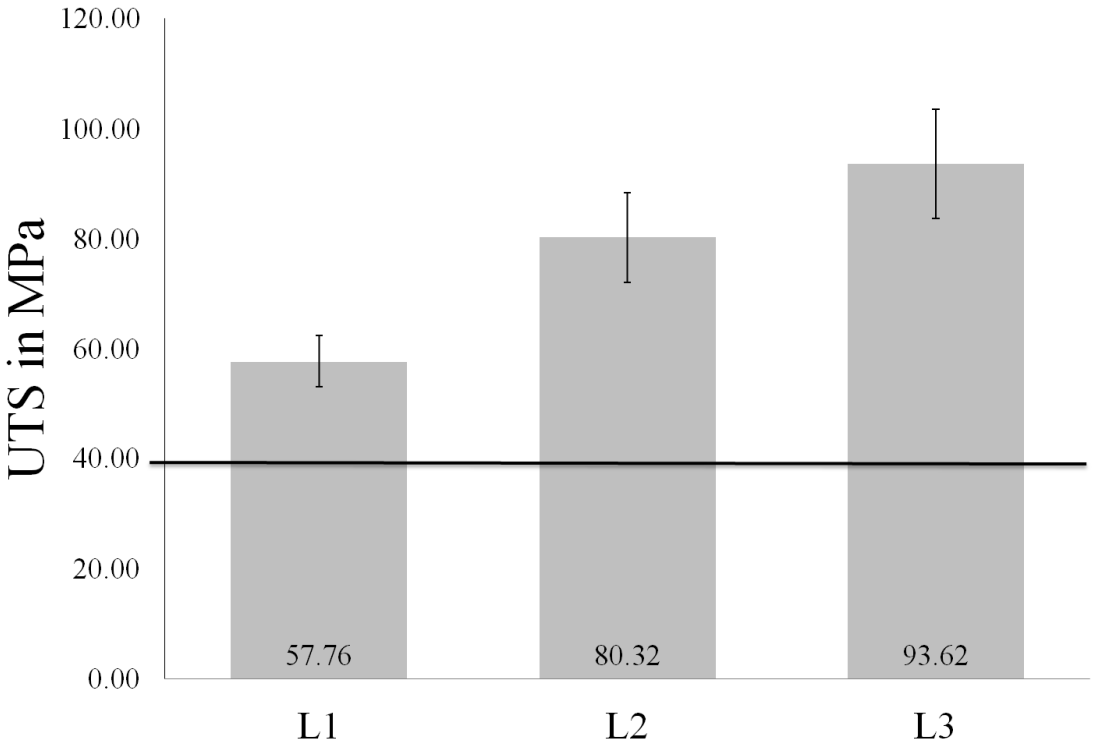

Figure 58: Ultimate tensile strength (σ_{max}) of the three different laminates. The black line shows the tensile strength of a layer of rayon fabric. Error bars indicate one standard deviation.

Similarly, the trend in Young's modulus followed that of the ultimate tensile strength. L1 yielded the lowest stiffness with 2.03 GPa, followed by L2 with 3.04 GPa and 4.67 GPa for L3 (Figure 59). The higher values of tensile strength and stiffness correlate with the improved interlaminar adhesion with L3. The more compacted laminae, lower void content and smaller void size with L3 (Figure 56) provides more efficient load bearing and load transfer throughout the composite, increasing the strength and stiffness, respectively. L1 and L2 failed in tension by delamination. Delamination is likely to be the result of insufficient matrix phase between the individual lamina [307]. The longer dissolution time used with L2 may also contribute to the lower strength and stiffness compared to L3. It has been shown that "over-dissolution" causes a significant decrease in tensile properties in all-cellulose composites based on ramie fibre [105].

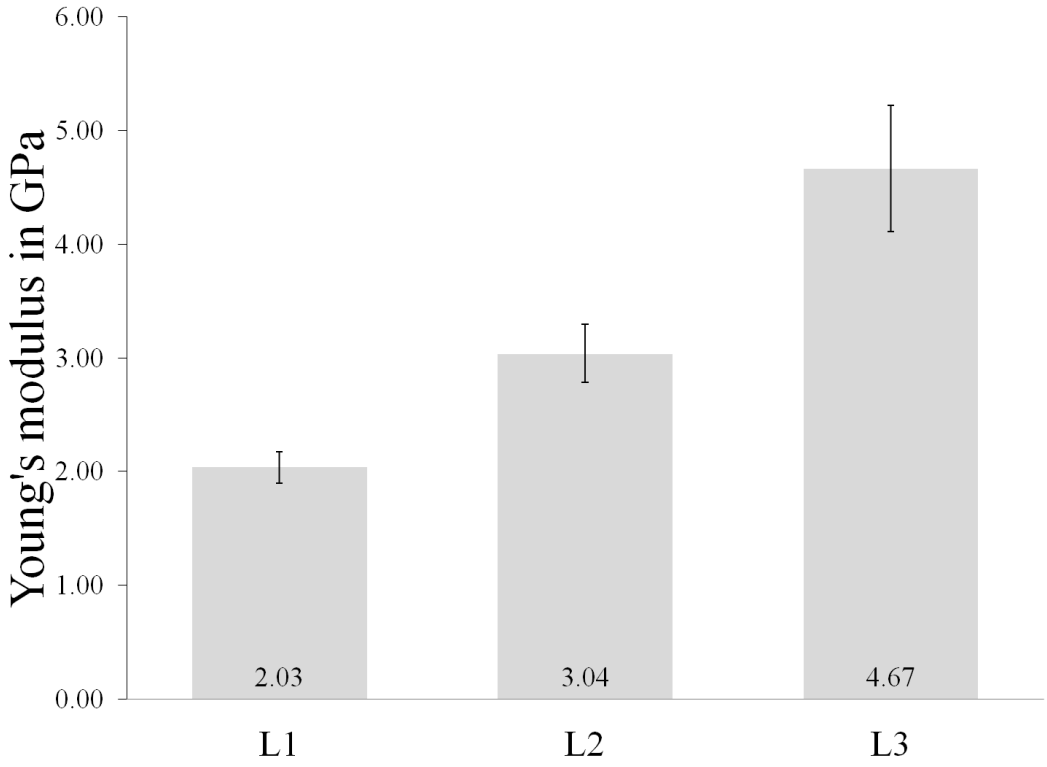

Figure 59: Average values of the Young's modulus of the three different laminates with standard deviation. Error bars indicate 1 standard deviation.

The tensile properties of the rayon laminates from the present study fit well within the reported range of ACCs (see Chapter 3, Table 5). However, it is difficult to compare the quality of the laminates with other ACCs due to the large differences in the raw materials and processing.

Rayon fibres have also been used as reinforcement in thermoplastic polymers such as polypropylene combined with the coupling agent MAPP [308], polypropylene (PP), polyethylene (PE), high impact polystyrene (HIPS) [204, 309] and the biopolymer and the bio-based polymer polylactic acid (PLA) ([185, 204, 309]). In all of these investigations the materials were produced *via* injection moulding using short rayon fibres. Mapping of the Young's modulus and tensile strength from these studies is performed to compare with the properties of the rayon ACCs from the present work (Figure 60). Bax and Müssig [185] observed the tensile strength and Young's modulus of

10-30 vol.% rayon fibre-PLA composites were up to 58 MPa and 4.85 GPa (no. 1 in Figure 60) . Khan *et al.* reported the tensile strength and modulus of a 25 vol.% rayon fibre-MAPP composite as 72.1 MPa and 2.67 GPa (no. 2 in Figure 60), respectively [308]. Ganster *et al.* [309] investigated composites made of 30 mass% rayon fibre-PP, 25 vol.% rayon fibre-PE, 25 vol.% rayon fibre-HIPS, and rayon fibre-PLA. They found the strength of these composites varied from 58 MPa to 108 MPa while the Young's modulus varied from 2.94 GPa to 4.2 GPa (no. 3-6 in Figure 60). In comparison, the laminate L3 made in the present study shows a similar strength and stiffness. One reason for the relatively high properties associated with L3 is due to a unique microstructure. The single fibrils of L3 are connected by a very thin layer of matrix phase that originates from cellulose regeneration during SIP (Figure 56). A remarkable fibre volume fraction of up to ~90 % results from the highly restricted and localised dissolution that occurs at the rayon fibre surface. The higher fraction of load bearing fibres and their increased length compared to the other rayon based composites are very likely to be the main reason for the higher mechanical properties. The presented SIP process allows the manufacturing of composites with high fibre volume fractions while providing, in case of uniform solvent distribution, a minimum of matrix phase surrounding each fibre. Thus, the applied load can be equally transferred to each fibre; subsequently each fibre can contribute to the composite strength and stiffness.

It is thought that the underlying reasons for the higher tensile strength in the present work compared with other rayon fibre composites reported in the literature are as follows: (I) superior interfacial properties as a result of similar chemistry between fibre and matrix; (II) greater rayon fibre lengths of up to 120 mm; and (III) control over fibre orientation through the use of a rayon textile.

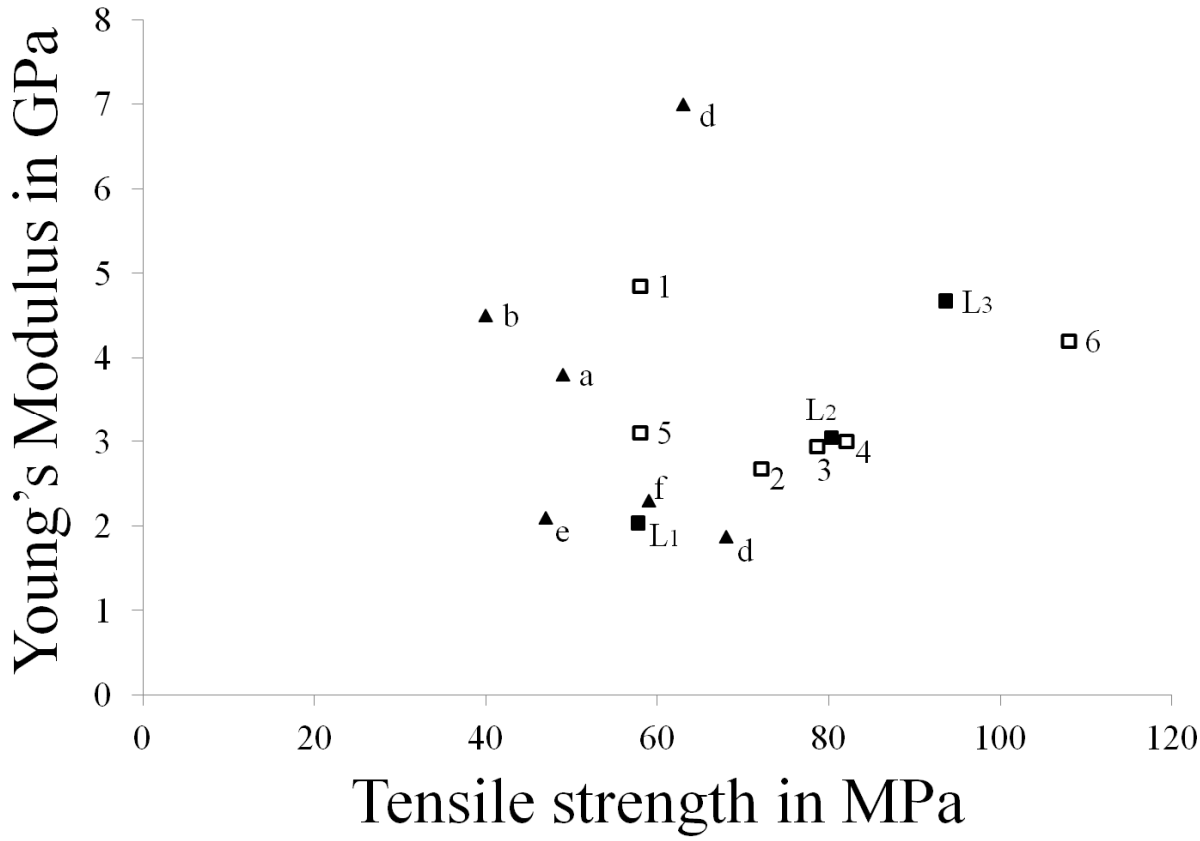

Figure 60: Young's modulus vs. strength of the produced rayon composites from the present study (L1-L3), compared to other rayon-based composites (1-6) and other biocomposites (a=PBS-flax [12];b=PHB-flax [12]; c=polyester resin-banana fibres [186], d=PTP-hemp [23], e=PLA cellulose nano whiskers [184]; f=PLA-cellulose nano fibrils [184]).

It can be seen that the rayon-based composites are in the same range as other biocomposites, but L3 shows higher strength and stiffness than the others except the composite reported by Ganster *et al.* [204], whose high properties could however be mainly the result of the used PLA compound, as pointed out by Bax and Müssig [185]. It can be assumed that the here demonstrated SIP allows to take full advantage of the fibre properties resulting in the higher tensile properties.

1.4 CASE STUDY FOR THE PRODUCTION OF SPORTS EQUIPMENT PROTOTYPES

To evaluate the potential of the developed process for the production of larger parts with a more complex geometry than the so-far produced flat panels, two case studies

were conducted. It was trialled to produce a shin pad and a skateboard deck using SIP process.

To produce the parts, an original shin and skateboard deck, respectively, were used a positive mould. The process is exemplarily described for the skateboard deck.

The deck was placed in a vacuum back, positioning inlet and vent at the nose and tail end of the board (Figure 61a). The deck was then covered with a layer of perforated plastic film. 6 layers of rayon textile and 5 strands of a rayon 3D braid (see Chapter VIII) were placed on the board and two strips of distribution medium under the inlet and vent (Figure 61b). The IL was infused into the textile layers applying a vacuum (Figure 61c). After infusion the bag was sealed and placed in an oven at 100 °C for 60 min to partially dissolve the cellulose. After dissolution the bag was infused with distilled water to regenerate the dissolved portion of the cellulose (Figure 61d). The ACC board was washed in distilled water for 48 hr to remove any remaining IL and then dried at room temperature for 72 hr clamped to the original board using G-clamps. Access material on the board edge was then removed using a hacksaw.

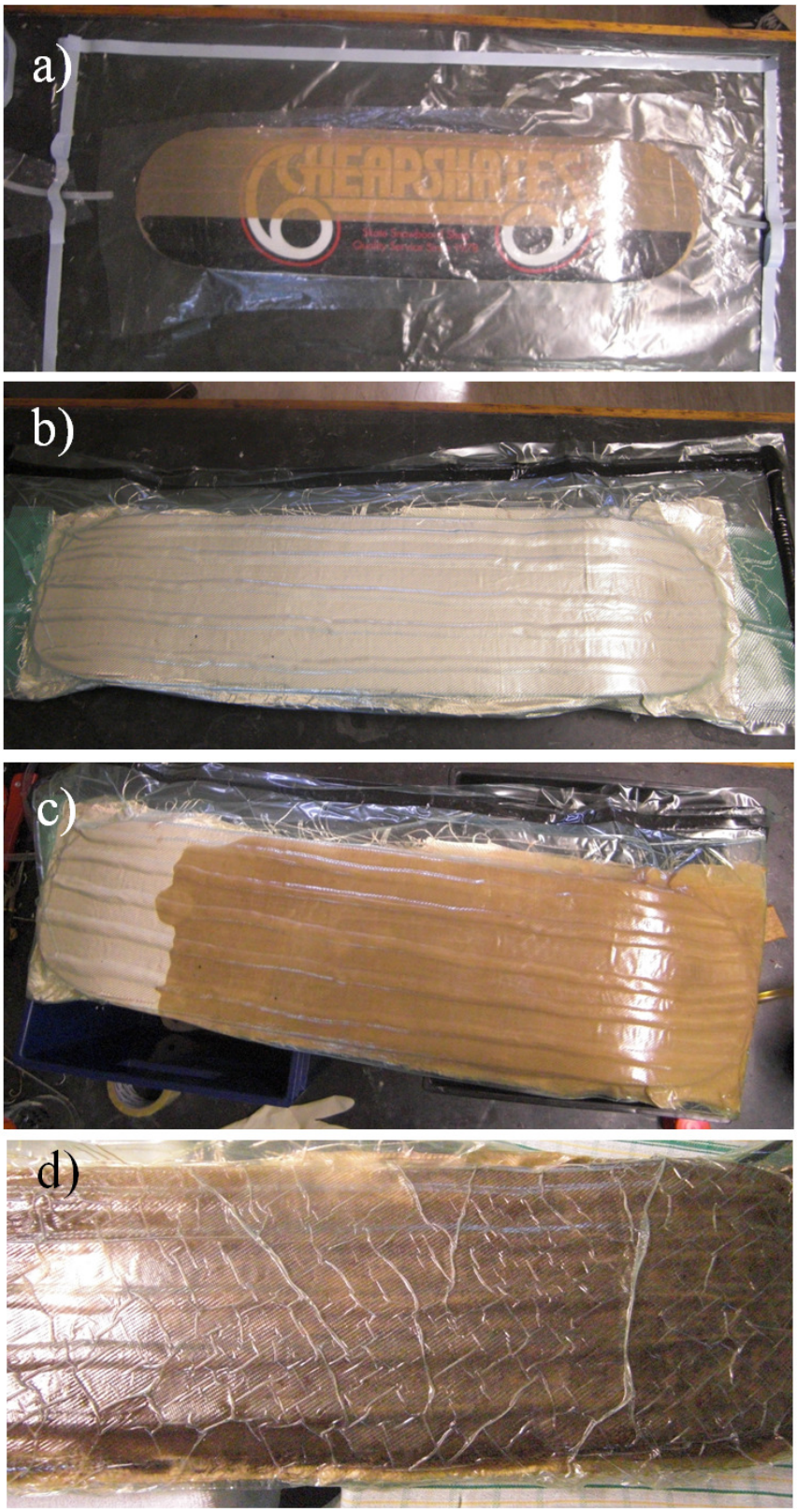

Figure 61: Photographs of the different stages used to produce an ACC skateboard deck. Displayed are the positioning of the board mould in the vacuum bag (a); the complete set-up before (b) and during (c) solvent infusion; and after infusion with water to regenerate the dissolved cellulose (d). The board length is 900 mm.

The shin pad was produced in the same manner but using 8 layers of rayon textile and no additional 3D braids. The final products can be seen in Figure 62.

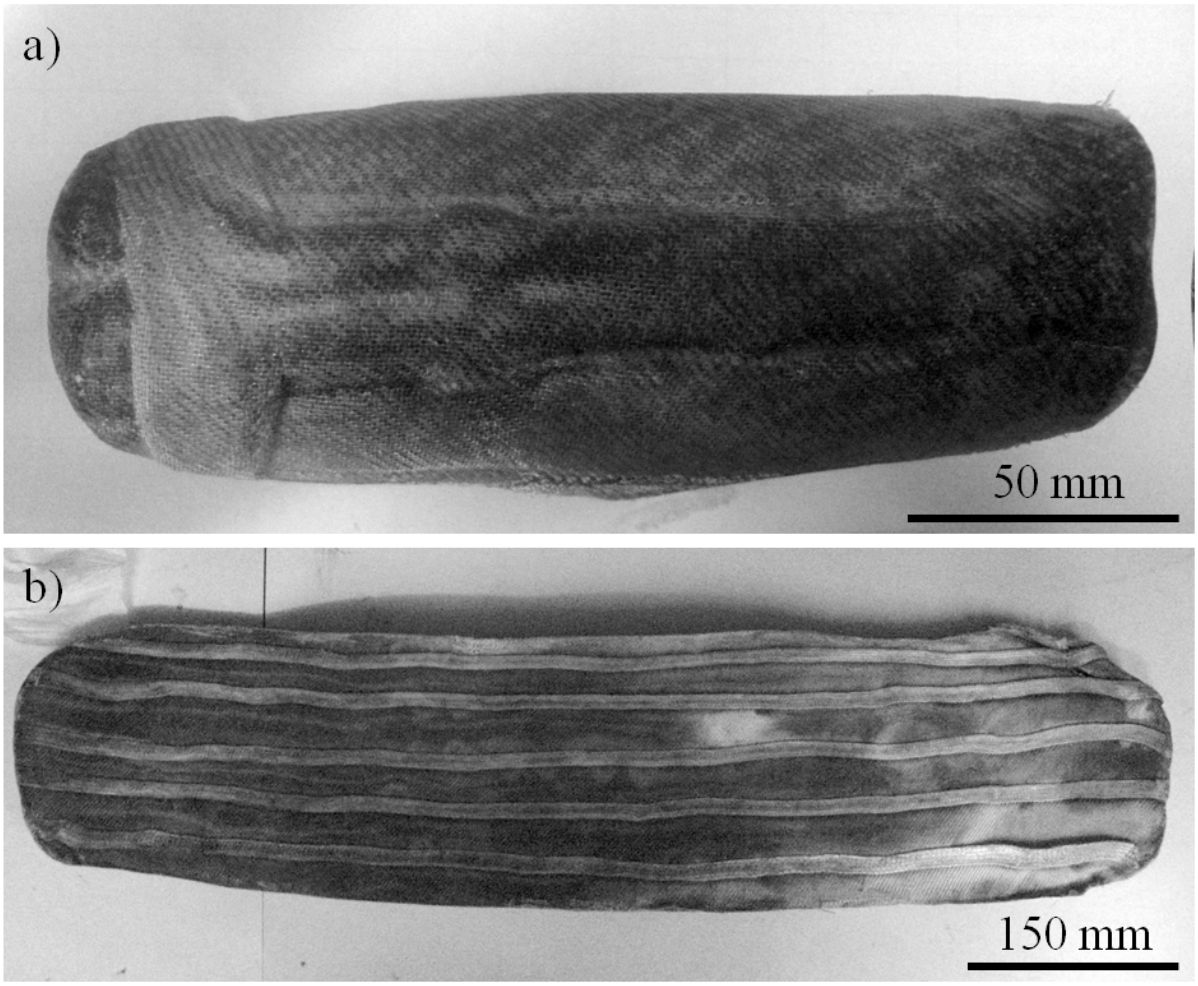

Figure 62: Photographs of the finished ACC shin pad (a) and skateboard deck (b) after SIP.

1.5 CONCLUSIONS

In this work, solvent infusion processing (SIP) that is conceptually based on vacuum-assisted resin transfer moulding has been developed to produce thick (> 1 mm) ACC laminates. SIP represents a first step toward an upscaled industrial processing method for ACCs. It allows a uniform distribution of the ionic liquid and good compaction of the composite can be achieved if additional pressure is applied during the dissolution step. Creating the matrix out of the fibre by partial dissolution does not only allow the

production of composites with a very high fibre volume fraction, but also provides a homogenous distribution of the matrix phase. The rectilinear infusion did provide the best wetting, resulting in the highest stiffness and strength, as a result of the applied pressure during dissolution. Therefore, only the rectilinear set-up will be used for following experiments.

The chemically identical phases allow a good adhesion between the reinforcing fibres resulting in good tensile properties. The composite properties are in most cases superior to other biocomposites using the same reinforcement material; however improved processing parameters could lead to even better properties.

The developed process could be successfully used to produce more complex shapes in the form of a shin pad and skateboard deck.

2. THE EFFECT OF SIP PROCESSING PARAMETERS ON ACC LAMINATE PROPERTIES AND MICROSTRUCTURE

2.1 INTRODUCTION

The previously described set of ACCs produced *via* SIP showed promising mechanical properties. The application of pressure during the dissolution stage of the process is necessary to achieve a strong interlaminar adhesion in ACC laminates.

However, there are several processing parameters for SIP that might influence the microstructure of the material and thus properties. Furthermore, it is necessary to investigate methods for improving the quality of ACC laminates and reduce the manufacturing cycle time to establish a feasible pathway to the industrial application of ACC laminates.

5 distinct stages have been identified during the solvent infusion process; in short those can be summarised as:

I. Vacuum-assisted infusion of IL
II. Dissolution of the fibre surface under conditions of elevated temperature and pressure
III. Infusion of a coagulant to regenerated the dissolved portion of cellulose
IV. Washing to completely remove the IL
V. Drying

Solvent infusion through the rayon textile (Step I) depends mainly on the geometry of the part, viscosity of the solvent and architecture of the fibre reinforcement which together determine the permeability of the textile. The set-up is of crucial importance to

infusion in traditional VARTM processes. Incorrect positioning of vents and outlets will hinder complete impregnation of the fibre preform before curing begins, leading to dry spots (*i.e.* void formation) in the final composite [310]. Similarly, the avoidance of air leaks and proper degassing of the resin are critical to laminate quality since any introduced air bubbles will lead to void formation in the final parts [284]. In contrast, a different set of problems can arise during SIP. Obviously, the risk of a resin curing before complete impregnation is not an issue for the solvent-based approach of SIP. However, it is preferable to minimise the infusion time with regards to the overall cycle time, particularly when handling the infusion of larger parts. At room temperature the IL will dissolve only very small fractions of cellulose if any at all ([311], see Chapter III). Thus, the ILs used in the dissolution of cellulose should not experience any noticeable change in viscosity during Step I of SIP. The introduction of air bubbles during SIP is not expected to drastically influence the quality of the final ACC since the pressure applied during Stage II acts to remove any voids present in the highly viscous cellulose-IL solution. Other processing parameters including the part geometry, textile architecture and solvent viscosity will influence the ease with which it is possible to synthesise ACCs *via* an infusion type process. However, since textile architecture and solvent viscosity are controlled by the selection of appropriate materials, these parameters are not the focus of the present work.

2.1.1 The Processing Parameters

The solvency of an ionic liquid for cellulose strongly depends on the dissolution temperature as was established earlier (see Section III.2.2). It is likely that the solvency is directly related to the viscosity of the IL, since it could be demonstrated that a lower viscosity enhances the dissolution of cellulose (see Section III.2.2). The viscosity of an IL

is known to decrease with increasing temperature [312], which was also be shown experimentally in Chapter III for the materials used in this analysis.

Furthermore, cellulose dissolution is a time dependent process. After the initial rapid dissolution of cellulose in 1-allyl-3-methylimidazolium chloride (AmimCl), the dissolution rate decreases due to undamaged crystalline fibre residues that are not dissolved by the IL [311]. Extending the dissolution time often leads to further dissolution of the cellulose until the maximum dissolution capacity is reached [311].

Cellulose dissolution is ultimately limited by the final dissolution capacity of the IL such that further increases in the dissolution temperature and/or time will not lead to further dissolution but rather degradation of the cellulose and/or IL. It was shown that 10 mass% of rayon fibre was the maximum amount that could be dissolved in BmimAc without visible occurrence of degradation (see Chapter III). It is therefore assumed that no more than 10 mass% of the rayon fibre will be dissolved during SIP.

Based on the observations of the L3 composite (see Chapter VI.1), it appears that 60 min at 95 °C is sufficient time to dissolve the maximum amount cellulose as the V_f of that composite was 92%. However, it is not known how much time is required for the cellulose dissolution. It is possible that the cycle time of Stage II could be reduced by reducing the dissolution time and increasing the dissolution temperature to enhance the rate of dissolution.

Another important factor to have an influence on the overall composite quality may be the type of coagulant used to remove the IL and, thus, regenerate the dissolved cellulose. For instance, the final crystallinity of the cellulose following fibre regeneration

in the Lyocell process is known to be dependent on the selected coagulant (*i.e.* distilled water versus methanol) [46].

The high availability of hydrogen groups along the cellulose molecule chains causes a significant amount of swelling when the cellulose is brought into contact with water, while less swelling occurs with other coagulants such as alcohol or acetone [273]. Different amounts of swelling may influence the formation and structure of the final regenerated cellulose matrix in an ACC, perhaps also affecting the mechanical behaviour of the composite. Duchemin *et al.* have reported severe swelling and shrinkage in ACCs [127]. Furthermore, Fink *et al.* reported that the precipitation medium (*i.e.* water or alcohol) has a significant effect on structure of the cellulose regenerated from a cellulose-NMMO solution [313]. It will therefore be important to determine whether water is a suitable coagulant or perhaps replacement with another coagulant can improve the properties of the final ACC.

A related parameter is the final drying step of the process. While a rapid removal of the coagulant is beneficial in terms of processing time it could lead to the formation of voids through evaporation processes. It is hypothesised that stress introduced into the system by more rapid drying conditions may cause greater shrinkage of the matrix phase compared to the reinforcing fibres, leading to the presence of cracks in the new created matrix phase and/or at the fibre-matrix interface (see Chapter IV).

Composite made *via* SIP but with altered parameters will be produced and analysed regarding their V_f , tensile properties, microstructure and crystallinity to quantify the influence of those parameters on the final composite and its properties.

2.2 EXPERIMENTAL PROCEDURES

2.2.1 Processing Parameters

Several processing parameters are investigated to elucidate their influence on the microstructure of ACCs synthesised *via* SIP.

Table 9: Overview over the composites made with different parameters

No.	Composite	Dissolution Time	Dissolution Temperature	Coagulation/Washing Medium	Drying Conditions
1	*Original SIP*	60 min	95 ˚C	Water/ Water-Ethanol mixture	4 hr at 60 ˚C and 4 hr at 100 ˚C
2	*125/30*	30 min	125 ˚C	Water/ Water-Ethanol mixture	4 hr at 60 ˚C and 4 hr at 100 ˚C
3	*Water SIP*	60 min	100 ˚C	Water/Water	4 hr at 60 ˚C and 4 hr at 100 ˚C
4	*Ethanol-Water SIP*	60 min	100 ˚C	Ethanol/Water	4 hr at 60 ˚C and 4 hr at 100 ˚C
5	*Low Temperature Drying (LTD) SIP*	60 min	100 ˚C	Water/Water	48 hr at 23 ˚C
6	*Ethanol SIP*	60 min	100 ˚C	Ethanol/Ethanol	4 hr at 60 ˚C
7	*24 hr SIP*	24 hr	100 ˚C	Water/Water	4 hr at 60 ˚C and 4 hr at 100 ˚C

The selected conditions are used to analyse the effects of dissolution time and temperature, coagulation and washing medium and drying conditions on the microstructure, fibre volume fraction and tensile properties of ACC laminates produced *via* SIP. The baseline conditions used in SIP are given by #1 in Table 9. The possibility of reducing the cycle time is examined by (i) increasing the dissolution temperature (#2) or (ii) replacing water with a more volatile coagulant such as ethanol to reduce drying time (#6). The influence of the coagulation and washing medium combined with different drying conditions will also be examined to determine any differences in interlaminar shrinkage that might introduce defects into the microstructure of the composites (#3-6). Furthermore, the possibility of over-dissolution or degradation is examined by increasing the dissolution time to 24 hr (#7).

The basic manufacturing method used to examine the above processing parameters follows that used for the original laminate L3 (see Chapter VII.1.2.1).

2.2.2 Materials

Four square layers of the rayon textile (125 mm × 125 mm) were used to process each composite after drying. BmimAc was used as the solvent. The used water was distilled water. Both, distilled water and ethanol, were used without further treatment.

2.2.3 Microscopy

For microscopical analysis, 3 samples each of approximately 5 mm × 3mm were cut from different sections of the laminates.

2.2.3.1 Optical Microscopy and Analysis

The mounted and polished samples were conditioned at 23 ˚C and 50 % RH prior to optical analysis to avoid the influence of a variable moisture content on the composite microstructure. The cross-sections of the composites were analysed with reflected light microscopy (Leica DR IRM microscope).

Captured images were further processed using the software GIMP v. 2.6.11 (GNU General Public License, 2011) to determine the fibre volume fraction. A colour threshold was applied manually to the picture to turn it into a black and white image, as exemplarily shown in Figure 63.

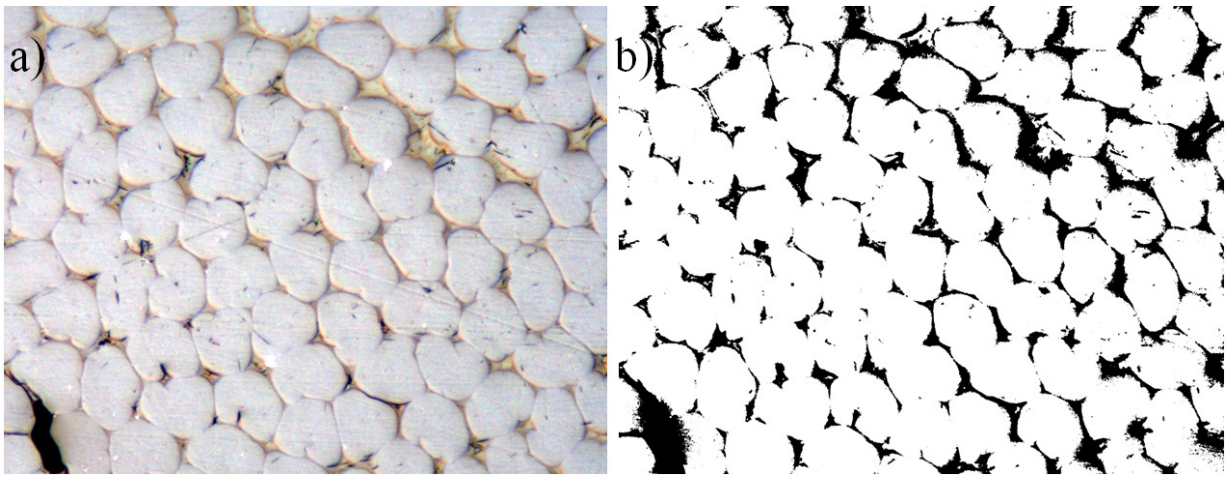

Figure 63: a) An optical micrograph of the cross-section of an ACC laminate and (b) the conversion of (a) into a black and white image *via* thresholding.

The matrix phase and eventual voids appear black, while the fibres remain white, following the image processing. The V_f and void content, respectively, can then easily be determined by counting the amount of black and white pixels for each image. Between 10 and 20 pictures were analysed for each composite and each picture was analysed three times to minimise the operator error. The used method applying a colour threshold to the pictures taken with an optical microscope produced almost

identical results as the before used technique of measuring fibre areas individually for composite L1 and L3 (see Section VI.1.3.3). It is therefore assumed that applied method is coherent with previous results.

2.2.3.2 Scanning Electron Microscopy

The mounted and polished samples were gold coated for 120 seconds at 25 mA. The fracture surface of tensile tested samples was analysed by cutting tested samples approximately 5 mm beneath the fracture. The samples were then mounted on carbon tabs and gold coated for 180 seconds at 25 mA.

2.2.4 Tensile Testing

8-10 ACC samples of each composite were tensile tested. Pneumatically-controlled grips with an applied pressure of 0.35 MPa were used to clamp the samples during testing. The length, width and thickness of the samples were 130 ± 2 mm, 10 ± 1 mm and 1.6 ± 0.15 mm. The used gauge length was 60 mm. All samples were conditioned at 50 % RH and 23 ˚C for 24 hr prior to testing.

2.2.5 Solid State Nuclear Magnetic Resonance (solid state NMR)

To analyse the influence of the coagulation medium on the crystalline structure of the composites, samples of the as-received fibre, composite 5 and composite 6 were analysed using solid-state NMR.

The samples were conditioned to a moisture content of 30 mass% for the measurements. To prepare samples of the ACCs, the composite were frozen and crushed to a particle size < 0.5 mm. Each moistened sample was packed into a 4 mm rotor fitted

with a Kel-F cap. A Bruker Advance DRX 200 spectrometer (Bruker AXS, Billerica, USA) was used to obtain 13C NMR spectra at 50.32 MHz. The rotor was spun at 5 kHz in a Bruker 4 mm SB doubly tuned H/X MAS probe. Each 90° proton preparation pulse was followed by a proton spin locking pulse (S' = 8 ms), 1 ms cross-polarisation contact time, 26.5 ms acquisition and a 2 s recycle delay. The proton decoupler output was > 83 kHz during data acquisition. All spectra were averaged over data accumulated for 10k (S) or 20k (S') transients. All spectra had a Gaussian line broadening of 25 Hz.

The software SpinWorks 3.1.8 (Kirk Marat, University of Manitoba, Canada) was used for data processing and analysis.

2.2.6 X-Ray Diffraction

Four different samples were analysed to determine the influence of the regeneration medium on the cellulose crystalline structure. Films of completely dissolved and regenerated cellulose II were produced by completely dissolving 5 g each of dried rayon fibre in BmimAc as described in detail in Chapter III.2.2. The dissolved cellulose was then regenerated and washed in distilled water and ethanol, respectively. The so manufactured were dried at room temperature. One sample of each, composite 5 and 6 were also analysed.

The four samples were analysed with an X'pert PRO diffractometer (PANalytical, Almelo, Netherlands) equipped with a copper anode (λ = 1.5418 Å). The radiation was filtered with a Kβ nickel filter. Pre-sample Soler slits were used with a 0.04 rad aperture, a post-sample anti-scatter slit was also used. The acquisition was made with a PIXcel 1D detector and the radiation $K\alpha_1$ was selected. Diffraction data was scanned from 2 θ =

5 to 90 ° in 8 min. The samples were scanned in their bulk form and placed on a sample spinner in order to cancel the orientation effects.

Data analysis was carried out using the software Fytik v.0.9.8 (Marcin Wojdyr, Institute of High Pressure Physics, Warsaw, Poland [314]).CrI calculations were carried out using formula 4.

3.2 RESULTS AND DISCUSSION

3.3.1 Influence of the Processing Parameters on the Fibre Volume Fraction

To analyse the effect of the different processing parameters on the overall structure of the composites their fibre volume fraction was determined (Figure 64).

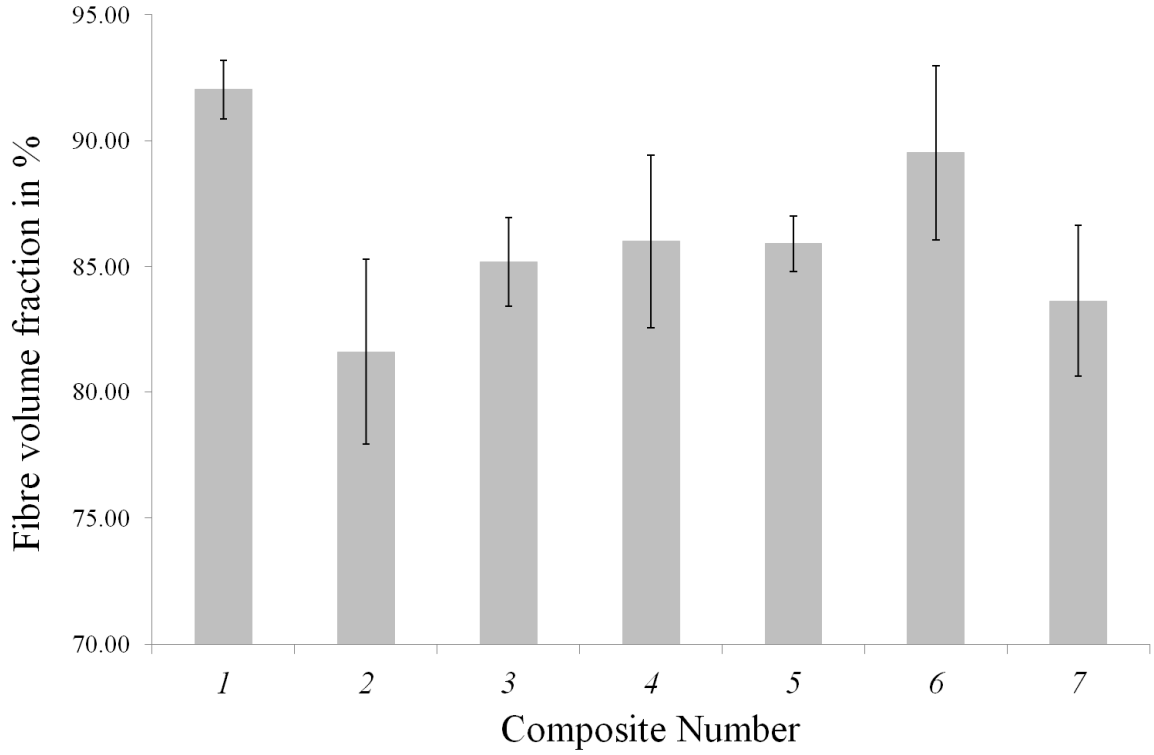

Figure 64: Mean values of the determined V_f of the composites produced with different processing parameters. The error bars represent one standard deviation. The composites are numbered according to Table 9.

All composites showed a high fibre volume fraction between 81.6 % (#5) and 92 % (#1). This demonstrates that SIP as a composites manufacturing route produces a relatively high fibre volume fraction, with only minor portions of the original rayon textile converted into matrix phase. The applied pressure results in thorough material compaction and, thus, minimal void as shown by the lowest Vf of composite #2. The shorter the dissolution time, the less likely is the formation of matrix phase. Consequently, a lack of matrix phase leads to an increased presence of voids between the elementary fibres of ACC laminates (Figure 65).

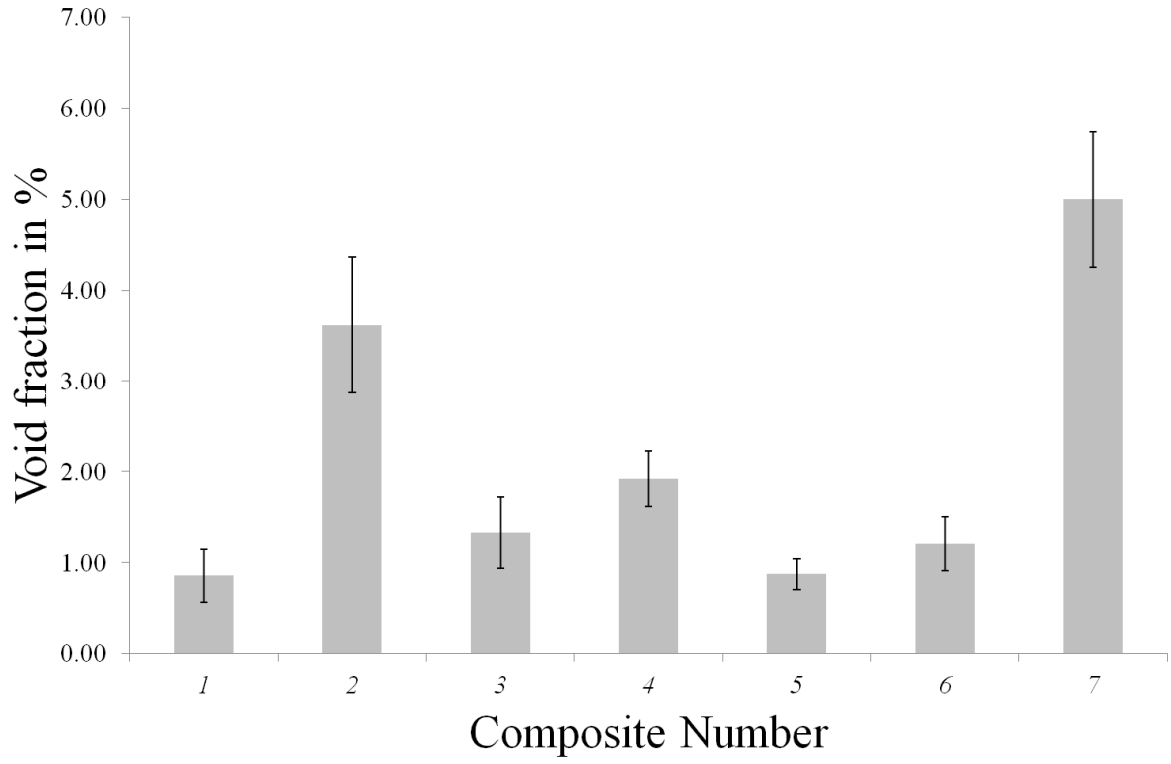

Figure 65: Mean values of the determined void fraction of the composites produced with different processing parameters. The error bars represent one standard deviation. The composites are numbered according to Table 9.

The differences in V_f are the result of the used coagulant and drying conditions. Interestingly, the three composites with the highest V_f were processed with ethanol as the coagulant. It is known that ethanol causes significantly less swelling of cellulose I and II than water. Specifically, cellulose I in the form of α-cellulose [273] , cellulose II in the form of mercerized cotton and eucalyptus [315] and cellulose II in the form of regenerated cellulose [316]. A reduction in swelling during regeneration and/or washing should translate into reduced tendency for shrinkage during drying. Moreover, a reduction in shrinkage results in lower stresses at the fibre-matrix interface, reducing interfibrillar cracking resembled in a low void formation (Figure 65) (and presumably leading to a higher V_f).

It can be seen in Figure 66 that a matrix phase has formed around the fibres, but has been cracked destroying the interfibrillar bond. On closer inspection, the fractured matrix phase takes on a jigsaw puzzle-like appearance where it is possible to see the matrix phase was initially a single phase that has separated apart during drying.

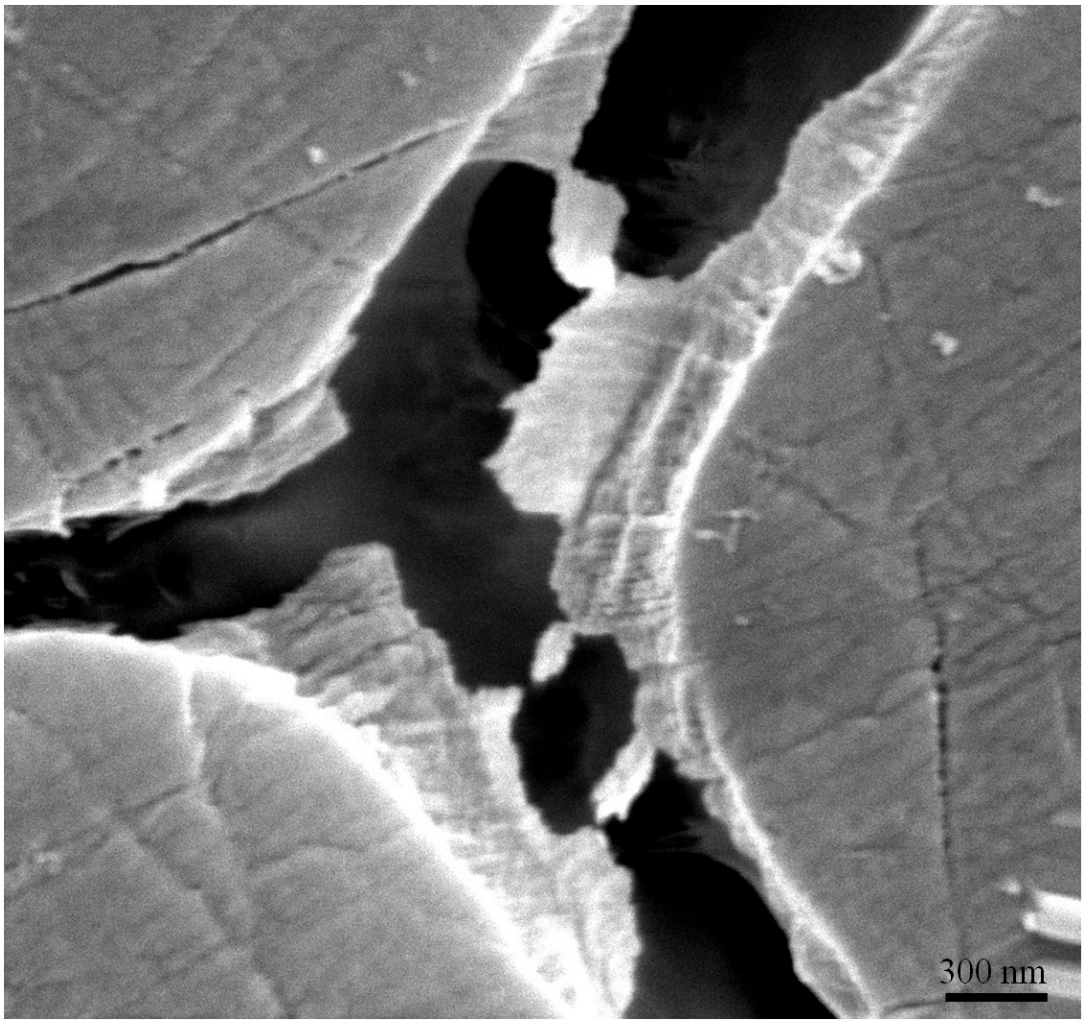

Figure 66: SEM micrograph that shows an example of drying-induced cracking within the matrix phase between elementary fibres (#2). An accelerating voltage of 5 kV was used.

3.3.2 Effect of the Processing Parameters on Tensile Properties

Figure 67-Figure 69 show the ultimate tensile strength (UTS), Young's modulus and strain at UTS of the 7 different composites.

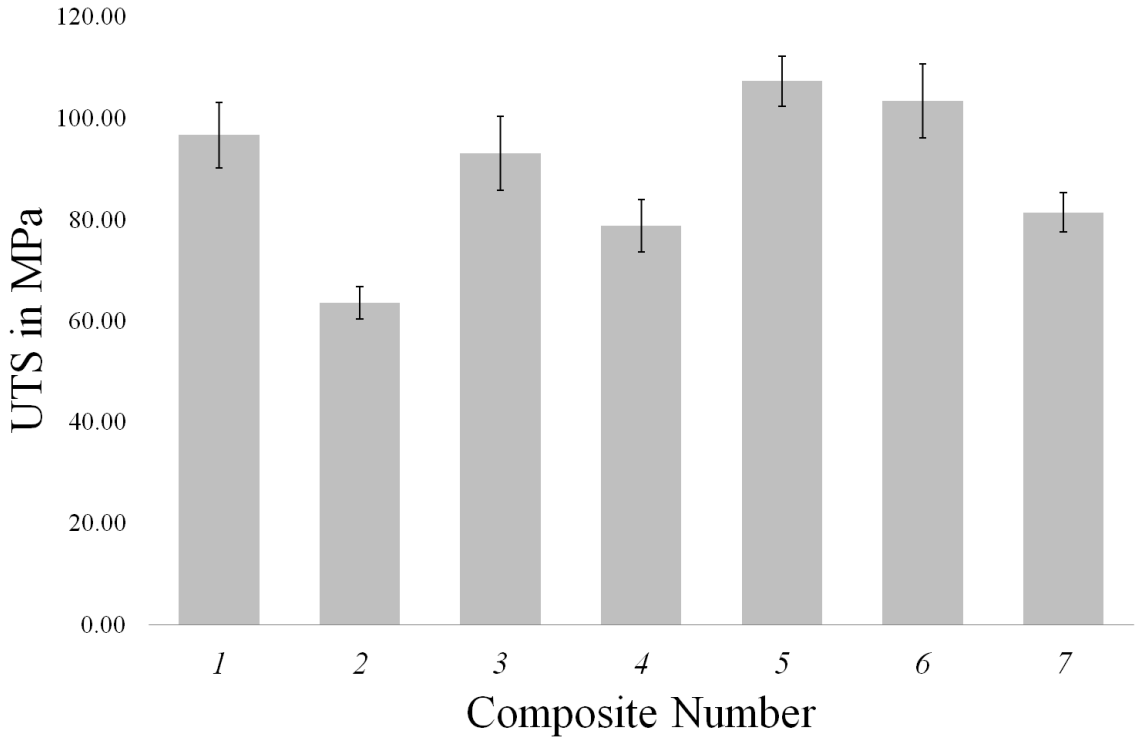

Figure 67: Ultimate tensile strength of the 7 different composites. The error bars represent one standard deviation.

Composite 2, 4 and 7 show the lowest strength and stiffness. In case of composite #2 this can be explained by the reduced dissolution time of 30 min and possibly by the increased dissolution temperature of 125 °C. As supported by the low V_f (Figure 64), the processing time appears to be insufficient to create a continuous matrix phase to achieve an even load transfer within the composite, resulting in a low UTS and Young's modulus and higher void content (Figure 65). The strain of 13.59 ± 0.79 % is almost identical to the untreated fibre [221], further indicating a dissolution time that was too short to cause a structural change of the fibres. Although not detectable by visual observation, the increased dissolution temperature could also have caused a small amount of degradation of the cellulosic fibres, contributing to the lower tensile properties of this composite.

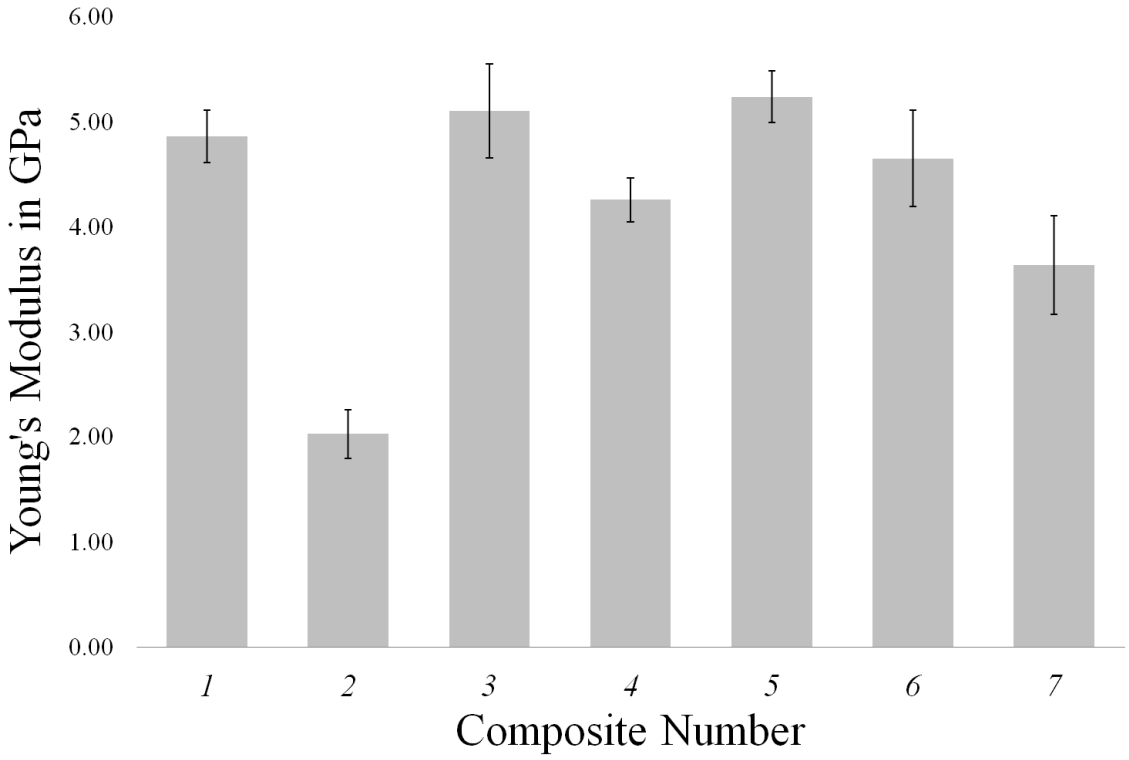

Figure 68: Young's modulus of the 7 different composites. The error bars represent one standard deviation.

Cellulose degradation could explain the tensile properties of composite 7. The extended dissolution time of 24 hr may have caused a complete dissolution of the amorphous fractions of the fibres (Figure 70 a) and perhaps also damage to the crystalline regions (Figure 70 b) as shown for elementary fibres within of composite 7 compared to composite 1 (Figure 70).

Although the matrix phases that surround the fibres look similar, there are gaps or cracks within the single fibres of composite 7 (Figure 70 b), also resembled in the highest void fraction of all described composites (Figure 65). This could indicate that the amorphous domains of the fibres have been completely dissolved creating voids within the fibre. It might be envisaged that these changes to the microstructure of the fibres lower the overall composite strength and stiffness. Void formation is also considered a major contributor to a low V_f.

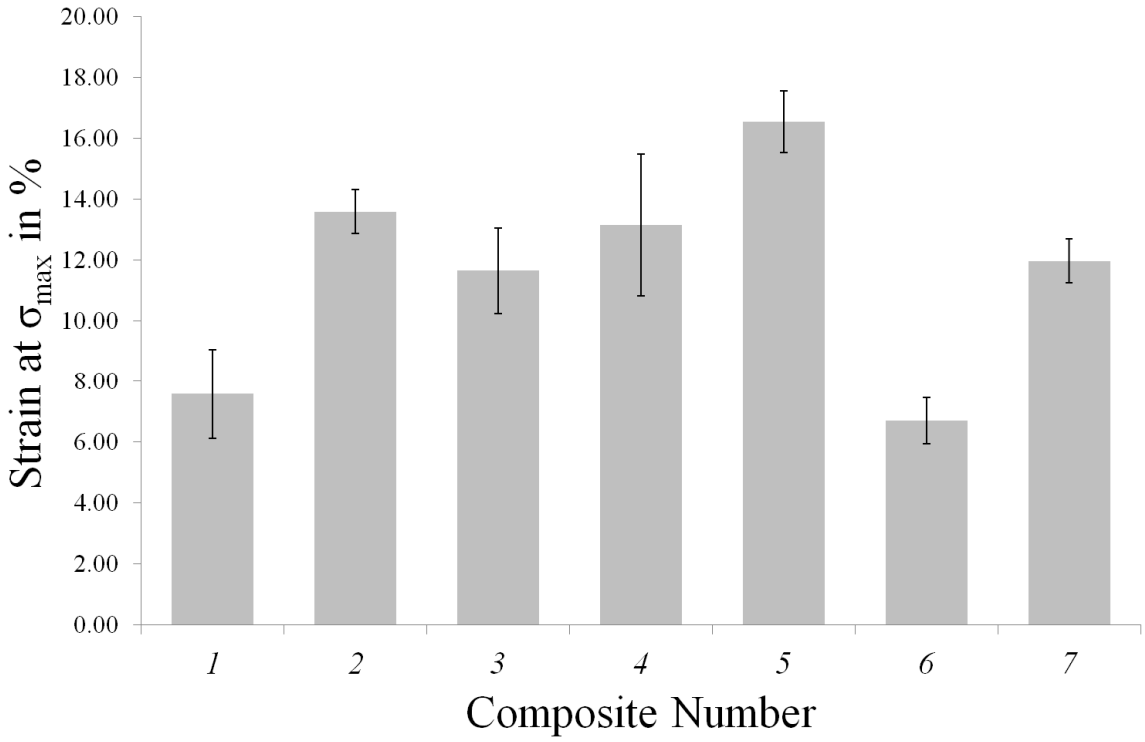

Figure 69: Strain at UTS of the 7 different composites. The error bars represent one standard deviation.

While composites 2 and 7 show low values for the V_f, UTS and Young's Modulus it could be assumed that ACC tensile properties depend primarily on the fibre volume fraction. It has been shown for many biocomposites that an increase in V_f causes an improvement of tensile strength and Young's modulus given a V_f between 10 and 60 % [317-319]. However, similar trends were not observed for the ACC laminates, with no clear correlation between the UTS or Young's modulus and V_f (Figure 71).

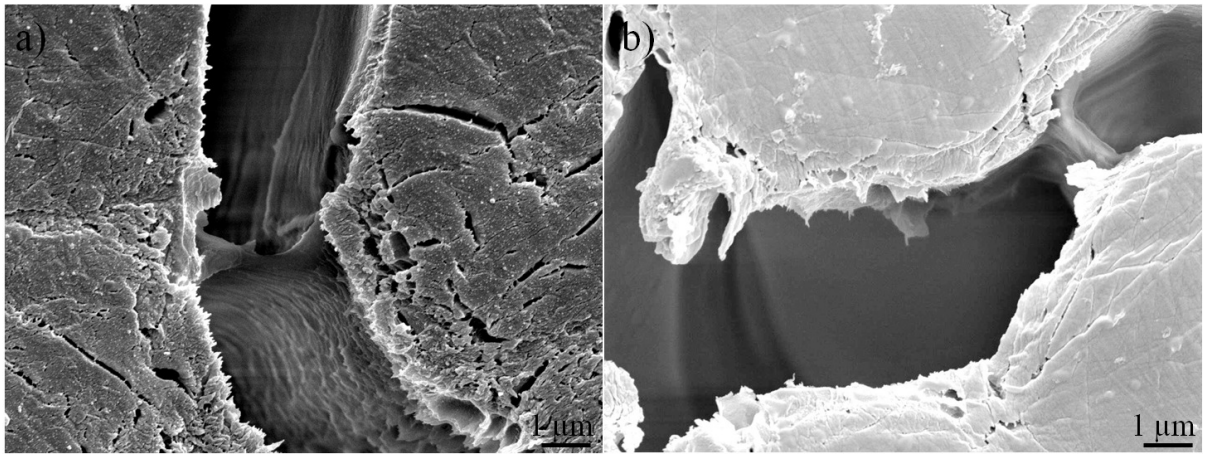

Figure 70: SEM micrographs of the cross-sections of (a) composite 7 and (b) composite 1, showing the details of the single fibres within the composites. An accelerating voltage of 5 kV was used.

It appears that for the biocomposites with a very high V_f, such as the ACC laminates in this work, that an increase in V_f does not necessarily improve the tensile properties. The composite properties are clearly dominated by the fibre properties and small changes in the amount of present matrix phase will not drastically change the composite performance, especially as only small fraction of the fibres are dissolved in the process.

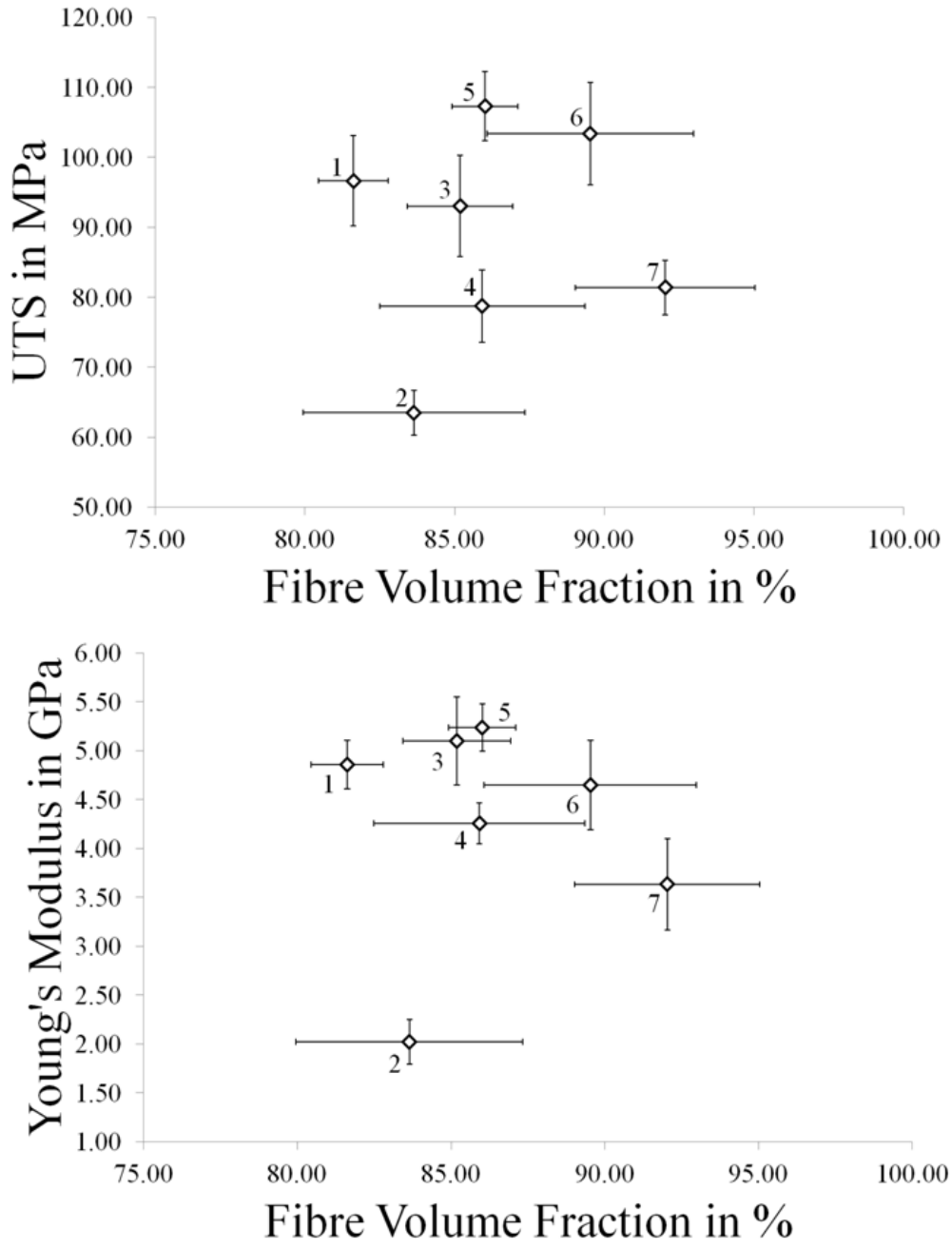

Figure 71: Plots of UTS and Young's modulus against V_f for the 7 produced composites. No statistical correlation can be identified.

A one-way ANOVA analysis combined with a Tuckey HSD test of the obtained values for UTS and Young's modulus was carried out to judge the statistical significance of the effect of the processing parameters. Composites 2 and 7, showed no significant difference between each other but a significantly lower UTS compare with the other composites. The lower UTS is likely to be the direct result of the low V_f and insufficient

fibre-matrix adhesion caused by either a too short (composite 2) or too long (composite 7) dissolution time.

No significant difference could be found between the UTS of composite 5 and 6 but the UTS of composite 5 was significantly higher ($p < 0.05$) than the UTS of all other composites. Furthermore, composite 6 showed a significantly higher UTS than composite 3 and 4 ($p < 0.05$). As no direct correlation to the V_f can be drawn it can be assumed that the drying conditions have a very strong influence on the final composite UTS. Composite 5 was dried at room temperature, allowing the absorbed water to slowly evaporate without causing too much disruption of the created fibre-matrix-interphase. The harsher drying conditions of the other composites, being heated up to 100 °C will cause strong shrinkage of the fibres and matrix phase.

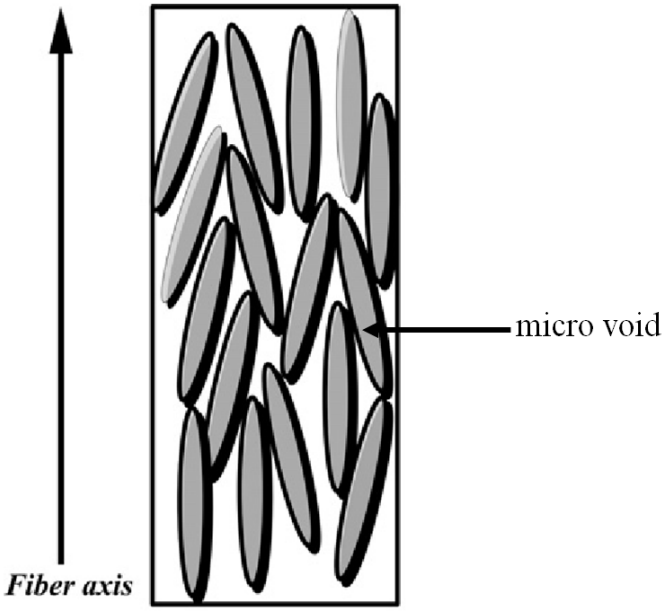

Figure 72: Orientation of micro voids within an elementary regenerated cellulose fibre. Taken from Jiang *et al.* [320], modified.

It is known that regenerated cellulose fibres contain microvoids between the elementary fibrils (Figure 72) [320, 321]. The presence of microvoids will likely result

in a greater uptake of water during the regeneration and washing stage of the ACC processing. The water is then removed during drying [316]. The drying process will lead to longitudinal shrinkage of the fibres. However, shrinkage in the transverse direction is also possible due to "zipping-up" of cellulose fibrils that results from the formation of new hydrogen bonds between cellulose fibrils [321]. It is thinkable that the orientation of crystalline, semi-crystalline and amorphous fractions, present in a rayon fibre, underwent different degrees of orientation during fibre processing. The orientation could in turn lead to an anisotropic shrinkage behaviour of the fibres. The abovementioned cracking of the newly formed matrix phase (Figure 66) is assumed to be related to the differences in the nature of the fibre and matrix shrinkage behaviour since the shrinkage of the matrix phase will be isotropic. A similar difference in shrinkage between reinforcing and matrix phase was observed for ACC films processed *via* the 2-ste-method and described in detail in Section IV.3.1.

The use of low temperature drying for composite 5 was useful for reducing shrinkage of the ACC laminate. Similarly, shrinkage of the ACC laminate was minimised by using ethanol or ethanol-water mixture as the washing medium for composites 1 & 6. It is known that ethanol is taken up less in the herein used cellulose II when compared with water [273, 315, 316]. For instance, the moisture uptake by mercerized cotton is at least 85% lower in ethanol than in water [315]. While for rayon viscose the moisture sorption was more 250 % lower in ethanol than in water [316]. As a result, the shrinkage within composite 1 & 6 will be lower than in the water-washed composites, resulting in a less cracked matrix phase and less debonding in the fibre-matrix interphase and therefore better load transfer through the composite. The better load

transfer is resembled in the high UTS of composite #1 (96.64 ± 6.47 MPa) and #6 (103.38 ± 7.30 MPa) (Figure 67).

The ANOVA analysis of the Young's modulus of composite 1, 3, 5 & 6 only showed a significant difference between regeneration and washing in distilled water followed by low temperature drying (composite 5) and regeneration and washing in ethanol (composite 6). No difference was observed between the use of water-ethanol mixture (composite 4) and pure ethanol (composite 6), although composite 4 showed a significantly higher Young's modulus than the composite dissolved for only 30 min (composite 2) and for 24 hr (composite 7), again supporting the assumption that a too short or too long dissolution time leads to a reduction in tensile properties.

Interestingly, the composites regenerated with ethanol (4 & 6) showed a lower Young's modulus than the composites regenerated with water. The effect of shrinkage has less impact on the Young's modulus than compared with the UTS. Thus, variations in moduli may be the result of differences in the crystalline structure of the regenerated portion of cellulose.

Almost no research has been conducted on the influence of the precipitation medium on the crystal structure of regenerated cellulose. However, Fink *et al.* reported that the crystallinity of NMMO fibre regenerated in methanol can be increased by instead regenerating the cellulose in water [46]. Thus, it is possible that the crystal structure of the newly created matrix phase does also depend on the precipitation and/or the washing media. Hence, the variation in Young's modulus may be the due to changes in crystal structure of the regenerated cellulose on the fibre surface. This hypothesis is supported by the measured strain to failure of composites 5 & 6 (Figure 69).

However, it has to be said that the analysis of Young's moduli and strain to failure is simply based on the cross-head displacement resulting in a relatively high uncertainty level of the reported values [322]. Available strain gauges did not produce reliable values due to the rough surface of the tested laminates. For a more reliable analysis an optical strain measurement system should be used to validate made observations.

Amorphous cellulose has been described as brittle by Czihak *et al.* [323]; therefore it could be assumed that using ethanol as the regeneration medium should lead to a more amorphous and therefore brittle matrix phase, lowering the overall strain of the composite.

The microfibrils within a single fibre show a higher degree of order in composite 5 than in composite 6 (Figure 73). This supports the assumption that gentle drying conditions lead to a microstructure with less interfibrillar cracks. However, a more detailed analysis of the portion of regenerated cellulose in close proximity to the fibres could show the formation of an "interphase" between fibre and matrix rather than a clear interface. The properties of this interphase depend on the used processing conditions and could therefore influence the overall composite properties.

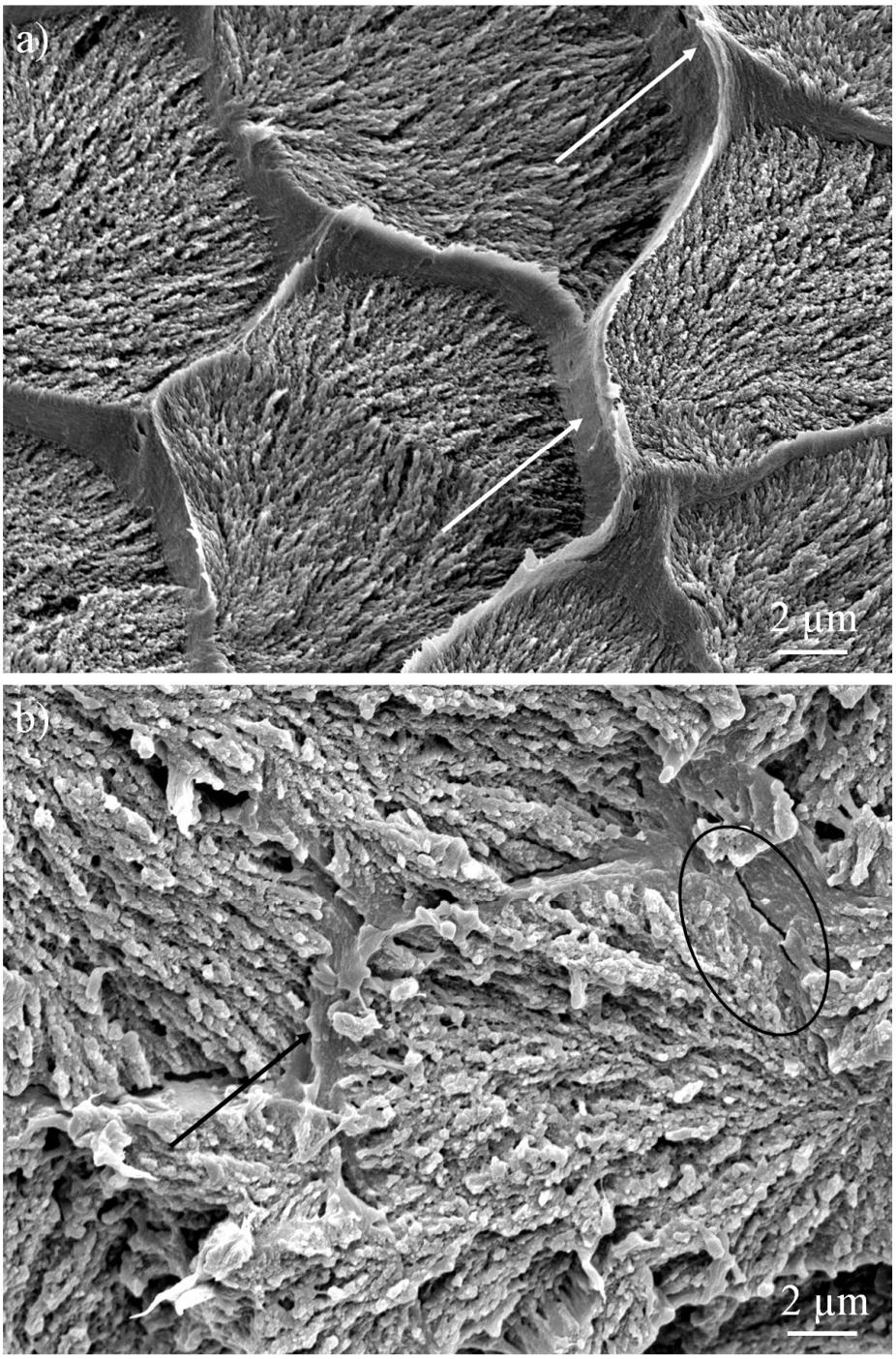

Figure 73: Fracture surface of composite 5 (a) and composite 6 (b) showing several single fibres connected by a thin layer of matrix phase, indicated by the arrows. An interfibrillar crack can be seen in composite 6 (b). An accelerating voltage of 5 kV was used.

In general, cellulose is a semi-crystalline polymer characterised by the presence of crystalline and low-ordered (amorphous) domains. Cellulose is often referred to as paracrystalline since the crystalline and amorphous domains or regions show a gradual

transition from crystalline to amorphous and vice versa along an elementary cellulose fibril, combined with low 3D ordering of the crystal lattice [324]. A distinction also needs to be made regarding the origin of the paracrystallinity since it may be due to either (I) the presence of a characteristic paracrystalline phase or (II) an imperfect crystal showing paracrystalline distortions [325]. The paracrystallinity of cellulose is attributed to paracrystalline distortions of the cellulose crystals since thin paracrystalline layers on the surface of crystallites have been identified [324].

Long molecular chain molecules such as cellulose, exert forces upon each other, leading to a mutual orientation also referred to as the "order in the smallest region" [326]. Hence, cellulose molecules exhibit tendencies toward parallelisation, especially in highly concentrated solutions [327]. Additionally, the examination of the interface of single-polymer composites such as self-reinforced PP or PE composites show the formation of a transcrystalline phase surrounding the fibres. The crystallites that make up the transcrystalline region tend to be orientated perpendicular to the fibre orientation [328-330]. Therefore, it seems possible that a similar trans- or paracrystalline "interphase" might be formed during the regeneration of the matrix phase in ACC laminates, with microfibrils arranged perpendicularly to the cellulosic fibres. The surface of the cellulose fibre can act as a nucleation side leading to crystal growth as it has been exemplarily shown for highly purified (>98.5% cellulose) wood fibres in combination with PP [331]. High magnification SEM micrographs indicate the presence of such an ordered paracrystalline phase in close proximity to the fibres (Figure 74). Shrinkage effects caused by the sample preparation that could contribute to the formation of those fibrillar structure cannot be ruled out completely. However, the structures can only be found on the surface of partially dissolved fibres within a

composite and neither in partially dissolved fibre yarns nor completely dissolved and regenerated cellulose.

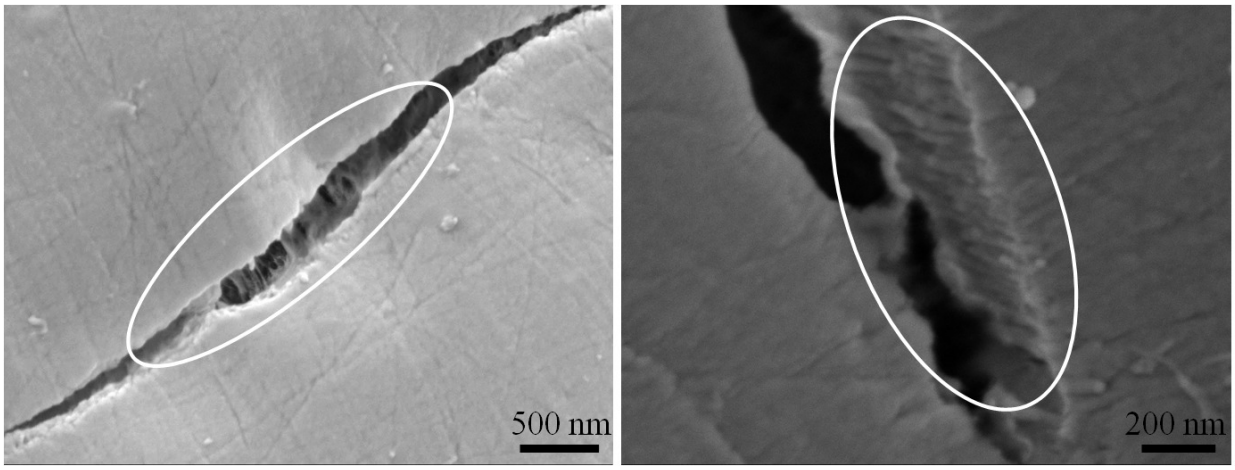

Figure 74: SEM micrographs of fibril-like structures orientated parallel to each other and perpendicular to the longitudinal axis of the fibre. The images are taken of fibrils that lie between two elementary fibres in an ACC laminate. An accelerating voltage of 5 kV was used.

3.3.3 The effect of the Processing Parameters on ACC Crystallinity and Interphase

A more thorough investigation of the molecular structure and orientation of the carbon atoms within the cellulose II chains and other allomorphs can be achieved by high resolution 13C solid state NMR [332]. An overview of the carbon atoms and the unit cell angles for a cellulose molecule is given in Figure 75.

Differences in the proton spin-lattice relaxation time constants $T_{1\rho}(H)$ influence the signal strength in cross-polarisation (CP) NMR experiments and therefore make it possible to distinguish between ordered and disordered areas within the cellulose chains [333, 334]. The carbon atom numbers are assigned to the different peaks as described in the first NMR spectrum reported for cellulose II by Atalla *et al.* [335].

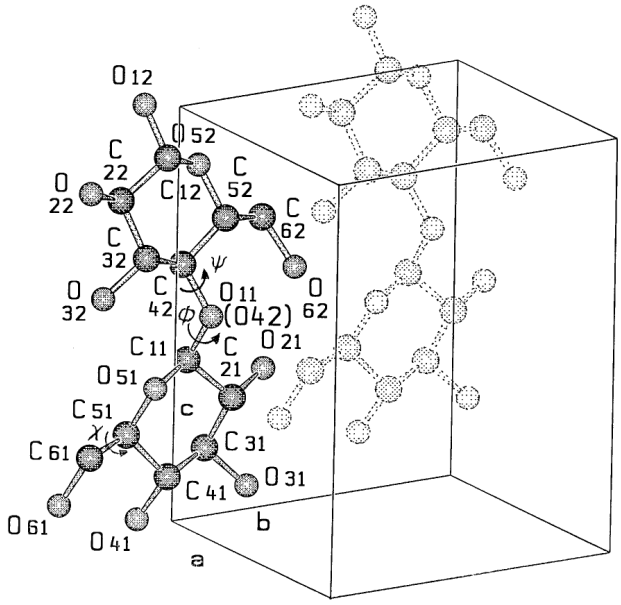

Figure 75: Cellulose chains with atom labelling; from [92].

The NMR data for the C-6 atom provides information on the crystallinity of the interior chains (I) and surface chains (s) for the cellulose II crystallites (Figure 76) [336].

The peak at C-6 was deconvoluted to determine the contribution from each of the different crystalline regions (interior, surface and non-crystalline) to the overall peak C-6 area by determining the single peak areas (i+s & s) (Table 10).

Composite 5 shows highest amount of crystalline phases in the combined 'i+s' area (88.65 %) compared to the fibre (66.83 %) and composite 6 (13.31%). For composite 6, the surface area is the largest contributor to the crystal structure (83.09 %) compared to the fibre (21.2 %) and composite 5 (9.16 %). The NMR results confirm that both the use of (I) water rather than ethanol and (II) longer drying times allows for a more ordered crystalline arrangement of the cellulose chains within in the fibre (Table 10).

.

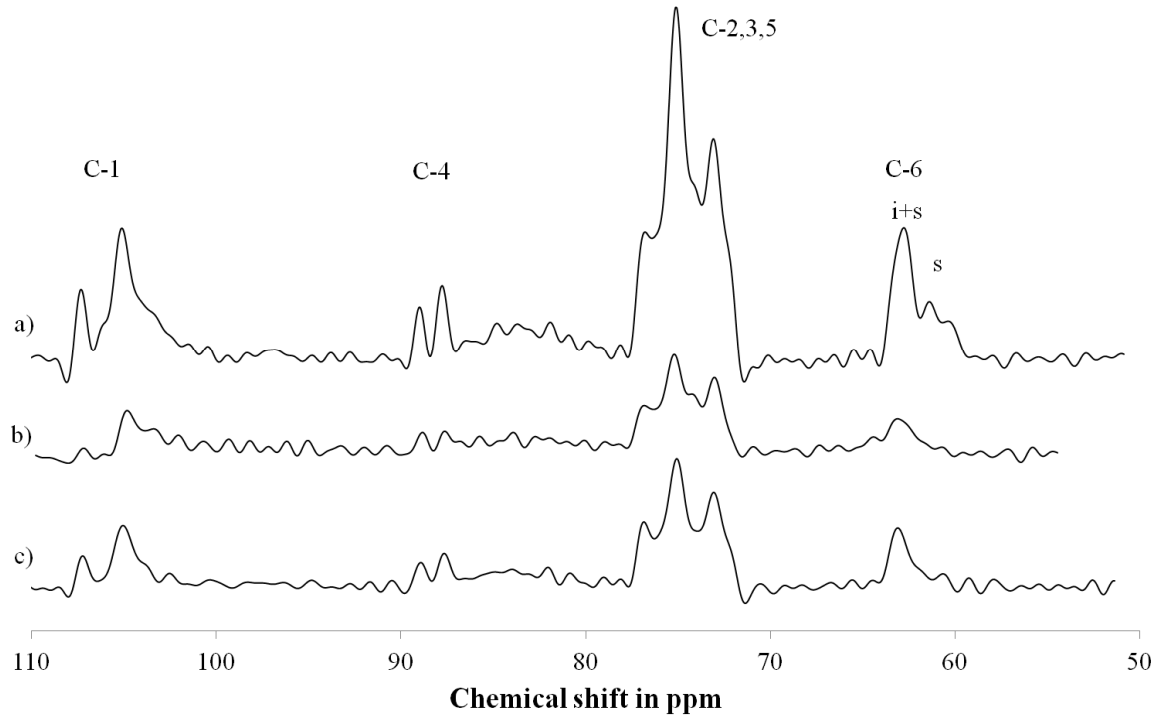

Figure 76: NMR spectra of the (a) as-received rayon fibre, (b) composite no. 5, and (c) composite no. 6. The peak at C-6 is divided between the order of the cellulose chains located in the interior (I) and at the surface (s) of the cellulose II crystal [336].

The C-4 "envelope", meaning the region between approximately 92 and 80 ppm, provides the most information on the crystalline structure, and especially partially-crystalline and non-crystalline regions within the cellulose molecule [337]. The C-4 region of the three different materials is shown in Figure 77. Ibbett *et al.* identified three different regions of crystalline order within this region for cellulose II; (I) two sharp peaks between 88 and 89 ppm resembling fully-ordered (crystalline) cellulose, meaning fixed φ, ψ and χ unit cell angles (Figure 75). (II) a broader peak around 86 ppm, accounting for partially-ordered regions with the glycocidic angles φ and ψ fixed in crystalline positions but with a flexible angle χ. (III) a very broad peak with its centre around 83 ppm, describing a disordered phase where all three angles φ, ψ and χ are flexible [338]. The contributions of those regions for the different materials are summarised in Table 10.

The as-received rayon fibre and composite 5 exhibit similar amounts of fully ordered phase (37.94 & 38.11 %), while composite 6 shows a lower amount of crystalline phase (32.74 %), suggesting that the use of water results in a higher crystallinity of the interphase (Table 10). Under these processing conditions significant recrystallisation occurs as shown by the presence of large amounts of paracrystalline phase (19.42 %) for composite 5.

Composite 6 shows a higher amount of partially ordered phase of (15.68 %) compared to the as-received fibre (8.12 %) (Table 10), indicating that the dissolution and regeneration of rayon fibres in BmimAc results in more ordered crystalline structure. One possible explanation for the increase in crystallinity following SIP is the preferential dissolution of the amorphous fractions of the fibres. Upon regeneration the dissolved portion of amorphous cellulose precipitates as a more crystalline or paracrystalline phase in a similar process as described by Ibbett *et al.* for acid hydrolysis of regenerated cellulose fibres [339]. The use of water as the regeneration medium combined with gentle drying conditions (*i.e.* composite 5) increases the crystallinity of the material, while the use of ethanol during regeneration results in a decrease in crystallinity to a partially-ordered phase.

The increased crystallinity of the created fibre-matrix-interphase will increase its stiffness and could therefore be a contributor to the higher Young's modulus of composite 5. It is also thinkable that the semi-crystalline achieves its highest order on the fibre surface therefore increasing the crystallinity of the fibres and correspondingly their Young's modulus. However, a more detailed analysis of the mechanical properties

of the interphase by using for example techniques such as nano-indentation would be necessary to validate this assumption.

Table 10: Signal distribution for assigned peak regions for the C-4 and C-6 peak analysis, calculated for each material.

C-4 analysis

Sample	Fully ordered region	Partially-ordered region	Disordered region
Rayon Fibre	0.3794	0.0812	0.5194
Composite 5	0.3811	0.1942	0.4262
Composite 6	0.3274	0.1568	0.5166

C-6 analysis

Sample	interior + surface	surface	Disordered region
Rayon Fibre	0.6683	0.212	0.1197
Composite 5	0.8865	0.0916	0.0247
Composite 6	0.1331	0.8309	0.0325

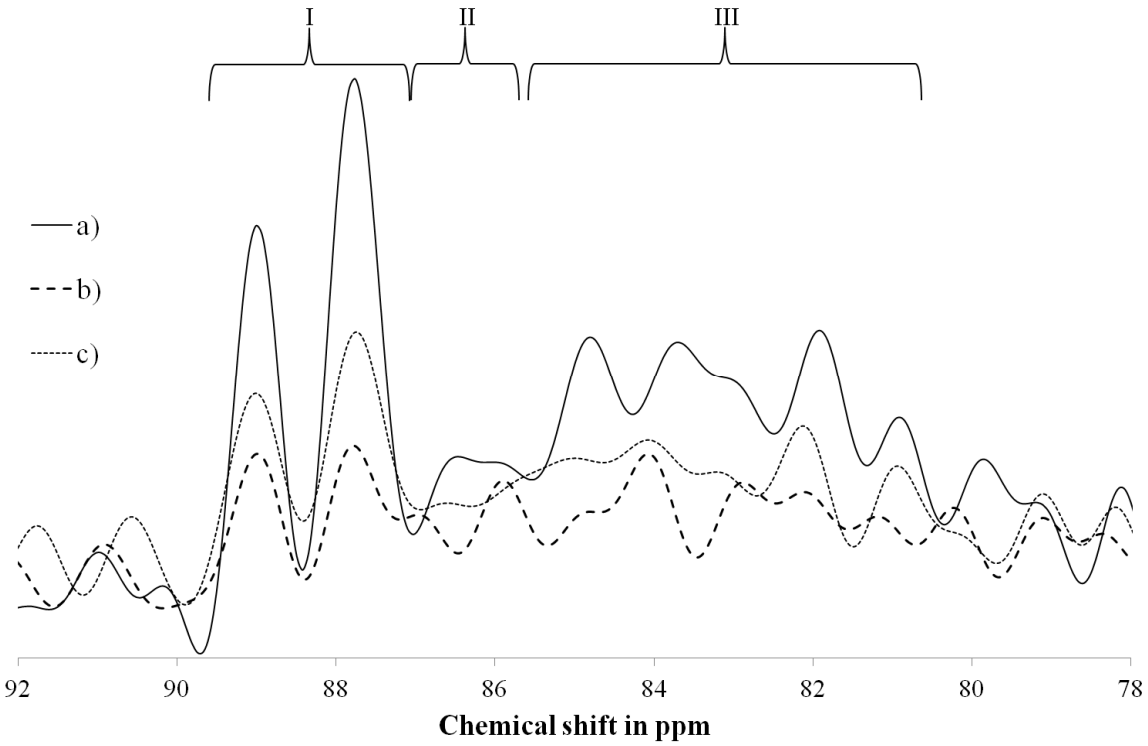

Figure 77: NMR spectra of the C-4 region of the as-received rayon fibre (a), composite 5 (b) and composite 6 (c). The different peaks have been assigned to well-ordered (I), partially-ordered (II) and disordered (III) regions according to Ibbett *et al.* [338].

3.3.4 WAXD OF ACCS AND RAYON FIBRE

The WAXD spectra of composite 5 and composite 6 did not differ greatly (Figure 78). The CrI values for composite 5 and 6 were calculated as 77 and 79%, respectively, indicating only minor differences in the crystallinity. It is likely that the WAXD pattern of the composites is dominated by the larger proportion of rayon fibres present in the ACC samples compared with the matrix phase. Accordingly, the CrI of the ACC laminates was very similar to that of the as-received rayon textile (77%) (see Section V.3.2).

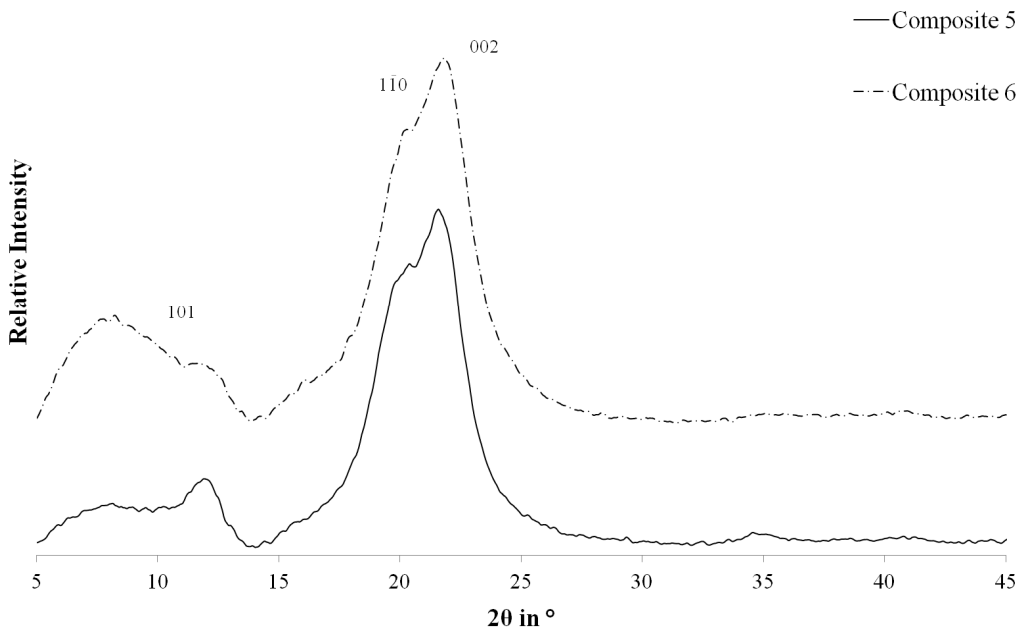

Figure 78: WAXD spectra of composite 5 and composite 6. The data plots have been offset from each other. The peaks are assigned according to Hindeleh *et al.* [340].

Thus, the effect of the type of regeneration medium on the crystallinity of the matrix phase was investigated instead by *completely* dissolving selected samples of the rayon textile. The WAXD spectra of the fully dissolved and regenerated rayon textile indicate that using ethanol as the regeneration medium leads to drastically reduced CrI of regenerated cellulose (13%) compared with using water (74%) (Figure 79). It is proposed that the water present in cellulose allows for further rearrangement of the cellulose chains to form a more crystalline (cellulose II) network which is a result of water weakening the intra- and intermolecular bonds responsible for the molecular arrangement of the cellulose chains [341]. It has also been shown that the molecular (re-)arrangement can be achieved for cellulose I as well as dissolved cellulose [342]. The sample of completely dissolved cellulose regenerated in distilled water suggests that a higher crystallinity can be achieved when using water over ethanol.

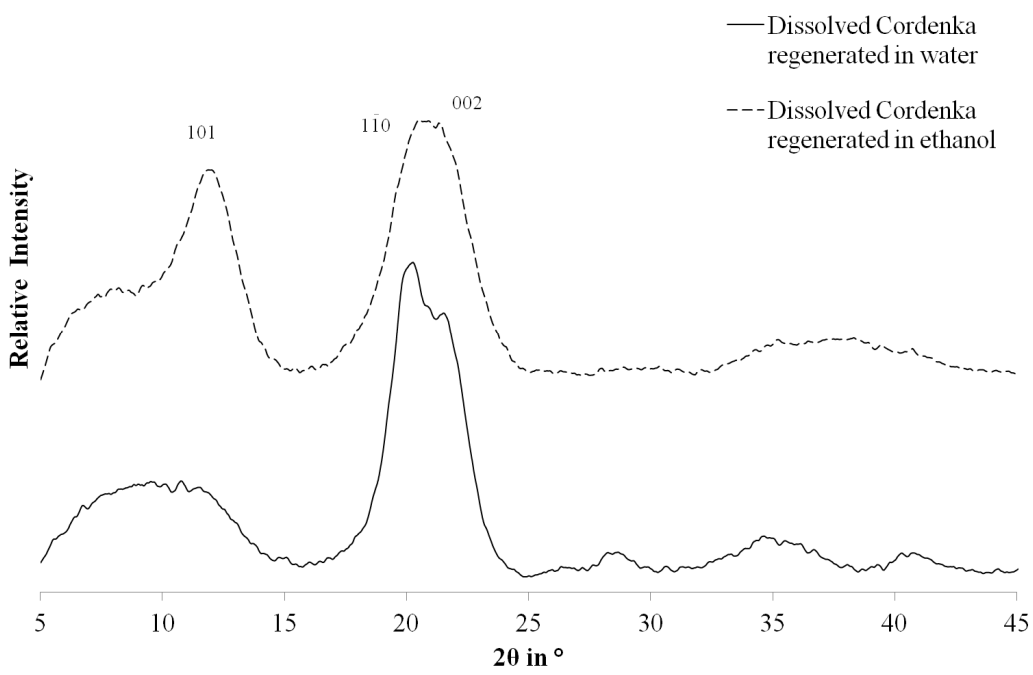

Figure 79: WAXD spectra of completely dissolved rayon fibre regenerated and washed in distilled water and ethanol. The data plots have been offset from each other. The peaks are assigned according to Hindeleh *et al.* [340].

3.3 CONCLUSIONS

It could be shown that the processing parameters affect the microstructure and tensile properties of ACCs processed *via* SIP. A V_f of over 80 to 92 % can be achieved for ACC laminates depending on the chosen dissolution time and temperature, washing and drying conditions. It could be shown that a reduction of the dissolution time to 30 min leads to less formation of matrix phase compared to a dissolution time of 60 min, even at higher dissolution temperatures (*e.g.* 125 °C). Over-dissolution is considered to occur for a drastically extended dissolution time of 24 hr, resulting in a reduced UTS and Young's modulus of the ACC laminate. A minimum dissolution time of 60 min is required under these SIP conditions and with the selected materials so that mechanical properties are not compromised.

The use of different regeneration and washing medium greatly influences the crystallography of the "interphase" created between fibre surface and matrix. As a result the area between fibre and matrix in an ACC should be referred to as "interphase" rather than a clear interface. However, since the matrix phase is a minor constituent phase in the ACC laminates it does not result in major changes to the tensile properties of the laminates.

The most important factors are the moisture uptake and corresponding shrinkage generated by the drying conditions since these influence the fibre-matrix interphase and therefore the mechanical properties of the ACC laminates. If water is used for the regeneration and washing, excess water needs to be removed slowly from the composite to avoid damage to the matrix due to material shrinkage. Alternatively, ethanol can be used to reduce swelling of the cellulose and therefore decrease the impact of the drying conditions on the fibre-matrix interphase.

3. FLEXURAL AND IMPACT PROPERTIES OF ALL CELLULOSE COMPOSITE LAMINATES

3.1 INTRODUCTION

Generally, biocomposites that are based on hemp, flax, ramie, sisal or wood fibre demonstrate adequate mechanical properties (strength and modulus) for many industrial applications. However, biocomposites are well known for exhibiting quite poor impact resistance [343]. The relatively low impact strength of biocomposites prevents the broader application of these materials since impact resistance is often a key requirement in product design [344]. Recently, improved impact properties have been achieved by either using polymer matrices with inherent impact resistance [185] or introduction of highly ductile fibres based on regenerated cellulose (*e.g.* Lyocell [60]). However, improved impact strength in biocomposites can often be the result of a poor fibre-matrix adhesion resulting in reduced tensile properties [185, 345]. To date, neither the impact nor flexural properties of ACCs have been investigated. In the present work, the impact resistance and flexural properties of ACC laminates based on a rayon textile were analysed by 3-point bending, puncture impact and Charpy impact testing to assess their potential as alternative "green" engineering material.

3.2 EXPERIMENTAL PROCEDURES

2.1.1 Materials

The same ionic liquid and rayon textile were used to produce samples for flexural and impact testing.

2.1.2 Sample Preparation

To produce panels of the ACCs, 5 layers of the rayon textile (120 × 120 mm) were used. The laminates were synthesised *via* SIP with the rectilinear infusion set-up.

2.1.3 Impact Testing

Two different tests were chosen to analyse the impact response of the ACC laminates. Charpy impact testing is routine used in production monitoring and developmental laboratories and therefore offers the most comprehensive comparison of ACCs to the impact strength of other biocomposite reported in the scientific literature. The puncture impact testing allows for a better understanding of complex loading conditions similar to actual use in real life [346].

2.1.3.1 Puncture Impact Testing

Impact tests were performed in accordance with EN ISO 6603-2:2000 using an Imatek IM10 drop mass impact tester (Imatek Ltd., Old Knebworth, UK). A 20 mm hemispherical striker was used from a falling height of 1 m. The total striking mass was 9.54 kg and the impact velocity was 4.43 m/s, resulting in a total impact energy of 94 J. Five samples of 60 mm × 60 mm were cut from the laminates using a band saw and conditioned for 24 h at 23 ± 1°C and 50 ±1 % RH. Sample thickness was 2 ± 0.05 mm. The testing was performed using a 40 mm diameter support ring, and the samples were clamped.

2.1.3.2 Charpy Impact Testing

Additional impact tests were executed in accordance with DIN EN ISO 179 to determine the unnotched Charpy impact strength. 12 samples of 80 × 10 × 3 mm were tested in

flatwise impact direction parallel to the fibres using a 4 J pendulum. Before testing, the samples were conditioned for 24 h at 23 ± 1°C and 50 ± 1% RH and sample dimensions were accurately measured using a digital vernier calliper (Mitutoyo Absolute, Mitutoyo Deutschland GmbH, Neuss, Germany).

2.1.4 Flexural Testing

3-point bending tests were conducted on samples of 2 mm thickness, 10-11 mm width and a length of 45 mm, cut from the laminates using a band saw. Eight samples were tested after conditioning for 48 h at 23 ± 2°C and 50 ± 2% RH.

2.1.5 Scanning Electron Microscopy

SEM analysis on the fracture surfaces of tested impact and bending samples was performed as described in Section 1.2.3.

3.3 RESULTS AND DISCUSSION

3.3.1 The Impact Behaviour of ACCs

3.3.1.1 Puncture Impact Testing

Table 11 shows the results of the puncture impact test.

Table 11: Mean results of the puncture impact tested samples with standard deviation

	Impact energy in J	Peak force in kN	Peak displacement in mm	Peak energy in J	Puncture Deflection in mm	Maximum strength in kN/mm^2
Mean	83.71	3.52	7.25	9.44	7.55	1.96
S.D.	0.17	0.35	0.49	1.98	0.44	0.19

The four typical failure modes following puncture impact testing have been identified as (1) matrix failure, observed as cracking of the matrix phase parallel to the fibres; (2) delamination of the laminate layers due to interlaminar stresses; (3) fibre failure such as fibre breakage and fibre buckling and (4) full penetration of the laminate [347]. A strong compaction of the laminates could be observed as a result of the *in situ* formation of the matrix phase under pressure during SIP. SIP results in small volume fraction of well distributed matrix phase throughout the ACC laminate. The force as a function of the displacement during puncture impact can be divided broadly into 4 different stages that can be loosely associated with the observed failure modes (Figure 80). At Stage 1, the sample remains undamaged. With increasing load, the first damage in the composite appears (Stage 2) most likely within the matrix phase but rapidly spreading to the fibres. The increasing load will lead to fibre-matrix debonding and delamination during Stage 3. Extensive delamination, fibre breakage and finally complete failure occurs during Stage 4.

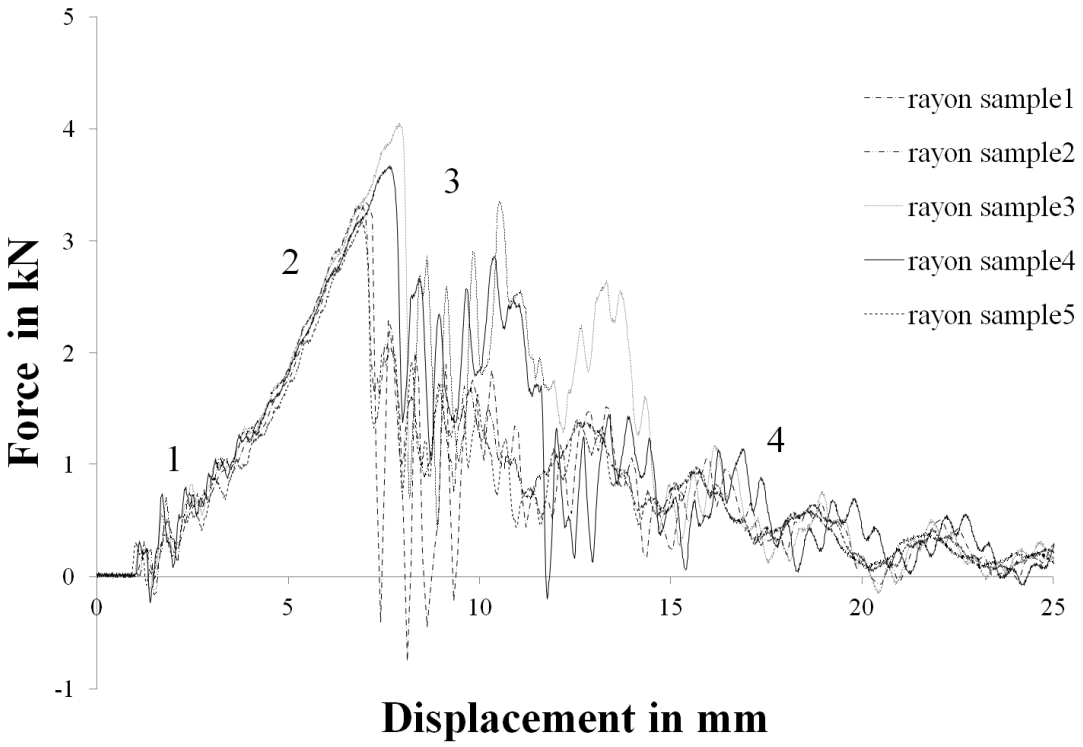

Figure 80: A plot of the impact force as a function of displacement for each of the 5 samples of ACC, with the various stages of failure as indicated by the numbers 1-4.

It is interesting to note that the samples only exhibited significant variation during Stage 3. The variations during Stage 3 are likely caused by variations in crack propagation through the samples.

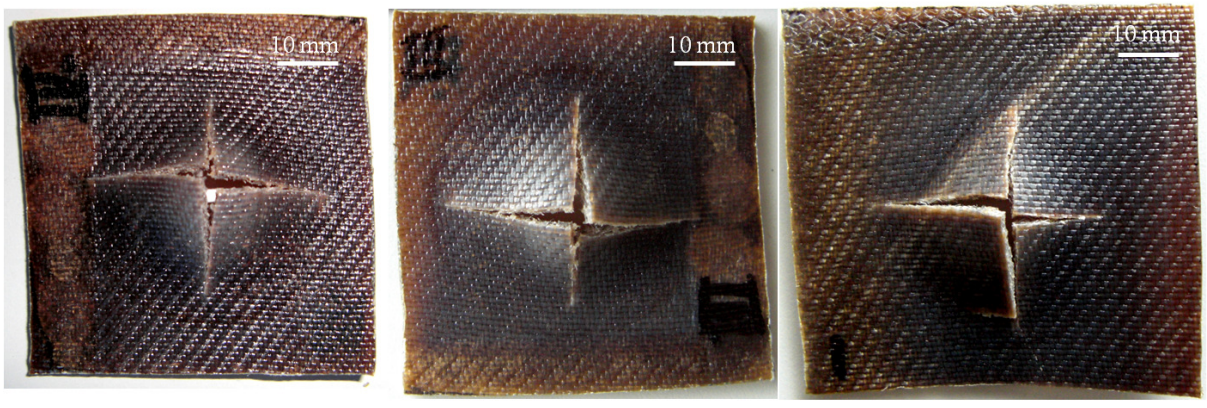

Figure 81: Photographs displaying the typical failure mode of the tested ACCs shown for three different samples.

Pyramidal type failures following the puncture impact tests were observed for all tested samples, indicative of a rigid matrix composite (Figure 81), while a flexible matrix composite would suffer from extensive deformation, a bulged failure mode and fibre pull-out [348]. No visual proof for delamination of the single laminae within the laminate could be found in the sample fracture surface. This indicates a strong interlaminar adhesion. Therefore delamination probably occurs between individual fibres within the composites.

SEM micrographs of the fracture surface support the assumptions of strong interlaminar adhesion within the ACCs produced in this work (Figure 82). It was clearly observed that the single plies of the laminate were well bonded with no observable interlaminar failure (Figure 82a). Three failure modes were observed: (i) fibre fracture (Figure 82b-1); (ii) fibre delamination, splitting fibre or small fibre bunches along the fibre axis (Figure 82b-2); and (iii) fracture of complete fibre yarns (Figure 82b-3). Delamination was also observed within the ACCs (Figure 82c). It was clearly seen that the fibres in the yarn were "peeled off". The aligned structures at the fracture surface left behind could resemble traces of single fibres. Figure 82-d and Figure 82-f show the fracture surface of individual fibres while Figure 82-e shows delamination between single fibres.

It would seem likely that some fibres undergo greater dissolution, resulting in a correspondingly larger fraction of matrix phase. Following fibre fracture, it is apparent that the failed fibres may remain bonded *via* the matrix phase (Figure 82f). In contrast, weak adhesion, and thus delamination, occurs in regions in which the fibre dissolution is less extensive. Both failure modes, fibre fraction and delamination, will contribute to

the high impact strength of ACCs, as both matrix phase and fibre undergo a strong elongation before breaking (Figure 82d).

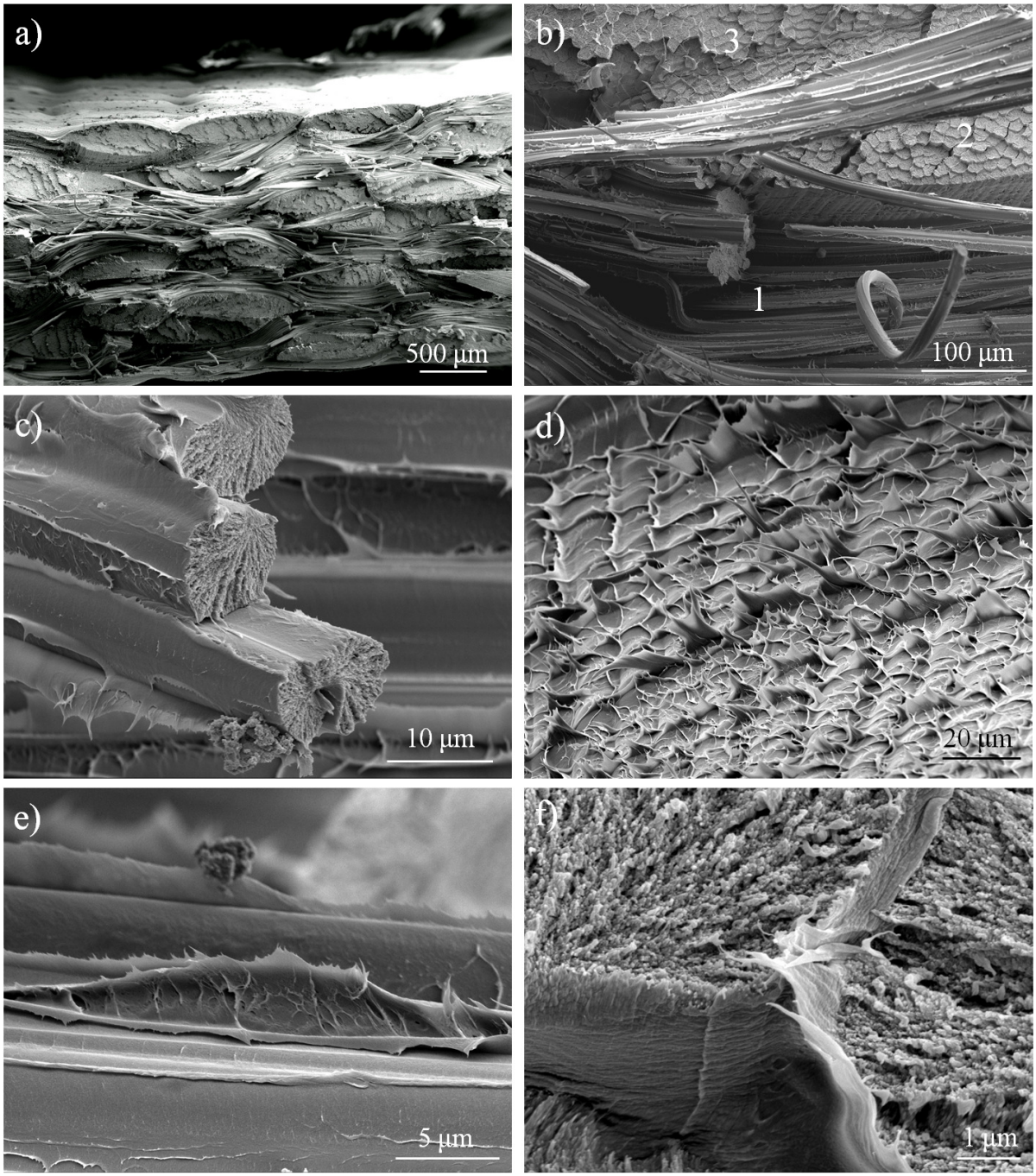

Figure 82: SEM images of the fracture surface of an impacted tested ACC laminate. Figure 82 a) shows the complete cross-section, Figure 82 b) shows occurring failure modes with (1) fibre fracture, (2) fibre delamination, (3) complete fracture of fibre yarns. Figure 82 c) shows fractured fibres, Figure 82 d) the delamination of a polyfil, Figure 82 e) delaminated fibres and Figure 82 f) the fracture surface of two single fibres. An accelerating voltage of 5 kV was used.

3.3.1.2 The Charpy Impact Strength of Unnotched ACC Laminates

The average unnotched Charpy impact strength of the four tested samples was 41.54 (±4.44 kJ/m^2). All samples showed hinge break behaviour. This type of impact failure is characterised by an incomplete break such that both parts of the sample are only held together by a thin peripheral layer in the form of a hinge of low residual stiffness. The Charpy impact strength of the ACCs was higher than other biocomposites (*e.g.* jute fibre–reinforced polyester is reported as (31. 87 kJ/m^2 [240], 29 kJ/m^2 and 27 kJ/m^2 [349]). It is interesting to compare the here reported ACCs to another form of composite made entirely from cellulosic material, so-called "all-plant fibre composites" (see Section I.3.2.2.2). Being made from sisal fibre and benzylated wood those composite only show an impact strength of 5.6 kJ/m^2, being more than 700 % lower.

The high elongation of the rayon fibre is a major contributor to the impact behaviour of the ACCs in addition to the aforementioned impact strengthening mechanisms. It has been shown that the impact strength of a natural fibre composite can be enhanced by the addition of high strain fibres [185].

3.3.2 Mechanical Behaviour of ACC Laminates in Bending

The average flexural strength of the tested samples was 135.24 MPa (± 11.16 MPa); the average flexural modulus was 3.72 GPa (±0.34 GPa) (Figure 83). The step-wise decrease in stress after reaching the maximum before complete ply failure observed for all samples is indicative of a progressive failure of the individual plies.

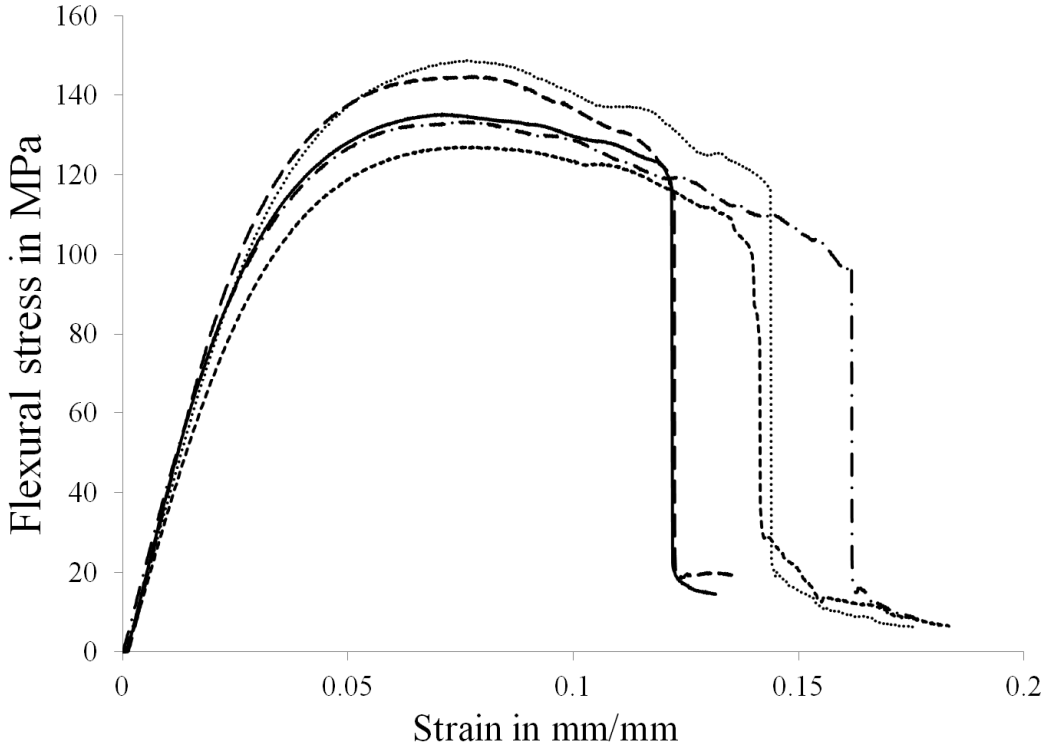

Figure 83: Comparisons of the flexural stress as a function of strain for 5 replicates of the ACC laminate. The failed samples did not exhibit interlaminar failure (Figure 84).

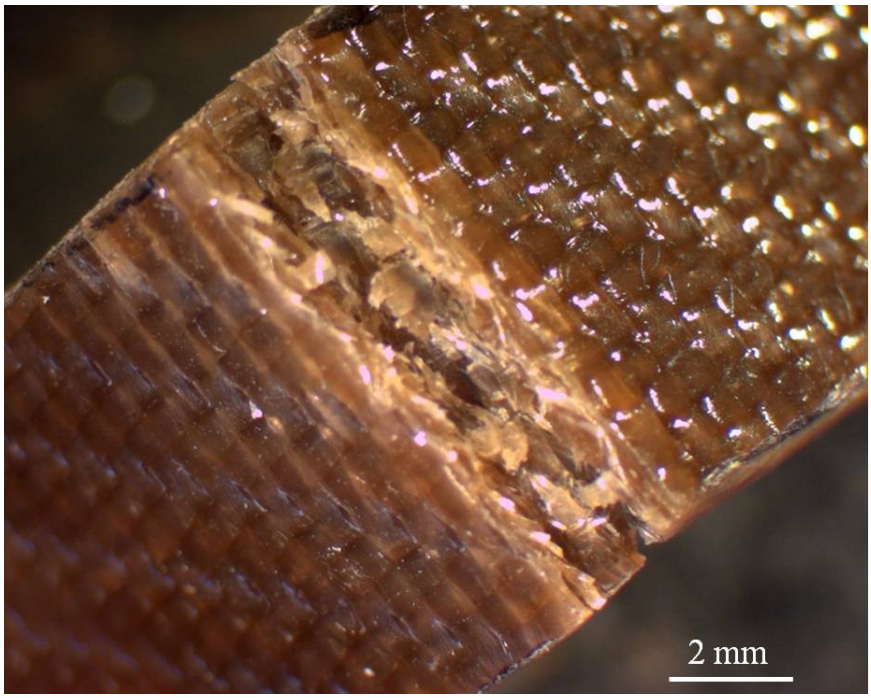

Figure 84: Fracture Photograph of the fracture surface of an ACC laminate following a 3-point bending test.

The characteristics of the failure following the bending test resemble that of the Charpy impact samples. Thus, it appears that in both cases there is delamination of bundles of fibres and individual fibres before the complete failure of the laminate. The gradual and/or step-wise decrease in strength following the maximum peak in stress is also indicative of delamination processes preceding the complete failure of the laminate.

As for impact testing, delamination of individual plies was not observed after bend testing (Figure 85). The dominant failure mode during bending is fibre breakage (Figure 85). Some pull-out of groups of fibres is evident after bend testing (Figure 85-a). It is apparent that fibres have also been peeled from the fracture surface (Figure 85-b), leaving a similar microstructural "imprint" as observed after impact testing (Figure 82). It is concluded that the strong interphase between individual fibres and matrix phase results in laminates with high flexural strength [70].

However, direct microstructural observation of the fracture surfaces does imply disbonding occurs between the fibres and matrix phase. Thus, ACCs cannot be thought of as having an interfaceless microstructure, but having a distinct interphase between fibre and matrix. This is explained by the structural changes that the cellulose crystals will undergo during dissolution and regeneration. Zhao *et al.* reported that cellulose I that is dissolved in an IL (BmimCl) and then regenerated will reprecipitate as cellulose II [167]. Presently, it is not known exactly what structural changes might occur when cellulose II is dissolved and regenerated in an IL. Next to the above discussed formation of a para-crystalline interphase, a phase transformation from cellulose II to cellulose IV_2 is possible under certain conditions [46, 350]. Thus, differences in the crystallinity between the matrix and reinforcing phase cannot be ruled out. Nishino *et al*. and

Soykeabkaew *et al*. observed an overall decrease in crystallinity of dissolved and regenerated cellulose [105, 129] and could also be shown for the use of ethanol as regeneration medium in Section VI.2.3.3.3. Furthermore, as proposed by Duchemin *et al.* and discussed earlier (Section VI.2) dissolved and undissolved portions of cellulose will swell by different amounts which upon regeneration again can cause differential shrinkage during regeneration, leading to the formation of voids in the fibre-matrix interphase [127]. It can therefore be assumed that in spite of being chemically identical, structural changes between matrix and reinforcing phase inhibit the formation of an interfaceless composite.

Externally applied loads are transferred *via* the matrix phase to the fibres due to the manufacturing process and the *in situ* generated matrix phase. Cracks will propagate along the full fibre length breaking the strong hydrogen bond network that exists between fibres and matrix phase before the fibres start to fail catastrophically.

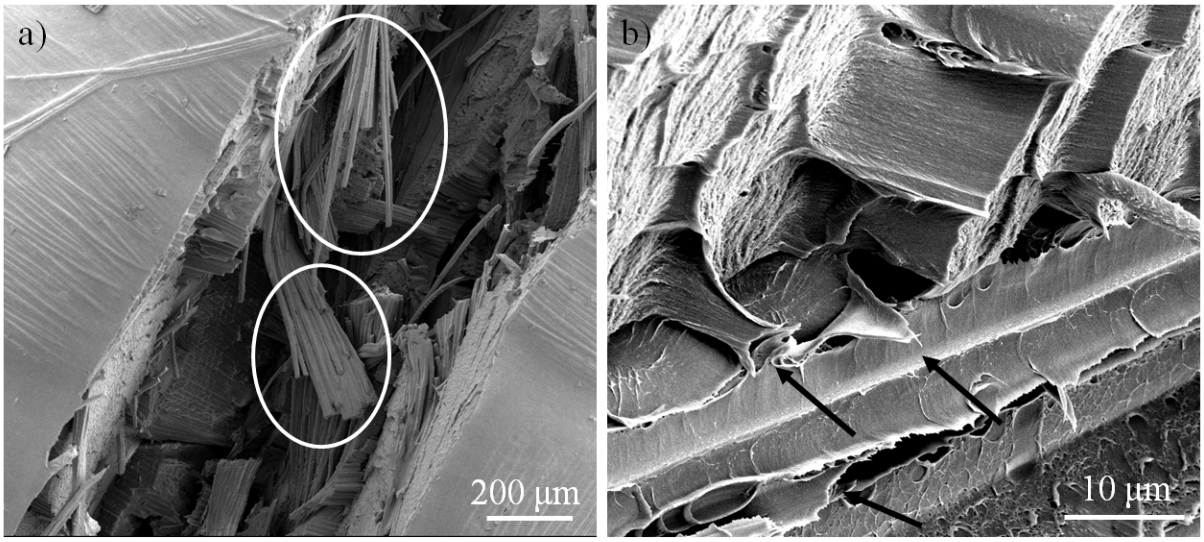

Figure 85: SEM micrographs of (a) fracture surfaces of an ACC sample tested in 3-point bending showing pulled-off fibres and (b) imprint left by fibres peeled from the fracture surface. An accelerating voltage of 5 kV was used.

The ACC laminates exhibited high flexural strength when compared with biocomposites based on natural fibres and petroleum- or bio-derived polymer matrices (Table 12 and Figure 86).

Table 12: overview over flexural strength and modulus of other biocomposites.

No.	Reference	Reinforcement (Fibre Volume Fraction in %)	Matrix	Flexural modulus in GPa	Flexural strength in MPa
1	O'Donnell *et al.,* 2003 [351]	recycled paper (45.3%)	soybean oil based resin	3.10	60.00
		flax fibre mat (14.06 %)	soybean oil based resin	1.70	44.00
2	Akesson *et al.,* 2009 [352]	air laid flax fibre mat (70 %)	acrylate modified soybean oil resin	6.90	98.00
		air laid flax fibre mat-PET (70%)	acrylate modified soybean oil resin	5.30	72.00
		coarse hemp fibre mat (70 %)	acrylate modified soybean oil resin	3.70	46.00
3	Pervaiz&Sain, 2003 [353]	non-woven hemp fibre needle felt (64 %)	polypropylene	4.90	63.00
4	Dhakal *et al.*, 2007 [347]	non-woven hemp fibre needle felt (26 %)	unsaturated polyester resin	6.49	110.00
5	Ahmed *et al.,* 2006 [354]	jute woven (46 %)	polyester resin	7.64	121.80
		jute-25% glass woven (46 %)	polyester resin	12.38	158.85

6	Goutianos *et al.*, 2006 [301]	flax fibre (270 g/mm^2) woven (< 30%)	vinyl ester resin	5.10	81.00
		flax fibre (325 g/mm^2) woven (35 %)	vinyl ester resin	8.90	130.00
7	Adekunle *et al.,* 2009 [355]	flax fibre woven (70 %)	styrene blended soy bean oil resin	6.14	110.00
8	Khondker *et al.,* 2005 [356]	half bleached jute fibre woven (20 %)	vinyl ester resin	4.10	78.00
		full bleached jute fibre woven (20 %)	vinyl ester resin	3.80	80.00
9	Jannah *et al,.* 2008 [357]	banana plant fibre woven treated with NaOH (sodium hydroxide) (10 %)	polyester resin	2.40	80.00

An approximately linear relationship is observed between the flexural strength and flexural modulus for natural fibre-reinforced polymers (Figure 86). In contrast, the flexural strength of the rayon-based ACC laminate is higher than the majority of the other biocomposites, although the flexural stiffness is modest in comparison. The comparatively lower flexural modulus of the ACC is explained by the use of rayon fibres which are well known to be strong but exhibit high elongation to failure. In contrast, many biocomposites are based on stiff and strong fibres with low strain to failure such as flax, hemp or jute fibres (Figure 86) [38]. Moreover, the rayon fibres used to produce the ACC laminate have been classified as a strong but high strain fibre compared to natural fibres [358]. It can be assumed that the good fibre-matrix bonding in the ACC allows the full potential of the fibre properties to be exploited, while the other biocomposites might suffer from an inefficient load-transfer from matrix to fibre due to weak fibre adhesion.

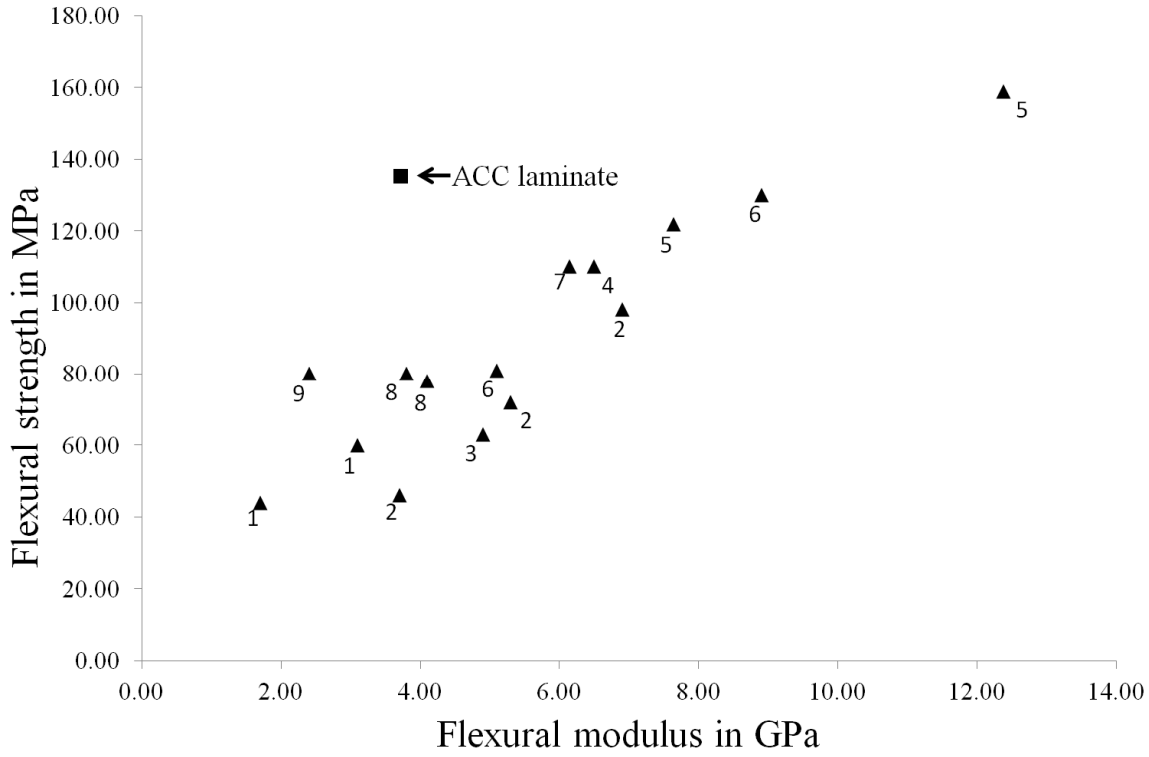

Figure 86: Graphical representation of the data provided in Table 12. The ACC laminate from the present work is shown for comparison.

3.4 CONCLUSIONS

It has been demonstrated that all-cellulose composite based on a rayon textile and manufactured *via* SIP exhibit high impact strength. The response of the ACC laminate to puncture impact shows two different modes: (I) fibre failure and (II) fibre delamination. As a result of the manufacturing process, all fibres in the composite are surrounded by a continuous cellulosic matrix phase. The strong fibre-matrix interphase is likely to dissipate large amounts of the impact energy in the process of breaking the hydrogen bond network present between fibre and matrix. The high strain to failure of regenerated cellulose fibre such as that of rayon also contributes to the higher impact strength when compared with biocomposites based on natural bast fibres. This assumption is supported by the high Charpy impact strength of the ACC laminates.

The flexural strength of the ACC laminates has been shown to be superior to many other biocomposites, and this also results from the strong interfacial adhesion present in these materials. In particular, the unusual combination of high flexural and impact strength is not a characteristic of the bast fibre-reinforced composite, emphasising the potential of ACCs as a new class of biocomposite.

4. BIODEGRADABILITY AND FIRE RESISTANCE OF ALL CELLULOSE COMPOSITE LAMINATES

The previous work in this Chapter shows that the mechanical properties of ACCs produced *via* SIP are very competitive with respect to the range of other biocomposites presently available. However, the issues of sustainability and eco-friendliness are also crucially important to assess this new class of biocomposite in relation to other green composites. Options for end-of-life (EOL) disposal of ACCs might include (I) recycling of the ACC waste as a cellulose source for new ACCs, (II) the use of the waste 'biomass' for the production of biofuels; or (III) the most likely scenario which is ACCs being sent to landfill as is the case for many other biocomposites [359]. Thus, the biodegradation of an ACC is an important physical property to assess, particularly if EOL disposal involves landfill.

Another physical property that is particularly relevant to the application of biocomposites is flammability [360]. However, the fire resistance of biocomposites in general, and more specifically cellulosic fibres, is an issue that has received little attention [361]. Nevertheless, it is commonly agreed that natural or regenerated cellulosic fibres behave poorly in terms of fire resistance [362, 363]. In this work, the flammability of rayon-based ACCs is compared with a rayon-reinforced PLA biocomposite.

4.1 INTRODUCTION

4.1.1 Biodegradation Behaviour of Biocomposites

There is a strong commercial need for polymer-based materials that are specifically designed for short life spans in many applications such as packaging [364]. Waste

materials that are generated by the petrochemically-derived polymers are often difficult to recycle nor do they easily biodegrade which increasing the demand for biodegradable alternatives [365].

Recently, the disposal of plastics in the USA and the European Union exceeded 10 million tons per annum [38]. Discarded plastics make up more than 20% of the urban waste by volume in the USA [366]. Only around 10% of waste plastics are recycled or incinerated, with the vast majority ending up in landfill. In response to the increasing amount of plastic waste, the European Union has introduced the European Community (EC) 2000/53 ELV - ‘‘End-of-Life Vehicles’’ standard, stating the need for recyclable and/or compostable automotive parts [367]. Additionally a “Landfill Directive” was issued by the EU in 1999 to ““to prevent or reduce as far as possible negative effects on the environment, in particular the pollution of surface water, groundwater, soil and air, and on the global environment, including the greenhouse effect, as well as any resulting risk to human health, from the landfilling of waste, during the whole lifecycle of the landfill” [368]. Therefore, ACCs could prove to be a valuable addition to the family of green composites, as they do not only show competitive mechanical properties but are also made entirely from a biodegradable biopolymer.

The term “biodegradation” has caused some confusion regarding the actual processes involved. Four different pathways to degradation in aquatic and terrestrial environments can be distinguished: (I) microbial degradation by fungi and/or bacteria; (II) macroorganism degradation meaning the consumption of the polymeric material as a food source by, for example, insects or fish, often causing great harm to the involved animal; (III) photodegradation caused by UV-light and (IV) chemical degradation [369].

Furthermore, although “biodegradation” implies a predominance of biological factors acting during the degradation process, in nature it is a combination of biotic and abiotic processes that work synergistically to break down polymeric materials. The abovementioned pathways to degradation are all active in the first step of the overall biodegradation process also referred to as biodeterioration. Biodeterioration is followed by depolymerisation, consumption by an organism and, finally, mineralisation [364].

Biodegradation of cellulosic polymers in nature can be classified as a microbial degradation process. A variety of cellulolytic fungi, bacteria and other microorganisms are able to convert the cellulose molecule into cellobiose and glucose monomers, which can then be assimilated by living cells [370]. This process is catalyzed by enzymes known as cellulases, which belong to the family of glycoside hydrolase enzymes, responsible for the hydrolysis of the different polysaccharides in plant cell walls. Cellulose degradation is based on the hydrolysis of the β-1,4 glucosidic linkages catalyzed by cellulase [371]. The decomposition of the cellulose on the molecular level is either achieved by enzyme activity (proteolysis) or fission by water molecules (hydrolysis) [372]. The depolymerisation processes invoked by cellulases are widely discussed in the research community and more detailed information is found in reviews by Galbe *et al*., Gilbert *et al.*, and Sun *et al.*[373-375].

PLA has emerged as one of the most promising biodegradable biopolymers for use in fully biodegradable biocomposites. PLA-based biocomposites exhibit considerable mechanical properties that allow them to compete with GFRPs [185, 204, 309, 376]. However, industrial composting conditions of high humidity and temperature (40 to

60°C) are required to achieve reasonable a degradation rate for the PLA [377]. Saadi *et al.* compared the degradation rates of poly(L-lactide) (PLLA) and cellulose. PLLA was found to rapidly degrade at a temperature of 58°C. However, PLLA exhibited a low degradation rate at a temperature of 30°C when compared with cellulose. The degradation rate was found to be most rapid in natural compost which is composed of a mixture of different fungi and bacteria [378]. The biodegradability of biocomposites can also be controlled by additives such as fungicides [379].

In the present work, soil burial experiments were carried out to simulate the biodegradation of rayon-based ACC laminates in a biologically active environment. A rayon-reinforced PLA composite was also tested to compare the biodegradability of conventional biocomposite with an ACC laminate. The effect of a fungicide on the biodegradation of ACCs was also examined to explore the possibility of controlling the biodegradation rate during soil burial experiments.

4.1.2 Fire Resistance of ACC laminates

All polymers undergo thermal and thermal-oxidative decomposition when exposed to fire or heat, producing smoke and volatiles. The exact nature of the evolved volatiles depends on the chemical composition of the polymer, but may consist of carbon monoxide and dioxide, hydrocarbons and/or hydrogen halides [362].

One way to compare the flammability of polymers is the limiting oxygen index (LOI) whereas a low LOI mean a high flammability and vice versa [362, 380].

The thermal decomposition of cellulosic fibres follows several steps that include desorption of adsorbed water, crosslinking of cellulose chains with the evolution of

water to form dehydrocellulose, followed by decomposition of the dehydrocellulose that yields char and volatiles. During this process, levoglucosan is formed and the decomposition of the levoglucosan yields gases, tar, and char [362]. The flammability of natural fibres depends on their chemical composition, crystallinity, DP, and microfibril orientation A high cellulose content and low crystallinity seems to increase flammability, while a high DP and strong fibrillar orientation have been reported to decrease pyrolysis [360, 362]. The limiting oxygen index (LOI) is used to compare the flammability of polymers, where a low LOI indicates higher flammability [362, 380]. For instance, rayon fibre has a lower LOI than cotton [380] which is expected given the relatively low DP and crystallinity compared to the natural fibre.

Next to the LOI level, a set of flammability tests developed by Underwriters Laboratories (Northbrook, USA) (UL 94) is often used to categorise the flammability behaviour of polymeric materials [381]. Samples are exposed twice to an open flame for 10 seconds and their response is classified by a V-2, V-1 or V-0 rating according to afterflame or afterglow time and potential flaming dripping [381]. The UL 94 test has been described as a test to assess a local ignition risk and self-extinguishing time, making it a suitable test to asses for example integral ignition of for example electronic appliances [382, 383].

The flammability of ACCs has not been reported in the literature. However, it is expected that the high cellulose content of ACCs will result in a low fire resistance based on the observed behaviour of other biocomposites. Nevertheless, a strong fibre-matrix interfacial bond improves the thermal stability of a biocomposite [362]. Therefore, it

will be of interest to analyse and compare the fire resistance of ACCs using a UL 94 ignition test and thermogravimetric analysis (TGA).

4.2 EXPERIMENTAL PROCEDURES

4.2.1 Biodegradation

4.2.1.1 ACC Samples

The standard ACCs samples were manufactured using the solvent infusion processing (SIP) as described above (see Chapter VI.1) using four layers of rayon textile. Ethanol (97 % purity) was used for regeneration and washing of the composites.

4.2.1.2 Fungicide treated ACC

In order to determine the influence of a fungicide on the degradation kinetics, samples of the ACC laminate were treated with Mycostat fungicide (Mycostat, Kiotechagil, UK-Aldermaston). 0.3 g of the fungicide was applied on each of the rayon textile layers before composite processing via SIP procedure. The presence of the fungicide in the composite could be confirmed by visual observation. The active ingredients in the fungicide and their concentrations in the manufactured laminate were: propionic acid (2.8-2.9 mass%), ammonium propionate (0.1-1 mass%) and sorbic acid (0.1-1 mass%). The fungicide treated ACC was regenerated by ethanol (97% purity, Thermo Fisher Scientific).

4.2.1.3 Rayon-PLA Composites

The cellulose fibre reinforced PLA granules were supplied by Cordenka GmbH (Obernburg, Germany). The granules were produced in an extruder using Cordenka fibres with a standard PLA injection moulding grade from NatureWorks LLC (Minnesota, USA).The composites with a fibre mass content of 20 % were injection

moulded into dog bone shape according to DIN EN ISO 527. The injection moulding pellets were dried for 3 h at 85 °C prior to injection moulding. The samples were injection moulded using a Plus 250/50 injection moulder (Battenfeld Kunststoffmaschinen GmbH, Kottingbrunn, Austria) supplied by J.H. Tönnjes Gmbh & Co. KG, (Delmenhorst, Germany). The processing temperature was kept under 190 °C to avoid degradation of the cellulose fibres. The mould temperature was set to 40-50 °C.

4.2.1.4 Soil Burial Test

ACC and fungicide-treated ACC samples were cut to the dimensions of 30 × 30 mm. The PLA samples dimensions were 20 × 22 mm. The mean thickness of the ACC and PLA samples was 2 and 3 mm, respectively. Ten samples of each of the tested materials were prepared. Six control samples of each material were also prepared. All soil burial samples were dried at 80 °C in a vacuum oven for at least 48 hr and weighed. Before burial, the samples were washed with distilled water and weighed again to establish a "wet mass".

The biodegradation test was performed at two different temperatures (23 °C and 38 °C) in two different growths cabinets (Plant Growth Cat 620, Contherm Scientific Company, Lower Hut, New Zealand). All samples were buried at a depth of at least 50 mm in plant pots. The used soil was a 1: 1 mixture of mature leaf compost and soil taken from local flowerbeds at the University of Canterbury, Christchurch, New Zealand. The approximate moisture content of the soil-compost mixture was 51 % (at 23 °C) and 28 % (at 38 °C), respectively. To ensure a sufficient moisture content of the soil, a sprinkling system was set up to dispense about 300 ml of tab water within the cabinets twice a day.

In order to determine any mass loss, the samples were removed from the soil, carefully washed and weighed in wet state after 28, 42, 56 and 70 days using a Sartorius ED224S analytical lab balance (precision 0.1 mg, Sartorius, Göttingen, Germany). For visual comparison and examination photos were taken after 28, 42, 56 and 70 days and before the samples were buried, respectively.

After 56 days 3 samples of each material for the two different experimental temperatures were removed from the soil, washed and dried for 48 hr at 100 °C in a vacuum oven. The dried samples were then prepared to be analysed using scanning electron microscopy (SEM) and optical microscopy to examine the surfaces as well as the cross sections of the samples.

After 70 days all remaining samples were finally washed and weighed, followed by drying for at least 48 hr at 100 °C in a vacuum oven. The samples were then weighed again to calculate the total dry mass loss.

4.2.1.5 Scanning Electron and Optical Microscopy

To analyse the composite cross-section, samples of approximately 5 × 10 mm were cut from each material and prepared according to Section II.2.1.1.

To analyse the surface of the composites, samples of approximately 2 × 2 mm were cut from the samples and mounted on carbon tabs. All samples were gold coated for 120 seconds at 25 mA.

To analyses any occurring fungal or microbial growth on the composite surface, pictures of the sample surface were taken using an Olympus SZH10 stereo microscope with the attached Zeiss AxioCam camera.

4.2.2 Fire Resistance

4.2.2.1 Thermogravimetric Analysis (TGA)

TGA was carried out on the same specimens as per the biodegradation studies using ethanol during regeneration and washing (Section 4.2.1.1). Some samples were also produced using water as the regeneration/washing medium and applying low temperature drying (see Chapter VI.2) and compared with as-received rayon fibre. The testing was performed using an STD Q600 (Texas Instruments, Dallas, TX, USA). The samples were heated starting from 23 to 550 °C at a heating rate of 10°C/min. Nitrogen was used as a protective purge gas with a flow rate of 100 ml/min. The samples were dried in a vacuum oven at 100 °C for at least 24 hr prior to TGA.

4.2.2.2 UL 94 Ignition Test

The ignition test was carried out in accordance with the standard "UL 94 - Test for Flammability of Plastic Materials for Parts in Devices and Appliances" in a laboratory fume hood with deactivated fan. The samples were tested using the set-up for the vertical burning test. For this test, the lower end of a sample is exposed to an open blue flame from a Bunsen burner for 10 seconds. The burner is removed and the afterflame time (t_1) is measured, meaning the time the sample keeps o burning. Once the afterflame has ceased the burner is placed under the sample again for 10 seconds followed by measuring the second afterflame time (t_2). Based on t_1 and t_2 the material can be classified as V-0, V-1 or V-2, V-0 describing the best resistance to ignition,

meaning the shortest afterflame time and no afterglow of the sample. The test was carried out on samples of ACC laminates and PLA-rayon composites. The samples were conditioned for 48 hr at 23 °C and 50 % RH prior to testing.

4.3 RESULTS AND DISCUSSION

4.3.1 Biodegradation Behaviour of Green Composites

4.3.1.1 The Effect of Soil Exposure on Sample Mass Change

Clear differences in the degradation as a function of time and temperature were observed for the ACC laminate, fungicide-treat ACC laminate and rayon-PLA biocomposite (Figure 87).

All samples show an increase in sample mass after 28 days, most likely the result of a strong moisture uptake caused by the hydrophilic nature of the rayon fibres [57]. The ACC laminates with or without fungicide treatment exhibit mass losses of 17 and 36%, respectively, after 56 days at 38 °C; the mass losses increased further to 55 and 35%, respectively, after 70 days. In contrast, the rayon-PLA biocomposite showed little change in mass at either temperature. This indicates that cellulose degrading microorganisms are highly active in this temperature range. It is likely that the degradation is dominated by fungal microorganisms at this temperature as the mass loss of the ACC laminate without fungicide treatment was almost double that of the fungicide-treated laminates.

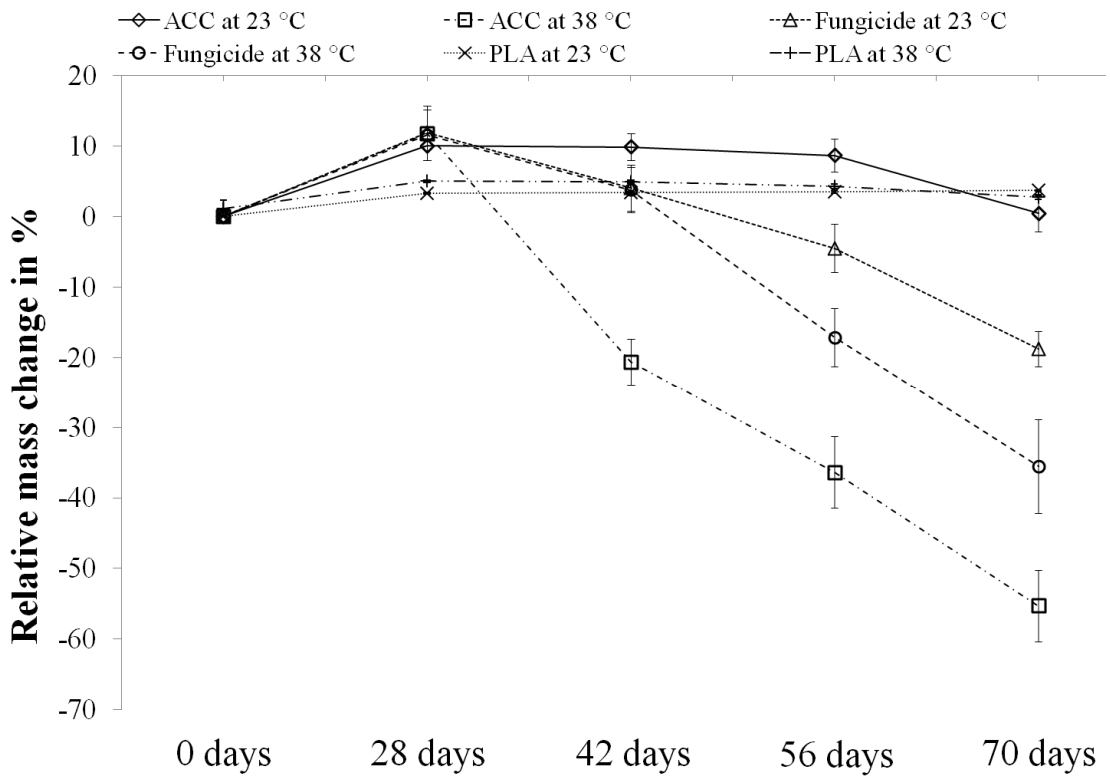

Figure 87: Sample mass change of the tested composite materials recorded before soil burial and after 4, 6, 8 and 10 weeks. Displayed is the relative mass change of the samples kept in soil at 23 °C and 38 °C. The error bars represent one standard deviation.

However, only minor changes in the standard sample mass are observed at 23 °C, showing a strongly reduced microorganism activity at room temperature compared to 38 °C. Interestingly, the fungicide treated samples shows a higher mass loss, compared to the standard ACC sample. This could mean that the applied fungicide could promote a stronger activity of other microorganisms. Simultaneously, a growing fungus in the standard sample could prohibit a stronger bacterial degradation [384].

4.3.1.2 Visual Examination

The change of sample appearance at 23 °C & 38 °C over time is displayed in Figure 88 and Figure 89 respectively.

When compared to a non-degraded sample of a rayon-ACC (Figure 54-d) it is obvious how rapidly both rayon composites start to degrade. At both temperatures, and despite the application of the fungicide, the rayon composite show a strong discolouration and the formation of a black, possibly fungal, substance on the surface after only 28 days (top row in Figure 88, Figure 89).

Interestingly, the fungicide-treated ACC seems to be attacked more strongly at 23 °C than the untreated ACC, judging by a more advanced change in colour (Figure 88, Figure 89). In contrast, the ACC without fungicide treatment exhibits greater degradation at 38 °C than the ACC with fungicide treatment, as seen by the onset of delamination (Figure 89). However, visual differences in the degradation of the ACC laminate with or without fungicide treatment are negligible after 70 days (bottom row in Figure 88, Figure 89). Thus, it is likely that different microorganisms are actively involved in the degradation process at different temperatures as also supported by SEM micrographs of the progression of the degradation (Figure 92 and Figure 93) [367, 369]. This could be the result of the strong influence of the environmental temperature on reaction rates in bioactive composting environments. For example, the ideal temperature for microorganisms in wastewater treatment sludge with pine bark is reported to be ~40°C [385].

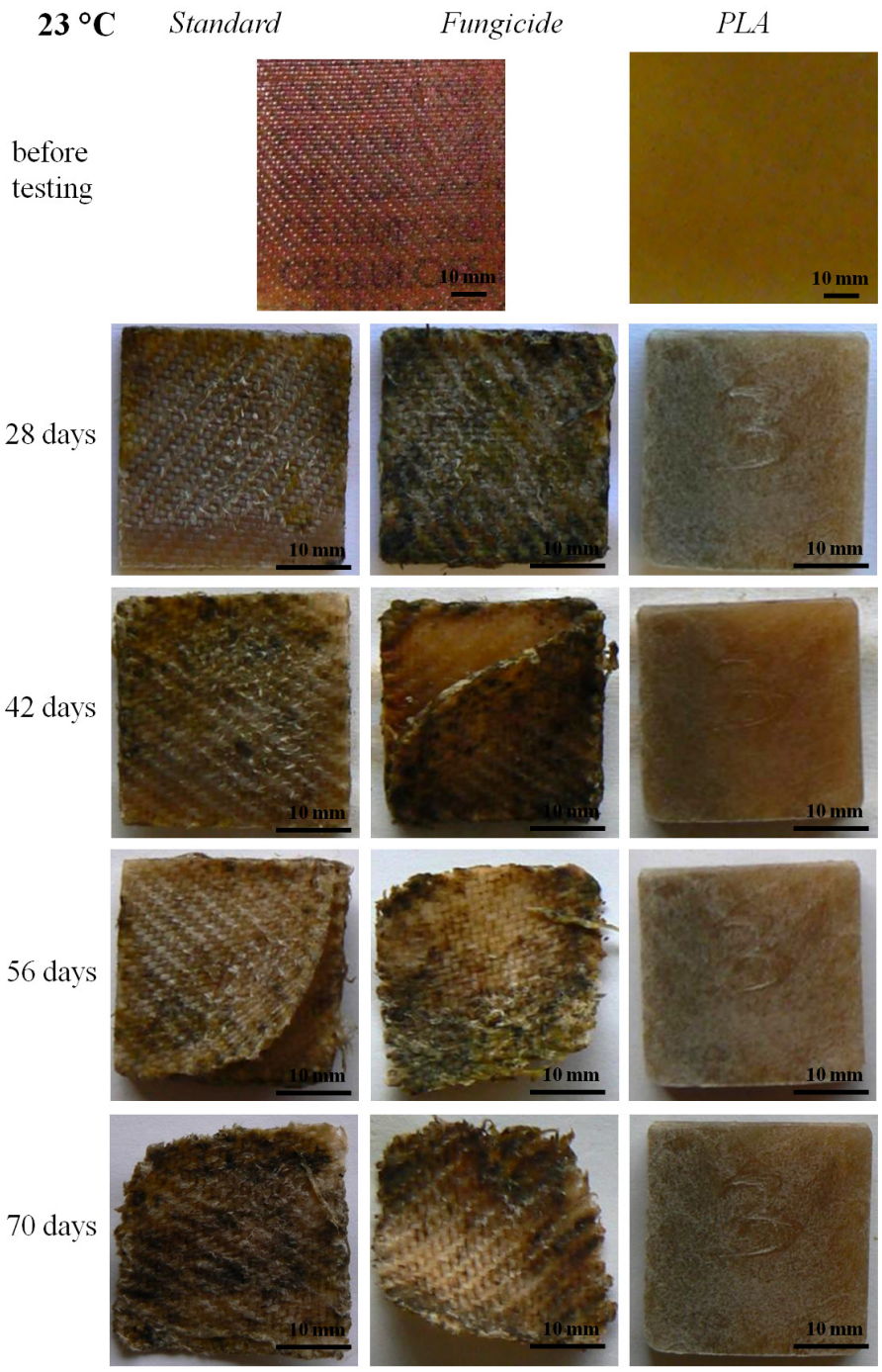

Figure 88: Photographs of the exterior appearance of the ACC laminate (standard), ACC treated with fungicide (fungicide), and rayon-PLA biocomposite (PLA) as a function of soil burial time at a temperature of 23 °C.

All rayon samples have either been completely or partially delaminated after 42 and 56 days (Figure 88, Figure 89). This indicates that the interlaminar interface is degraded.

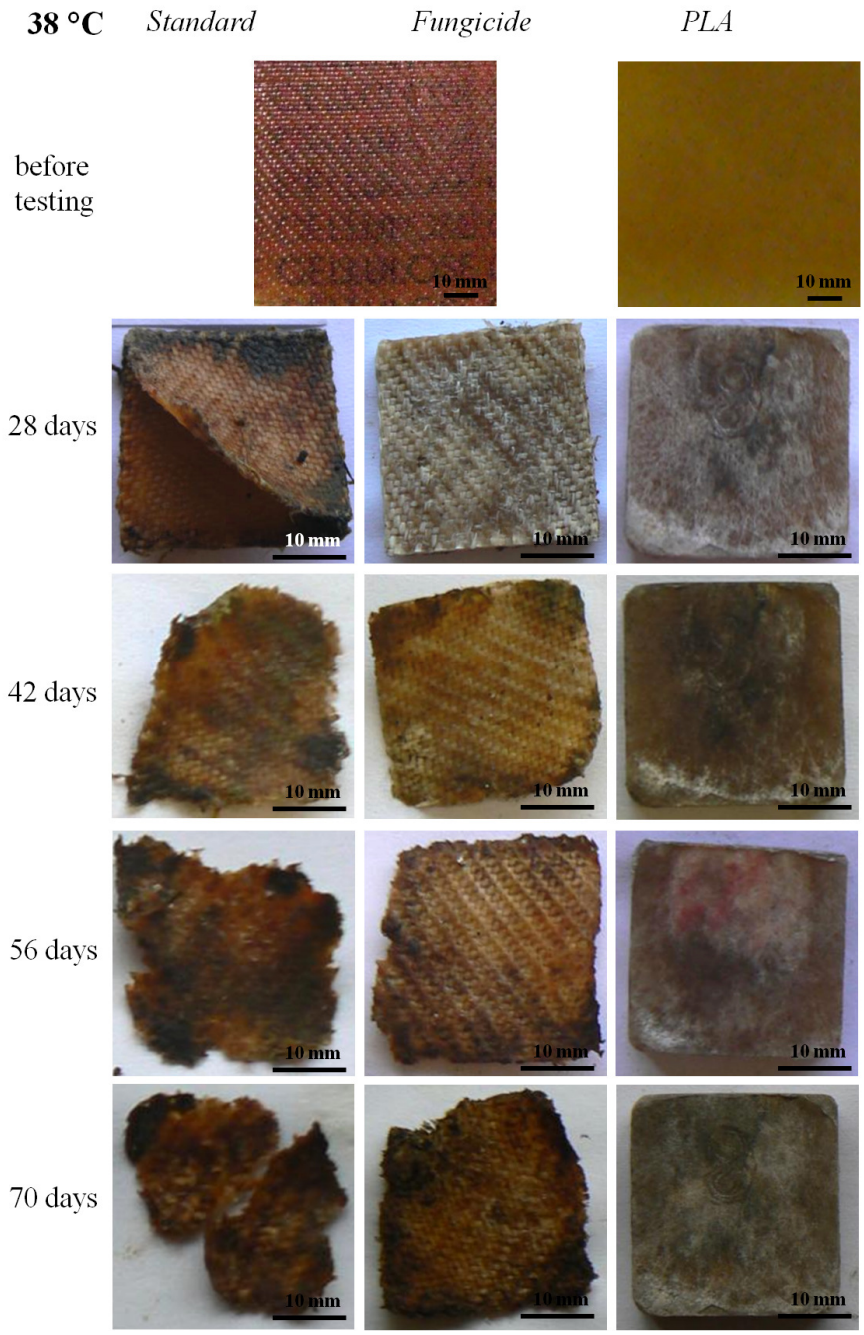

Figure 89: Photographs of the exterior appearance of the ACC laminate (standard), ACC treated with fungicide (fungicide), and rayon-PLA biocomposite (PLA) as a function of soil burial time at a temperature of 38°C.

At 38 °C, the samples have clearly started to disintegrate and some material has been completely degraded leaving the composite with frayed edges (Figure 89). Again, it is noteworthy that at 23 °C, the fungicide treated sample shows stronger signs of degradation (Figure 88 and Figure 89). However, at 38 °C, the standard sample

degrades very rapidly and after 56 days the sample barely resembles the original structure and is further degraded and broken up into smaller fractions after 70 days (Figure 89). It is possible that a fungus that normally causes rapid degradation of cellulose is hindered by the presence of the fungicide at 38 °C (Figure 92 & Figure 93) [384], while other microorganisms (bacterial, etc.) cause cellulose degradation at 23°C but not at 38°C [386]. It is known that microorganisms do not always work synergistically but may compete against one another during the degradation process [387, 388]. Hence, the fungicide might actually promote bacterial degradation at 23 °C. Another possible explanation would be that some fungi are partially suppressed by the fungicide while others that are unaffected are in a better position to degrade the ACC [389]. It should be noted that some of the fungicide components (propionic acid, sorbic acid and ammonium propionate) are soluble in ethanol which was used during regeneration in SIP. Hence, it is possible that the active components of the fungicide have been partially or even completely removed from the composite. Although remaining fungicide particles can be directly observed on the sample surface (Figure 90), it is possible the fungicidal activity is affected by the washing process.

Additionally, the introduction of the fungicide might have affected the dissolution process during composite processing and could therefore be responsible for a weakened interlaminar adhesion in the fungicide composite. Based on the photographs in Figure 88 and Figure 89 it can be assumed that the regenerated cellulose is initially attacked as shown by the strong tendency for delamination and fibre separation. In summary, a temperature of ~40°C promotes greater degradation of the cellulose based samples in the given bioactive environment [385].

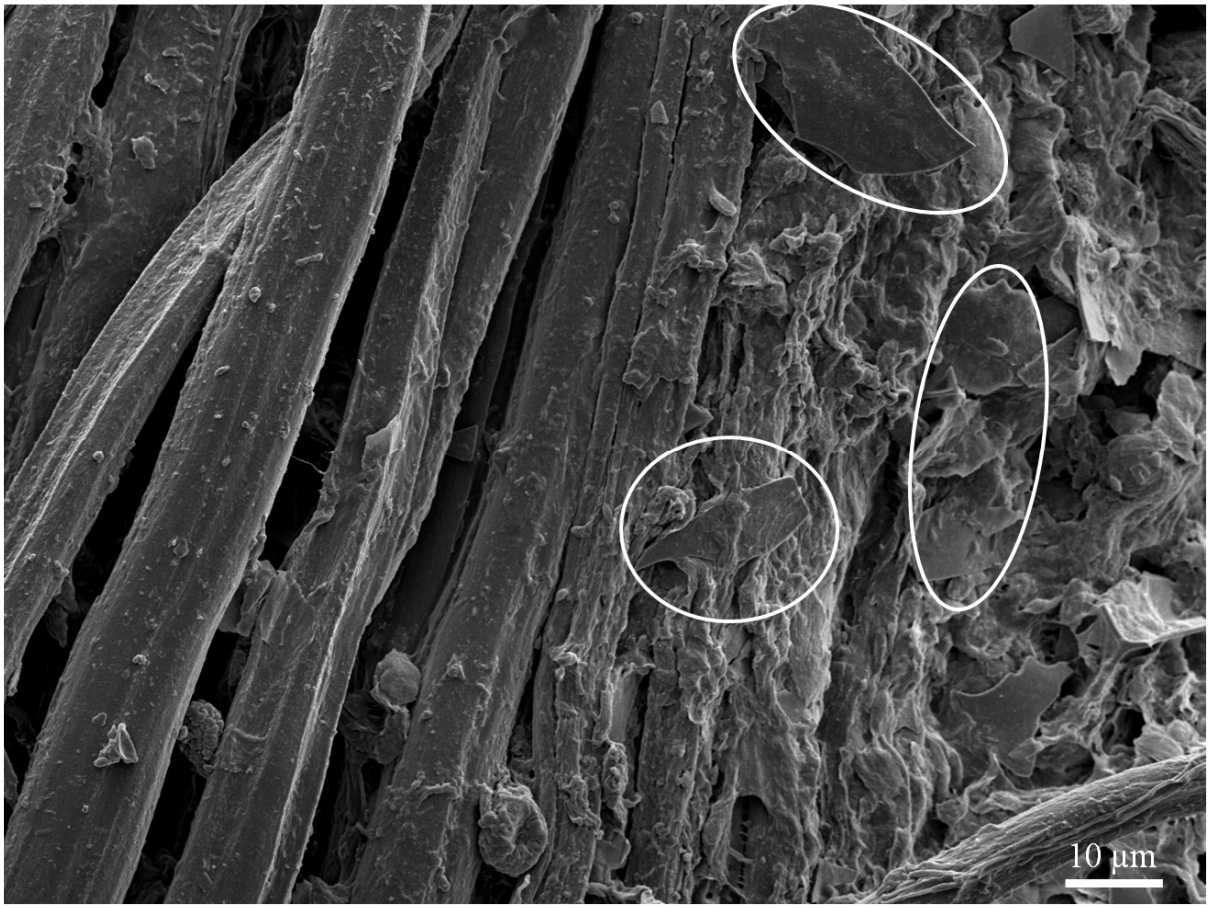

Figure 90: Fungicide treated samples kept at 23 °C for 56 days. Marked are particles of the used fungicide.

In contrast to the ACC laminates, the rayon-PLA biocomposite is almost unaffected by the soil burial test. At 23 °C almost no colour change can be observed compared to the original material (Figure 88) and even at 38 °C only a slight change towards a lighter colour can be observed on a macroscopic scale (Figure 89). This is a typical reaction of PLA to soil degradation [390]. However, this work shows that PLA degrades very slowly, if at all, at moderate conditions, particularly when compared with an ACC [391]. Higher humidities and temperatures are necessary to achieve full biodegradation of PLA (*e.g.* Shah *et al.* [386]).

There was obvious enhancement of the degradation of the ACC laminate after 56 days of soil burial at 38°C (Figure 91). A black fungus was observed to spread over the sample

surface. However, the separation of single fibres from the original rayon yarns is clearly evident at a temperature of 23°C. This supports the assumption that different microorganisms are responsible for the degradation processes at different temperatures [386].

The fungicide treated samples show a less severe colour change, possibly the result of the applied fungicide. The disbonding of single fibres is also observed (Figure 91).

Micrographs of the rayon-PLA biocomposite confirm the above observation that, apart from a slight discolouration, neither the PLA matrix nor the rayon fibres seem strongly degraded (Figure 91). Further analysis of the microorganism growth was carried out by examining the cross-section (Figure 92) and surface (Figure 93) of the specimens by SEM. The above made observations regarding the PLA-rayon composite are confirmed by the SEM micrographs. The PLA matrix appears to not be affected at by all the degradation testing (Figure 92 a-c). However, single rayon fibres close to the composite surface appear to be partially degraded at 23 °C (Figure 92 b, Figure 93 a) and have fully disappeared at 38 °C (Figure 92 c, Figure 93 b). A similar degradation behaviour has been reported for Lyocell fibre reinforced PLA composites [392].

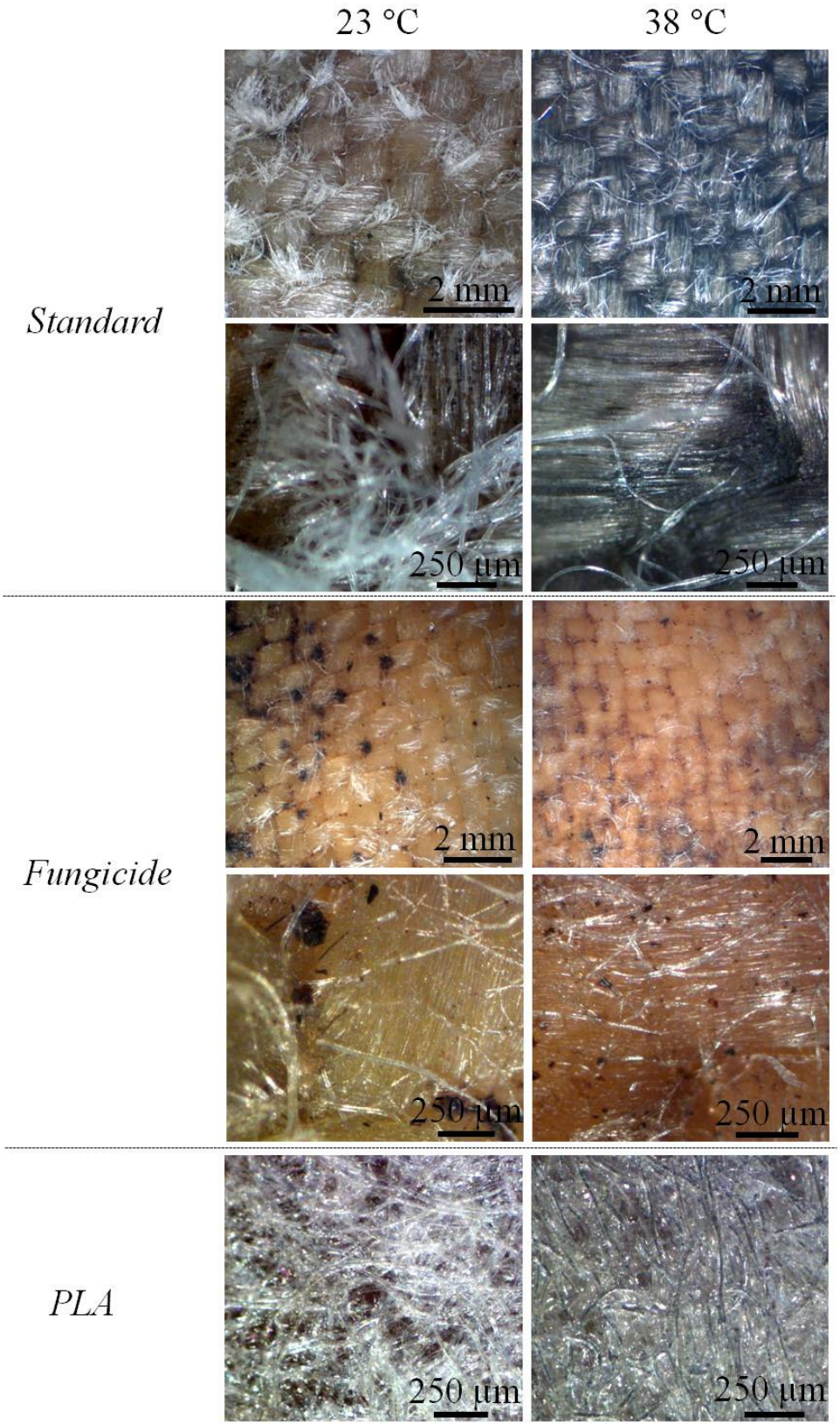

Figure 91: Reflected light micrographs of the surface structure of the various samples (ACC laminate (Standard), ACC laminate treated with fungicide (fungicide) and rayon-PLA biocomposite (PLA)). All specimens were subjected to 56 days of soil burial.

The suspected vulnerability of the ACC laminate to fungal degradation was clearly seen in the SEM micrographs. At 23 °C a thin layer of fungal growth is observed on the surface of the fibres that mainly seems to degrade the fibre-matrix interphase (Figure 92 e), also causing defibrillation (Figure 93 c). Fungal growth is strongly increased at 38°C and a much thicker growth layer of microorganisms is observed (Figure 92 f). In fact, the surface of the sample seems to be almost completely covered by microorganisms (Figure 93 d). Filamentous type species are observed that are likely to be *Phanerochaete chrysosporium* or *Postia placenta*, well known for digesting cellulose [393].

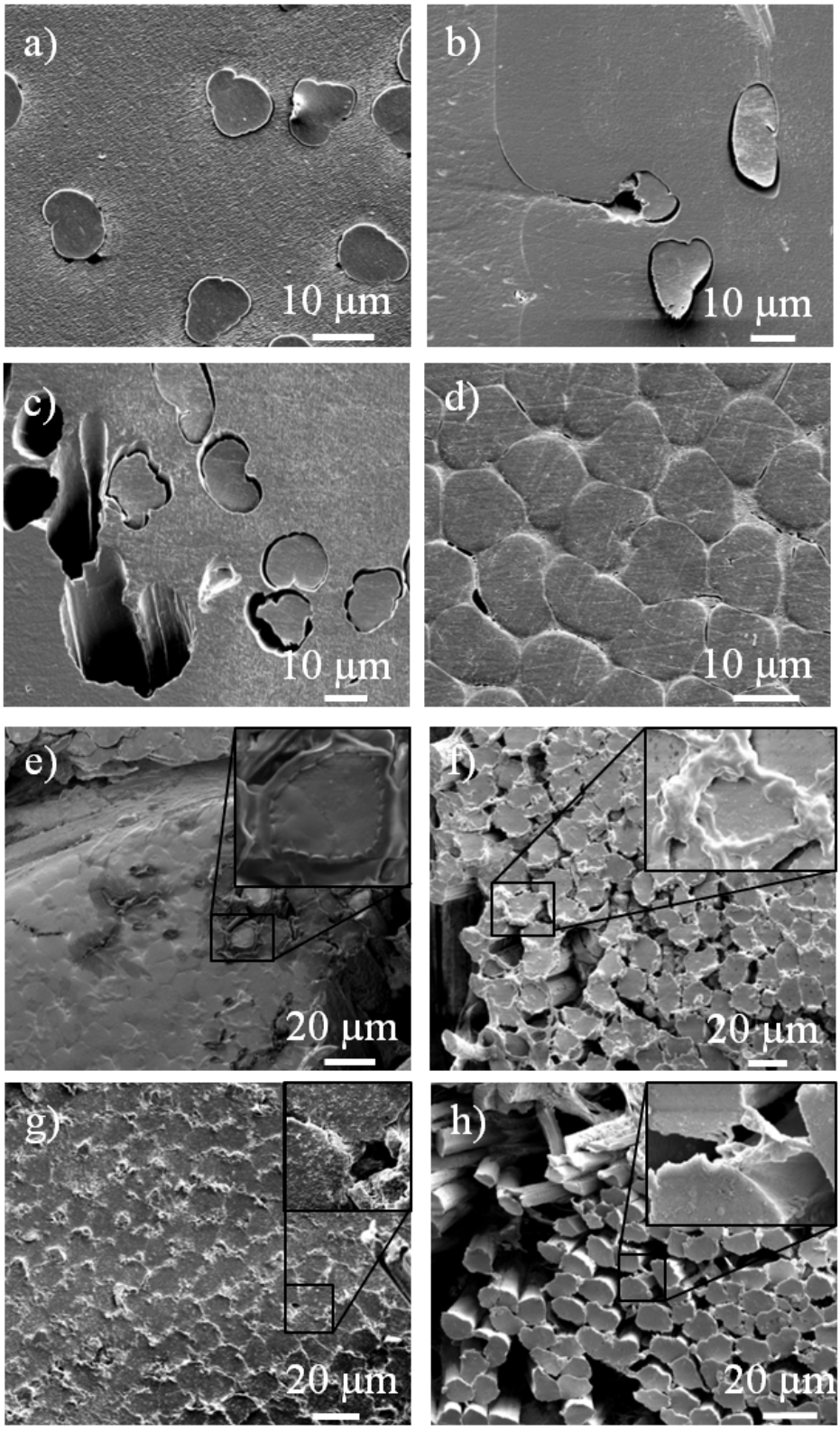

Figure 92: Scanning electron micrographs of the cross-sections of the (a) as-received rayon-PLA biocomposite; rayon-PLA biocomposite tested at (b) 23 and (c) 38°C; (d) as-received ACC laminate; ACC laminate tested at (e) 23 and (f) 38°C; fungicide-treated ACC laminate tested at (g) 23 and (h) 38 °C. All tested specimens were analysed after 56 days of soil burial. An accelerating voltage of 5 kV was used.

A different type of microorganism growth is observed on the ACC laminate treated with the fungicide. Once more, the fibre-matrix interphase appears to be attacked more strongly than the rayon fibres. Due to the dissolution and regeneration process the fibre-matrix interphase is likely to be of lower crystallinity than the fibres it surrounds [129], making it more accessible to microorganisms [394] (Figure 92 g & f).

At 23 °C the formation of small particles, can be seen on the single fibres (Figure 93 e). Similar types of particles cover large areas of the sample surface when degradation takes place at elevated temperature. Most of the particles appear to be conglomerated around single fibres (Figure 93 f), and their morphology is indicative of spore or fruit bodies. These observations suggest that although the fungicide prevents fungal growth, it does not stop other microorganism from attacking the ACC laminate [384].

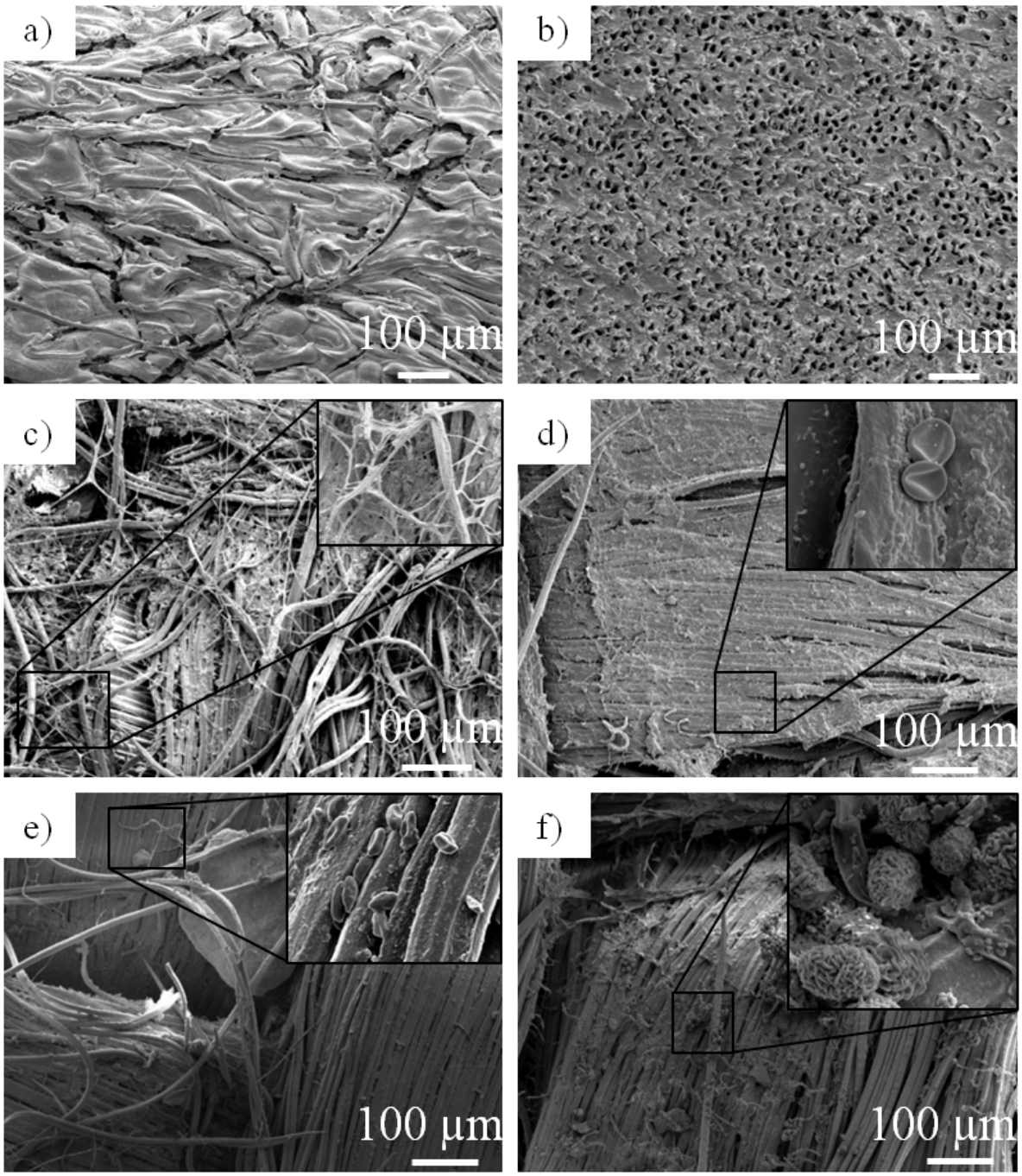

Figure 93: Scanning electron micrographs of the surface of the rayon-PLA biocomposite after 56 days of soil burial at (a) 23 °C and (b) 38 °C; the corresponding micrographs for the ACC laminate and ACC laminate treated with fungicide are shown in (c-d) and (e-f), respectively. An accelerating voltage of 5 kV was used.

4.3.2 Thermal Properties and Fire Resistance of ACC Laminates

4.3.2.1 TGA

A small reduction in sample mass of the rayon fibre at temperatures up to 100 °C is explained by the removal of residual moisture (Figure 94). It is interesting to note that the as-received rayon fibre and low temperature drying ACC both exhibit almost identical mass loss behaviour with a dramatic loss in mass in the region of 260 to 270°C. In contrast, the ethanol washed ACC exhibits far less thermal stability with a dramatic loss in mass at 220°C, likely due to the lower crystallinity of the ethanol washed composite (see Section VII.3). Similar behaviour has been reported for cellulosic fibre electrospun from a cellulose-ionic liquid solution [395].

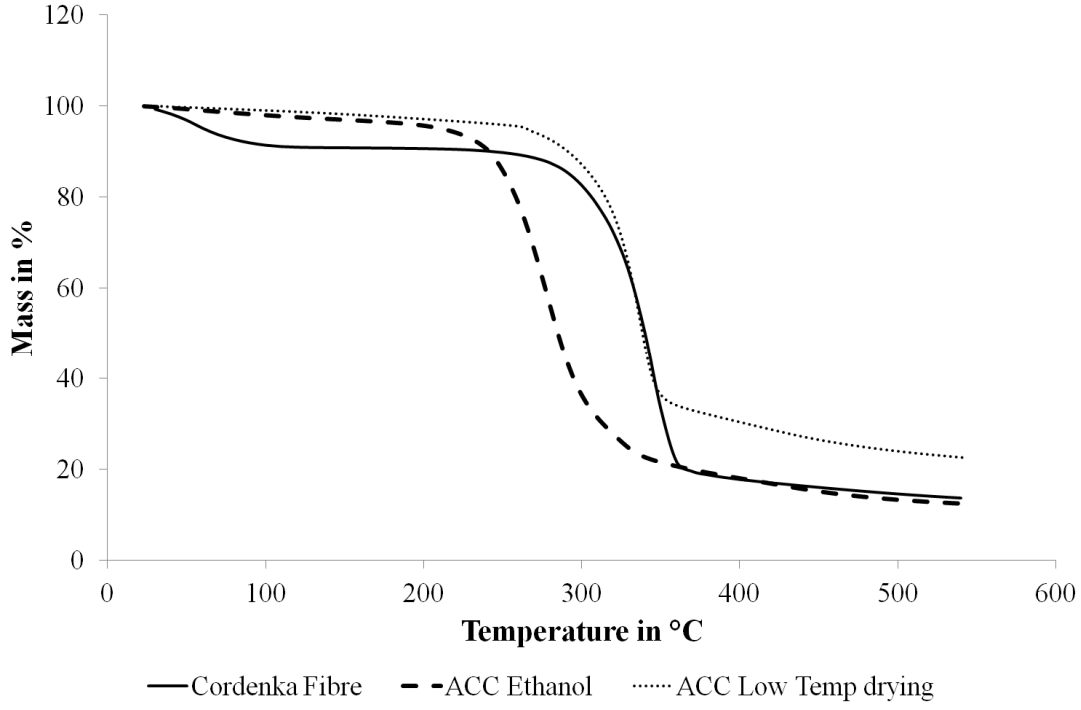

Figure 94: TGA results of the tested as-received rayon fibre, Ethanol regenerated and washed ACC and the ACC washed and regenerated with distilled water, dried at room temperature.

4.3.2.2 Ignition Test

The ACC laminate and rayon-PLA biocomposite failed the ignition test, as the flame did not cease after the first ignition and eventually the whole of the specimen was burnt completely. This was expected since cellulosic fibre (natural and regenerated) is well known to have high flammability and additional treatments are required to reduce the flammability ([396, 397]). The application of flame retardants to Lyocell fibres has been successfully demonstrated [363] and could be potentially applied to rayon fibres. However, whether those flame retardants would interact and influence the dissolution behaviour is not known and requires further study.

All of the specimens were completely burned after approximately 80 s, with significant charring occurring during the burning process. Specimen fragments of the rayon-PLA biocomposite began dripping after 50 to 60 s (Figure 95).

As cellulose, PLA is known for its high flammability [398] and the need for additional flame retardants to achieve a V-2 rating has been previously addressed in literature [399, 400]. This study shows that a biocomposite based on PLA does not show greater fire resistance than an ACC laminate and thus offers no competitive advantage regarding its flammability.

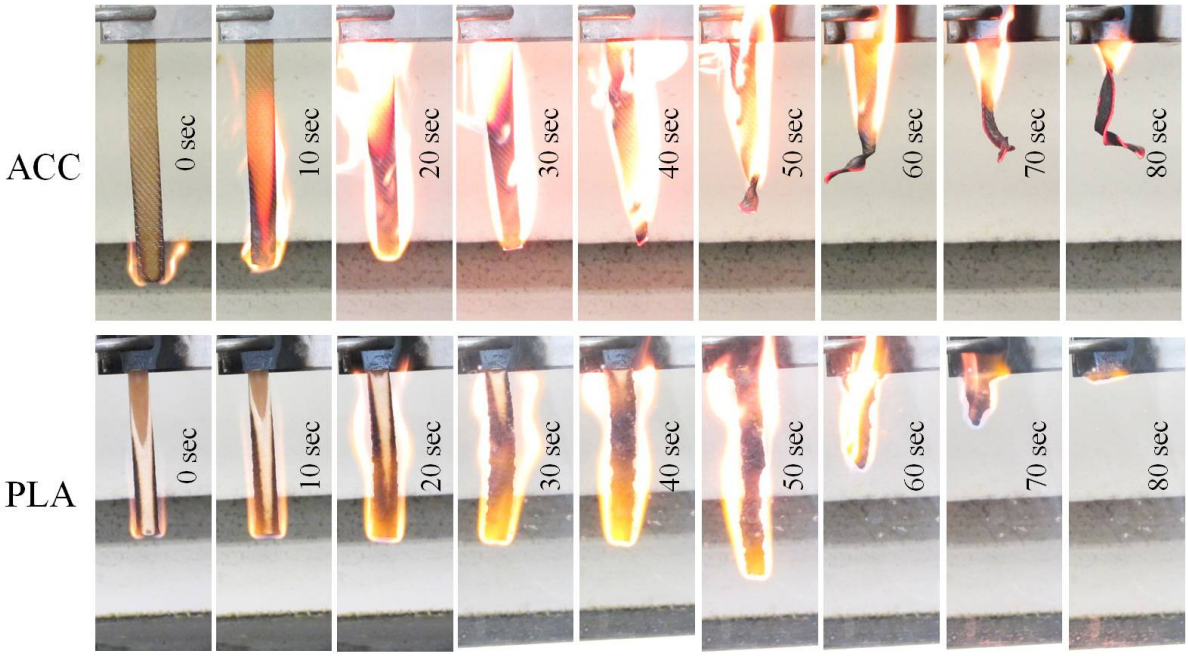

Figure 95: The burning behaviour of a sample of the ACC laminate and rayon-PLA composite shown from the removal of the flame up to complete burning.

4.4 CONCLUSIONS

Rayon based ACCs degrade rapidly in active soil even at moderate temperatures of 23°C and 38°C, making them an attractive alternative for applications with short life spans. A slightly increased degradation progress is observed at 38°C. It is possible to influence microorganism growth on the composites by adding a fungicide. Although a fungicide appears to have an effect on fungal growth it cannot significantly slow down degradation in active soil due do the vast number of organisms that are able to degrade cellulose. Perhaps the greatest advantage of a fungicidal additive would be to prevent or hinder fungal growth in high humidity and elevated temperature environments.

In contrast to the ACCs, “biodegradable” rayon-PLA biocomposite exhibited only minor degradation at the selected test temperatures and humidities, and the slight degradation that did occur is attributed to the rayon fibres.

It was shown that rayon-PLA biocomposite has no advantage over ACC laminates in terms of flammability. This work emphasises the need for additives in both types of biocomposite to improve fire resistance. TGA experiments showed that the degradation temperature of an ACC depends strongly on its crystallinity.

VII. RIGID MOULD PROCESSING OF ACCs

1. INTRODUCTION

The processing of composites *via* a completely closed and non-flexible mould, also termed "rigid mould processing", represents yet another alternative to the manufacturing processes described in Chapters V and VI. Two-sided rigid mould processing of ACCs is examined in the present Chapter through adaptation of the Resin Transfer Moulding (RTM) process. Here, this adapted RTM-based process is referred to as "Solvent Transfer Moulding" (STM) to distinguish it from SIP.

Two-sided rigid mould processing is expected to improve the surface finish of the SIP-based ACCs, while a closed cavity will also minimise moisture uptake as for SIP [401, 402].

A successful adaption of the RTM process for processing of ACCs can also be seen as the foundation for extending ACC processing to other closed-mould processes such as injection moulding for example. In fact, RTM has been identified as one of the most promising processes for the processing of conventional and natural fibre reinforced composites in the automotive industry [7, 403]. RTM has also been successful in the processing of natural fibre preforms including hemp fibre non-wovens [404] and flax fibre mats [405].

The herein described approach of ACC processing *via* RTM will be based on SIP as described in Chapter VI. The vacuum bag used in SIP is replaced by a second rigid tool in STM. The basic processing steps remain the same:

- Positioning layers of cellulosic fabric in the mould;
- Vacuum assisted infusion of the solvent through the fabric layers;
- Heating under pressure to achieve partial dissolution and consolidation;
- Vacuum assisted infusion of a coagulant to regenerate the dissolved portion of the cellulose; and
- Removal of the composite from the mould to further washing and drying.

In a similar way to traditional composite processing *via* VARTM the positioning of the inlets and vents and therefore resin or solvent flow is important to the quality of the composite. Poor flow behaviour will lead to an uneven saturation of the fabric by the resin or solvent, resulting in dry spots within the final composite [406].

Furthermore, the second infusion of the coagulant could pose an additional challenge to the mould design as supplementary cavity space will be necessary to allow additional fluids to enter.

A mould will be designed that allows the production of ACC panels of different thicknesses to examine the feasibility of rigid mould processing of ACCs.

2. EXPERIMENTAL PROCEDURES

2.1 MOULD DESIGN

The mould is to be mounted in a hot press that will apply pressure for consolidation and maintain elevated temperatures for cellulose dissolution. Various inlets/vents were designed to allow different infusion paths for the IL. The mould was also designed with a rubber seal to prevent possible leakage of IL and/or the used coagulant (Figure 96).

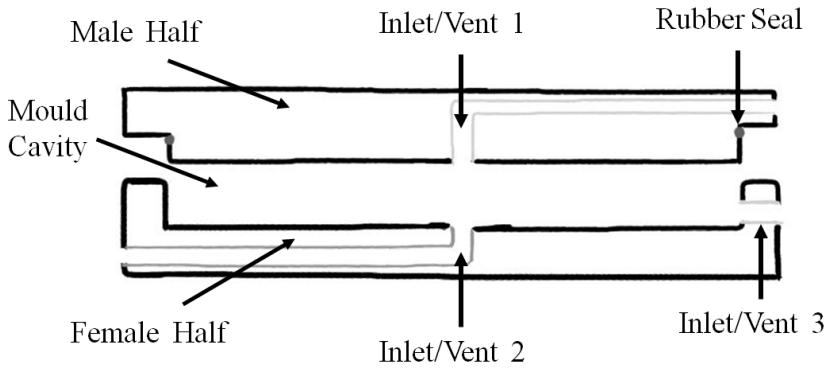

Figure 96: Sketch of the basic mould design developed for Solvent Transfer Moulding.

Flanges were then added to the original design (Figure 96) to allow mounting in the hot press (Figure 97). Aluminium was chosen as mould material due to its easy machinability and high thermal conductivity. The mould was designed to produce ACC panels 1 mm in thickness. However, the height of the mould cavity is adjustable *via* the use of spacer plates or shims to allow customisable panel thicknesses. The mould design work was carried out using SolidWorks 2008 SP4 (Dassault Systèmes SolidWorks Corporation, Waltham, MA, USA). Detailed technical drawings of the mould are provided in the Appendix).

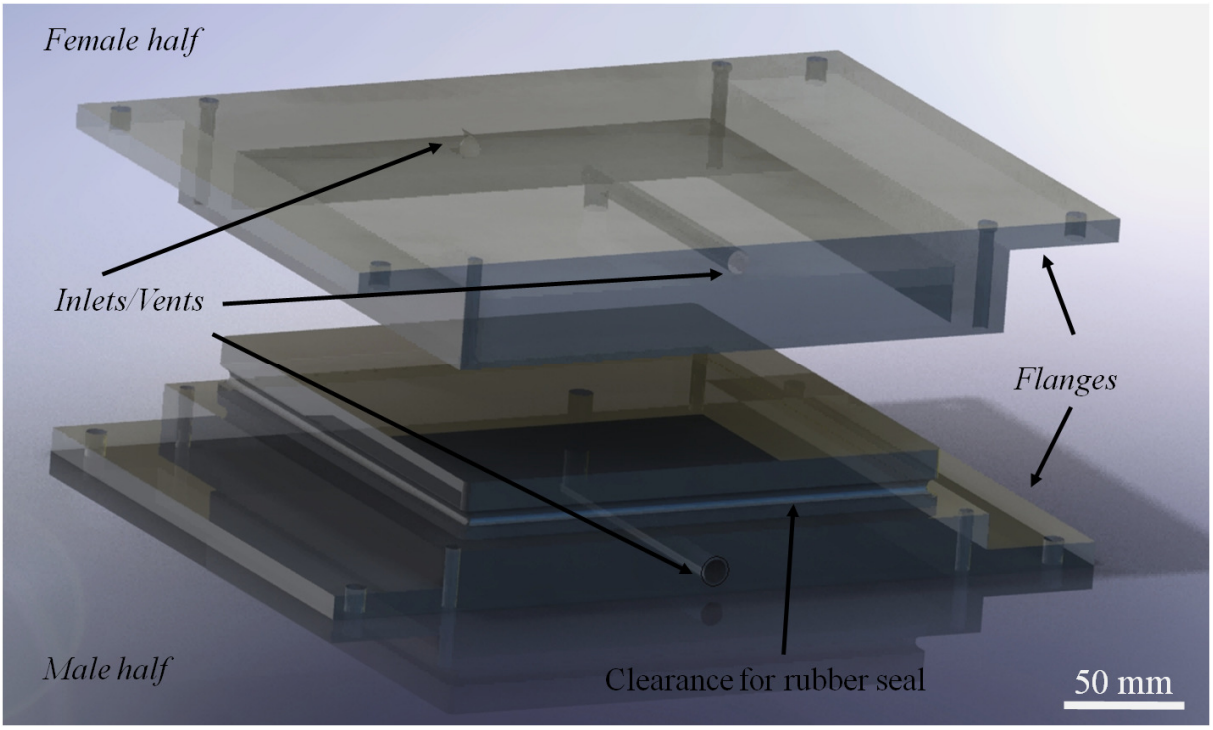

Figure 97: Rendered SolidWorks model of the STM mould.

The individual steps of STM can be identified as:

I. Placement of the cellulosic textile in the heated mould;
II. Closure of the mould;
III. Injection of the ionic liquid;
IV. Partial dissolution of the fibre surface at elevated temperatures;
V. (Vacuum assisted) infusion of the coagulant for cellulose regeneration;
VI. Removal of the composite from the mould;
VII. Post-STM washing; and
VIII. Post-STM drying.

During SIP the flexibility of the vacuum bag and the presence of a distribution medium enable the coagulant to easily access the infused solvent and partially dissolved textile. In contrast, Step V of STM requires an adjustment of the mould height to allow additional fluids to enter the mould cavity. Thus, the mould was partially opened just

prior to Step V to allow the insertion of stainless steel shims of 0.1-0.5 mm thickness between the male and female halves increase the cavity volume.

2.2 MATERIALS AND COMPOSITE PROCESSING

Sheets of 200 mm x 200 mm were cut from the rayon textile and dried before processing. BmimAc was used as the IL.

All composites were processed at a temperature of 100˚C and 0.5 MPa of applied pressure using the laboratory hot press. Two layers of the rayon textile were used as a dry fibre preform. Distilled water was used as the coagulant for regeneration and washing. Four different processing set ups were used as follows (refer to Figure 96 for the inlet and vent positions):

a) Using the central inlets/vents (No. 1&2) for infusion and removal of IL/coagulant (STM-A);
b) Using the central inlet (No. 1) for IL/coagulant infusion and the peripheral inlet/vent (Figure 96, no. 3) for removal (STM-B);
c) Using the central inlets/vents (No. 1&2) for infusion and removal of IL/ coagulant with an additional layer of peel-ply for improved IL/ coagulant distribution (STM-C); and
d) Using the central inlet (No. 1) for IL/ coagulant infusion and the peripheral inlet/vent (No. 3) for removal with two additional top and bottom layers of porous plastic film (hole diameter *ca.* 1 mm, hole spacing *ca.* 2 mm) for improving IL/ coagulant distribution(STM-D).

A 10 L pressure pot (Blastquip, Christchurch, New Zealand) with an applied pressure of 0.2 MPa was used to inject the IL and water into the mould. An additional vacuum of 0.1 MPa was applied at the vent using a Hitachi 3VP-C vacuum pump (Hitachi Ltd., Tokyo, Japan) to improve the flow of the IL/water.

2.3 ACC ANALYSIS

2.3.1 Fibre Volume Fraction

3-4 sections were prepared for optical microscopy from the manufactured laminates close to the inlet position, middle region and outer region to determine V_f. The mounted samples were conditioned at 23 ˚C and 50% RH prior to optical microscopy and then analysed using the colour threshold method as described in detail in Chapter VI.2.2.3.1. 7 to 8 micrographs were analysed from each region. The average values of V_f were statistically analysed using a one-way ANOVA analysis.

2.3.2 Scanning Electron Microscopy

The mounted and polished samples were gold coated for 120 seconds at 25 mA.

3. RESULTS AND DISCUSSION

3.1 THE POTENTIAL OF SOLVENT TRANSFER MOULDING IN ACC FABRICATION

All four variations of the processing set-up (*i.e.* STM-A, B, C and D) posed difficulties with regard to the injection and removal of the IL and water. The complete cycle was only possible for STM-D. Water could not be injected into the mould using STM-A; thus, the partially dissolved textile layers had to be removed from the mould by hand and put in a bath of distilled water for regeneration. The injected water could not be removed automatically from the mould using STM-B or STM-C, in spite of the shims placed between the mould halves.

An improved surface finished was not observed in any of the ACCs produced *via* STM. The close contact of the materials with the mould surface during dissolution, consolidation and regeneration is considered a prerequisite for obtaining a smooth surface finish. However, close contact between the materials and mould surfaces was

not possible for the entire process due to the difficulties in performing all the processing steps *within* the mould.

Further examination of the composite surfaces offers some explanations for the observed processing behaviours (Figure 98). An increase in the volume of the mould cavity by the addition of the steel shims did not improve the water flow. A deep imprint of the circular inlet/vent is visible for STM-A, C and D (Figure 98). The presence of an imprint indicates that dissolved cellulose [407] may have been forced into the inlet and vent, effectively blocking them and preventing the flow of water into the cavity. STM-A and C exhibited only a slight colour change, indicating that an insufficient amount of IL had permeated into the textile during the dissolution step. It is appears that most of the IL was forced directly through a region of the textile layers immediately between the inlet and vent in preference to spreading throughout the mould [408]. The two layers of rayon textile for STM-A and C were also observed to separate during the drying process, confirming that insufficient dissolution had taken place.

The additional layer of peel ply (STM-C) appears to improve the distribution of the IL slightly, as the peel ply was inseparable from the rayon textile after processing. The bond between the peel ply and rayon textile is due to the IL wetting the peel ply upon injection and then slightly dissolving the surface of the neighbouring rayon fibres. As a result of partial dissolution the rayon fibre becomes malleable [407], allowing some of the rayon to be forced into the pores of the peel ply (Figure 99). The two different layers of peel ply and cellulosic textile can be clearly identified by the different fibre geometry. Following regeneration, mechanical interlocking of the peel ply and rayon textile layer ensues in a similar fashion to the blocked inlet and vent.

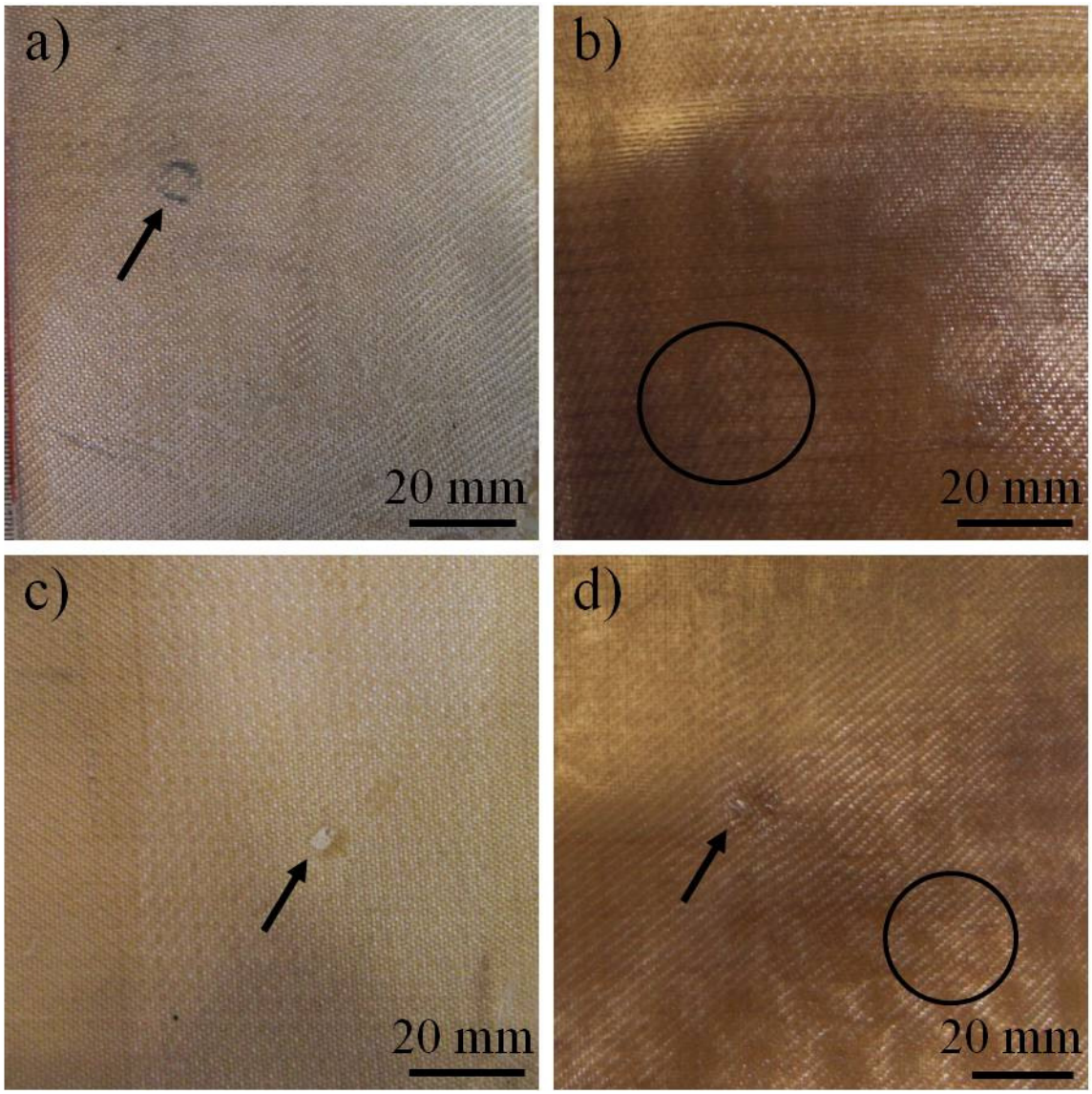

Figure 98: Photographs of the top view of (a) STM-A, (b) STM-B, (c) STM-C and (d) STM-D. The arrows indicate an imprint originating from the central inlet/vent. The circles in (b) and (d) indicate areas of uneven solvent distribution.

STM-B exhibits greatly improved dissolution of the rayon textile, indicating that a sufficient IL had permeated through the rayon textile layers prior to the dissolution step. However, the final composite exhibited non-uniform solvent distribution as indicated by colour variations across the laminate (Figure 98b and d, Figure 100).

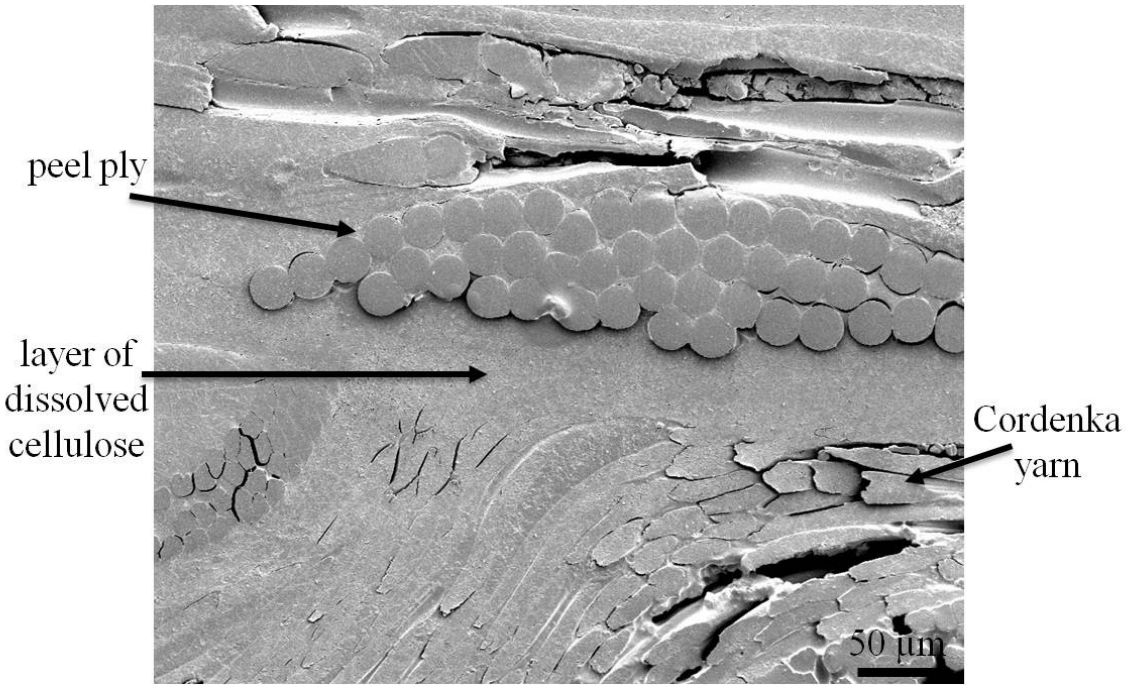

Figure 99: SEM micrograph of the interface between the peel ply and rayon textile. A layer of dissolved cellulose has formed on top of the cellulosic layer and has bonded to the peel ply. An accelerating voltage of 5 kV was used.

Flow behaviour within the mould during infusion is often improved through the use of an additional porous layer [408]. Therefore, it was not surprising that the addition of porous films (STM-D) led to a more even distribution of the solvent. The pattern of the pores was also replicated in the surface of the composite (Figure 98d). The plastic film also prevents dissolved cellulose from entering the vent and inlet, allowing STM-D to proceed through a complete processing cycle.

Backlighting the ACC laminates was useful for photographing and recording the variation in coloration due to non-uniform distribution of solvent (Figure 100). Based on these visual observations, the positioning of vent and inlet are of crucial importance in achieving good saturation of the textiles with IL. This of course also implies that the positioning of vent and inlet are important for obtaining an evenly distributed matrix phase in the final ACC laminate [401, 406]. The distribution of solvent is also worsened

by possible variation of the cavity height due to local pressure differences within the cavity that are known to occur in rigid RTM moulds [408]. The presence of a porous intermediate layer between the inlet and rayon textile appears to be beneficial for distribution of the solvent given that STM-C and D both indicate a more regular pattern of dissolution. Additionally, the high viscosity of the solvent (see Chapter III) may also contribute to the non-uniform wetting behaviour [409].

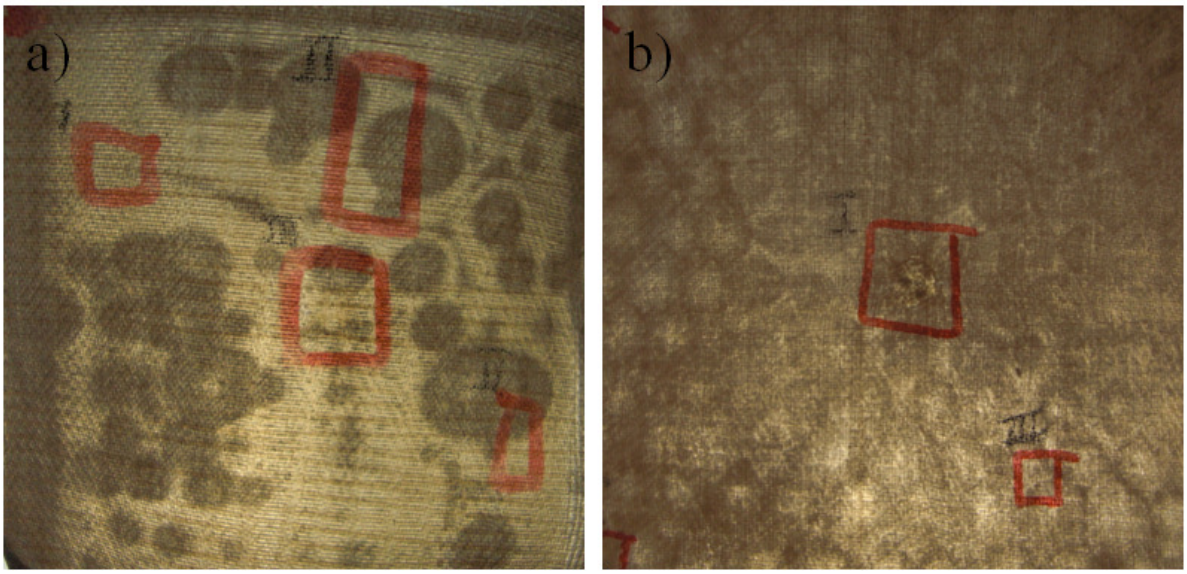

Figure 100: Backlit photographs of (b) STM-B and (d) STM-D that exhibit non-uniform coloration indicating uneven solvent distribution. STM-B shows a more random dissolution pattern, while STM-D displays a spotted pattern caused by the porous film. The marked areas indicate the sections that were taken from the composites for determining V_f.

The final ACC laminates produced *via* STM were judged to be too inhomogeneous for meaningful tensile testing of the mechanical properties. Therefore, the different ACC laminates were compared at the microstructural level in terms of their fibre volume fraction. Unfortunately, the V_f of STM-A was not determinable as a result of delamination during drying.

3.2 FIBRE VOLUME FRACTION

The V_f of STM-B, C and D was examined as a function of their location within the laminate (Figure 101). There was no statistically significant difference in V_f for the different regions within each laminate, although visual inspection suggests an uneven distribution of the solvent through the textile layers. A layer of completely dissolved cellulose can be observed for all samples (STM-B, C and D) adjacent to the surface of the textile layer (Figure 99). However, the inhomogeneous IL distribution leads to regions in the laminate that remain untouched by the solvent. This will cause dry patches within the composite and therefore areas with no present matrix phase after the dissolution stage. An insufficient matrix phase will lead to debonding of fibre yarns and consequently delamination of the whole composite, causing a drastic decrease in composite properties. In fact, the uneven dissolution can also be seen in the micrographs of the composite cross-sections (Figure 102). The large, vertical cracks within a yarn indicate poor distribution of the solvent and a lack of fibre dissolution. As a result, no matrix phase has been created that could bond single fibres within a yarn together during the dissolution and consolidation phase. Instead, the applied pressure has pushed the fibres apart, resulting in the large cracks. Similar cracks could not be observed during SIP (see Chapter VI), indicating superior distribution of the solvent during flexible mould processing..

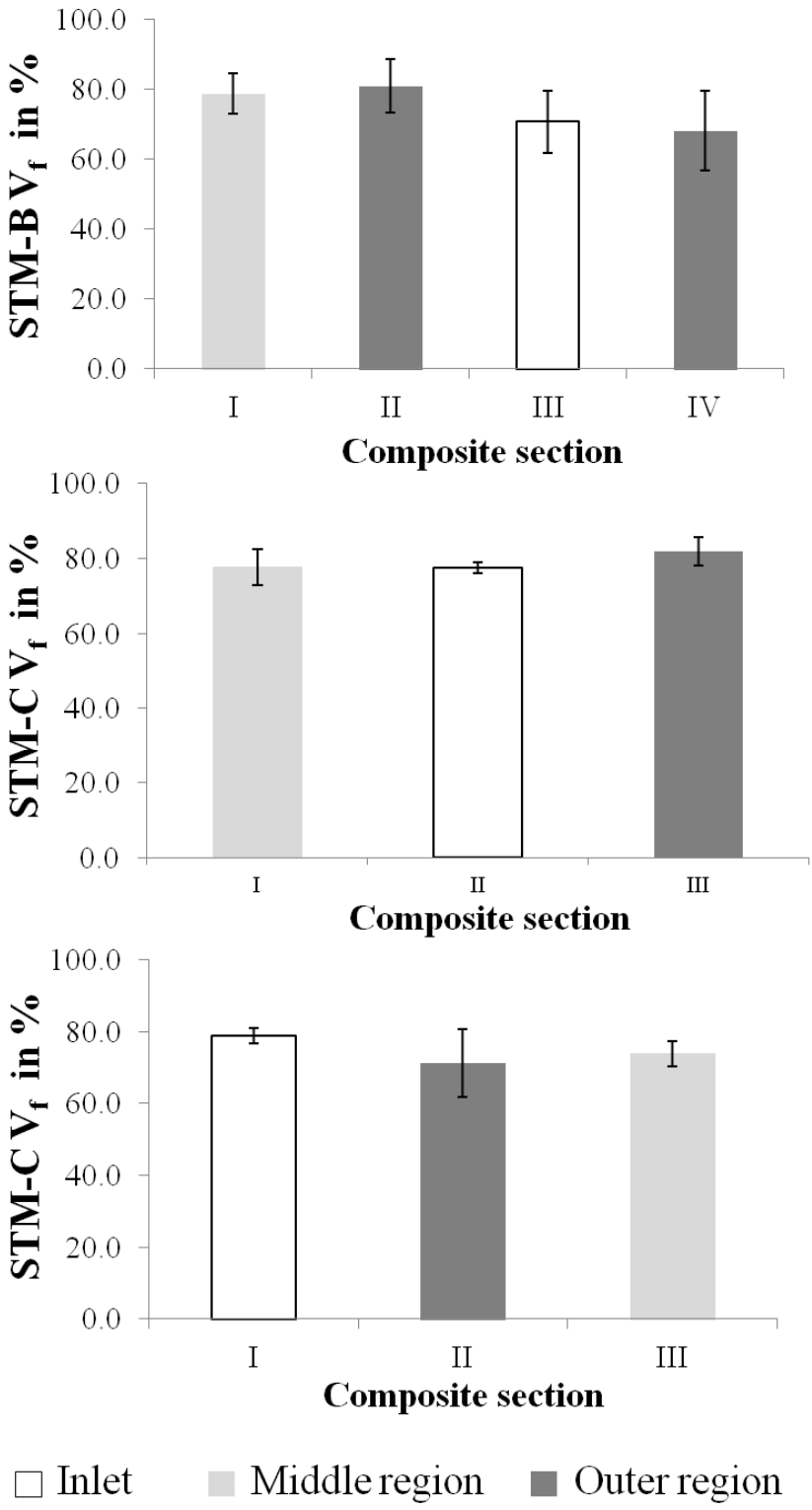

Figure 101: V_f of STM-B, C and D as a function of the region (inlet, middle or outer) within the laminate. Error bars indicate one standard deviation..

No statistically significant difference could be found between the different sections of each composite although the optical appearance indicates an uneven distribution of the

solvent through the textile layers. This could indicate that the optical irregularities are mere superficial and don't affect the overall V_f too severely in a two layer laminate as both layers will still be in contact with the IL. A layer of dissolved cellulose located on the textile surface can also be seen in Figure 99. However, the inhomogeneous IL distribution could lead to completely undissolved regions in a multi-layer laminate, causing a drastic decrease in composite properties. In fact, the uneven dissolution can also be seen in the micrographs of the composite cross-sections (Figure 102).

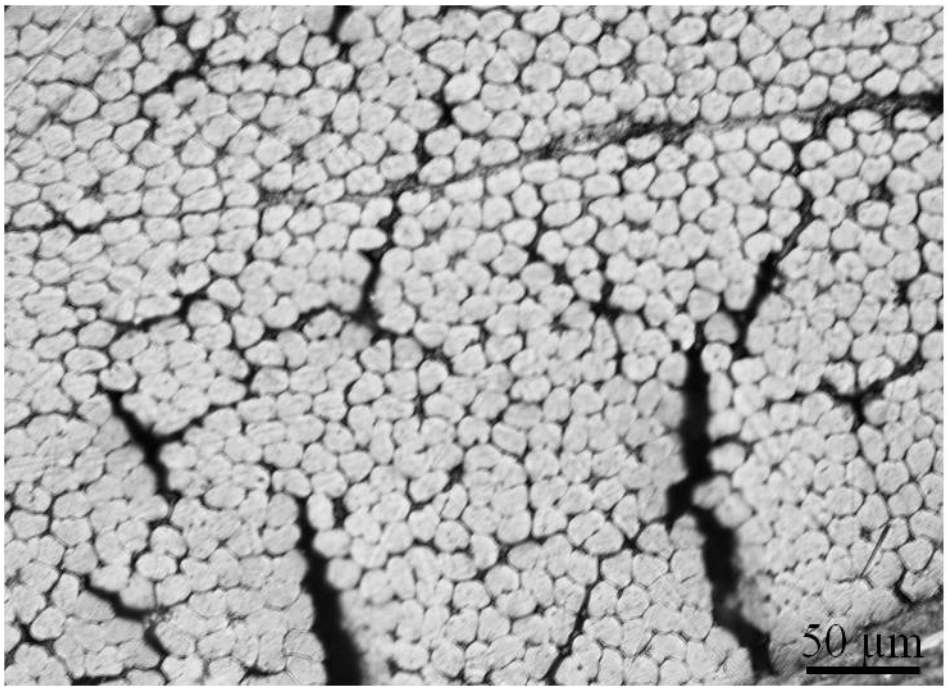

Figure 102: Reflected light micrograph of the cross-section of the ACC laminate produced *via* STM-D. The sample is taken from the middle region of the laminate.

The large, vertical cracks within a yarn can be seen as an indicator for a poor solvent distribution and little fibre dissolution. As a result, no matrix phase has been created that could bond single fibres within a yarn together during the dissolution and consolidation phase. Instead, the applied pressure has pushed the fibres apart, resulting in the large cracks. Similar cracks could not be observed during SIP (see Chapter VI) indicating a superior solvent distribution during the flexible mould processing.

3.3 STM COMPARED TO SIP

The direct result of the observed cracks is an overall lower V_f for the STM composites compared to the SIP composites (Figure 103). The average V_f of the STM composites was 75.91 ± 4.45 %, while that of the SIP composites was 87.01 ± 3.4 %, mainly due to a vast amount of crack and void formation in the STM composites. Clearly, these results demonstrate that SIP has greater capacity for providing a homogenous distribution of the solvent. Aside from the positioning of the inlet and vent, the main reason for a reduction in the distribution of the solvent is due to the non-flexible nature of the mould material. It is presumed that uniform distribution of the solvent is hindered since capillary flow paths are closed under the applied pressure. In contrast to that, during SIP, the flexible vacuum bag in combination with the used distribution medium and porous film (see Figure 52) allow a constant flow of solvent through the textile layers. The improved flow leads to better solvent distribution and as a result a higher fibre volume fraction.

Furthermore, any dissolved cellulose needs to be stopped from entering the inlet and vent so they will not be blocked during the regeneration stage. This problem is avoided by SIP through placing a layer of distribution medium between the textile layers and vent/inlet. Completely dissolved cellulose is trapped in the distribution medium and cannot block the actual vent/inlet and therefore stop the flow of the regeneration medium.

Additionally, using transparent vacuum bags allows an inspection of the ongoing infusion process in contrast to the rigid aluminium mould. Suboptimal solvent

distribution can be identified before the textiles are partially dissolved and therefore corrected by improving the inlet/vent placement.

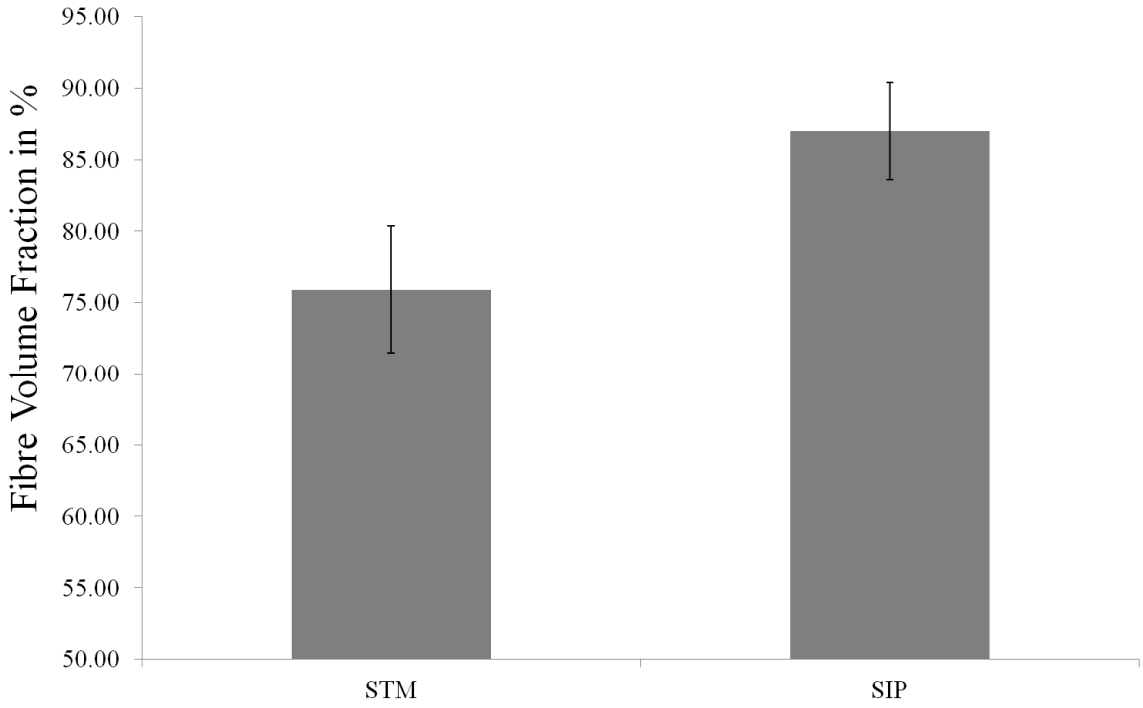

Figure 103: A comparison of the average Vf of all STM and SIP samples. Error bars indicate one standard deviation.

4. CONCLUSIONS

It is concluded that STM as an upscaled fabrication route does not improve the quality of ACC laminates. On the contrary, STM was found to significantly reduce the V_f of ACC laminates. The produced composites have shown that using certain inlet/vent combinations prevents a homogenous solvent distribution and a solvent/coagulant exchange for cellulose regeneration is made difficult using rigid moulds. While changes in the inlet and vent positions may slightly improve the process, a redesign of the mould may bring more promising results. The use of a porous medium such as a perforated

film or peel ply tends to improve the IL distribution. Thus, it is possible that both, IL distribution and solvent/coagulant exchange can be strongly improved by using either a porous intermediate layer between actual mould surface and cellulosic material or manufacturing the mould completely from a porous material. Careful design would need to take into account an appropriate pore size since the pore structure may be imprinted into the final surface of the composite if the pore size is too large. Conversely, pores that are too fine may lead to an inefficient exchange of solvent and coagulant, or blocking of the pores.

Comparing STM with SIP showed a clearly better processability of ACCs *via* SIP. The flexible mould seems to enhance solvent flow, leading to a more uniform matrix phase and therefore better load transfer and mechanical properties.

.

VIII. ALL-CELLULOSE COMPOSITE BASED ON 3D-BRAIDED TEXTILE PREFORMS

1. INTRODUCTION

1.1 3D TEXTILES

Composite laminates that are based on 2D textile layers have become commonplace in the aircraft, maritime craft, high performance automotive and civil infrastructure industries over the last few decades [410]. In combination with a thermosetting resin matrix, 2D textiles form very lightweight, stiff structures. Composite laminates are able to be designed through their stacking sequence and orientation of 2D layers to withstand high in-plane loads in the required directions, which gives them an advantage over conventional materials such as steel or aluminium in lightweight structural applications [411, 412]. However, the poor drapeability of many textiles may hinder the fabrication of complex 3D designs as a single integral structure (*i.e.* without the need for secondary bonding and fastening) [413].

Another option to produce 3D composites is through the use of 3D textiles. Technically, even 2D textiles are 3D in nature, although a definition put forward by Gries *et al.* provides a simple method to distinguish between 2D- and 3D textiles. According to this definition "a textile is defined as 2D if it does not extend in more than two directions, neither in yarn architecture nor in textile architecture" while "a textile is defined as 3D textile if its yarn architecture extends in three directions, regardless of whether it is made in a one-step-process or a multiple-step-process." [414]. One-step processes are based on technologies such as 3D braiding, 3D weaving or 3D knitting, whereas multiple-step processes involve stitching or over-braiding of 2D textiles. Typical fibres used for the

production of 3D textiles are carbon, aramide and to some extent glass fibre. The fibres are mainly used in the form of twisted or untwisted yarns, also known as rovings. During processing, the fibres are exposed to various bending and tensile stresses as well as frictional forces occurring between the fibres and/or the fibres and processing equipment. Twisting of the yarns reduces the risk of fibre damage [414, 415].

Composites based on 3D textiles are generally assumed to result in better properties than their 2D counterparts due to improved through-thickness or out-of-plane strength [416]. Composites based on 3D textiles may improve the shear strength, interlaminar tensile strength and flexural strength by 300, 200 and 65%, respectively [415]. However, in general the in-plane properties of 3D textile based composites are reduced at the expense of improving the out-of-plane properties. This is explained by the overall reduction in fibre volume fraction in the in-plane directions as some of the volume must be taken up by fibres orientated out-of-plane [417].

1.2 3D-BRAIDING

Of the abovementioned one-step processes, 3D braiding was the first process used to manufacture a 3D textile structure for a composite application [411]. Several different 3D braiding processes have been developed since then including the 4-step process and its successors such as 6-step and multistep braiding, two-step braiding and multi-layer interlocking braiding [414]. The latest development in 3D braiding technology is 3D rotary braiding. Recently, 3D braiding has been declared as one of the most promising 3D textile processes [411] since it also allows a more complex microstructure due to a 3D yarn course during braiding. 3D braided composites have a higher delamination

resistance, improved impact resistance and lower notch sensitivity when compared with traditional 2D laminates [411].

The decisive factor determining the mechanical properties of a 3D braided composite is the microstructure of the braid. The microstructure is a result of several processing factors such as braid angle and pattern or yarn tension [418, 419]. The braiding angle can be defined as the angle between the yarn direction in the braid and longitudinal direction of the braid (Figure 104).

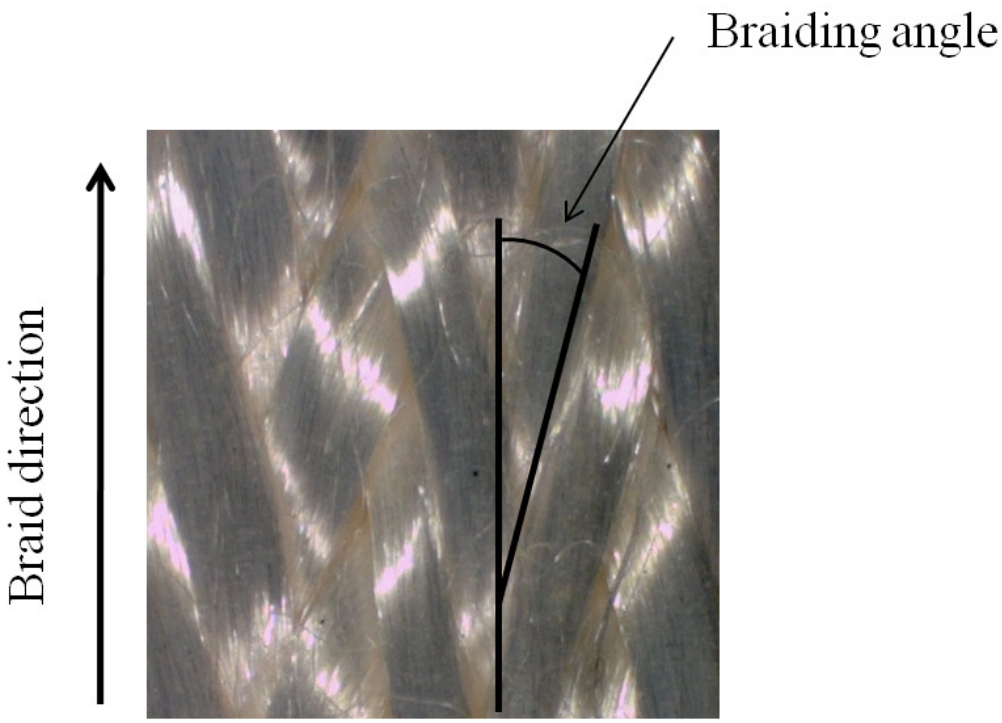

Figure 104: Definition of the braiding angle as shown on the surface on 3D-rayon braid.

Braiding machines use yarn carriers to deposit continuous rovings to create the desired braid architecture [414]. Usually, in 2D braiding machines, half of the carriers move clockwise and the other half counter clockwise in an intertwining motion to produce a certain braid pattern [420]. In 3D rotary braiding the motion of the yarn carriers takes place by rotating horn gears that rotate in counter direction. In contrast to conventional

braiding machines the horn gears are assembled in rows and columns to form a braiding bedplate. Each horn gear can carry one to four bobbins holding the yarns. Two different 3D rotary braiding technologies have been invented: the ITA-Herzog-3D rotary–braiding invented by ITA and Herzog and the 3TEX-3D rotary-braiding invented by 3TEX. The ITA-Herzog technology uses switches between the horn gears to control the yarn carrier movement. In each step of the braiding process it can be decided for every horn gear whether a yarn carrier is transferred to a neighbouring horn gear or remains on the former horn gear and is rotated by 90˚. Complex yarn architectures can be achieved by computer controlled individual switches and horn gears resulting in an individual path of each yarn carrier. Rather than switches, the 3TEX-3D technology has gripping forks positioned between the horn gears. Hence, two yarn carriers can be present between two horn gears simultaneously. At this stage the carriers can either swap places or remain on their former horn gears. While the 3TEX technology can employ more yarn carriers on the same area and can be exercised faster, the ITA-Herzog machinery uses yarn carriers with a higher yarn capacity and allows for more complex designs (Figure 105) [414].

Presently, there are no reported studies of 3D braiding of regenerated cellulose fibres and subsequent processing of the braids into 3D preforms for composite materials. The present work, examines the possibility of processing a rayon yarn into a 3D-braided preform using braiding equipment that has been developed for glass and carbon fibres. The 3D braided preforms will be then be used in the fabrication of all-cellulose composites. Finally, the mechanical properties of the 3D textile-based ACC will be compared with the standard ACC laminates processed *via* SIP (Chapter VI).

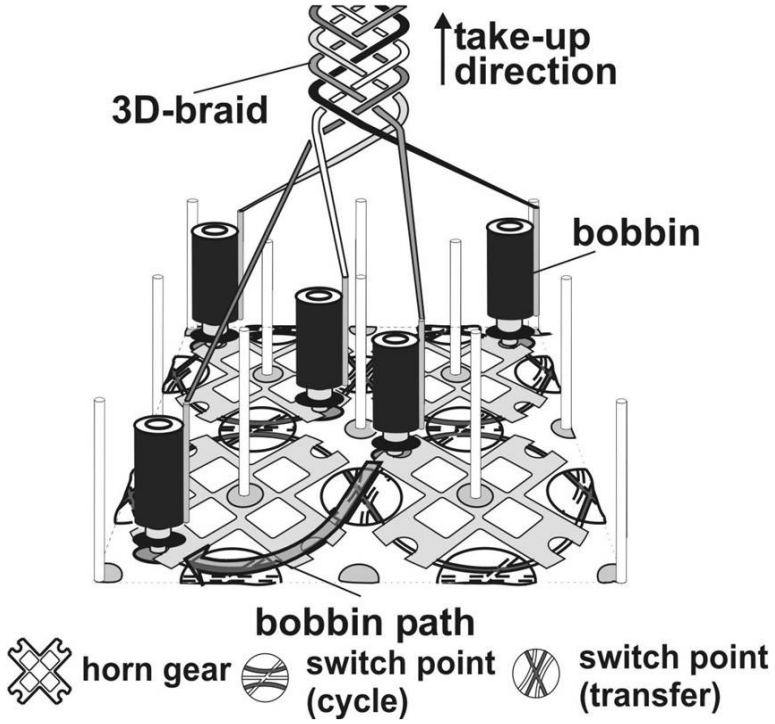

Figure 105: Schematic of the 3D rotary braiding technology Shown are 4 horn gears with 5 attached bobbins [414].

2. EXPERIMENTAL PROCEDURES

2.1 3D-BRAIDING

A rayon yarn with 10,000 single fibres per yarn with a fibre fineness of 1440 dtex was used for the braiding process. The ITA-Herzog technology was used to produce preforms for all-cellulose composite processing. The used braiding machine was a CAB-9-32-220 3D rotary braider (August Herzog Maschinenfabrik GmbH & Co. KG, Oldenburg, Germany) (Figure 107). A total of 8 steps were used to produce a three dimensional rectangular braid, with every second step being a blank step due to software (Herzog CAB-0.20-04, August Herzog Maschinenfabrik GmbH & Co. KG, Oldenburg, Germany) requirements. 32 horns gears supplied with 68 bobbins were necessary to produce the braid.

Figure 106 shows the 4 non-blank braiding steps, direction of rotation of the horn gears and position of the bobbins in each step. Approximately 80 m of the yarn was spooled to a bobbin using a Herzog 280/PN rewinding machine applying a rewinding speed of 25 m/min.

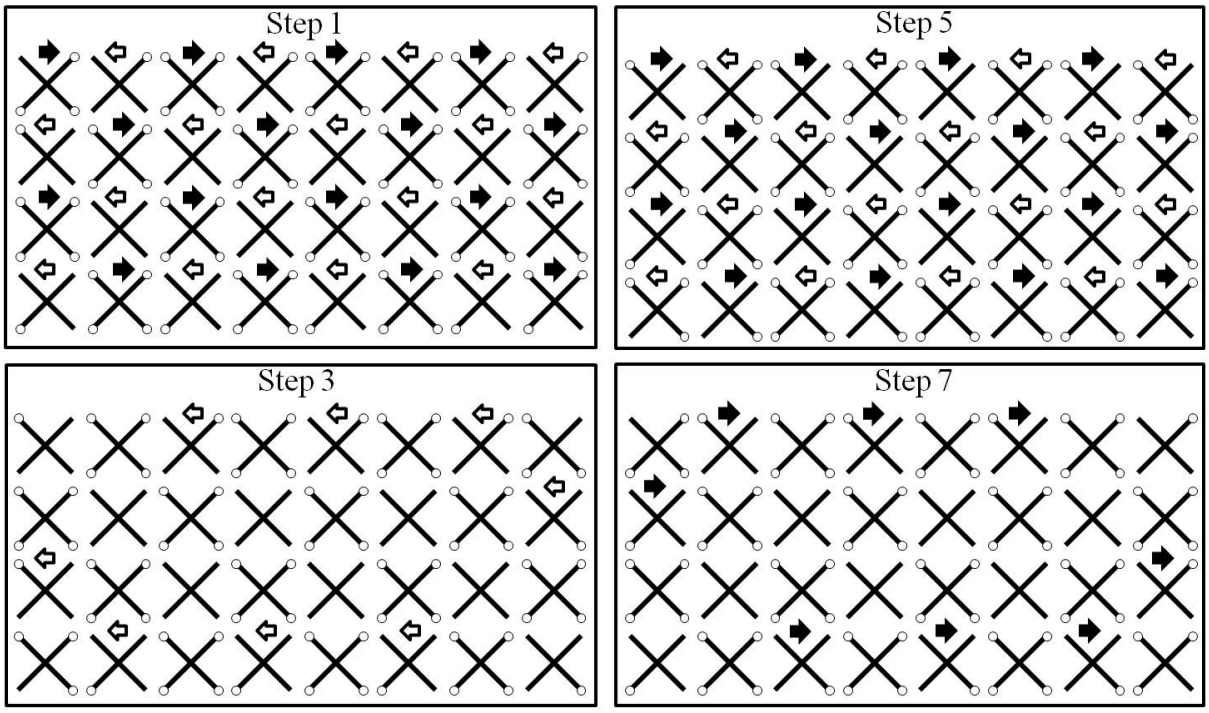

Figure 106: Schematic representation of the active braiding steps of programmed braiding path to manufacture a rectangular rayon preform. The crosses resemble the horn gears with the circles representing the attached bobbins. The arrows indicate the rotation direction of each horn gear in each step.

2.1.1 Fibre Tensile Testing

30 single fibres were taken from each of the yarn bobbins and final braid to investigate the influence of spooling and braiding on the fibre properties. The fibres were tensile tested according to DIN EN ISO 5079 using a Fafegraph M (Textechno, Herbert Stein GmbH & Co. KG, Mönchengladbach, Germany). For testing, the fibres were clamped using pneumatic clamps with a clamping pressure of 0.4 MPa and testing length of 20 mm. The tensile test rate was 20 mm/min and load changes were recorded using a 0.1 N load cell.

A pre-load of 0.0001 N was applied before testing using a 100 mg weight to avoid fibre crimping. The fibres were conditioned at 20 °C and 65% RH prior to testing. The average values of the determined fibre properties were statistically compared using a Wilcoxon signed-rank test.

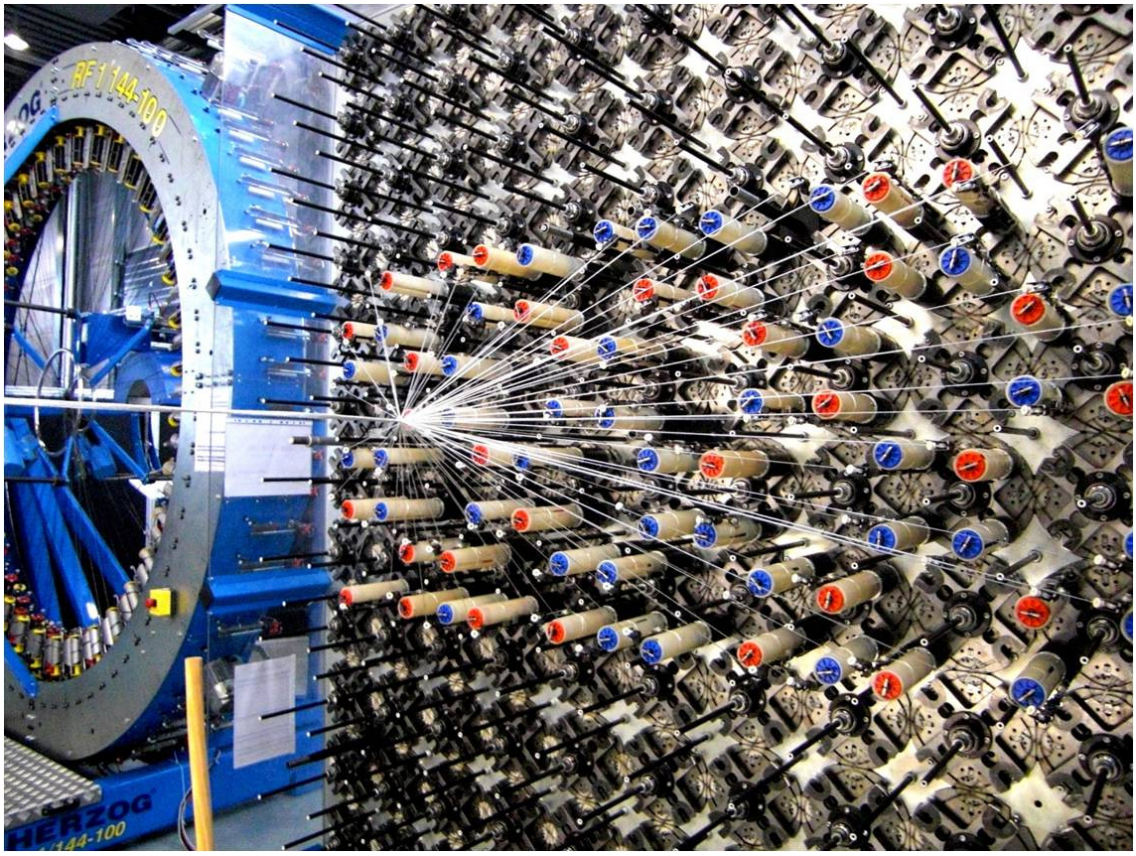

Figure 107: **Photograph of the 3D rotary braider loaded with bobbins. The rayon yarns in each bobbin intersect in the braiding point to form the braid.**

2.1.2 Analysis of the Braiding Structure

Four reflected light micrographs were taken of the surface of 8 different samples using an Olympus SZH10 stereo microscope (Olympus Corporation, Tokyo, Japan) with an attached Zeiss AxioCam camera (Carl Zeiss AG, Jena, Germany) in order to measure the braiding angle of the rectangular rayon braid. The braiding angle was measured using the software ImageJ. 100 measurements of the braiding angle were taken along the

longitudinal axis of each sample. Each measurement was performed 3 times to minimize the influence of manual measurements, resulting in a total of 300 measurements.

A 5 mm long section was cut from the braid to observe changes in the microstructure after processing. The sections were then mounted along their longitudinal axis and prepared for optical analysis of the braids.

The average values of the measured braiding angle were compared using a one way ANOVA analysis. All statistical analysis was carried out using the software "R" (Bell Laboratories, Murray Hill, NJ, USA).

2.2 COMPOSITE PROCESSING

The principle of partial fibre surface dissolution was used to process the 3D braids into all cellulose composites. Sections of about 200 mm in length were cut from the braid and the ends secured with cable binders to prevent any loosening of the braid. The braid sections were dried in a vacuum oven at 100˚C for 24 hr. The sections were then weighed individually and placed in a Petri dish. BmimAc was selected as the cellulose solvent. The Petri dish was filled with the IL until the braid was completely submerged. A lid was placed over the Petri dish. Braids were submerged in the IL for 30 min in order to achieve thorough saturation of the yarns with the solvent. The submerged braid was kept at 4°C during this infiltration stage to avoid any premature dissolution of the fibres. After 30 min the braid was removed from the Petri dish, excess IL was wiped from the surface and reweighed. The infiltration stage resulted in the braid section being impregnated with a mass of IL similar to the as-received section of braid (~ 4 g). Up to four of the IL-soaked braids were then placed on a sheet of HDPE (200 × 200 mm), aligned and straightened

(Figure 108). The ends of the braids were clamped with two narrow sheets of HDPE (15 × 200 mm) using 6 hex cap screws (ø 6.35 mm) and matching nuts to prevent movement of the braid during dissolution.

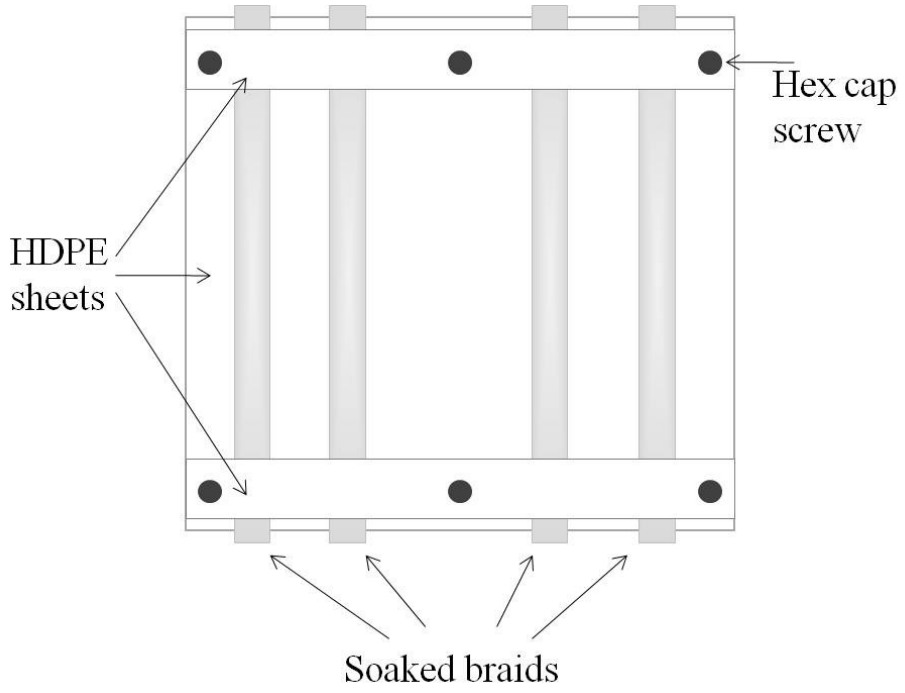

Figure 108: Schematic of the set-up used for processing 3D braids into ACCs.

The soaked and secured braids were put in a furnace at 100 ˚C for 60 min to partially dissolve the fibre surface. After 60 min the HDPE clamps were removed and the braids were sprayed with 1:1 mixture of distilled water and ethanol using a fine hand sprayer to regenerate the dissolved cellulose. After the surface has been solidified the composites were taken off the bottom HDPE sheet and washed in a mixture of distilled water and ethanol (ratio 1:1) for 48 hr to remove the remaining ionic liquid. After washing, the wet composites were dried in the hot press under light pressure (0.1 MPa) at 65 ˚C for 4 hr followed by 4 hr at 100 ˚C.

2.3 MATERIALS CHARACTERISATION

The cold mounted samples, fracture surface and sample surface of mechanically tested samples were analyzed using FE-SEM. The samples were gold-coated for 120 s at 25 mA, of the tensile tested samples were also analysed using FE-SEM.

To determine the difference in void size between ACCs based on 3D braids and SIP, 50 voids selected from SEM micrographs of the above described cold mounted samples and SEM micrographs of SIP composite 1 (see Table 9) were analysed using ImageJ.

2.4 MECHANICAL TESTING

12 samples were tensile tested on a MTS810 Servo-hydraulic load frame (MTS, Eden Prairie, MN, USA) with a 100 kN load cell. A gauge length of 60 mm and a cross-head speed of 2mm/min were used. Pneumatic clamps with a clamping pressure of 2 MPa were used. To avoid clamping damage, cap strips cut from a glass-fibre epoxy laminate were glued to the samples. Before testing, the samples were conditioned at 23 ± 1°C and 50 ± 1% RH for 24 hr.

6 samples of approximately 2.1 mm thickness, 8 mm in width and a length of 50 mm for 3-point bending testing were prepared using a band saw. The samples were tested after conditioning for 48 h at 23 ± 2°C and 50 ± 2% RH Before testing the sample dimensions were accurately measured using a digital vernier calliper.

Charpy impact tests were executed in accordance with DIN EN ISO 179 [421] to determine the unnotched Charpy impact strength. 7 samples of 70 × 6 × 3 mm were tested in parallel impact direction using a 4 J pendulum. Before testing, the samples were

conditioned for 24 h at 23 ± 1°C and 50 ± 1% RH and sample dimensions were accurately measured using a digital Vernier calliper.

3. RESULTS AND DISCUSSION

3.1 ANALYSIS OF THE BRAIDING PROCESS

A 3D braiding consisting of 68 yarns, with a thickness and width of ~4 and 10 mm, respectively, was successfully fabricated (Figure 109). The braid appeared to be of regular consistency, showing no obvious defects. However, some single fibres were observed to have separated from the yarns, protruding from the surface.

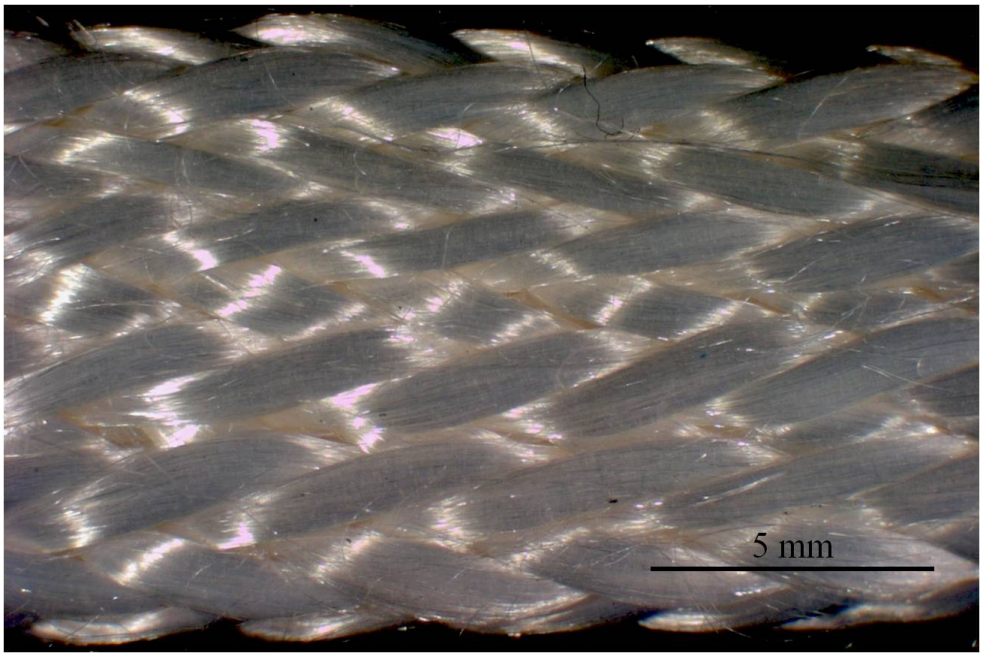

Figure 109: Top view of the produced 3D braid.

3.1.1 Fibre Damage

The ultimate tensile strength (UTS) and strain to failure (ε_f) of the as-received rayon fibre was found to be 427.13 ± 62.77 MPa and 10.60 ± 2.13%, respectively (Figure 110); the fibre supplier (Cordenka) report values of 830 MPa and 13%, respectively [221]. The reduction in strength and elongation is likely due to fibre damage caused during the

braiding process [422]. In fact, the precise test method used will influence the mechanical properties observed and may contribute to discrepancies between literature and measured values.

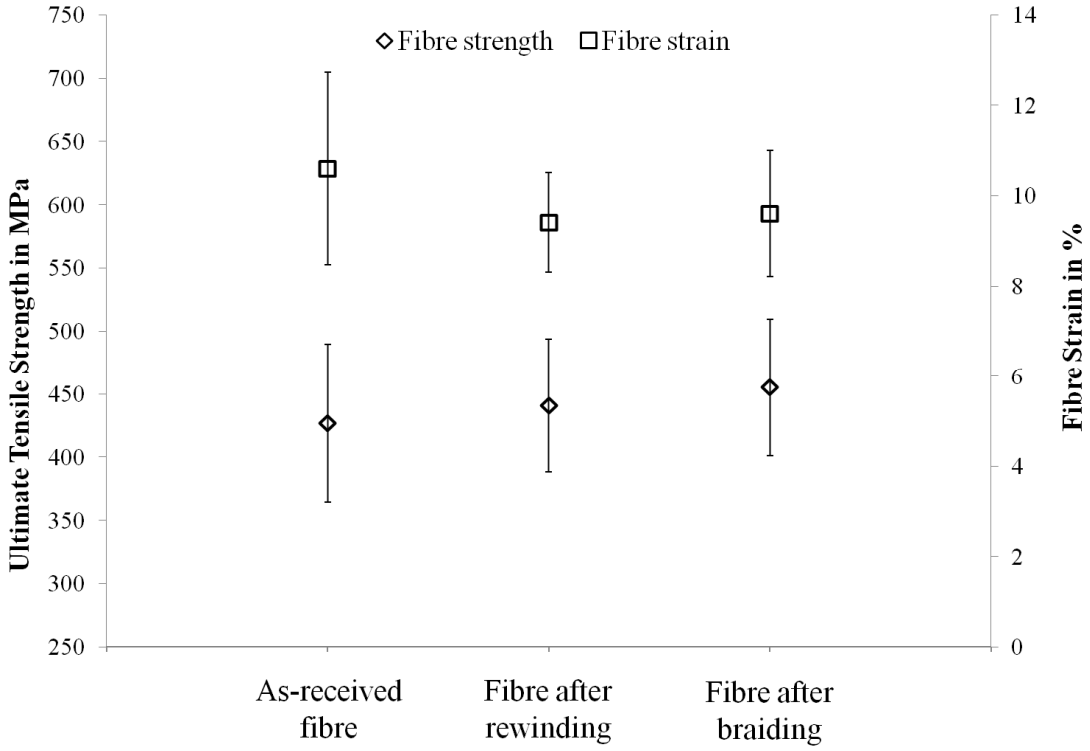

Figure 110: Ultimate tensile strength and strain of single fibres taken from the as-received yarn, after rewinding to a bobbin and after the braiding process. Shown are average values (n=30) with one standard deviation.

No statistically significant difference in the fibre strength was observed at any stage of the braiding process, showing that the 3D braiding process was sufficiently gentle on the rayon fibres and will not reduce the fibre strength under the selected conditions (Figure 110). However, there was a small, yet statistically significant, reduction in the strain to failure from 10.06 ± 2.13 % for the as-received rayon fibres to 9.41 ± 1.1 % and 9.61 ± 1.4 % after rewinding and braiding, respectively (Figure 110). No significant difference was found between strain to failure of the rewound and braided fibres.

Interestingly, the braiding process does not cause a reduction in the strength of rayon fibres although decreases have been reported for carbon fibre [423], glass fibres used in 2D braiding processes [424], and glass fibres used in 3D weaving [425]. It is proposed that the higher ductility of the rayon fibres is an important characteristic for the minimisation of fibre damage since damage readily occurs after braiding in more brittle carbon and glass fibres.

3.1.2 Braiding Angle

The measured braiding angles show a range from 17.17˚ to 23.81˚ (Figure 111). However, no statistical difference could be found due to the relatively large standard deviation. The variations in braiding angle are thought to be due to splicing processes that occur between the rayon yarns during braiding. Individual fibres are able to separate from the yarn since no-twist yarns were used.

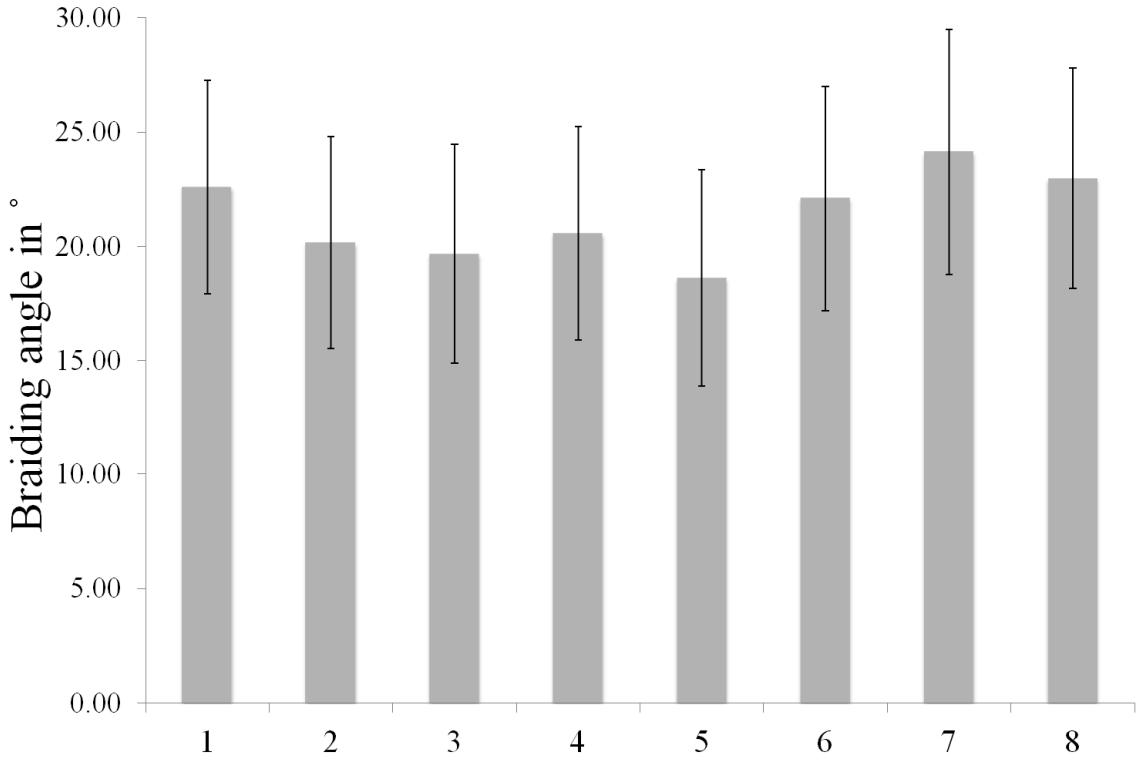

Figure 111: Average values of the measured braiding angle for 8 specimens taken from the 3D rectangular braid. Error bars indicate one standard deviation.

The moving yarn carriers with the attached horn gears will cause an interweaving of individual fibres just prior to the actual braiding point, creating small tensile forces on individual yarns that may influence the final braiding angle. The interweaving of single fibres creates a cobweb-like structure between the yarns (Figure 112).

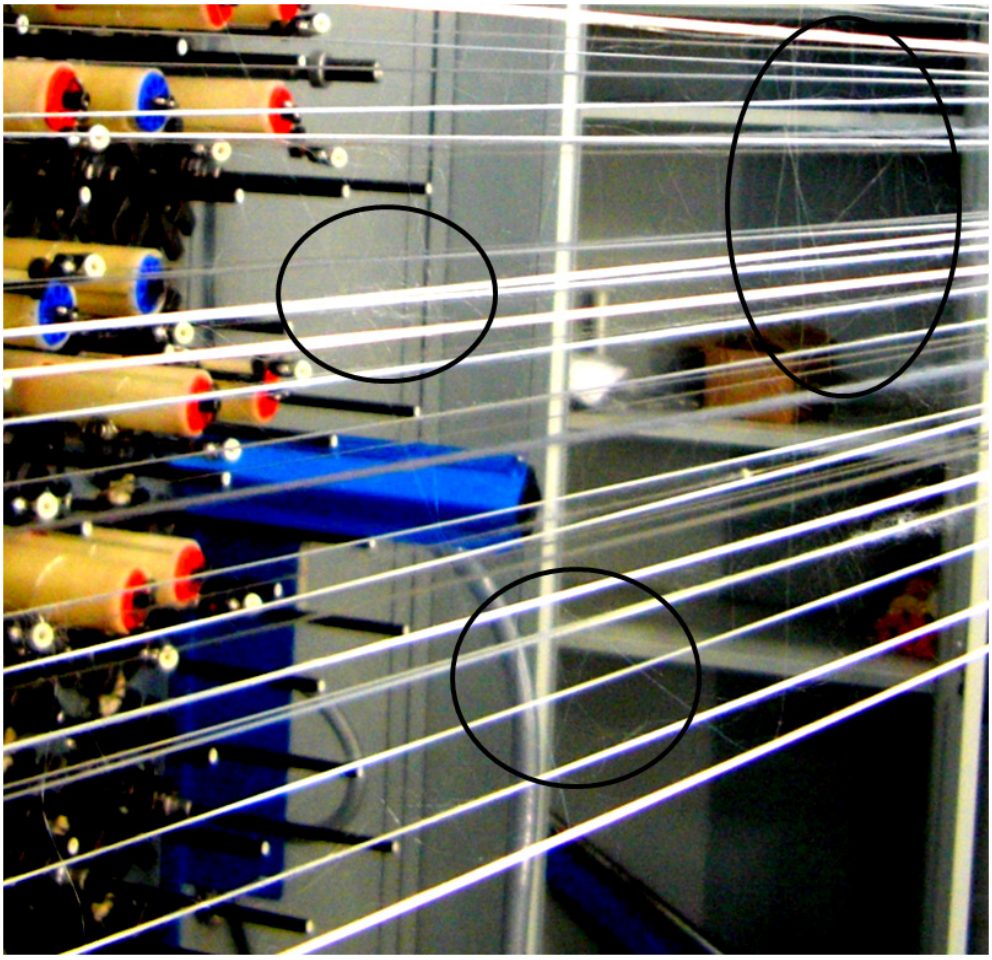

Figure 112: Photograph of single fibres that have separated from the rayon yarns. The single fibres are interwoven between the yarns, creating a cobweb-like structure that may change the overall braiding angle.

The braiding angle is an important characteristic since it determines the mechanical properties of the resulting composite [420]. In addition, the misplaced fibres could create voids during composite processing thereby lowering the overall properties.

3.2 ANALYSIS OF COMPOSITE PROCESSING

As shown earlier, shrinkage of the material often accompanies the regeneration and drying stages in the synthesis of ACCs. Lateral shrinkage and shrinkage through the thickness of the final ACC are mainly observed in the 3D braided rayon due to removal of voids within the braid due to the combination of compaction and cellulose dissolution. Shrinkage in the longitudinal direction was constrained by fixing of the specimen ends during processing. The average shrinkage in the width and thickness was approximately 19.5 % and 43 %, respectively.

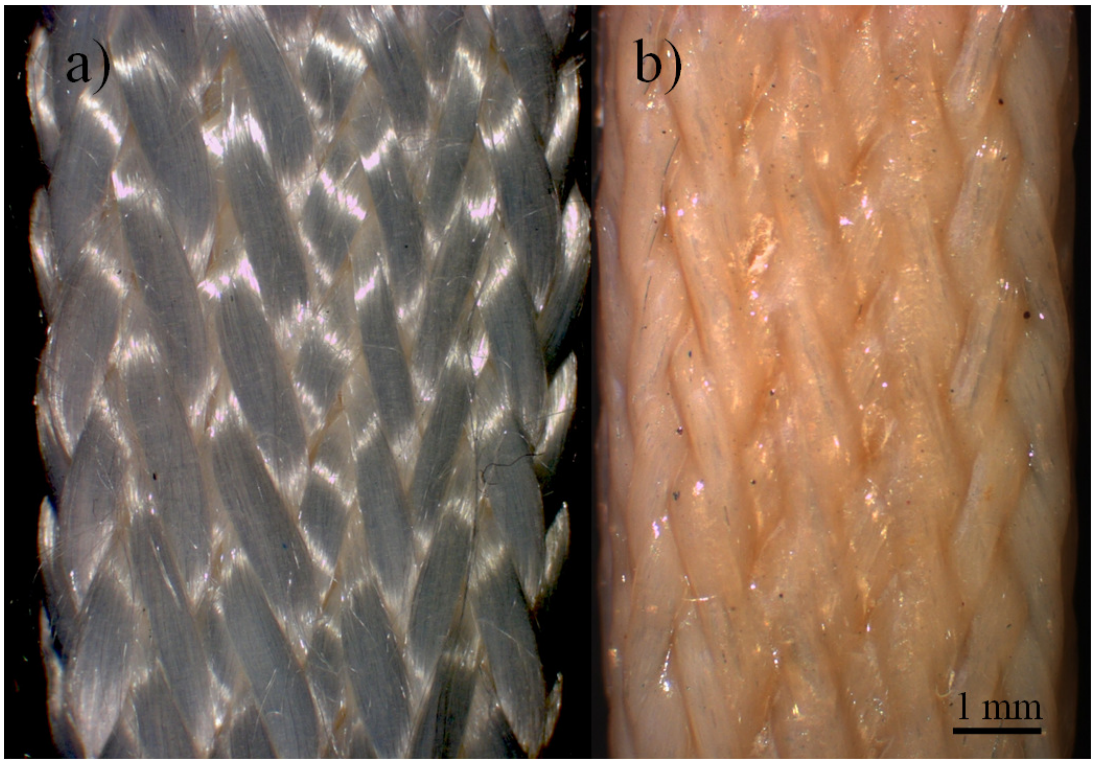

Figure 113: Photographs of the 3D rayon-based braid as-received (a) and following composites processing (b).

A very thin layer of transparent cellulose (~0.1 mm) was observed on the surface of the composite (Figure 113b) giving it a plastic-like appearance when compared with the as-received braid (Figure 113a). Figure 115-a shows a low magnification image of several

different yarns and their various orientations in the cross-section of the braid. Not all of the yarns were observed to neighbour each other closely, most likely a result of the aforementioned variations in the braiding angle. The separation of single fibres from the yarn is also observed (Figure 115-b) as are gaps between single fibres within a single yarn (Figure 115-c). In general, thorough compaction of the final composite was observed (Figure 115-d). However, some voids did persist that indicates the process may benefit from additional applied pressure (Figure 115-d). The appearance of inter-fibre cracking appears to be due to matrix cracking that probably occurs during drying due to difference in the swelling and drying behaviour of the rayon and regenerated matrix (Figure 115-e). Similar observations have been reported by Duchemin *et al.* [127]. Nevertheless, it can be clearly seen in Figure 115-f that the processing lead to small amounts of matrix phase, connecting the single fibres in the yarn. The used processing method results in a drastically increased void size compared to SIP Figure 114.

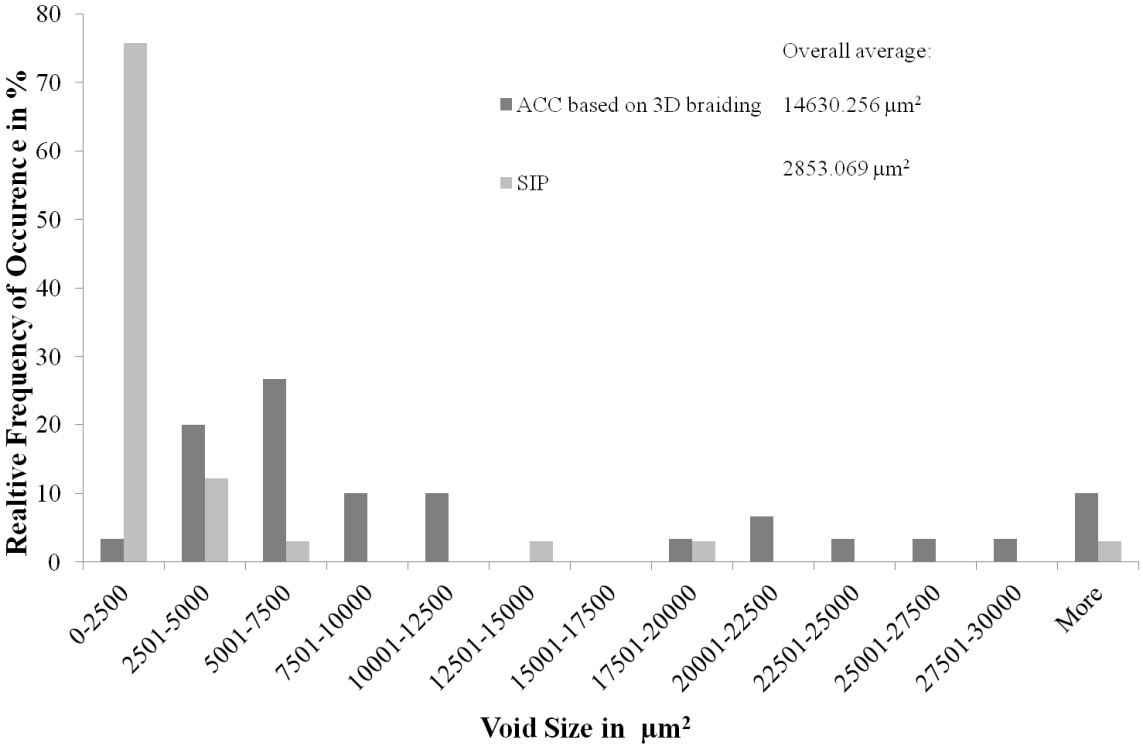

Figure 114: Relative distribution and overall average of void size in the produced ACCs based on 3D braidings compared to SIP.

The change in cross-sectional area is due to shrinkage caused by tension in the samples resulting in a realigning of the yarns in the braid, causing decrease in braiding angle of 17.25 % (**Figure 117**).

.

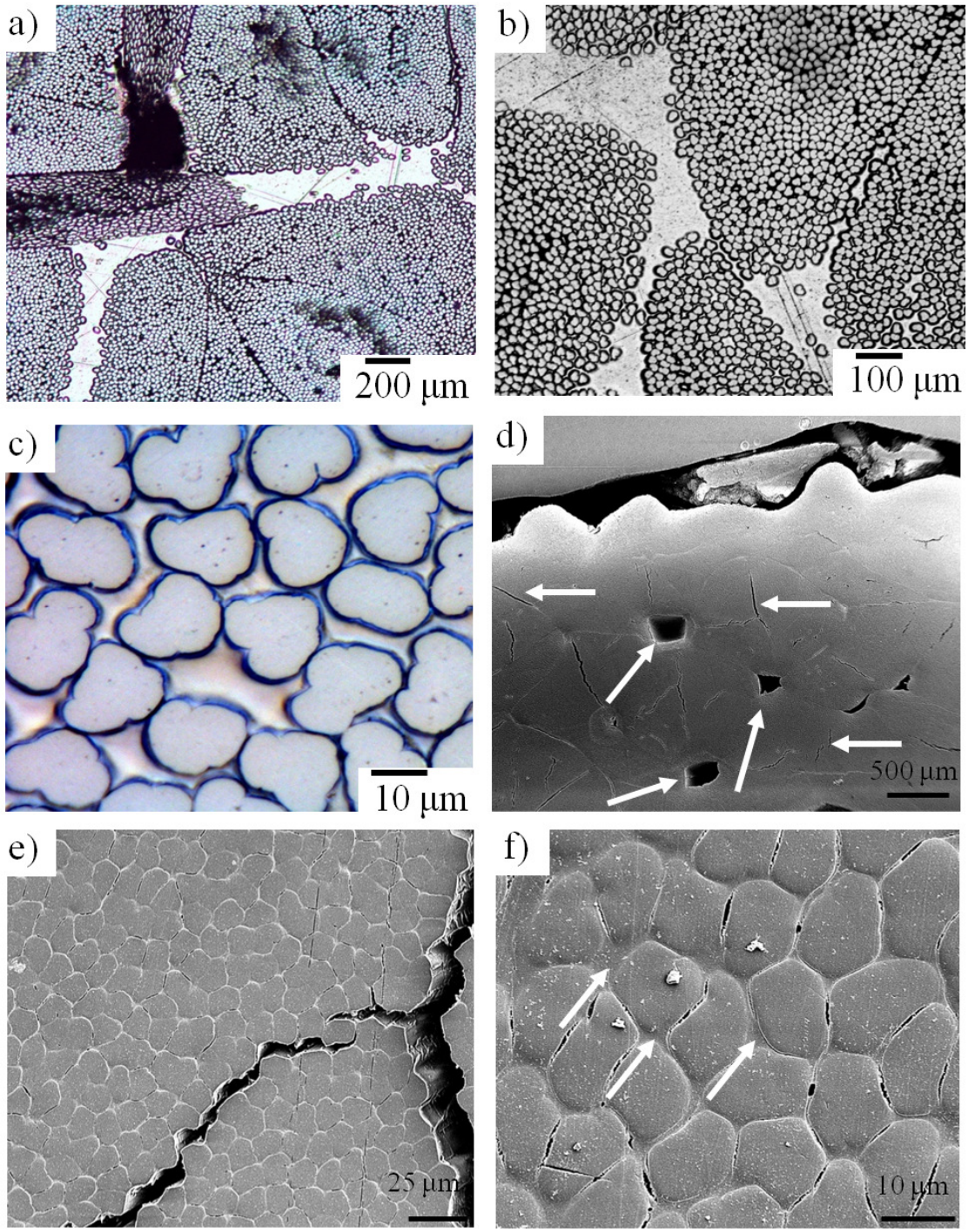

Figure 115: Cross-sectional views of the microstructure of the as-received braid (a-c) and final composite (d-f). Arrows mark large voids as well as cracks between single yarns in figure d. Areas of created matrix phase are pointed out in figure f. Figures a-c are reflected light micrographs, while d-f are scanning electron micrographs obtained with an acceleration voltage of 5 kV.

3.3 TENSILE PROPERTIES OF ACCs BASED ON 3D BRAIDS

The tested samples showed an increased UTS (143.56 MPa, Figure 116) compared to the ACC laminates prepared *via* SIP (107.28 MPa, Section VI.3.3.2, Figure 123: Mechanical Properties of an ACC made from a 3D-braid compared to an ACC made *via* SIP from 2D textiles.). For composites based on 3D-braidings this cannot necessarily expected as it was reported before that the UTS of 3D braided composite is lower than for their 2D counterparts with an equivalent mass fraction of in-plane fibres [411]. However the increase in UTS for ACCs could be the result of the improved delamination resistance of 3D-braids compared to 2D-wovens [411], preventing premature failure of the rayon fibres. Furthermore the exact amount of in-plane fibres couldn't be determined for the used 3D braids due to high variation in braiding angle present in produced the braids. Due to the twill weave structure of the woven used for SIP based composites, it could therefore be possible that higher mass fraction of in-plane fibres are present in the rayon braids contributing to the increased UTS.

There was a further decrease in the braiding angle of the ACC caused by tensile stress. A realignment of the yarns following tensile testing resulted in a decrease in braiding angle by 28.3% (Figure 117). Hence, the reorientation of the yarn appears to be an important contributor to the strain observed at σ_{max}. The rearranging of the yarns within the composite can be seen in the stress-strain plots of the tested samples (Figure 116). After an initial elastic region the slope of the stress-strain curve changes (~0.01 mm/mm strain). It is thinkable that after this point the created matrix phase begins to break and the yarns start to align themselves in the load direction until catastrophic failure occurs. Although composites based on 3D braided preforms are not widely discussed in the

scientific literature, the observed behaviour seems typical for 3D braided preforms. A similar behaviour was for example reported by Mei *et al.* for testing composites based on 3D braids of carbon fibre and a silicon carbide matrix [426] and by Promis *et al.* for E-glass 3D braids reinforcing a phosphate cement matrix [427].

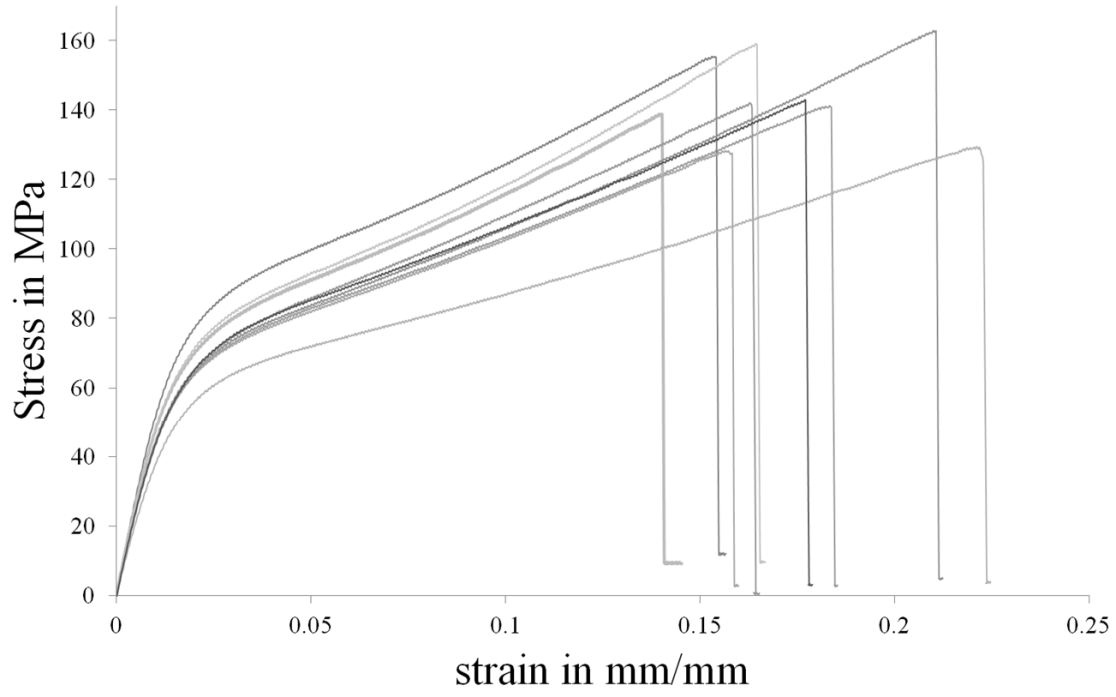

Average values		
Young's modulus in GPa	UTS in MPa	strain at σ_{max} in mm/mm
5.26 ± 0.43	143.56 ± 11.42	0.17 ± 0.03

Figure 116: Tensile stress as a function of strain of ACCs based on the 3D braid textile. Shown are the plots of all tested samples. The average Young's modulus (GPa), ultimate tensile strength (UTS)(MPa) and strain at UTS are also given (inset).

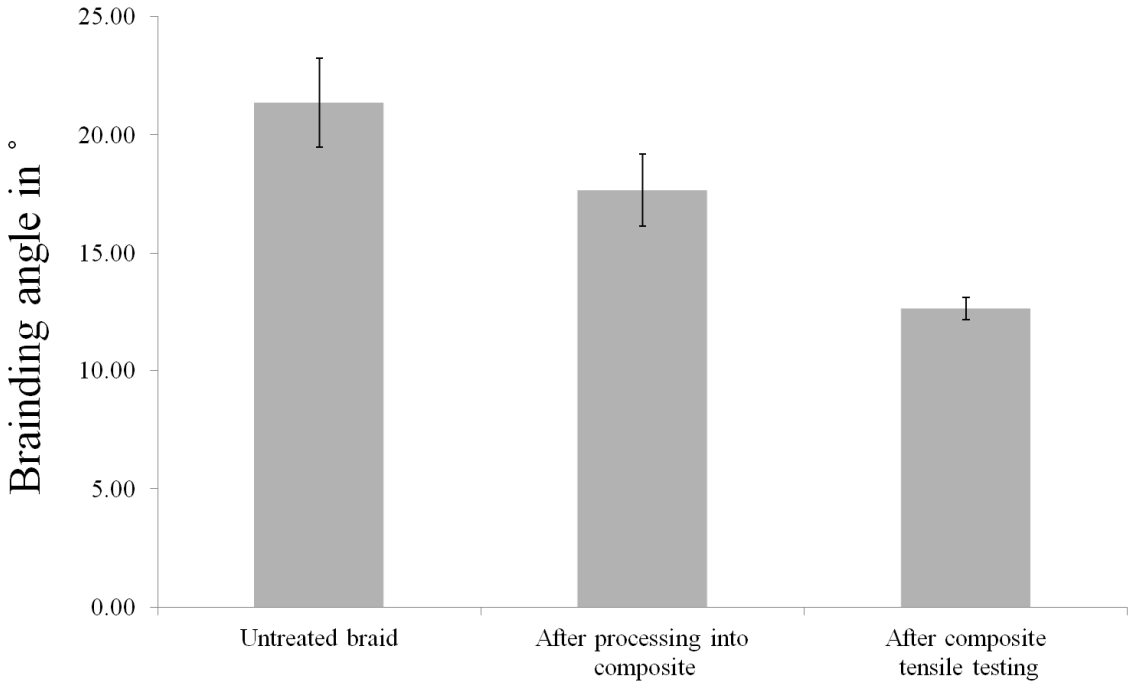

Figure 117: Average braiding angle of the as-received rayon braid, ACC and following tensile testing of the ACC. Error bars indicate one standard deviation.

Observations of the fracture surface following tensile testing indicate that some of the yarns remain intact and cracking appears to propagate along the inter-yarn boundary (Figure 118a). Some yarns exhibit bunches of fibres or individual fibres being pulled out from the yarn, perhaps indicating some variation in the fibre-matrix adhesion. Many of the single fibres still seem strongly attached to neighbouring fibres while some are completely separated (Figure 118b). The failure modes indicate large differences in fibre-matrix adhesion, most likely the result of the processing route. The applied method of simply soaking the braids in the solvent is likely to have caused an uneven distribution of the solvent in the sample and therefore different amounts of dissolved cellulose between the fibres. In combination with the observed variations in spacings between the single yarns (Figure 115b), this will likely lead to an uneven distribution of matrix phase in the composite. Consequently, this leads to an uneven load transfer during tensile testing causing stress concentration in matrix-free areas where fibres remain unbonded (Figure

118b) and follow-on failure. Additionally, the large voids created by non-contacting braids will act as a point of weakness contributing to premature failure (Figure 118b, Figure 115d, Figure 114).

At higher magnification is it possible to observe the detailed bonding behaviour between adjacent single fibres. For example, the three fibres in the upper part of Figure 118c are well bonded and it is difficult to distinguish an interface between them. However, a poor connection appears to occur with other fibres in the lower part of the micrograph. The observation of "peeled-off" surface structures are the only indication that the fibres were bonded at all (Figure 118c). The rough surfaces that are observed on the cross-section of the fibres (Figure 118c) hint at the internal structure of synthetic cellulose fibres that consist of many microfibrils [36].

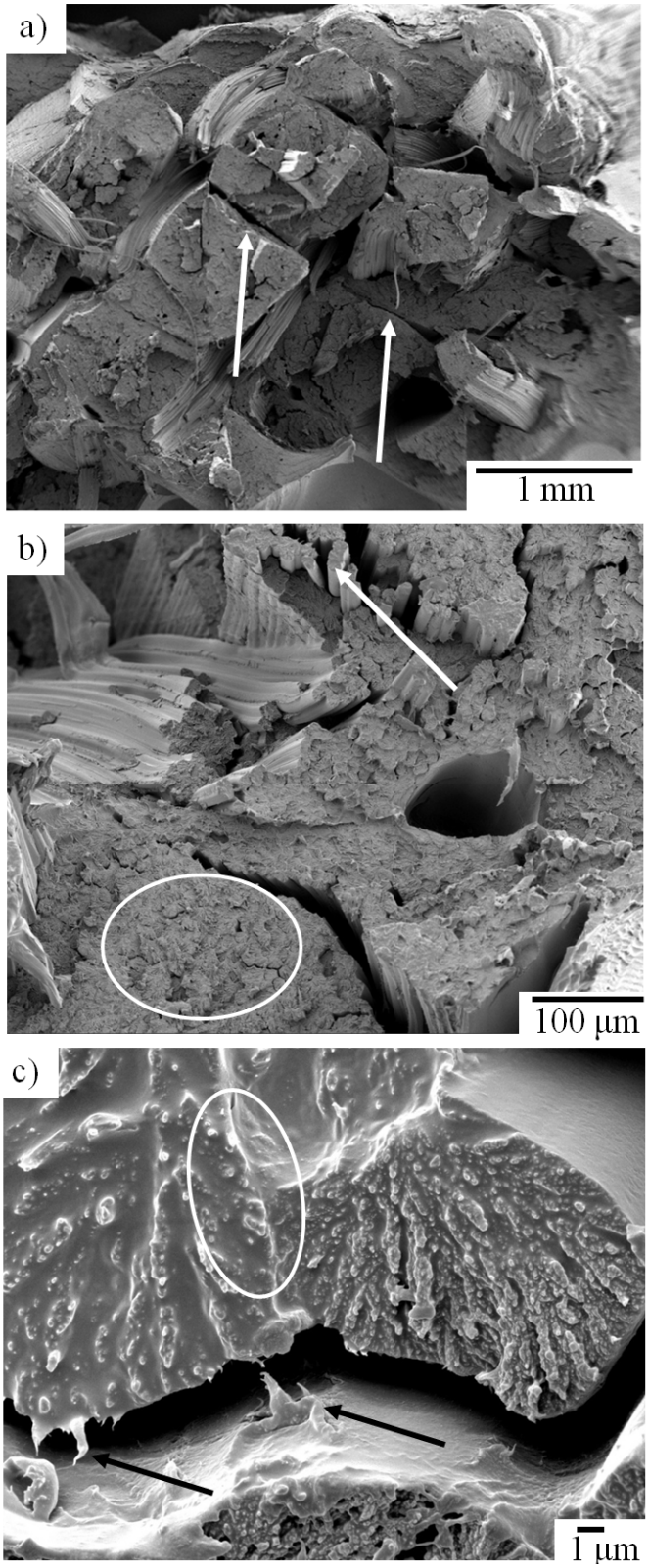

Figure 118: **Scanning electron micrographs of the fracture surface of an ACC following tensile testing. Shown is an overview of the fracture surface with inter-yarn cracking (a); several yarns showing closely bonded and separated fibres within a yarn (b); and (c) the interfacial region between 5 individual fibres. Both, an almost interfaceless bonding and peeled-off structures are visible. The micrographs were obtained using an accelerating voltage of 10 kV.**

A similar topography is observed on the surface of the tensile tested samples in the boundary region of a former yarn (Figure **119**). Therefore, it is likely that the microfibrils were formed during the regeneration of dissolved cellulose. Although a tensile load reorientates the yarns (Figure 111), the yarns remain bonded to each other (Figure **119**). It is possible the network of microfibrils play a role here in accommodating strains so as to maintain bonding between the yarns.

Another possible explanation for this fibrillar network could be the formation of an aerogel-like structure on the surface on the sample. As a result of the used soaking process, it is likely that more IL was present on the surface of the braid causing a stronger local dissolution of cellulose. Due to the high viscosity of the so-created cellulose-IL solution (see Chapter III) large areas of dissolved cellulose will have formed on the sample surface. Upon regeneration and drying, the water removal could have a partial collapse of this structure leaving a foam-like arrangement behind. A similar process is used for the processing of cellulose aerogels [428].

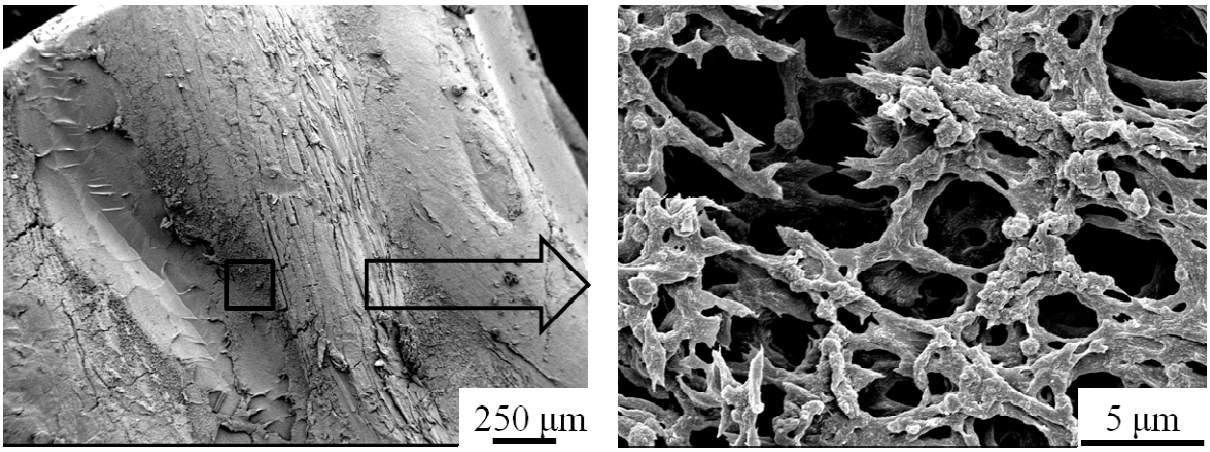

Figure 119: Scanning electron micrograph of the fracture surface of a tensile tested ACC (left). The inset region is shown at higher magnification (right) to highlight where microfibrils could be observed. The micrographs were obtained using an accelerating voltage of 10 kV.

3.4 FLEXURAL PROPERTIES OF ACCs BASED ON 3D BRAIDS

In all cases flexural testing was halted at a strain of ~0.2 since the samples reached the bottom of the sample fixture without failing. Therefore, reported strain values do not represent the strain to failure (**Figure 120)**. However, the average strain at σ_{max} is 0.07 (standard deviation = 0.004). The ACC composite exhibits a decrease in stress after reaching the maximum stress. Interestingly, the decrease in stress appears to occur in discreet steps. This may indicate a rearrangement of yarns in the composite in the direction of the applied in similar to the one observed in the tensile tested samples. Another possibility for such stepped deformation behaviour is that fibre bundles or yarns fail progressively within the composite that act to reduce the load bearing ability of the specimen as the flexural strain continues to increase.

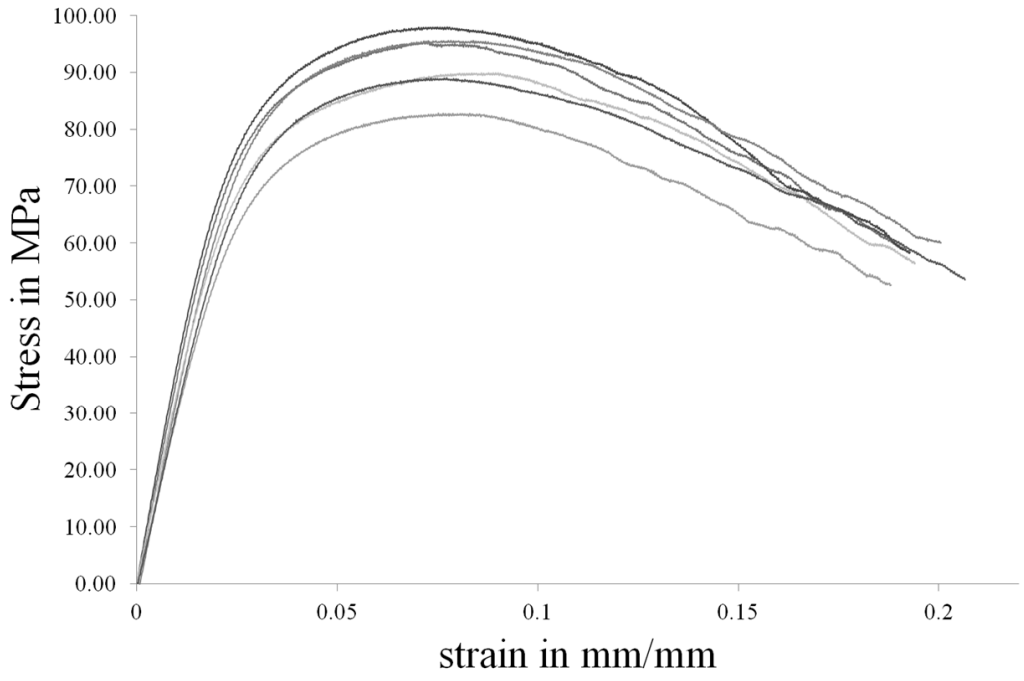

Average values		
Flexural modulus in GPa	Flexural strength in MPa	strain at σ_{max} in mm/mm
3.57 ± 0.46	91.43 ± 5.22	0.07 ± 0.00

Figure 120: Stress over strain plots of the tested samples and calculated average values for flexural modulus in GPa, flexural strength σ_f in MPa and strain at σ_{tmax} in mm/mm.

The yarns on the surface of the flexural specimen rearranged into an almost parallel orientation in the longitudinal direction, although no widespread damage is observed in the yarns (Figure 121a). Local damage is observed between the yarns within the matrix phase at the inter-yarn boundary, having a slightly crimped appearance (Figure 121b). A lamellae like structure of the film of regenerated cellulose can be seen Figure 121c that has also been reported by Duchemin *et al.* [127].

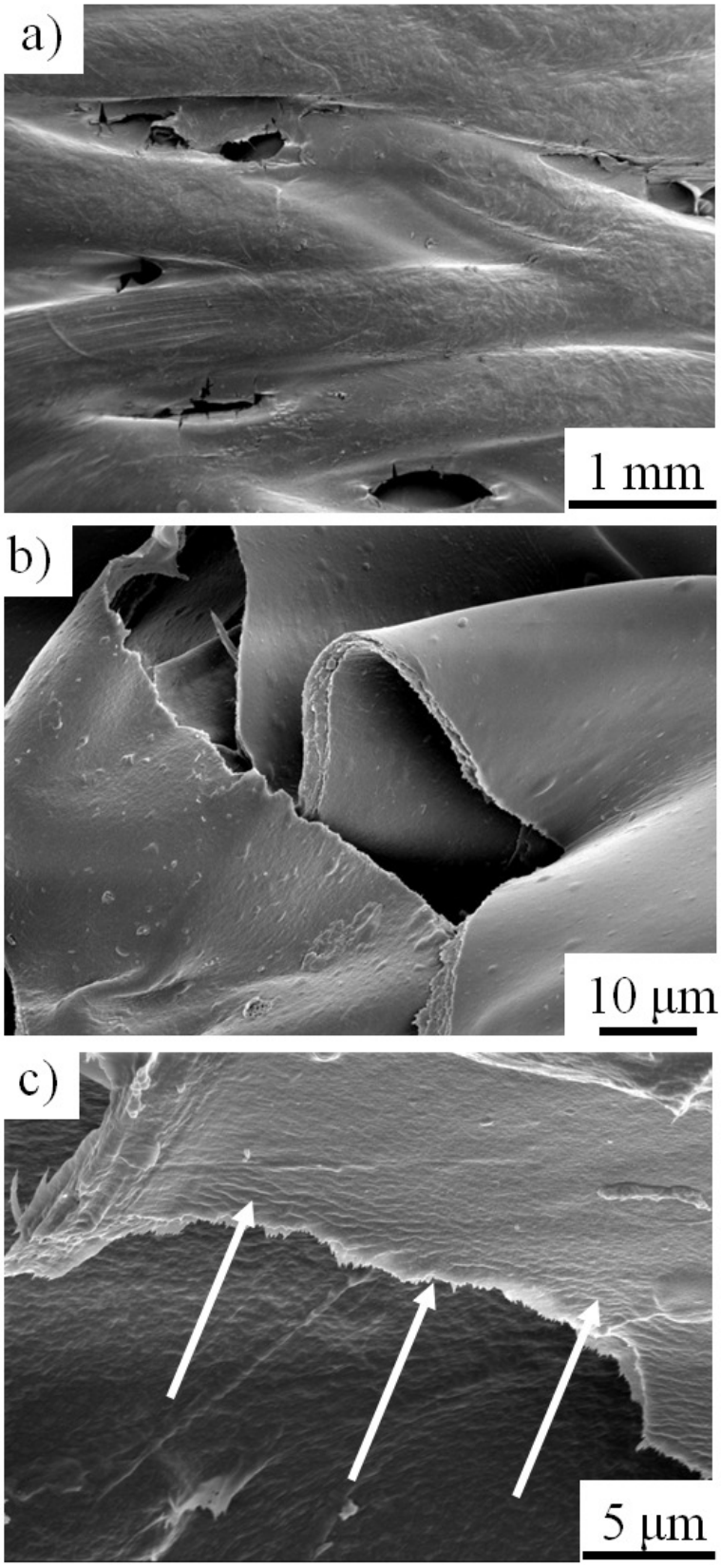

Figure 121: SEM micrographs of the (a) surface of an ACC specimen following flexural testing. Higher magnification shows the crimped matrix phase (b) and the lamellae structure of the matrix phase (c). An acceleration voltage of 5 kV was used to obtain the micrographs.

3.5 IMPACT PROPERTIES

The average unnotched Charpy impact strength of the ACC made from the 3D braid was 125.33 kJ/m^2 with a standard deviation of 13.66 kJ/m^2. All tested sample either showed partial or non-break behaviour (Figure 122). The 3D braid based composites show a clearly improved impact strength compared to the previously tested ACC laminates based on 2D-textiles (41.54 kJ/m^2, Section VI.3.3.1.2). The clear improvement in impact strength is expected for 3D-braided composites and can be explained by the complex yarn architecture and more flexible yarns, distributing a higher amount of stress throughout the sample [411]. Correspondingly, ACCs based 3D textile show an clearly superior impact strength to other jute fibre based biocomposites (31. 87 kJ/m^2 [240], 29 kJ/m^2 and 27 kJ/m^2 [349]) and especially all-plant composites (5.6 kJ/m^2,see Section I.3.2.2.2).

Strong improvements (~60%) are also reported for the step from 2D woven textiles to 3D woven textiles as shown for carbon–bismaleimide composite by Chou *et al.* [429]. The improvement can be explained by the presence of through-thickness binder yarns able to stop or at least slow the growth of delamination cracks during impact loading [429].

The improved impact behaviour of composites based on 3D textiles mainly depends on the presence of those through-thickness yarns [425] preventing delamination and allowing higher local shear stresses [430]. It is therefore assumed that the uneven solvent distribution has only minor effects on the Charpy impact properties of ACCs based on 3D braids.

Figure 122: Photographs of the ACC samples after Charpy impact testing.

3.6 ACC COMPARISON

It is instructive to compare the mechanical properties of the herein described ACCs based on 3D textiles with ACCs made *via* SIP using 2D textiles (Figure 123). The ACC based on the rayon textile with a 3D architecture exhibited superior mechanical properties apart from the flexural strength and stiffness. The 3D braid allows a mechanical interlocking of the fibre yarns significantly improving the interlaminar shear strength of the composites. It cannot be ruled out that the more complex yarn architecture contributes to the observed uneven solvent distribution.

The relatively low flexural strength of ACCs based on 3D braided textiles is likely to originate from the significant amounts of voids found to be present in the final microstructure (Figure 114). Optimisation of the processing route would minimise the void content and achieve better compaction so as to improve the mechanical properties of these ACCs. However, it can also be assumed that the introduced third dimension in fibre orientation reduces the fibre volume fraction, resulting in slightly lower in-plane properties compared to the SIP-based ACCs [417].

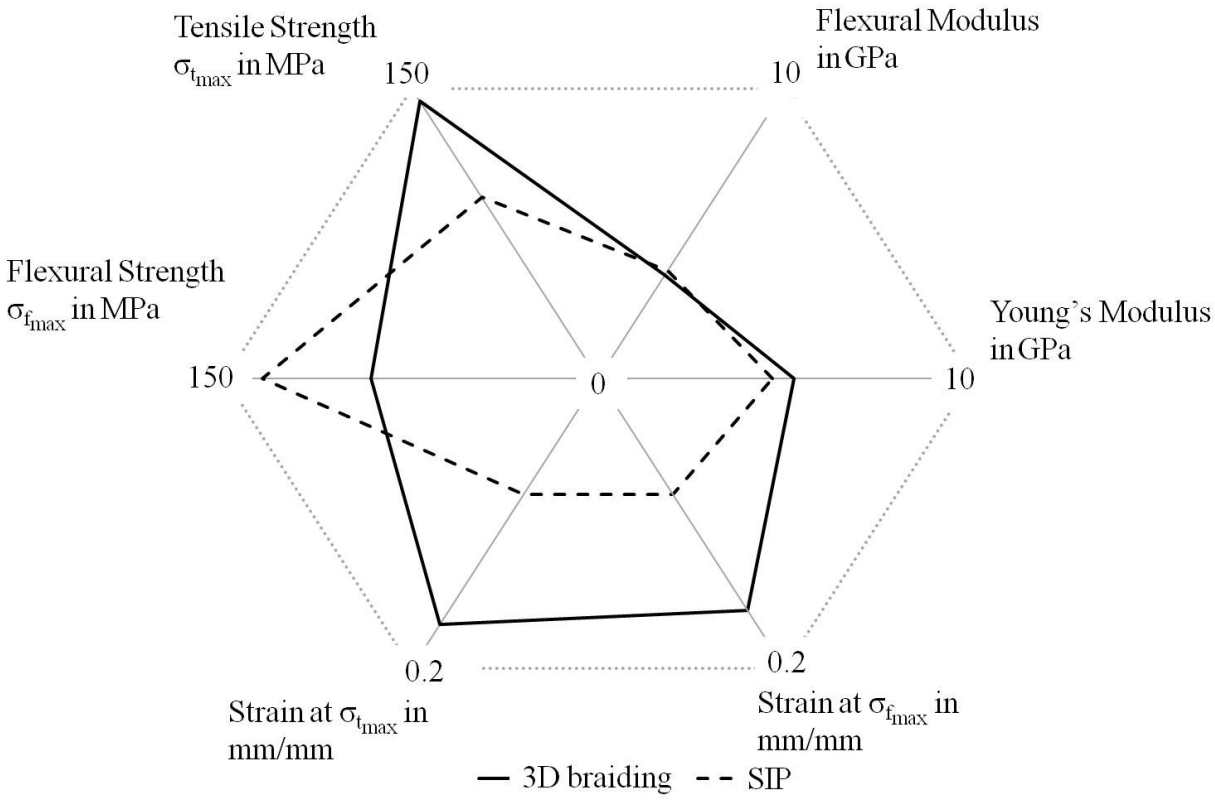

Figure 123: Mechanical Properties of an ACC made from a 3D-braid compared to an ACC made *via* SIP from 2D textiles.

4. CONCLUSIONS

It could be shown for the first time that the ITA-Herzog-3D rotary braiding process can be applied to synthetic cellulose fibres to create a rayon fibre preform having a 3D architecture. The resulting 3D braids are able to be converted into ACCs using a partial fibre surface dissolution approach wherein the solvent was applied to the textile by submersion. The resulting ACC exhibits a homogenous appearance, although larger voids were present in the microstructure. Void formation is thought to be a result of yarn splicing during the braiding process leading to non-constant braiding angles. Voids occurring between yarns cannot be completely filled by the created matrix phase leading to large voids within the composite. Additionally, the immersion in IL results in a non-uniform distribution of the solvent during processing causing local under-dissolution and

unbonded fibres. However, ACCs based on 3D braided textiles displayed improved mechanical properties over SIP-based ACC laminates. The improved mechanical efficiency is thought to be due to the mechanical interlocking in all three directions. Finally, it is arguable whether the improvement in mechanical properties is sufficient to justify the more complex processing steps involved in the production of the 3D braided preform.

IX. CONCLUSIONS AND OUTLOOK

1. CONCLUDING REMARKS

The excellent specific mechanical properties of the cellulose molecule seemingly appear to make cellulose an ideal raw material for a high performance, lightweight engineering materials. In spite of the promise of cellulose, exploiting the full properties of cellulose has proven to be difficult in the development of biocomposites. Based on the carried out work, all-cellulose composites can represent a crucial solution to existing problems of biocomposites especially the incompatibility of cellulosic fibre and non-cellulosic matrix phase. The characteristics of cellulose must be considered in the development of a process that allows the application of ACCs to real world applications. Due to its strong hydrogen bonding network, cellulose needs adequate solvents to be processed therefore demanding an adaption of common processes developed for thermoplastics and thermosets.

1.1 CELLULOSE DISSOLUTION IN IONIC LIQUIDS

Millions, if not trillions of different cation and anion combinations and possible IL blends allow for a distinct tailoring of the IL according to the selected process. The chosen IL, BmimAc, showed a high solvency compared to other solvent systems which combined with a possible recyclability makes this IL an attractive solvent for cellulosic raw materials.

The amount of dissolvable cellulose strongly depends on the cellulose source as shown by the studies of microcrystalline and rayon cellulose. More precisely the solvency depends on the DP and resulting interaction or entanglement of single cellulose chains in the IL. Cellulose chain entanglement also strongly influences the viscosity of the

cellulose-IL solution. The viscosity of the solution can be controlled by the applied temperature, yet care needs to be taken to not overheat the solution to avoid cellulose degradation. Over- or under dissolution of the cellulose will markedly reduce the properties of ACCs due to fibre damage or poor fibre-matrix bonding, respectively.

1.2 MOISTURE SENSITIVITY OF ACCS PROCESSED VIA COMPLETE DISSOLUTION

Microcrystalline cellulose was completely dissolved in BmimAc to create a liquid matrix phase. This phase can be combined with additional MCC or wood fibre to create a precursor for a cellulose-reinforced cellulose composite. This was achieved by pressing the precursor into flat films and regenerating the dissolved fraction in water. However, upon drying a separation between reinforcing and matrix could be observed on the microscopic level due to variations in water uptake and shrinkage behaviour between the regenerated cellulose, MCC and wood fibre. Overall, strong dimensional shrinkage could be observed for all so-produced composites. The processing of ACCs *via* a complete cellulose dissolution route can be suitable for the production of ACCs with an intimate bond between fibre and matrix but no to produce truly interfaceless ACCs.

1.3 ACCS PROCESSED VIA PARTIAL FIBRE DISSOLUTION FOR THE PRODUCTION OF "THICK" COMPOSITES

The concept of partial fibre surface dissolution allows for processing of multilayered, cellulose composites or composite laminates. This can be realized by using a very simple hand-layup approach to impregnate cellulosic textiles with the solvent. After dissolution at elevated temperatures, a regeneration of the dissolved fibre matrix results in a matrix formation *in situ.* This process allows for the easy production of thick laminate composites in 2D and simple 3D geometries.

However, care must be taken to achieve an even solvent distribution to create a homogeneous fibre-matrix interphase. Furthermore, it could be shown that the dissolution time needs to be chosen carefully according to the composition and structure of the fibres to achieve adequate amounts of dissolved cellulose for formation of the matrix phase. Compared with a flax fibre textile, regenerated cellulose fibres allowed for controlled dissolution conditions due to their uniformity of structure and quality compared to natural fibres.

The newly developed solvent infusion process conceptually based on VARTM and applying the principle of fibre surface dissolution, allows for an even solvent distribution, producing ACC laminates with an extremely high fibre volume fraction of up to 92%. In a similar manner to the hand layup approach, multilayered laminates were produced from cellulosic textiles up to at least 4.8 mm in thickness. An improved fibre-matrix interphase was created as a result of a more uniform distribution of the solvent. It could be established that applied pressure during the dissolution stage of the process is crucial to achieve good inter- and intralaminar adhesion. No dimensional shrinkage or warpage is observed since only small amounts of cellulose are dissolved and regenerated under the applied pressure. SIP is favoured over hand layup as the ACCs exhibited superior tensile properties. Using the high strength, high strain rayon fibre textiles for ACC processing does not only lead to good tensile properties but also to excellent flexural and impact properties, especially compared to other conventional bio- and green composites.

It could be shown that processing conditions during SIP are critical to the final composite properties. The type of regeneration and washing media selected will affect

the structure of the interphase that bonds the single fibres; it could be established that ethanol yields a more amorphous interphase, while water results in higher crystallinity. The interphase structure affects the tensile properties of the composite. Observations of the ACC cross-section revealed a matrix phase bonding single fibre together. However, the matrix phase has a different crystalline structure compared to the fibres according to results from both WAXD and solid-state NMR. Thus, it is confirmed that the ACC laminates cannot be classified as *interfaceless* composites as they possess a distinct fibre-matrix-interphase.

From a processing point of view, the drying conditions have a greater effect on the final ACC laminate properties if processed *via* complete cellulose dissolution. The use of ethanol causes less swelling of the composite during washing, while the alcohol evaporates more easily than water, resulting in less shrinkage induced stress within the interphase. On the contrary, washing the ACC laminate with water during the regeneration stage leads to greater swelling of the material. Rapid drying at elevated temperature will encourage shrinkage-induced fracture of the interphase between fibre and matrix, reducing the tensile properties of the laminate. However, the highly crystalline interphase stays intact when dried slowly at room temperature, resulting in the highest tensile properties observed for ACC laminates produced *via* SIP.

ACC laminates produced *via* SIP were showed to be readily degradable under active composting conditions compared to a rayon-PLA composite, providing a viable pathway to end-of-life disposal. A combination of different microorganisms is responsible for cellulose degradation and especially less crystalline regions (*i.e.* the matrix phase) are

prone to microbial attack. Correspondingly, ACC laminates require additives to avoid premature degradation in hot and humid conditions.

1.4 CLOSED MOULD PROCESSING OF ACCS

Closed mould processing (*i.e.* solvent transfer moulding) of ACCs was examined as a means to improve the surface finish and further improve the composite properties. However, the inflexibility of the moulds used in STM caused problems with the solvent exchange as the regeneration medium (*i.e.* water or alcohol) is prevented for freely entering the tightly filled mould. Furthermore, the applied pressure that is needed for improving the surface finish obstructs the infusion of the solvent, leading to an uneven flow of the solvent through the rayon textile preform. Consequently, the fibre volume fraction of the resulting composites falls short compared with the SIP counterparts. Alternative approaches to the mould design are required for closed mould processing of ACCs to comply with their unique requirements that differ significantly from the infusion of thermosetting resins.

1.5 ACCS BASED ON 3D-BRAIDED TEXTILES

A 3D braid was produced as a textile preform to further explore the (i) possibility of creating 3D textiles based on rayon fibre and (ii) effect of textile architecture on the mechanical properties of ACCs. It was established that rayon fibre was suitable for processing on a conventional braiding machine developed for carbon and glass fibres. The 3D braid could be easily converted into ACCs by submerging the preform in solvent to partially dissolve the surface of the fibres. The 3D composites exhibited large voids between individual yarns within the braid. In spite of this, a further increase in the tensile and impact strengths was achieved over ACCs based on 2D textiles. This is

primarily due to an increased through-thickness strength of the 3D braid compared to the 2D woven textiles.

2. FUTURE OUTLOOK

2.1 ACCS AS GREEN COMPOSITES

The industrial world will have to face major challenges in terms of polymer and composite development in the coming decades. Not only is the demand for crude oil rising due to rapid industrial growth in Asia and South America, but also are long maintained supply routes threatened by regional and global conflicts and increasing difficulties in accessing and exploiting new oil fields [431]. This will inevitably lead to increasing oil prices and therefore create the incentive to find sustainable, independent alternatives for crude oil based polymers. Furthermore, increasing oil prices will cause a rise of fuel prices making lightweight materials such as composites an attractive alternative to metals in especially the transportation sector [432].

Important steps have been undertaken in the present study to make ACCs a true alternative to conventional biocomposites. Due to an increasing demand for lightweight, strong and petroleum-free materials, ACCs will have the potential to become an important class of materials in the longer term future. However, as a result of the novelty of ACC research in general and especially in terms of their industrial adaptability, a large amount of work will be necessary to establish a first ACC application. Theoretical models are still required for the prediction of ACC quality and selection of processing parameters.

Although the price of ILs is expected to decrease in the foreseeable future, they still are considerably more expensive than many other solvent systems for cellulose [227].

Nonetheless they should still be considered as a solvent system at industrial scales as they are easy to handle and could be potentially recycled [228]. Furthermore, it is likely that a higher dissolution capacity than the reported herein can be achieved by newly developed ILs in the future, further increasing their effectiveness. Additionally, due to their versatile character it is likely that ILs will be developed for the selective dissolution of non-cellulosic components in natural fibres to improve the properties of natural fibre as high quality precursors for ACCs.

2.2 SELECTION OF RAW MATERIALS FOR ACCS

Commercially-produced regenerated cellulose fibres such as rayon are shown to be well suited to the production of ACCs. However, the industrial processing of ACCs should be extended to the use of natural fibres as they usually provide a cheaper and greener source of cellulose that inherently have higher strengths and stiffnesses. Natural fibres offer a source of raw material that requires less energy or chemical treatment in their processing and should therefore improve the overall carbon dioxide balance of ACCs [13]. However, a full life cycle assessment is still needed to confirm the ecofriendliness of ACCs. Using natural fibres instead of regenerated cellulose does offer the advantage of stronger and stiffer fibres compared to rayon and Lyocell. However, providing natural fibres of constant quality, especially on industrial scale, remains a challenge for fibre producers due to variations in climatic and harvesting conditions. Variations in fibre diameters and cellulose content are important since these will require a process that is either widely adaptable to the dissolution of different batches of natural fibres or manipulation of the process to suit the fibres being utilised.

2.3 ENVIRONMETAL RESISTANCE OF ACCS

One of the challenges of ACCs is their strong hydrophilicity and resulting moisture uptake. The development of low-cost, ecofriendly post-processing treatments are required to reduce the moisture uptake of ACCs. Coatings, surface treatments and/or derivatisation of the surface cellulose are possibilities for improving the environmental resistance.

Additives to reduce the composite flammability and decrease the speed of biodegradability could be beneficial to increase the application potential. However, a way to integrate those additives into the ACC processing needs to be developed that does not affect the cellulose dissolution or reduce the composite properties. On the other hand, ease of biodegradation and/or incineration are distinct advantages for the end-of-life disposal of ACCs.

2.4 IMPROVEMENTS IN ACC PROCESSING

A deeper understanding of the regeneration process of the dissolved portion of the cellulose and possible interactions with the surrounding undissolved cellulose is still necessary. A detailed understanding of the formation of the interphase would be advantageous to further increase the composite properties through improvements to the interfacial properties. Variations in the regeneration media and mixtures thereof, dissolution temperature and dissolution time will affect the structure of the interphase although a detailed picture requires further research.

The developed hand layup process and SIP both allow the manufacture of thick 2D structures and simple three-dimensional shapes. While this work represents notable progress in the field of ACCs, methods for the manufacturing of complex 3D components needs to be addressed in future work. Ideally, an adaptation for closed mould

processing can be developed so that ACCs might be manufactured using RTM, injection moulding or other extrusion based processes. Furthermore, processing simulation tools should be developed that allow the calculation of ideal inlet and vent positioning and solvent distribution to ensure uniform partial dissolution of the fibres. It will be important to design processes that eliminate strong dimensional shrinkage or at least result in controllable, homogenous shrinkage behaviour.

2.5 APPLICATION POTENTIAL

ACCs require easily adaptable processing routes and low processing costs to compete with conventional polymers and composite materials. A possible application of ACCs is in the sports equipment industry. Rayon-based ACCs exhibit good tensile properties and impressive impact and flexural properties, making them strong, tough and lightweight materials suitable for many applications in the sporting sector. Examples of a shin pad and skateboard deck fabricated *via* SIP illustrate the concept. While the sports sector is a smaller application sector for composites than the transportation sector it still represents an attractive field as it is highly innovative and offers larger margins in terms of processing and material costs than for example the automotive sector.

The preliminary work carried out with 3D textiles showed a clear improvement in composite properties and also allowed the production of true three-dimensional composites. However, the production of those textiles will increase the processing costs drastically. Moreover, process optimisation is required to avoid void formation in such 3D structures. Similar to composites made from preforms based on glass, carbon or petrochemical based polymer fibres, applications would only be feasible in a high-tech sector such as the biomedical or space-and aircraft industry. However, the moisture

sensitivity and flammability of the ACCs require further process development to be applicable to the special conditions of such applications.

REFERENCES

[1] Mohanty, A., M. Misra, and L. Drzal: Sustainable bio-composites from renewable resources: opportunities and challenges in the green materials world. Journal of Polymers and the Environment, **10** (1) 19-26 (2002).

[2] Jacob John, M. and S. Thomas: Review: Biofibres and biocomposites. Carbohydrate Polymers, **71** 343-364 (2008).

[3] Gray, D.: Polypropylene transcrystallization at the surface of cellulose fibers. Journal of Polymer Science: Polymer Letters Edition, **12** (9) 509-515 (1974).

[4] McAllister, D.H., P. Pearson, and H. Wells. Potential of Cellulosic Fibres as Reinforcement for Reinforced Plastics. in Proceedings of the Reinforced Plastics Congress. Brighton, UK3-6 (1982).

[5] Kanari, N., J.L. Pineau, and S. Shallari: End-of-life vehicle recycling in the European Union. JOM Journal of the Minerals, Metals and Materials Society, **55** (8) 15-19 (2003).

[6] Zervas, E. and C. Lazarou: Influence of European passenger cars weight to exhaust CO2 emissions. Energy Policy, **36** (1) 248-257 (2008).

[7] Bledzki, A.K. and J. Gassan: Composites reinforced with cellulose based fibres. Progress in Polymer Science, **24** (2) 221-274 (1999).

[8] Eichhorn, S.J., C.A. Baillie, N. Zafeiropoulos, L.Y. Mwaikambo, M.P. Ansell, A. Dufresne, K.M. Entwistle, P.J. Herrera-Franco, G.C. Escamilla, L. Groom, M. Hughes, C. Hill, T.G. Rials, and P.M. Wild: Review Current international research into cellulosic fibres and composites. Journal of Materials Science, **36** (9) 2107-2131 (2001).

[9] Saheb, D.N. and J.P. Jog: Natural Fiber Polymer Composites: A Review. Advances in Polymer Technology, **18** 351-363 (1999).

[10] Wambua, P., J. Ivens, and I. Verpoest: Natural fibres: can they replace glass in fibre reinforced plastics? Composites Science and Technology, **63** 1259-1264 (2003).

[11] Anandjiwala, R.D. and S. Blouw. Composites from Bast Fibres - Prospects and Potential in the Changing Market Environment. in Proceedings of the FAO Global Workshop: Bast Fibrous Plants for Healthy Life. Banja Luka, Bosnia-Herzegovina(2004).

[12] Bodros, E., I. Pillin, N. Montrelay, and C. Baley: Could biopolymers reinforced by randomly scattered flax fibre be used in structural applications? Composites Science and Technology, **67** 462-470 (2007).

[13] Carus, M., C. Gahle, C. Pendarovski, D. Vogt, S. Ortmann, F. Grotenhermen, T. Breuer, and C. Schmidt, Studie zur Markt- und Konkurrenzsituation bei Naturfasern und Naturfaserwerkstoffen (Deutschland und EU), nova-Institut, Editor. 2008, Fachagentur Nachwachsende Rohstoffe (FNR): Gülzow, Germany.

[14] Karus, M. and M. Kaup: Natural Fibres in the European Automotive Industry. Journal of the International Hemp Association, **7** (1) 119-131 (2002).

[15] Karus, M., S. Ortmann, and D. Vogt: Naturfasern im Automobil: Innen alles Natur? Kunststoffe, **7** 51-53 (2005).

[16] Elliot-Sink, S. Special report: cars made of plants? Online news release. 2005.

[17] Shen, L. and M.K. Patel: Life cycle assessment of polysaccharide materials: a review. Journal of Polyimers and the Environment, **16** (2) 154-167 (2008).

[18] Joshi, S.V., L. Drzal, A. Mohanty, and S. Arora: Are natural fiber composites environmentally superior to glass fiber reinforced composites? Composites Part A: Applied Science and Manufacturing, **35** (3) 371-376 (2004).

[19] Cheung, H.Y., K.T. Lau, X.M. Tao, and D. Hui: A Potential material for tissue engineering: silkworm silk/pla biocomposite. Composites Part B, **39** (6) 1026-1033 (2008).

[20] Czaja, W.K., D.J. Young, M. Kawecki, and R.M. Brown: The Future Prospects of Microbial Cellulose in Biomedical Applications. Biomacromolecules, **8** (1) 1-12 (2007).

[21] Habibi, Y. and A. Dufresne: Highly Filled Bionanocomposites from Functionalized Polysaccharide Nanocrystals. Biomacromolecules, **9** (7) 1974-1980 (2008).

[22] Hong, L., Y.L. Wang, S.R. Jia, Y. Huang, C. Gao, and Y.Z. Wan: Hydroxyapatite/bacterial cellulose composites synthesized via a biomimetic route. Materials Letters, **60** (13-14) 1710-1713 (2006).

[23] Müssig, J., M. Schmehl, H.B. Von Buttlar, and U. Schönfeld: SMC-Werkstoff aus Naturfasern und Pflanzenölharz - Entwicklung eines Karosseriebauteils auf Basis Nachwachsender Rohstoffe. Kunststoffe, **96** (2006).

[24] Bledzki, A.K., V. Sperber, and O. Faruk: Natural and wood fibre reinforcement in polymers. Rapra Technology Ltd. Shawbury, UK(2002).

[25] Bos, H., The Potential of Flax Fibres as Reinforcement for Composite Materials. 2004, Technische Universität Eindhoven: Eindhoven.

[26] Fowler, P.A., J.M. Hughes, and R.M. Elias: Review Biocomposites: technology, environmental credentials and market forces. Journal of the Science of the Food and Agriculture, **86** (12) 1781–1789 (2006).

[27] Gassan, J. and A.K. Bledzki: Möglichkeiten zur Kontrolle der Festigkeit und Impactzähigkeit in naturfaserverstärkten Kunststoffen. Die Angewandte Makromolekulare Chemie, **272** 17-23 (1999).

[28] Oksman, K., L. Wallstrom, L.A. Berglund, and R.D. Toledo: Morphology and mechanical properties of unidirectional sisal-epoxy composites. Journal of Applied Polymer Science, **84** (13) 2358-2365 (2002).

[29] Wollerdorfer, M. and H. Bader: Influence of natural fibres on the mechanical properties of biodegradable polymers. Industrial Crops and Products, **8** (2) 105-112 (1998).

[30] Müssig, J.: Untersuchung der Eignung heimischer Pflanzenfasern für die Herstellung von naturfaserverstärkten Duroplasten - vom Anbau zum Verbundwerkstoff. VDI Verlag GmbH. Düsseldorf, Germany(2001).

[31] Keller, A., M. Leupin, V. Mediavilla, and E. Wintermantel: Influence of the growth stage of industrial hemp on chemical and physical properties of the fibres. Industrial Crops and Products, **13** (1) 35-48 (2001).

[32] Müssig, J. and E. Baur. Naturfaserverstärkte Kunststoffe: Entwicklung und Anwendung. in BIO-raffinieret III - Von der Vision zur Machbarkeit(2006).

[33] Müssig, J., G. Cescutti, and H. Fischer: Le management de la qualité appliqué à l'emploi des fibres naturelles dans l'industrie. in Le chanvre industriel - production et utilisations(eds.: Editor^Editors), GROUPE FRANCE AGRICOLE (Editions France Agricole): Paris, France **1** 235-269(2006).

[34] Bledzki, A.K., A. Jasziewicz, M. Murr, V.E. Sperber, R. Luetzkendorf, and T. Reussmann: Processing techniques for natural- and wood-fibre composites. in Properties and performance of natural-fibre composites(eds.: Editor^Editors), Woodhead Publishing Limited: Cambridge, England **1** 163-192(2008).

[35] Woodings, C.: Regenerated cellulose fibres. Woodhead Publishing Ltd. Boca Ranton,FL, USA(2001).

[36] Bredereck, K. and F. Hermanutz: Man–made cellulosics. Review of Progress in Coloration and Related Topics, **35** (1) 59-75 (2005).

[37] Shen, L. and M.K. Patel: Life cycle assessment of man-made cellulose fibres. Lenzinger Berichte, **88** 1-59 (2010).

[38] Mohanty, A.K., M. Misra, and G. Hinrichsen: Biofibres, biodegradable polymers and biocomposites: An overview. Macromolecular Materials and Engineering, **276/277** (1) 1-24 (2000).

[39] Jacob, M., S. Joseph, L. Pothan, and S. Thomas: A study of advances in characterization of interfaces and fiber surfaces in lignocellulosic fiber-reinforced composites. Composite Interfaces, **12** (1) 95-124 (2005).

[40] Biagotti, Puglia, and Kenny: A Review on Natural Fibre-Based Composites – Part I: Structure, Processing and Properties of Vegetable Fibres. Journal of Natural Fibers, **1** 32 (2004).

[41] Bismarck, A. and A.B. y Jimenez. Truly Green Composites: Fibre, Polymer & Interface Characterisation. in Biobased/Green Materials and Processing Technology - The Annual Meeting. Cincinnati, USA(2005).

[42] Akin, D.E.: Chemistry of Plant Fibres. in Industrial Applications of Natural Fibres Structure, Properties and Technical Applications(eds.: Editor^Editors), John Wiley & Sons Ltd: Chichester, UK(2010).

[43] Thielemans W. and Wool R.P.: Kraft Lignin as Fiber Treatment for Natural Fiber-Reinforced Composites. Polymer Composites, **26** (5) 695-705 (2005).

[44] Röder, T., J. Moosbauer, G. Kliba, S. Schlader, G. Zuckerstätter, and H. Sixta: Comparative Characterisation of Man-Made Regenerated Cellulose Fibres. Lenzinger Berichte, **87** 98-105 (2009).

[45] Purz, H.J., H.P. Fink, and H. Graf: Zur Struktur cellulosischer Naturfasern Teil 1: Struktur von Bastfasern und deren Veränderung infolge Beuche und Mercerisierung mittels Licht- und Elektronenmikroskopie. Das Papier, **52** (6) 315-324 (1998).

[46] Fink, H., P. Weigel, H. Purz, and J. Ganster: Structure formation of regenerated cellulose materials from NMMO-solutions. Progress in Polymer Science, **26** (9) 1473-1524 (2001).

[47] Charlet, K., J.P. Jernot, J. Breard, and M. Gomina: Scattering of morphological and mechanical properties of flax fibres. Industrial Crops and Products, **32** (3) 220-224 (2010).

[48] Eichhorn, S.J., Baillie C A, Zafeiropoulos N, Mwaikambo L Y, Ansell M P, Dufresne A, Entwistle K M, Herrera-Franco P J, Escamilla G C, Groom L, Hughes M, Hill C, Rials T G, and Wild P M: Review: Current international research into cellulosic fibres and composites. Journal of Material Science, **36** (9) 2107-2131 (2001).

[49] Adusumali, R.-B., M. Reifferscheid, H. Weber, T. Roeder, H. Sixta, and W. Gindl: Mechanical Properties of Regenerated Cellulose Fibres for Composites. Macromolecular Symposia, **244** 119-125 (2006).

[50] Sfiligoj Smole, M., Z. Peršin, T. Kreže, K. Stana Kleinschek, V. Ribitsch, and S. Neumayer: X-ray study of pre-treated regenerated cellulose fibres. Material Research Innovation, **7** (5) 275-282 (2003).

[51] Goda, K. and Y. Cao: Research and Development of Fully Green Composites Reinforced with Natural Fibers. Journal of Solid Mechanics and Materials Engineering, **1** (9) 1073-1084 (2007).

[52] La Mantia, F. and M. Morreale: Green composites: A brief review. Composites Part A: Applied Science and Manufacturing, **42** (6) 579-588 (2011).

[53] Satyanarayana, K.G., G.G.C. Arizaga, and F. Wypych: Biodegradable composites based on lignocellulosic fibers—An overview. Progress in Polymer Science, **34** (9) 982-1021 (2009).

[54] Avérous, L. and P.J. Halley: Biocomposites based on plasticized starch. Biofuels, Bioproducts and Biorefining, **3** (3) 329-343 (2009).

[55] Pouteau, C., S. Baumberger, B. Cathala, and P. Dole: Lignin–polymer blends: evaluation of compatibility by image analysis. Comptes Rendu Biologies, **327** (9-10) 935-943 (2004).

[56] Breitel, J., M. Sommer, R. Schledjewski, and P. Mitschang. Plastifizierpressen naturfaserverstärkter Thermoplaste. Plastifying presses for natural fiber reinforced thermoplastics. in 4th International Wood and Natural Fibre Composites Symposium. Kassel, Germany(2002).

[57] Garlotta, D.: A Literature Review of Poly(Lactic Acid). Journal of Polymers and the Environment, **9** (11) 63-84 (2001).

[58] Flieger, M., M. Kantorova, A. Prell, T. Rezanka, and J. Votruba: Biodegradable Plastics from Renewable Ressources. Folia Microbiologica, **48** (1) 27-44 (2003).

[59] Inoue, K., S. Serizawa, M. Yamashiro, and M. Iji. Highly Functional Bioplastics (PLA compounds) Used for Electronic Products. in 6th International Conference on Polymers and Adhesives in Microelectronics and Photonics. Tokyo, Japan73-76 (2007).

[60] Graupner, N.: Improvement of the Mechanical Properties of Biodegradable Hemp Fiber Reinforced Poly (lactic acid)(PLA) Composites by the Admixture of Man-made Cellulose Fibers. Journal of Composite Materials, **43** (6) 689 (2009).

[61] Lee, S.H. and S. Wang: Biodegradable polymers/bamboo fiber biocomposite with bio-based coupling agent. Composites: Part A, **37** 80-91 (2006).

[62] Suryanegara, L., A.N. Nakagaito, and H. Yano: The effect of crystallization of PLA on the thermal and mechanical properties of microfibrillated cellulose-reinforced PLA composites. Composites Science and Technology, **69** (7-8) 1187-1192 (2009).

[63] Huber, T., J. Müssig, O. Curnow, S. Pang, S. Bickerton, and M. Staiger: A critical review of all-cellulose composites. Journal of Materials Science, **47** (3) 1171-1186 (2012).

[64] van Voorn, B., H.H.G. Smit, R.J. Sinke, and B. de Klerk: Natural fibre reinforced sheet moulding compound. Composites Part A, **32** (9) 1271-1279 (2001).

[65] De Bruijn, J.: Natural fibre mat thermoplastic products from a processor's point of view. Applied Composite Materials, **7** (5) 415-420 (2000).

[66] Riedel, U. and J. Nickel: Konstruktionswerkstoffe aus nachwachsenden Rohstoffen (BioVerbunde). Structural materials from renewable resources (Biocomposites). Materialwissenschaft und Werkstofftechnik, **32** (5) 493-498 (2001).

[67] Romhany, G., J. Karger-Kocsis, and T. Czigany: Tensile fracture and failure behavior of thermoplastic starch with unidirectional and cross-ply flax fiber reinforcements. Macromolecular Materials and Engineering, **288** (9) 699-707 (2003).

[68] Huber, T. and J. Müssig: Fibre matrix adhesion of natural fibres cotton, flax and hemp in polymeric matrices analyzed with the single fibre fragmentation test. Composite Interfaces, **15** (2-3) 335-349 (2008).

[69] D´Almeida, J.R.M.: Fibre-matrix interface and natural fibre composites. Journal of Materials Science Letters, **10** (10) 578-580 (1991).

[70] Drzal, L.T. and M. Madhukar: Fibre-matrix adhesion and its relationship to composite mechanical properties Journal of Material Science, **28** 569-610 (1993).

[71] Arbelaiz, A., B. Fernandez, J. Ramos, A. Retegi, R. Llano-Ponte, and I. Mondragon: Mechanical properties of short flax fibre bundle/polypropylene composites: Influence of matrix/fibre modification, fibre content, water uptake and recycling. Composites Science and Technology, **65** (10) 1582-1592 (2005).

[72] George, J., M.S. Sreekala, and S. Thomas: A Review on Interface Modification and Characterization of Natural Fiber Reinforced Plastic Composites. Polymer Engineering and Science, **41** (9) 1471-1485 (2001).

[73] Caulfield, D., D. Feng, S. Prabawa, R. Young, and A. Sanadi: Interphase effects on the mechanical and physical aspects of natural fiber composites. Die Angewandte Makromolekulare Chemie, **272** (4757) 57–64 (1999).

[74] Tu, X., R. Young, and F. Denes: Improvement of bonding between cellulose and polypropylene by plasma treatment. Cellulose, **1** (1) 87-106 (1994).

[75] Huber, T., U. Biedermann, and J. Müssig: Enhancing the Fibre Matrix Adhesion of Natural Fibre Reinforced Polypropylene by Electron Radiation Analyzed with the Single Fibre Fragmentation Test. Composite Interfaces, **17** (4) 371-381 (2010).

[76] Bodin, A., S. Concaro, M. Brittberg, and P. Gatenholm: Bacterial cellulose as a potential meniscus implant. Journal of Tissue Engineering and Regenerative Medicine, **1** (5) 406-408 (2007).

[77] Piao, H., B. Duchemin, S. Dean, S. Schrecker, A. Pietak, P.A. Gostomski, and M.P. Staiger. Bacterial Cellulose-Reinforced Polylactide Eco-Composites. in Proceedings of the Ecocomposites. Stockholm, Sweden(2005).

[78] Bhatnagar, A. and M. Sain: Processing of Cellulose Nanofiber-reinforced Composites. Journal of Reinforced Plastics and Composites, **12** 1259-1268 (2005).

[79] Orts, W.J., J. Shey, S.H. Imam, G.M. Glenn, M.E. Guttman, and J.F. Revol: Application of Cellulose Microfibrils in Polymer Nanocomposites. Journal of Polymers and the Environment, **13** (4) 301-306 (2005).

[80] Oksman, K., A. Mathew, D. Bondeson, and I. Kvien: Manufacturing process of cellulose whiskers/polylactic acid nanocomposites. Composites Science and Technology, **66** (15) 2776-2784 (2006).

[81] Azizi Samir, M.A.S., F. Alloin, and A. Dufresne: Review of Recent Research into Cellulosic Whiskers, Their Properties and Their Application in Nanocomposite Field. Biomacromolecules, **6** (2) 612-626 (2005).

[82] Helbert, W., J. Cavaille, and A. Dufresne: Thermoplastic nanocomposites filled with wheat straw cellulose whiskers. Part I: processing and mechanical behavior. Polymer Composites, **17** (4) 604-611 (1996).

[83] Kohler, R. and K. Nebel: Cellulose-Nanocomposites: Towards High Performance Composite Materials. Macromolecular Symposia, **244** (1) 97-106 (2006).

[84] Holbery, J. and D. Houston: Natural-fiber-reinforced polymer composites in automotive applications. JOM Journal of the Minerals, Metals and Materials Society, **58** (11) 80-86 (2006).

[85] Klemm, D., B. Heublein, H.P. Fink, and A. Bohn: Cellulose: Fascinating biopolymer and sustainable raw material. Angewandte Chemie-International Edition, **44** (22) 3358-3393 (2005).

[86] Perepelkin, K.E.: Polysaccharides as renewable plant polymers for fibers: their today position and future forecast. in Conference Proceedings, 4. Internationales Symposium "Werkstoffe aus Nachwachsenden Rohstoffen". Erfurt (Germany)(2003).

[87] Zugenmaier, P.: Crystalline cellulose and derivatives: characterization and structures. Springer Verlag. Berlin, Heidelberg, Germany(2007).

[88] Nishiyama, Y.: Structure and properties of the cellulose microfibril. Journal of wood science, **55** (4) 241-249 (2009).

[89] Kolpak, F. and J. Blackwell: Determination of the structure of cellulose II. Macromolecules, **9** (2) 273-278 (1976).

[90] Brown Jr, R. and I. Saxena: Cellulose biosynthesis: a model for understanding the assembly of biopolymers. Plant Physiology et Biochemistry, **38** (1-2) 57-67 (2000).

[91] O'Sullivan, A.: Cellulose: the structure slowly unravels. Cellulose, **4** (3) 173-207 (1997).

[92] Zugenmaier, P.: Conformation and packing of various crystalline cellulose fibers. Progress in Polymer Science, **26** (9) 1341-1417 (2001).

[93] French, A.D. and G.P. Johnson: Cellulose shapes. Cellulose: Molecular and Structural Biology, 257-284 (2007).

[94] Nishiyama, Y., P. Langan, and H. Chanzy: Crystal Structure and Hydrogen-Bonding System in Cellulose I [beta] from Synchrotron X-ray and Neutron Fiber Diffraction. Journal of the American Chemical Society, **124** (31) 9074-9082 (2002).

[95] Kadla, J.F. and R.D. Gilbert: Cellulose structure: A review. Cellulose chemistry and technology, **34** (3-4) 197-216 (2000).

[96] Klemm, D., B. Phillip, T. Heinze, U. Heinze, and W. Wagenknecht: Comprehensive Cellulose Chemistry. Volume 1: Fundamentals and analytical methods. Wiley-VCH. Weinheim, Germany(1998).

[97] Kroon-Batenburg, L., J. Kroon, and M. Northolt: Chain modulus and intramolecular hydrogen bonding in native and regenerated cellulose fibers. Polymer Communications, **27** (10) 290-292 (1986).

[98] Matthews, J.F., Molecular Mechanics simulations of cellulose and cellobiose. 2009, CORNELL UNIVERSITY.

[99] Stone, B.: Cellulose: Structure and distribution. eLS, (2005).

[100] Stipanovic, A.J. and A. Sarko: Packing analysis of carbohydrates and polysaccharides. 6. Molecular and crystal structure of regenerated cellulose II. Macromolecules, **9** (5) 851-857 (1976).

[101] Kroon-Batenburg, L., B. Bouma, and J. Kroon: Stability of Cellulose Structures Studied by MD Simulations. Could Mercerized Cellulose II Be Parallel? Macromolecules, **29** (17) 5695-5699 (1996).

[102] Raymond, S., Å. Kvick, and H. Chanzy: The structure of cellulose II: a revisit. Macromolecules, **28** (24) 8422-8425 (1995).

[103] Wada, M., H. Chanzy, Y. Nishiyama, and P. Langan: Cellulose IIII crystal structure and hydrogen bonding by synchrotron X-ray and neutron fiber diffraction. Macromolecules, **37** (23) 8548-8555 (2004).

[104] Ciolacu, D., L. Pitol-Filho, and F. Ciolacu: Studies concerning the accessibility of different allomorphic forms of cellulose. CELLULOSE, **19** (1) 55-68

[105] Soykeabkaew, N., N. Arimoto, T. Nishino, and T. Peijs: All-cellulose composites by surface selective dissolution of aligned ligno-cellulosic fibres. Composites Science and Technology, **68** (10-11) 2201-2207 (2008).

[106] Soykeabkaew, N., T. Nishino, and T. Peijs: All-Cellulose Composites of Regenerated Cellulose Fibres by Surface Selective Dissolution. Composites: Part A, **16** (3) 435-444 (2009).

[107] Stubičar, N., I. Šmit, M. Stubičar, A. Tonejc, A. Janosi, J. Schurz, and P. Zipper: An X-ray diffraction study of the crystalline to amorphous phase change in cellulose during high-energy dry ball milling. Holzforschung-International Journal of the Biology, Chemistry, Physics and Technology of Wood, **52** (5) 455-458 (1998).

[108] Duchemin, B.J.C., Structure, property and processing relationships of all-cellulose composites, in Mechanical Engineering. 2008, University of Canterbury Christchurch, New Zealand.

[109] Wadehra, I. and R. Manley: Recrystallization of amorphous cellulose. Journal of Applied Polymer Science, **9** (7) 2627-2630 (1965).

[110] Chen, W., G. Lickfield, and C. Yang: Molecular modeling of cellulose in amorphous state. Part I: model building and plastic deformation study. Polymer, **45** (3) 1063-1071 (2004).

[111] Sakurada, I., Y. Nukushina, and T. Ito: Experimental determination of the elastic modulus of crystalline regions in oriented polymers. Journal of Polymer Science, **57** (165) 651-660 (1962).

[112] Nishino, T., K. Takano, and K. Nakamae: Elastic modulus of the crystalline regions of cellulose polymorphs. Journal of Polymer Science Part B: Polymer Physics, **33** (11) (1995).

[113] Ishikawa, A., T. Okano, and J. Sugiyama: Fine structure and tensile properties of ramie fibres in the crystalline form of cellulose I, II, IIII and IVI. Polymer, **38** (2) 463-468 (1997).

[114] Nishino, T., I. Matsuda, and K. Hirao, Cellulose Self-reinforced Composite, in Ecocomposites. 2003: University of London.

[115] Wegst, U. and M. Ashby: The mechanical efficiency of natural materials. Philosophical Magazine, **84** (21) 2167-2186 (2004).

[116] Lyons, W.: Crystal Density of Native Cellulose. The Journal of Chemical Physics, **9** 377-378 (1941).

[117] Staiger, M.P. and N. Tucker: Natural-fibre composites in structural applications. in Properties and performance of natural-fibre composites(eds.: Editor^Editors), Woodhead Publishing Limited: Cambridge, England **1** 269-300(2008).

[118] Nishino, T., I. Matsuda, and K. Hirao: All-cellulose composite. Macromolecules, **37** (20) 7683-7687 (2004).

[119] Capiati, N. and R. Porter: The concept of one polymer composites modelled with high density polyethylene. Journal of Materials Science, **10** (10) 1671-1677 (1975).

[120] Alcock, B., N. Cabrera, N.M. Barkoula, J. Loos, and T. Peijs: The mechanical properties of unidirectional all-polypropylene composites. Composites Part A: Applied Science and Manufacturing, **37** (5) 716-726 (2006).

[121] Zhang, J.M., Z. Mousavi, N. Soykeabkaew, P. Smith, T. Nishino, and T. Peijs: All-Aramid Composites by Partial Fiber Dissolution. ACS Applied Materials & Interfaces, **2** (3) 919-926 (2010).

[122] Matabola, K., A. De Vries, F. Moolman, and A. Luyt: Single polymer composites: a review. Journal of Materials Science, **44** (23) 6213-6222 (2009).

[123] Mead, W. and R. Porter: The preparation and tensile properties of polyethylene composites. Journal of Applied Polymer Science, **22** (11) 3249–3265 (1978).

[124] Teishev, A. and G. Marom: The effect of transcrystallinity on the transverse mechanical properties of single-polymer polyethylene composites. Journal of Applied Polymer Science, **56** (8) 959–966 (1995).

[125] Alcock, B., N. Cabrera, N.M. Barkoula, J. Loos, and T. Peijs. Processing and Properties of Recyclable All-Polypropylene Composites. in Proceedings of the EcoComposite. London, UK(2003).

[126] Pegoretti, A., A. Zanolli, and C. Migliaresi: Flexural and interlaminar mechanical properties of unidirectional liquid crystalline single-polymer composites. Composites Science and Technology, **66** (13) 1953-1962 (2006).

[127] Duchemin, B.J.C., R.H. Newman, and M.P. Staiger: Structure-property relationship of all-cellulose composites. Composites Science and Technology **69** (7-8) 1225-1230 (2009).

[128] Gindl, W. and J. Keckes: All-cellulose nanocomposite. Polymer, **46** (23) 10221-10225 (2005).

[129] Nishino, T. and N. Arimoto: All-Cellulose Composite Prepared by Selective Dissolving of Fiber Surface. Biomacromolecules, **8** 2712-2716 (2007).

[130] Swatloski, R., S. Spear, J. Holbrey, and R. Rogers: Dissolution of cellose with ionic liquids. Journal of the American Chemical Society, **124** (18) 4974-4975 (2002).

[131] Zhao, H., S. Xia, and P. Ma: Review: Use of ionic liquids as 'green' solvents for extractions. Journal of Chemical Technology & Biotechnology, **80** (10) 1089–1096 (2005).

[132] Heinze, T., K. Schwikal, and S. Barthel: Ionic liquids as reaction medium in cellulose functionalization. Macromolecular Bioscience, **5** (6) 520-525 (2005).

[133] Yang, Z. and W. Pan: Ionic liquids: Green solvents for nonaqueous biocatalysis. Enzyme and Microbial Technology, **37** (1) 19-28 (2005).

[134] Rogers, R., K. Seddon, and A.C.S. Meeting: Ionic liquids as green solvents: progress and prospects. American Chemical Society Washington, DC. Washington, DC, USA(2003).

[135] Graenacher, C., Cellulose solution. 1934, United States Patent 1943176

[136] Johnson, D., Process for strengthening swellable fibrous material with an amine oxide and the resulting material. 1969, United States Patent 3447956

[137] McCormick, C., Novel cellulose solutions. 1981, United States Patent 4278790

[138] Isogai, A. and R. Atalla, Alkaline method for dissolving cellulose. 1995, United States Patent 5410034

[139] Rosenau, T., A. Potthast, H. Sixta, and P. Kosma: The chemistry of side reactions and byproduct formation in the system NMMO/cellulose (Lyocell process). Progress in Polymer Science, **26** (9) 1763-1837 (2001).

[140] McCorsley III, C., Process for shaped cellulose article prepared from a solution containing cellulose dissolved in a tertiary amine N-oxide solvent. 1981, United States Patent 5410034

[141] Turbak, A., A. El-Kafrawy, F. Snyder Jr, and A. Auerbach, Solvent system for cellulose. 1981, United States Patent 4302252

[142] Ishii, D., D. Tatsumi, and T. Matsumoto: Effect of solvent exchange on the solid structure and dissolution behavior of cellulose. Biomacromolecules, **4** (5) 1238-1243 (2003).

[143] Ishii, D., Y. Kanazawa, D. Tatsumi, and T. Matsumoto: Effect of solvent exchange on the pore structure and dissolution behavior of cellulose. Journal of Applied Polymer Science, **103** (6) 3976 - 3984 (2007).

[144] Seurin, M.J. and P. Sixou: Comportement des solutions d'hydroxypropylcellulose en présence d'un sel inorganique. European Polymer Journal, **23** (1) 77-87 (1987).

[145] Bianchi, E., A. Ciferri, G. Conio, A. Cosani, and M. Terbojevich: Mesophase Formation and Chain Rigidity in Cellulose and Derivatives .4. Cellulose in N,N-Dimethylacetamide Lithium-Chloride. Macromolecules, **18** (4) 646-650 (1985).

[146] Gindl, W., K.J. Martinschitz, P. Boesecke, and J. Keckes: Structural changes during tensile testing of an all-cellulose composite by in situ synchrotron X-ray diffraction. Composites Science and Technology, **66** (15) 2639-2647 (2006).

[147] Gindl, W., K.J. Martinschitz, P. Boesecke, and J. Keckes: Changes in the molecular orientation and tensile properties of uniaxially drawn cellulose films. Biomacromolecules, **7** (11) 3146-3150 (2006).

[148] Gindl, W., T. Schoeberl, and J. Keckes: Structure and properties of a pulp fibre-reinforced composite with regenerated cellulose matrix. Journal of Applied Physics Part A, **83** (1) 19-22 (2006).

[149] Nishino, T. and N. Arimoto. All-cellulose composites by partial dissolving of fibers. in Conference Proceedings of the EcoComposite. Tokyo, Japan(2005).

[150] Soykeabkaew, N., C. Sian, S. Gea, T. Nishino, and T. Peijs: All-cellulose nanocomposites by surface selective dissolution of bacterial cellulose Cellulose, **16** (3) 435-444 (2009).

[151] Qin, C., N. Soykeabkaew, N. Xiuyuan, and T. Peijs: The effect of fibre volume fraction and mercerization on the properties of all-cellulose composites. Carbohydrate Polymers, **71** (3) 458-467 (2008).

[152] Sobue, H., H. Kiessig, and K. Hess: The cellulose-sodium hydroxide-water system as a function of the temperature. (1990).

[153] Vehviläinen, M., T. Kamppuri, M. Rom, J. Janicki, D. Ciecha ska, S. Grönqvist, M. Siika-Aho, K. Elg Christoffersson, and P. Nousiainen: Effect of wet spinning parameters on the properties of novel cellulosic fibres. CELLULOSE, **15** (5) 671-680 (2008).

[154] Ruan, D., L. Zhang, A. Lue, J. Zhou, H. Chen, X. Chen, B. Chu, and T. Kondo: A rapid process for producing cellulose multi-filament fibers from a NaOH/thiourea solvent system. Macromolecular Rapid Communications, **27** (17) 1495 - 1500 (2006).

[155] Cai, J., L. Zhang, J. Zhou, H. Li, H. Chen, and H. Jin: Novel fibers prepared from cellulose in NaOH/urea aqueous solution. Macromolecular Rapid Communications, **25** (17) 1558 - 1562 (2004).

[156] Kamida, K., K. Okajima, T. Matsui, and K. Kowsaka: Study on the solubility of cellulose in aqueous alkali solution by deuteration IR and 13 C NMR. Polymer Journal, **16** (12) 857-866 (1984).

[157] Cuissinat, C. and P. Navard: Swelling and Dissolution of Cellulose Part II: Free Floating Cotton and Wood Fibres in NaOH-Water-Additives Systems. Macromolecular Symposia, **244** (1) 19–30 (2006).

[158] Jin, H., C. Zha, and L. Gu: Direct dissolution of cellulose in NaOH/thiourea/urea aqueous solution. Carbohydrate Research, **342** (6) 851-858 (2007).

[159] Kuo, Y. and J. Hong: Investigation of solubility of microcrystalline cellulose in aqueous NaOH. Polymers For Advanced Technologies, **16** (5) 425-428 (2005).

[160] Cao, Y. and H. Tan: Preparation and properties of microporous cellulose membranes from novel cellulose/aqueous sodium hydroxide solutions. Journal of Applied Polymer Science, **102** (1) 920 - 926 (2006).

[161] Liang, S., C. Liu, and L.F. Song: Soluble microbial products in membrane bioreactor operation: Behaviors, characteristics, and fouling potential. Water Research, **41** (1) 95-101 (2007).

[162] Isogai, A. and R. Atalla: Dissolution of cellulose in aqueous NaOH solutions. CELLULOSE, **5** (4) 309-319 (1998).

[163] Yamashiki, T., T. Matsui, M. Saitoh, K. Okajima, K. Kamide, and T. Sawada: Characterisation of cellulose treated by the steam explosion method. Part 1: Influence of cellulose resources on changes in morphology, degree of polymerisation, solubility and solid structure. British Polymer Journal, **22** (1) 73 - 83 (1990).

[164] Kunze, J. and H. Fink: Structural changes and activation of cellulose by caustic soda solution with urea. Macromolecular Symposia, **223** (1) 175–188 (2005).

[165] Ramnial, T., D. Ino, and J. Clyburne: Phosphonium ionic liquids as reaction media for strong bases. Chemical Communications, **2005** (3) 325-327 (2005).

[166] Forsyth, S., J. Pringle, and D. MacFarlane: Ionic Liquids-An Overview. ChemInform, **35** (20) 113-119 (2004).

[167] Zhao, Q., R.C.M. Yam, B. Zhang, Y. Yang, X. Cheng, and R. Li: Novel all-cellulose ecocomposites prepared in ionic liquids. CELLULOSE, **16** (2) 217-226 (2009).

[168] Remsing, R., R. Swatloski, R. Rogers, and G. Moyna: Mechanism of cellulose dissolution in the ionic liquid 1-n-butyl-3-methylimidazolium chloride: a 13C and 35/37Cl NMR relaxation study on model systems. Chemical Communication (Camb), **28** (12) 1271-1273 (2006).

[169] Pinkert, A., K. Marsh, S. Pang, and M. Staiger: Ionic Liquids and Their Interaction with Cellulose. Chemical Reviews, **109** 6712–6728 (2009).

[170] Duchemin, B.J.C., R.H. Newman, and M.P. Staiger: Phase transformations in microcrystalline cellulose due to partial dissolution. CELLULOSE, **14** (4) 311-320 (2007).

[171] Ouajai, S. and R.A. Shanks: Preparation, Structure and Mechanical Properties of All-Hemp Cellulose Biocomposites. Composites Science and Technology, **69** (13) 2119-2126 (2009).

[172] Bledzki, A.K., Fink, H.P., Specht, K.: Unidirectional hemp and flax EP- and PP-composites: Influence of defined fiber treatments. Journal of Applied Polymer Science, **93** (5) 2150-2156 (2004).

[173] Zhou, L.M., K.W.P. Yeung, and C.W.M. Yuen: Effect of NaOH Mercerization on the Crosslinking of Ramie Yarn Using 1,2,3,4-Butanetetracarboxylic Acid. Textile Research Journal, **72** (6) 531-538 (2002).

[174] Qi, H., J. Cai, L. Zhang, and S. Kuga: Properties of Films Composed of Cellulose Nanowhiskers and a Cellulose Matrix Regenerated from Alkali/Urea Solution. Biomacromolecules, **10** (6) 1597–1602 (2009).

[175] Qin, C., N. Soykeabkaewa, N. Xiuyuan, and T. Pejis: The effect of fibre volume fraction and mercerization on the properties of all-cellulose composites. Carbohydrate Polymers, **71** 458-468 (2008).

[176] Niu, P., B. Liu, X. Wei, X. Wang, and J. Yang: Study on mechanical properties and thermal stability of polypropylene/hemp fiber composites. Journal of Reinforced Plastics and Composites, **30** (1) 36-44 (2010).

[177] Pullawan, T., A. Wilkinson, and S. Eichhorn: Discrimination of matrix–fibre interactions in all-cellulose nanocomposites. Composites Science and Technology, **70** (16) 2325-2330 (2010).

[178] Baur, E. and F. Otremba: Design, Material Properties and Databases. in Industrial Applications of Natural Fibres Structure, Properties and Technical Applications(eds.: Editor^Editors), John Wiley & Sons, Ltd.: Chichester **1** 397-406(2010).

[179] Soykeabkaew, N., C. Sian, S. Gea, T. Nishino, and T. Peijs: All-cellulose nanocomposites by surface selective dissolution of bacterial cellulose. CELLULOSE, **16** (3) 435-444 (2009).

[180] Duchemin, B.J.C., A.P. Mathew, and K. Oksman: All-cellulose composites by partial dissolution in the ionic liquid 1-butyl-3-methylimidazolium chloride. Composites Part A: Applied Science and Manufacturing, **40** (12) 2031-2037 (2009).

[181] Arevalo, R., O.T. Picot, R.M. Wilson, N. Soykeabkaew, and T. Peijs: All-Cellulose Composites by Partial Dissolution of Cotton Fibres. Journal of Biobased Materials and Bioenergy, **4** (2) 129-138 (2010).

[182] Han, D. and L. Yan: Preparation of All-Cellulose Composite by Selective Dissolving of Cellulose Surface in PEG/NaOH Aqueous Solution. Carbohydrate Polymers, **79** (3) 614-619 (2010).

[183] Petersson, L. and K. Oksman: Preparation and Properties of Biopolymer-Based Nanocomposite Films Using Microcrystalline Cellulose. in Cellulose Nanocomposites - Processing, Characterization and Properties(eds.: Editor^Editors), American Chemical Society **1** 133-150(2006).

[184] Mathew, A.P., A. Chakraborty, K. Oksman, and M. Sain: The Structure and Mechanical Properties of Cellulose Nanocomposites Prepared by Twin Screw Extrusion. in Cellulose Nanocomposites - Processing, Characterization and Properties(eds.: Editor^Editors), American Chemical Society **1** 115-131(2006).

[185] Bax, B. and J. Müssig: Impact and tensile properties of PLA/Cordenka and PLA/flax composites. Composites Science and Technology, **68** (7-8) 1601-1607 (2008).

[186] Sreekumar, P.A., P. Albert, G. Unnikrishnan, K. Joseph, and S. Thomas: Mechanical and water sorption studies of ecofriendly banana fiber-reinforced polyester composites fabricated by RTM. Journal of Applied Polymer Science, **109** (3) 1547-1555 (2008).

[187] Madsen, B., Lilholt H.: Physical and mechanical properties of unidirectional plant fibre composites - an evaluation of the influence of porosity. Composites Science and Technology, **63** (9) 1265-1272 (2003).

[188] Khondker, O.A., U.S. Ishiaku, A. Nakai, and H. Hamada: A novel processing technique for thermoplastic manufacturing of unidirectional composites reinforced with jute yarns. Composites: Part A, **37** (12) 2274-2284 (2006).

[189] Van de Weyenberg, I., T.C. Truong, B. Vangrimde, and I. Verpoest: Improving the properties of UD flax fibre reinforced composites by applying an alkaline fibre treatment. Composites Part a-Applied Science and Manufacturing, **37** (9) 1368-1376 (2006).

[190] Ochi, S.: Mechanical properties of kenaf fibers and kenaf/PLA composites. Mechanics of Materials, **40** (4-5) 446-452 (2008).

[191] Yano, S., H. Hatakeyama, and T. Hatakeyama: Effect of hydrogen bond formation on dynamic mechanical properties of amorphous cellulose. Journal of Applied Polymer Science, **20** (12) 3221 - 3231 (1976).

[192] Szczesniak, L., A. Rachocki, and J. Tritt-Goc: Glass transition temperature and thermal decomposition of cellulose powder. CELLULOSE, **15** (3) 445-451 (2008).

[193] Shen, T. and S. Gnanakaran: The Stability of Cellulose: A Statistical Perspective from a Coarse-Grained Model of Hydrogen-Bond Networks. Biophysical Journal, **96** (8) 3032-3040 (2009).

[194] Jafarpour, G., E. Dantras, A. Boudet, and C. Lacabanne: Study of dielectric relaxations in cellulose by combined DDS and TSC. Journal of non-crystalline solids, **353** (44-46) 4108-4115 (2007).

[195] Montes, H., K. Mazeau, and J. Cavaille: Secondary mechanical relaxations in amorphous cellulose. Macromolecules, **30** (22) 6977-6984 (1997).

[196] Montes, H., K. Mazeau, and J. Cavaille: The mechanical ß relaxation in amorphous cellulose. Journal of non-crystalline solids, **235** 416-421 (1998).

[197] Manabe, S., M. Iwata, and K. Kamide: Dynamic Mechanical Absorptions Observed for Regenerated Cellulose Solids in the Temperature-Range from 280-K to 600-K. Polymer Journal, **18** (1) 1-14 (1986).

[198] Hongo, T., C. Yamane, M. Saito, and K. Okajima: Super-molecular structures controlling the swelling behavior of regenerated cellulose membranes. Polymer Journal, **28** (9) 769-779 (1996).

[199] Yamane, C., M. Mori, M. Saito, and K. Okajima: Structures and mechanical properties of cellulose filament spun from cellulose/aqueous NaOH solution system. Polymer Journal, **28** (12) 1039-1047 (1996).

[200] Duchemin, B.J.C., M.P. Staiger, and R.H. Newman: High-temperature viscoelastic relaxation in all-cellulose composites. (submitted).

[201] Zickler, G.A., W. Wagermaier, S.S. Funari, M. Burghammer, and O. Paris: In situ X-ray diffraction investigation of thermal decomposition of wood cellulose. Journal of Analytical and Applied Pyrolysis, **80** (1) 134-140 (2007).

[202] Nogi, M., K. Handa, A.N. Nakagaito, and H. Yano: Optically transparent bionanofiber composites with low sensitivity to refractive index of the polymer matrix. Applied Physics Letters, **87** (24) 243110 1-3 (2005).

[203] Edgar, K.J., C.M. Buchanan, J.S. Debenham, P.A. Rundquist, B.D. Seiler, M.C. Shelton, and D. Tindall: Advances in cellulose ester performance and application. Progress in Polymer Science, **26** (9) 1605-1688 (2001).

[204] Ganster, J. and H. Fink: Novel cellulose fibre reinforced thermoplastic materials. CELLULOSE, **13** (3) 271-280 (2006).

[205] Heinze, T., T. Liebert, K. Pfeiffer, and M. Hussain: Unconventional cellulose esters: synthesis, characterization and structure–property relations. CELLULOSE, **10** (3) 283-296 (2003).

[206] Seavey, K., I. Ghosh, R. Davis, and W. Glasser: Continuous cellulose fiber-reinforced cellulose ester composites. I. Manufacturing options. CELLULOSE, **8** (2) 149-159 (2001).

[207] Glasser, W.G.: 6. Prospects for future applications of cellulose acetate. Macromolecular Symposia, **208** (1) 371-394 (2004).

[208] Glasser, W.G., R. Taib, R.K. Jain, and R. Kander: Fiber-reinforced cellulosic thermoplastic composites. Journal of Applied Polymer Science, **73** (7) 1329-1340 (1999).

[209] Lorand, E.J. and E.A. Georgi: The mechanism of cellulose benzylation. Journal of the American Chemical Society, **59** (7) 1166-1170 (1937).

[210] Wolfrom, M.L. and M.A. Eltaraboulsi: Benzylation and Xanthation of Cellulose Monoalkoxide. Journal of the American Chemical Society, **76** (8) 2216-2218 (1954).

[211] Lu, X., M.Q. Zhang, M.Z. Rong, G. Shi, and G.C. Yang: All-plant fibre composites: Self reinforced composites based on sisal. Advanced Composites Letters, **10** (2) 73-79 (2001).

[212] Lu, X., M.Q. Zhang, M.Z. Rong, G. Shi, and G.C. Yang: All-Plant fiber composites. I: Unidirectional sisal fiber reinforced benzylated wood. Polymer Composites, **23** (4) 624-633 (2002).

[213] Lu, X., M.Q. Zhang, M.Z. Rong, G. Shi, and G.C. Yang: Self-reinforced melt processable composites of sisal. Composites Science and Technology, **63** (2) 177-186 (2003).

[214] Zhang, M.Q., M.Z. Rong, and X. Lu: Fully biodegradable natural fiber composites from renewable resources: All-plant fiber composites. Composites Science and Technology, **65** (15-16) 2514-2525 (2005).

[215] Lu, X., M.Q. Zhang, M.Z. Rong, G. Shi, G.C. Yang, and H.M. Zeng: Natural vegetable fibre/plasticised natural vegetable fibre - A candidate for low cost and fully biodegradable composite. Advanced Composites Letters, **8** (5) 231-236 (1999).

[216] de Menezes, A.J., D. Pasquini, A.A.D. Curvelo, and A. Gandini: Self-reinforced composites obtained by the partial oxypropylation of cellulose fibers. 2. Effect of catalyst on the mechanical and dynamic mechanical properties. CELLULOSE, **16** (2) 239-246 (2009).

[217] de Menezes, A.J., D. Pasquini, A.A.D. Curvelo, and A. Gandini: Self-reinforced composites obtained by the partial oxypropylation of cellulose fibers. 1. Characterization of the materials obtained with different types of fibers. Carbohydrate Polymers **76** (3) 437-442 (2009).

[218] Gandini, A., A.A.D. Curvelo, D. Pasquini, and A.J. de Menezes: Direct transformation of cellulose fibres into self-reinforced composites by partial oxypropylation. Polymer, **46** (24) 10611-10613 (2005).

[219] Matsumura, H. and W.G. Glasser: Cellulosic nanocomposites. II. Studies by atomic force microscopy. Journal of Applied Polymer Science, **78** (13) 2254-2261 (2000).

[220] Matsumura, H., J. Sugiyama, and W.G. Glasser: Cellulosic nanocomposites. I. Thermally deformable cellulose hexanoates from heterogeneous reaction. Journal of Applied Polymer Science, **78** (13) 2242-2253 (2000).

[221] Wunderlich, D. and B. Zimmerer, Technical Rayon: Present and Future, in 50th Dornbirn Man-Made Fibers Congress. 2011: Dornbirn, Austria.

[222] ASTME3, Standard Guide for Preparation of Metallographic Specimens. 2007, ASTM International: West Conshohocken, PA, USA.

[223] ASTMD790, Standard Test Methods for Flexural Properties of Unreinforced and Reinforced Plastics and Electrical Insulating Materials. 2010, ASTM International: West Conshohocken, PA, USA.

[224] Kubisa, P.: Ionic liquids as solvents for polymerization processes--Progress and challenges. Progress in Polymer Science, **34** (12) 1333-1347 (2009).

[225] Thuy Pham, T.P., C.W. Cho, and Y.S. Yun: Environmental fate and toxicity of ionic liquids: A review. Water Research, **44** (2) 352-372 (2010).

[226] Swatloski, R.P., J.D. Holbrey, and R.D. Rogers: Ionic liquids are not always green: hydrolysis of 1-butyl-3-methylimidazolium hexafluorophosphate. Green Chemistry, **5** (4) 361-363 (2003).

[227] Khodadoust, A.P., S. Chandrasekaran, and D.D. Dionysiou: Preliminary assessment of imidazolium-based room-temperature ionic liquids for extraction of organic contaminants from soils. Environmental science & technology, **40** (7) 2339-2345 (2006).

[228] Gordon, C.M.: New developments in catalysis using ionic liquids. Applied Catalysis A: General, **222** (1-2) 101-117 (2001).

[229] Pinkert, A., D.F. Goeke, K.N. Marsh, and S. Pang: Extracting wood lignin without dissolving or degrading cellulose: investigations on the use of food additive-derived ionic liquids. Green Chem., **13** (11) 3124-3136 (2011).

[230] Scammells, P.J., J.L. Scott, and R.D. Singer: Ionic liquids: The neglected issues. Australian journal of chemistry, **58** (3) 155-169 (2005).

[231] Abu-Eishah, S.I.: Ionic Liquids Recycling for Reuse. in Ionic Liquids - Classes and Properties(eds.: Editor^Editors), InTech: Rijeka, Croatia **1** 239-272(2011).

[232] Meng, F., S.-R. Chae, A. Drews, M. Kraume, H.-S. Shin, and F. Yang: Recent advances in membrane bioreactors (MBRs): Membrane fouling and membrane material. Water Research, **43** (6) 1489-1512 (2009).

[233] Feng, W., J.L. Brash, and S. Zhu: Non-biofouling materials prepared by atom transfer radical polymerization grafting of 2-methacryloloxyethyl phosphorylcholine: Separate effects of graft density and chain length on protein repulsion. Biomaterials, **27** (6) 847-855 (2006).

[234] Liebert, T. and T. Heinze: Interaction of ionic liquids with polysaccharides. 5. Solvents and reaction media for the modification of cellulose. BioResources, **3** (2) 576-601 (2008).

[235] Cao, Y., J. Wu, J. Zhang, H. Li, Y. Zhang, and J. He: Room temperature ionic liquids (RTILs): A new and versatile platform for cellulose processing and derivatization. Chemical Engineering Journal, **147** (1) 13-21 (2009).

[236] Kosan, B., C. Michels, and F. Meister: Dissolution and forming of cellulose with ionic liquids. CELLULOSE, **15** (1) 59-66 (2008).

[237] Kadokawa, J.-i., M.-a. Murakami, A. Takegawa, and Y. Kaneko: Preparation of cellulose–starch composite gel and fibrous material from a mixture of the polysaccharides in ionic liquid. Carbohydrate Polymers, **75** (1) 180-183 (2009).

[238] Hermanutz, F., F. Gähr, E. Uerdingen, F. Meister, and B. Kosan. New developments in dissolving and processing of cellulose in ionic liquids **262** 23-27 (2008).

[239] Viswanathan, G., S. Murugesan, V. Pushparaj, O. Nalamasu, P.M. Ajayan, and R.J. Linhardt: Preparation of biopolymer fibers by electrospinning from room temperature ionic liquids. Biomacromolecules, **7** (2) 415-418 (2006).

[240] Ahmed, K.S. and S. Vijayarangan: Tensile, flexural and interlaminar shear properties of woven jute and jute-glass fabric reinforced polyester composites. Journal of Materials Processing Technology, **207** (1-3) 330-335 (2008).

[241] Ma, H., B. Zhou, H.S. Li, Y.Q. Li, and S.Y. Ou: Green composite films composed of nanocrystalline cellulose and a cellulose matrix regenerated from functionalized ionic liquid solution. Carbohydrate Polymers, (2010).

[242] Aaltonen and O.A.O.J. Jauhiainen: The preparation of lignocellulosic aerogels from ionic liquid solutions. Carbohydrate Polymers, **75** 125–129 (2009).

[243] Tsioptsias, C., A. Stefopoulos, I. Kokkinomalis, L. Papadopoulou, and C. Panayiotou: Development of micro- and nano-porous composite materials by processing cellulose with ionic liquids and supercritical CO2. Green Chemistry, **10** (9) 965-971 (2008).

[244] Deng, M., Q. Zhou, A. Du, J. Van Kasteren, and Y. Wang: Preparation of nanoporous cellulose foams from cellulose-ionic liquid solutions. Materials Letters, **63** (21) 1851-1854 (2009).

[245] Vitz, J., T. Erdmenger, C. Haensch, and U.S. Schubert: Extended dissolution studies of cellulose in imidazolium based ionic liquids. Green Chem., **11** (3) 417-424 (2009).

[246] Marsh, K., J. Boxall, and R. Lichtenthaler: Room temperature ionic liquids and their mixtures--a review. Fluid Phase Equilibria, **219** (1) 93-98 (2004).

[247] Gericke, M., K. Schlufter, T. Liebert, T. Heinze, and T. Budtova: Rheological properties of cellulose/ionic liquid solutions: From dilute to concentrated states. Biomacromolecules, **10** (5) 1188-1194 (2009).

[248] El Seoud, O.A., A. Koschella, L.C. Fidale, S. Dorn, and T. Heinze: Applications of ionic liquids in carbohydrate chemistry: a window of opportunities. Biomacromolecules, **8** (9) 2629-2647 (2007).

[249] Cammarata, L., S. Kazarian, P. Salter, and T. Welton: Molecular states of water in room temperature ionic liquids. Phys. Chem. Chem. Phys., **3** (23) 5192-5200 (2001).

[250] Mazza, M., D.A. Catana, C. Vaca-Garcia, and C. Cecutti: Influence of water on the dissolution of cellulose in selected ionic liquids. CELLULOSE, **16** (2) 207-215 (2009).

[251] Strechan, A., Y. Paulechka, A. Blokhin, and G. Kabo: Low-temperature heat capacity of hydrophilic ionic liquids [BMIM][CF3COO] and [BMIM][CH3COO] and a correlation scheme for estimation of heat capacity of ionic liquids. The Journal of Chemical Thermodynamics, **40** (4) 632-639 (2008).

[252] Liu, Z., H. Wang, Z. Li, X. Lu, X. Zhang, S. Zhang, and K. Zhou: Characterization of the regenerated cellulose films in ionic liquids and rheological properties of the solutions. Materials Chemistry and Physics, **128** (1-2) 220-227 (2011).

[253] Fort, D.A., R.C. Remsing, R.P. Swatloski, P. Moyna, G. Moyna, and R.D. Rogers: Can ionic liquids dissolve wood? Processing and analysis of lignocellulosic materials with 1-n-butyl-3-methylimidazolium chloride. Green Chem., **9** (1) 63-69 (2006).

[254] Kilpeläinen, I., H. Xie, A. King, M. Granstrom, S. Heikkinen, and D.S. Argyropoulos: Dissolution of wood in ionic liquids. Journal of agricultural and food chemistry, **55** (22) 9142-9148 (2007).

[255] Zavrel, M., D. Bross, M. Funke, J. Büchs, and A.C. Spiess: High-throughput screening for ionic liquids dissolving (ligno-) cellulose. Bioresource Technology, **100** (9) 2580-2587 (2009).

[256] Nada, A. and M.L. Hassan: Thermal behavior of cellulose and some cellulose derivatives. Polymer Degradation and Stability, **67** (1) 111-115 (2000).

[257] Emsley, A. and G. Stevens: Kinetics and mechanisms of the low-temperature degradation of cellulose. CELLULOSE, **1** (1) 26-56 (1994).

[258] Anderson, J.L., D.W. Armstrong, and G.T. Wei: Ionic liquids in analytical chemistry. Analytical chemistry, **78** (9) 2892-2902 (2006).

[259] Frydrych, I., G. Dziworska, and J. Bilska: Comparative analysis of the thermal insulation properties of fabrics made of natural and man-made cellulose fibres. Fibres and Textiles in Eastern Europe, **10** (4) 40-44 (2002).

[260] Valkenburg, M.E.V., R.L. Vaughn, M. Williams, and J.S. Wilkes: Thermochemistry of ionic liquid heat-transfer fluids. Thermochimica Acta, **425** (1) 181-188 (2005).

[261] Lu, F., B. Cheng, J. Song, and Y. Liang: Rheological characterization of concentrated cellulose solutions in 1-allyl-3-methylimidazolium chloride. Journal of Applied Polymer Science, **124** (4) 3419-3425 (2011).

[262] Lv, Y., J. Wu, J. Zhang, Y. Niu, C.-Y. Liu, J. He, and J. Zhang: Rheological properties of cellulose/ionic liquid/Dimethylsulfoxide (DMSO) solutions. Polymer, **In Press** (2012).

[263] Lindman, B., G. Karlström, and L. Stigsson: On the mechanism of dissolution of cellulose. Journal of Molecular Liquids, **156** (1) 76-81 (2010).

[264] Zhang, H., J. Wu, J. Zhang, and J. He: 1-Allyl-3-methylimidazolium chloride room temperature ionic liquid: A new and powerful nonderivatizing solvent for cellulose. Macromolecules, **38** (20) 8272-8277 (2005).

[265] Zhao, D., H. Li, J. Zhang, L. Fu, M. Liu, J. Fu, and P. Ren: Dissolution of cellulose in phosphate-based ionic liquids. Carbohydrate Polymers, **87** (2) 1490-1494 (2011).

[266] Cuissinat, C., P. Navard, and T. Heinze: Swelling and dissolution of cellulose. Part IV: Free floating cotton and wood fibres in ionic liquids. Carbohydrate Polymers, **72** (4) 590-596 (2008).

[267] Mora-Pale, M., L. Meli, T.V. Doherty, R.J. Linhardt, and J.S. Dordick: Room temperature ionic liquids as emerging solvents for the pretreatment of lignocellulosic biomass. Biotechnology and Bioengineering, **108** (6) 1229-1245 (2011).

[268] Zhao, H., C.L. Jones, G.A. Baker, S. Xia, O. Olubajo, and V.N. Person: Regenerating cellulose from ionic liquids for an accelerated enzymatic hydrolysis. Journal of Biotechnology, **139** (1) 47-54 (2009).

[269] Chen, X., Y. Zhang, L. Cheng, and H. Wang: Rheology of concentrated cellulose solutions in 1-butyl-3-methylimidazolium chloride. Journal of Poymers and the Environment, **17** (4) 273-279 (2009).

[270] Sammons, R., J. Collier, T. Rials, and S. Petrovan: Rheology of 1-butyl-3-methylimidazolium chloride cellulose solutions. I. Shear rheology. Journal of Applied Polymer Science, **110** (2) 1175-1181 (2008).

[271] Sunthar, P.: Polymer Rheology. Rheology of Complex Fluids, 171 (2010).

[272] Yang, H., H. Kim, H. Park, B. Lee, and T. Hwang: Water absorption behavior and mechanical properties of lignocellulosic filler-polyolefin bio-composites. Composite Structures, **72** (4) 429-437 (2006).

[273] Boluk, Y.: Acid–base interactions and swelling of cellulose fibers in organic liquids. CELLULOSE, **12** (6) 577-593 (2005).

[274] Hansen, N.M.L. and D. Plackett: Sustainable films and coatings from hemicelluloses: A review. Biomacromolecules, **9** (6) 1493-1505 (2008).

[275] Weise, U., T. Maloney, and H. Paulapuro: Quantification of water in different states of interaction with wood pulp fibres. CELLULOSE, **3** (1) 189-202 (1996).

[276] Nakamura, K., T. Hatakeyama, and H. Hatakeyama: Studies on bound water of cellulose by differential scanning calorimetry. Textile Research Journal, **51** (9) 607-613 (1981).

[277] Berrocal, A., J. Baeza, J. Rodríguez, M. Espinosa, and J. Freer: Effect of tree age on variation of Pinus radiata D. DON chemical composition. Journal of the Chilean Chemical Society, **49** (3) 251-256 (2004).

[278] Araque, E., C. Parra, J. Freer, D. Contreras, J. Rodríguez, R. Mendonça, and J. Baeza: Evaluation of organosolv pretreatment for the conversion of Pinus radiata D. Don to ethanol. Enzyme and Microbial Technology, **43** (2) 214-219 (2008).

[279] Ping, Z., Q. Nguyen, S. Chen, J. Zhou, and Y. Ding: States of water in different hydrophilic polymers--DSC and FTIR studies. Polymer, **42** (20) 8461-8467 (2001).

[280] Bertran, M. and B. Dale: Determination of cellulose accessibility by differential scanning calorimetry. Journal of Applied Polymer Science, **32** (3) 4241-4253 (1986).

[281] Morton, W.E. and J.W.S. Hearle: Physical Properties of Textile Fibres. Butterworth & Co. LTD. London, UK(1962).

[282] Hatakeyama, T., Y. Ikeda, and H. Hatakeyama: Effect of bound water on structural change of regenerated cellulose. Die Makromolekulare Chemie, **188** (8) 1875-1884 (1987).

[283] Mazumdar, S.K.: Composites manufacturing: materials, product, and process engineering. CRC. (2002).

[284] Rudd, C.D., A.C. Long, K.N. Kendall, and C. Mangin: Liquid moulding technologies: Resin transfer moulding, structural reaction injection moulding and related processing techniques. Woodhead Pub Ltd. (1997).

[285] Piotrowski, S. and M. Carus: Natural Fibres in Technical Applications: Market and Trends. in Industrial Applications of Natural Fibres: Structure, Properties and Technical Applications(eds.: Editor^Editors), John Wiley & Sons Ltd.: Chichester, UK(2010).

[286] Baur, E., N. Graupner, S. Joas, and F. Otremba: Press formed parts from natural fibre-reinforced polymers. Kunststoffe Int, **3** 24-31 (2009).

[287] Mueller and Fries: Pure Natur im Automobil. Kunststoffe, **88** (4) 544-546 (1998).

[288] Müssig, J., M. Schmehl, H.B. von Buttlar, U. Schonfeld, and K. Arndt: Exterior components based on renewable resources produced with SMC technology--Considering a bus component as example. Industrial Crops and Products, **24** (2) 132-145 (2006).

[289] Akin, D.E.: Flax–Structure, Chemistry, Retting and Processing. Industrial Applications of Natural Fibres, 87-108 (2010).

[290] Kljun, A., T.A.S. Benians, F. Goubet, F. Meulewaeter, J.P. Knox, and R.S. Blackburn: Comparative analysis of crystallinity changes in cellulose I polymers using ATR-FTIR, X-ray diffraction, and carbohydrate-binding module (CBM) probes. Biomacromolecules, **12** (11) 4121-4126 (2011).

[291] Haverhals, L.M., W.M. Reichert, H.C. De Long, and P.C. Trulove: Natural Fiber Welding. Macromolecular Materials and Engineering, **295** (5) 425-430 (2010).

[292] Sun, N., M. Rahman, Y. Qin, M.L. Maxim, H. Rodríguez, and R.D. Rogers: Complete dissolution and partial delignification of wood in the ionic liquid 1-ethyl-3-methylimidazolium acetate. Green Chemistry, **11** (5) 646-655 (2009).

[293] Casas, A., M. Oliet, M. Alonso, and F. Rodríguez: Dissolution of< i> Pinus radiata</i> and< i> Eucalyptus globulus</i> woods in ionic liquids under microwave radiation: Lignin regeneration and characterization. Separation and Purification Technology, (2012).

[294] Kreze, T., S. Strnad, K. Stana-Kleinschek, and V. Ribitsch: Influence of aqueous medium on mechanical properties of conventional and new environmentally friendly regenerated cellulose fibers. Materials Research Innovation, **4** (2) 107-114 (2001).

[295] Isogai, A., M. Usuda, T. Kato, T. Uryu, and R. Atalla: Solid-state CP/MAS carbon-13 NMR study of cellulose polymorphs. Macromolecules, **22** (7) 3168-3172 (1989).

[296] Rihm, R., Röntgen-Strukturuntersuchungen an Celluloseregeneratfasern. 2003, Technische Universität Berlin, Universitätsbibliothek (Diss.-Stelle).

[297] Buleon, A. and H. Chanzy: Single crystals of cellulose IV 2: preparation and properties. Journal of Polymer Science Polymer Physics Edition, **18** 1209-1217 (1980).

[298] Singleton, A., C. Baillie, P. Beaumont, and T. Peijs: On the mechanical properties, deformation and fracture of a natural fibre/recycled polymer composite. Composites Part B, **34** (6) 519-526 (2003).

[299] Alix, S., S. Marais, C. Morvan, and L. Lebrun: Biocomposite materials from flax plants: Preparation and properties. Composites Part A, **39** (12) 1793-1801 (2008).

[300] Huang, X. and A. Netravali: Characterization of flax fiber reinforced soy protein resin based green composites modified with nano-clay particles. Composites Science and Technology, **67** (10) 2005-2014 (2007).

[301] Goutianos, S., T. Peijs, B. Nystrom, and M. Skrifvars: Development of flax fibre based textile reinforcements for composite applications. Applied Composite Materials, **13** (4) 199-215 (2006).

[302] Williams, C., J. Summerscales, and S. Grove: Resin infusion under flexible tooling (RIFT): a review. Composites Part A: Applied Science and Manufacturing, **27** (7) 517-524 (1996).

[303] Hammami, A. and B. Gebart: Analysis of the vacuum infusion molding process. Polymer Composites, **21** (1) 28-40 (2000).

[304] Li, W., J. Krehl, J. Gillespie, D. Heider, M. Endrulat, K. Hochrein, M. Dunham, and C. Dubois: Process and performance evaluation of the Vacuum-Assisted Process. Journal of Composite Materials, **38** (20) 1803-1814 (2004).

[305] Seemann III, W.H., G.C. Tunis III, A.P. Perrella, R.K. Haraldsson, W.E. Everitt, and E.A. Pearson, Large composite structures incorporating a resin distribution network. 1998, US Patent No 5721034.

[306] David, H.A., H.O. Hartleyand, and E.S. Pearson: The distribution of the ratio in a single normal sample of range to standard deviation. Biometrika, **41** 482-493 (1954).

[307] Pothan, L.A., P. Potschke, R. Habler, and S. Thomas: The static and dynamic mechanical properties of banana and glass fiber woven fabric-reinforced polyester composite. Journal of COMPOSITE MATERIALS, **39** (11) 1007-1025 (2005).

[308] Khan, M.A., G. Hinrichsen, and L.T. Drzal: Influence of novel coupling agents on mechanical properties of jute reinforced polypropylene composite. Journal of Material Science Letters, **20** (18) 1711-1713 (2001).

[309] Ganster, J., H.P. Finck, and M. Pinnow: High-tenacity man-made cellulose fibre reinforced thermoplastics – Injection moulding compounds with polypropylene and alternative matrices. Composites: Part A, **37** 1796-1804 (2006).

[310] Mallick, P.: Fiber-reinforced composites: materials, manufacturing, and design. CRC Press. (1993).

[311] Maki-Arvela, P., I. Anugwom, P. Virtanen, R. Sjoholm, and J. Mikkola: Dissolution of lignocellulosic materials and its constituents using ionic liquids--A review. Industrial Crops and Products, **32** (3) 175-201 (2010).

[312] Sescousse, R., K.A. Le, M.E. Ries, and T. Budtova: Viscosity of Cellulose–Imidazolium-Based Ionic Liquid Solutions. The Journal of Physical Chemistry B, **114** (21) 7222-7228 (2010).

[313] Fink, H.P., P. Weigel, H. Purz, and J. Ganster: Structure formation of regenerated cellulose materials from NMMO-solutions. Progress in Polymer Science, **26** (9) 1473-1524 (2001).

[314] Wojdyr, M.: Fityk: a general-purpose peak fitting program. Journal of Applied Crystallography, **43** (5) 1126-1128 (2010).

[315] El Seoud, O.A., L.C. Fidale, N. Ruiz, M.L.O. D'Almeida, and E. Frollini: Cellulose swelling by protic solvents: which properties of the biopolymer and the solvent matter? CELLULOSE, **15** (3) 371-392 (2008).

[316] Dollimore, D. and B. Holt: Sorption of vapors in cellulose film. Journal of Applied Polymer Science, **17** (6) 1795-1803 (1973).

[317] Bodros, E., I. Pillin, N. Montrelay, and C. Baley: Could biopolymers reinforced by randomly scattered flax fibre be used in structural applications? Composites Science and Technology, **67** (3-4) 462-470 (2007).

[318] Averous, L. and N. Boquillon: Biocomposites based on plasticized starch: thermal and mechanical behaviours. Carbohydrate Polymers, **56** (2) 111-122 (2004).

[319] Wambua, P., J. Ivens, and I. Verpoest: Natural fibres: can they replace glass in fibre reinforced plastics? Composites Science and Technology, **63** (9) 1259-1264 (2003).

[320] Jiang, G., W. Huang, L. Li, X. Wang, F. Pang, Y. Zhang, and H. Wang: Structure and properties of regenerated cellulose fibers from different technology processes. Carbohydrate Polymers, (2011).

[321] Crawshaw, J. and R. Cameron: A small angle X-ray scattering study of pore structure in Tencel® cellulose fibres and the effects of physical treatments. Polymer, **41** (12) 4691-4698 (2000).

[322] Czichos, H., T. Saito, and L. Smith: Springer handbook of materials measurement methods. Springer. (2006).

[323] Czihak, C., M. Müller, H. Schober, L. Heux, and G. Vogl: Dynamics of water adsorbed to cellulose. Physica B: Condensed Matter, **266** (1-2) 87-91 (1999).

[324] Ioelovich, M., A. Leykin, and O. Figovsky: Study of cellulose paracrystallinity. BioResources, **5** (3) 1393-1407 (2010).

[325] Lipatov, Y.S., V.V. Shilov, Y.P. Gomza, and N. Kruglyak: X-Ray Diffraction Methods for Investigation of Polymer Systems. Naukova Dumka, Kiev, 303 (1982).

[326] Hermans, P.H. and M. Hollander: Physics and Chemistry of Cellulose Fibres: With Particular Reference to Rayon. Elsevier Pub. Co. (1949).

[327] Stuart, H.: Form und Beweglichkeit von Fadenmolekülen im Modellversuch. Naturwissenschaften, **31** (11) 123-127 (1943).

[328] Kitayama, T., S. Utsumi, H. Hamada, T. Nishino, T. Kikutani, and H. Ito: Interfacial properties of PP/PP composites. Journal of Applied Polymer Science, **88** (13) 2875-2883 (2003).

[329] Loos, J., T. Schimanski, J. Hofman, T. Peijs, and P. Lemstra: Morphological investigations of polypropylene single-fibre reinforced polypropylene model composites. Polymer, **42** (8) 3827-3834 (2001).

[330] Quan, H., Z.M. Li, M.B. Yang, and R. Huang: On transcrystallinity in semi-crystalline polymer composites. Composites Science and Technology, **65** (7-8) 999-1021 (2005).

[331] Amash, A. and P. Zugenmaier: Morphology and properties of isotropic and oriented samples of cellulose fibre–polypropylene composites. Polymer, **41** (4) 1589-1596 (2000).

[332] Dudley, R., C. Fyfe, P. Stephenson, Y. Deslandes, G. Hamer, and R. Marchessault: High-resolution carbon-13 CP/MAS NMR spectra of solid cellulose oligomers and the structure of cellulose II. Journal of the American Chemical Society, **105** (8) 2469-2472 (1983).

[333] Teeäär, R., R. Serimaa, and T. Paakkarl: Crystallinity of cellulose, as determined by CP/MAS NMR and XRD methods. Polymer Bulletin, **17** (3) 231-237 (1987).

[334] Newman, R.H., J.A. Hemmingson, and I.D. Stuckling: Carbon-13 nuclear magnetic resonance studies of kraft pulping. Holzforschung, **47** (3) 234-238 (1993).

[335] Atalla, R.H., J. Gast, D. Sindorf, V. Bartuska, and G. Maciel: Carbon-13 NMR spectra of cellulose polymorphs. Journal of the American Chemical Society, **102** (9) 3249-3251 (1980).

[336] Newman, R.H. and J.A. Hemmingson: Carbon-13 NMR distinction between categories of molecular order and disorder in cellulose. CELLULOSE, **2** (2) 95-110 (1995).

[337] Newman, R.H. and T.C. Davidson: Molecular conformations at the cellulose–water interface. CELLULOSE, **11** (1) 23-32 (2004).

[338] Ibbett, R.N., D. Domvoglou, and M. Fasching: Characterisation of the supramolecular structure of chemically and physically modified regenerated cellulosic fibres by means of high-resolution Carbon-13 solid-state NMR. Polymer, **48** (5) 1287-1296 (2007).

[339] Ibbett, R., D. Domvoglou, F. Wortmann, and K.C. Schuster: Carbon-13 solid state NMR investigation and modeling of the morphological reorganization in regenerated cellulose fibres induced by controlled acid hydrolysis. CELLULOSE, **17** (2) 231-243 (2010).

[340] Hindeleh, A.: X-ray characterization of viscose rayon and the significance of crystallinity on tensile properties. TEXTILE RESEARCH JOURNAL, **50** (10) 581-589 (1980).

[341] Gindl, W. and J. Keckes: Drawing of self-reinforced cellulose films. Journal of Applied Polymer Science, **103** (4) 2703-2708 (2007).

[342] Ago, M., T. Endo, and T. Hirotsu: Crystalline transformation of native cellulose from cellulose I to cellulose ID polymorph by a ball-milling method with a specific amount of water. CELLULOSE, **11** (2) 163-167 (2004).

[343] Huber, T., J. Müssig, E. Baur, and F. Otremba: Verstärkung aus der Natur= Natural Reinforcement. Kunststoffe, **98** (7) 97-101 (2008).

[344] Hristov, V., R. Lach, and W. Grellmann: Impact fracture behavior of modified polypropylene/wood fiber composites. Polymer Testing, **23** (5) 581-589 (2004).

[345] Thomason, J.L. and M.A. Vlug: Influence of fibre length and concentration on the properties of glass fibre-reinforced polypropylene: 4. Impact properties. Composites Part A, **28 A** 12 (1997).

[346] Grellmann, W. and S. Seidler: Polymer testing. Hanser Gardner Publicationss. Cincinnati, Ohio, USA(2007).

[347] Dhakal, H., Z. Zhang, M. Richardson, and O. Errajhi: The low velocity impact response of non-woven hemp fibre reinforced unsaturated polyester composites. Composite Structures, **81** (4) 559-567 (2007).

[348] Faur-Csukat, G.: Development of composite structures for ballistic protection **537** 151-159 (2007).

[349] Munikenche Gowda, T., A. Naidu, and R. Chhaya: Some mechanical properties of untreated jute fabric-reinforced polyester composites. Composites Part A: Applied Science and Manufacturing, **30** (3) 277-284 (1999).

[350] Zugenmaier, P.: Überlegungen zur Symmetrie und Packung von kristallinen Cellulosen und Modell-verbindungen. in 4. internationales Symposium "Werkstoffe aus Nachwachsenden Rohstoffen"(2003).

[351] O'donnell, A., M. Dweib, and R. Wool: Natural fiber composites with plant oil-based resin. Composites Science and Technology, **64** (9) 1135-1145 (2004).

[352] Åkesson, D., M. Skrifvars, and P. Walkenström: Preparation of thermoset composites from natural fibres and acrylate modified soybean oil resins. Journal of Applied Polymer Science, **114** (4) 2502-2508 (2009).

[353] Pervaiz, M. and M. Sain: Sheet Molded Polyolefin Natural Fiber Composites for Automotive Applications. Macromolecular Materials and Engineering, **288** (7) 553-557 (2003).

[354] Ahmed, K., S. Vijayarangan, and C. Rajput: Mechanical behavior of isothalic polyester-based untreated woven jute and glass fabric hybrid composites. Journal of Reinforced Plastics and Composites, **25** (15) 1549 (2006).

[355] Adekunle, K., D. Åkesson, and M. Skrifvars. Biobased Composites Prepared by Compression Moulding using a Novel Thermoset Resin from Soybean oil and a Natural Fibre Reinforcement(2009).

[356] Khondker, O., U. Ishiaku, A. Nakai, and H. Hamada: Tensile, flexural and impact properties of jute fibre-based thermosetting composites. Plastics, Rubber and Composites, **34** (10) 450-462 (2005).

[357] Jannah, M., M. Mariatti, A. Abu Bakar, and H. Abdul Khalil: Effect of Chemical Surface Modifications on the Properties of Woven Banana-Reinforced Unsaturated Polyester Composites. Journal of Reinforced Plastics and Composites, **28** (12) 1519 (2009).

[358] Adusumali, R., M. Reifferscheid, H. Weber, T. Roeder, H. Sixta, and W. Gindl. Mechanical properties of regenerated cellulose fibres for composites **244** 119-125 (2006).

[359] Baillie, C.: Green composites: polymer composites and the environment. CRC. (2004).

[360] Kozłowski, R. and M. Władyka-Przybylak: Flammability and fire resistance of composites reinforced by natural fibers. Polymers For Advanced Technologies, **19** (6) 446-453 (2008).

[361] Matko, S., A. Toldy, S. Keszei, P. Anna, G. Bertalan, and G. Marosi: Flame retardancy of biodegradable polymers and biocomposites. Polymer Degradation and Stability, **88** (1) 138-145 (2005).

[362] Chapple, S. and R. Anandjiwala: Flammability of Natural Fiber-reinforced Composites and Strategies for Fire Retardancy: A Review. Journal of Thermoplastic Composite Materials, **23** (6) 871-893 (2010).

[363] Hall, M., A. Horrocks, and H. Seddon: The flammability of Lyocell. Polymer Degradation and Stability, **64** (3) 505-510 (1999).

[364] Lucas, N., C. Bienaime, C. Belloy, M. Queneudec, F. Silvestre, and J.E. Nava-Saucedo: Polymer biodegradation: Mechanisms and estimation techniques-A review. Chemosphere, **73** (4) 429-442 (2008).

[365] Aminabhavi, T., R. Balundgi, and P. Cassidy: A review on biodegradable plastics. Polymer-Plastics Technology and Engineering, **29** (3) 235-262 (1990).

[366] Swift, G.: Directions for environmentally biodegradable polymer research. Accounts of chemical research, **26** (3) 105-110 (1993).

[367] Salazar, V.L.P., A. Leão, D. Rosa, J.G.C. Gomez, and R.C.P. Alli: Biodegradation of Coir and Sisal Applied in the Automotive Industry. Jounral of Polymers and the Environment, **19** (3) 677-688 (2011).

[368] Directive, C.: PRODUCTION STORAGE EMISSIONS PRODUCT. Official Journal L, **393** 0001-0012 (1989).

[369] Wool, R., D. Raghavan, G. Wagner, and S. Billieux: Biodegradation dynamics of polymer–starch composites. Journal of Applied Polymer Science, **77** (8) 1643-1657 (2000).

[370] Wertz, J.L., O. Bédué, and J.P. Mercier: Cellulose science and technology. EFPL Press. (2010).

[371] Béguin, P. and J.P. Aubert: The biological degradation of cellulose. FEMS Microbiology Reviews, **13** (1) 25-58 (1994).

[372] Schnegelsberg, G.: Handbuch der Faser: Theorie und Systematik der Faser. Deutscher Fachverlag. Frankfurt/Main, Germany(1999).

[373] Galbe, M. and G. Zacchi: A review of the production of ethanol from softwood. Applied Microbiology and Biotechnology, **59** (6) 618-628 (2002).

[374] Gilbert, H.J. and G.P. Hazlewood: Bacterial cellulases and xylanases. Journal of General Microbiology, **139** (2) 187-194 (1993).

[375] Sun, Y. and J. Cheng: Hydrolysis of lignocellulosic materials for ethanol production: a review. Bioresource Technology, **83** (1) 1-11 (2002).

[376] Avella, M., A. Buzarovska, M.E. Errico, G. Gentile, and A. Grozdanov: Eco-Challenges of Bio-Based Polymer Composites. Materials, **2** (3) 911-925 (2009).

[377] Madhavan Nampoothiri, K., N.R. Nair, and R.P. John: An overview of the recent developments in polylactide (PLA) research. Bioresource Technology, **101** (22) 8493-8501 (2010).

[378] Saadi, Z., A. Rasmont, G. Cesar, H. Bewa, and L. Benguigui: Fungal Degradation of Poly (l-lactide) in Soil and in Compost. JOURNAL OF POLYMERS AND THE ENVIRONMENT, 1-10

[379] Kumar, R., M. Yakubu, and R. Anandjiwala: Biodegradation of flax fiber reinforced poly lactic acid. (2010).

[380] Tesoro, G.C. and C.H. Meiser: Some effects of chemical composition on the flammability behavior of textiles. Textile Research Journal, **40** (5) 430-436 (1970).

[381] Nelson, G.L.: Fire and polymers: an overview **599** 1-28 (1995).

[382] Morgan, A.B. and M. Bundy: Cone calorimeter analysis of UL 94 V rated plastics. Fire and materials, **31** (4) 257-283 (2007).

[383] Reti, C., M. Casetta, S. Duquesne, S. Bourbigot, and R. Delobel: Flammability properties of intumescent PLA including starch and lignin. Polymers For Advanced Technologies, **19** (6) 628-635 (2008).

[384] Munier-Lamy, C. and O. Borde: Effect of a triazole fungicide on the cellulose decomposition by the soil microflora. Chemosphere, **41** (7) 1029-1035 (2000).

[385] Tremier, A., A. De Guardia, C. Massiani, E. Paul, and J. Martel: A respirometric method for characterising the organic composition and biodegradation kinetics and the temperature influence on the biodegradation kinetics, for a mixture of sludge and bulking agent to be co-composted. Bioresource Technology, **96** (2) 169-180 (2005).

[386] Shah, A.A., F. Hasan, A. Hameed, and S. Ahmed: Biological degradation of plastics: a comprehensive review. Biotechnology Advances, **26** (3) 246-265 (2008).

[387] Boer, W., L.B. Folman, R.C. Summerbell, and L. Boddy: Living in a fungal world: impact of fungi on soil bacterial niche development. FEMS Microbiology Reviews, **29** (4) 795-811 (2005).

[388] el Zahar Haichar, F., W. Achouak, R. Christen, T. Heulin, C. Marol, M.F. Marais, C. Mougel, L. Ranjard, J. Balesdent, and O. Berge: Identification of cellulolytic bacteria in soil by stable isotope probing. Environmental microbiology, **9** (3) 625-634 (2007).

[389] Kozakiewicz, Z. and J. Clarke: Techniques for determining toxicity of propionic acid to fungi from stored grain. Transactions of the British Mycological Society, **61** (2) 355-367 (1973).

[390] Fukushima, K., C. Abbate, D. Tabuani, M. Gennari, and G. Camino: Biodegradation of poly (lactic acid) and its nanocomposites. Polymer Degradation and Stability, **94** (10) 1646-1655 (2009).

[391] Shibata, M., S. Oyamada, S.i. Kobayashi, and D. Yaginuma: Mechanical Properties and Biodegradability of Green Composites Based on Biodegradable Polyesters and Lyocell Fabric. Journal of Applied Composite Materials, **92** 3857–3863 (2004).

[392] Shibata, M., S. Oyamada, S. Kobayashi, and D. Yaginuma: Mechanical properties and biodegradability of green composites based on biodegradable polyesters and lyocell fabric. Journal of Applied Polymer Science, **92** (6) 3857-3863 (2004).

[393] Nutt, A.: Hydrolytic and oxidative mechanisms involved in cellulose degradation. Acta Universitatis Upsaliensis, Digital Comprehensive Summaries of Uppsala Dissertations from the Faculty of Science and Technology, **185** (2006).

[394] Siu, R.: Mechanism of microbiological decomposition of cellulose. TEXTILE RESEARCH JOURNAL, **20** (5) 281-288 (1950).

[395] Quan, S.L., S.G. Kang, and I.J. Chin: Characterization of cellulose fibers electrospun using ionic liquid. CELLULOSE, **17** (2) 223-230 (2010).

[396] Seddon, H., M. Hall, and A.R. Horrocks: The flame retardancy of lyocell fibres. Polymer Degradation and Stability, **54** (2) 401-402 (1996).

[397] Horrocks, A.: An introduction to the burning behaviour of cellulosic fibres. Journal of the Society of Dyers and Colourists, **99** (7-8) 191-197 (1983).

[398] Kimura, K. and Y. Horikoshi: Bio-Based Polymers. Fujitsu Scientific and Technical Journal, **41** (2) 173-180 (2005).

[399] Murariu, M., L. Bonnaud, P. Yoann, G. Fontaine, S. Bourbigot, and P. Dubois: New trends in polylactide (PLA)-based materials. Polymer Degradation and Stability, **95** (3) 374-381 (2010).

[400] Fontaine, G. and S. Bourbigot: Intumescent polylactide: a nonflammable material. Journal of Applied Polymer Science, **113** (6) 3860-3865 (2009).

[401] Cai, Z.: Analysis of mold filling in RTM process. Journal of Composite Materials, **26** (9) 1310-1338 (1992).

[402] Kendall, K., C. Rudd, M. Owen, and V. Middleton: Characterization of the resin transfer moulding process. Composites Manufacturing, **3** (4) 235-249 (1992).

[403] Rudd, C. and K. Kendall: Towards a manufacturing technology for high volume production of composite components. ARCHIVE: Proceedings of the Institution of Mechanical Engineers, Part B: Journal of Engineering Manufacture 1989-1996 (vols 203-210), **206** (22) 77-91 (1992).

[404] Sebe, G., N.S. Cetin, C.A.S. Hill, and M. Hughes: RTM hemp fibre-reinforced polyester composites. Applied Composite Materials, **7** (5) 341-349 (2000).

[405] Oksman, K.: High quality flax fibre composites manufactured by the resin transfer moulding process. Journal of Reinforced Plastics and Composites, **20** (7) 621-627 (2001).

[406] Liu, B., S. Bickerton, and S.G. Advani: Modelling and simulation of resin transfer moulding (RTM)--gate control, venting and dry spot prediction. Composites Part A: Applied Science and Manufacturing, **27** (2) 135-141 (1996).

[407] Swatloski, R.P., R.D. Rogers, and J.D. Holbrey, Dissolution and processing of cellulose using ionic liquids. 2011, EP Patent 2,325,246.

[408] Andersson, H.M.: Vacuum infusion of polymer composites. Licentiate Thesis, Department of Mechanical Engineering, Lulea University of Technology, Sweden, (2001).

[409] Sayre, J.R., Vacuum-assisted resin transfer molding (VARTM) model development, verification, and process analysis. 2000, Virginia Polytechnic Institute and State University.

[410] Daniel, I.M., J.J. Luo, and P.M. Schubel: Three-dimensional characterization of textile composites. Composites Part B: Engineering, **39** (1) 13-19 (2008).

[411] Mouritz, A.P., M.K. Bannister, P.J. Falzon, and K.H. Leong: Review of applications for advanced three-dimensional fibre textile composites. Composites Part A: Applied Science and Manufacturing, **30** (12) 1445-1461 (1999).

[412] Yang, C., Y.K. Kim, U.A. Qidwai, and A.R. Wilson: Related strength properties of 3D fabrics. Textile Research Journal, **74** (7) 634-639 (2004).

[413] Ren, J., Y.K. Kim, and J. Rice: Comparing the fracture toughness of 3-D braided preform composites with z-fiber-reinforced laminar composites. Textile Research Journal, **81** (4) 335 (2011).

[414] Gries, T., J. Stüve, and D. Veit: Textile structures for load-bearing applications in vehicles. in Textile advances in the automotive industry (Woodhead textiles series, N 79)(eds.: Editor^Editors), Woodhead Publishing Limited: Cambridge, UK **1** (2008).

[415] Mohamed, M.H.: Three-dimensional textiles. American Scientist, **78** (6) 530-541 (1990).

[416] Ayranci, C. and J. Carey: 2D braided composites: A review for stiffness critical applications. Composite Structures, **85** (1) 43-58 (2008).

[417] Stig, F. and S. Hallstrom: Assessment of the mechanical properties of a new 3D woven fibre composite material. Composites Science and Technology, **69** (11-12) 1686-1692 (2009).

[418] Ivanov, D., S. Ivanov, S. Lomov, and I. Verpoest: Strain mapping analysis of textile composites. Optics and Lasers in Engineering, **47** (3-4) 360-370 (2009).

[419] Wan, Y., G. Chen, Y. Huang, Q. Li, F. Zhou, J. Xin, and Y. Wang: Characterization of three-dimensional braided carbon/Kevlar hybrid composites for orthopedic usage. Materials Science and Engineering A, **398** (1-2) 227-232 (2005).

[420] Wang, Y.Q. and A. Wang: Microstructure/property relationships in three-dimensionally braided fiber composites. Composites Science and Technology, **53** (2) 213-222 (1995).

[421] ISO179-1, Determination of Charpy impact properties -- Part 1: Non-instrumented impact test, in Plastics. 2010, International Organization for Standardization: West Conshohocken, PA, USA.

[422] Chi, Z., T.W. Chou, and G. Shen: Determination of single fibre strength distribution from fibre bundle testings. Journal of Materials Science, **19** (10) 3319-3324 (1984).

[423] Falzon, P.J. and I. Herszberg: Mechanical performance of 2-D braided carbon/epoxy composites. Composites Science and Technology, **58** (2) 253-265 (1998).

[424] Dadkhah, M., J. Flintoff, T. Kniveton, and B. Cox: Simple models for triaxially braided composites. Composites, **26** (8) 561-577 (1995).

[425] Lee, L., S. Rudov-Clark, A. Mouritz, M. Bannister, and I. Herszberg: Effect of weaving damage on the tensile properties of three-dimensional woven composites. Composite Structures, **57** (1) 405-413 (2002).

[426] Mei, H., L. Cheng, and L. Zhang: Damage mechanisms of C/SiC composites subjected to constant load and thermal cycling in oxidizing atmosphere. Scripta materialia, **54** (2) 163-168 (2006).

[427] Promis, G., A. Gabor, G. Maddaluno, and P. Hamelin: Behaviour of beams made in textile reinforced mineral matrix composites, an experimental study. Composite Structures, **92** (10) 2565-2572 (2010).

[428] Innerlohinger, J., H.K. Weber, and G. Kraft. Aerocellulose: Aerogels and Aerogel-like Materials made from Cellulose **244** 126-135 (2006).

[429] Chou, S., H.C. Chen, and C.C. Wu: BMI resin composites reinforced with 3D carbon-fibre fabrics. Composites Science and Technology, **43** (2) 117-128 (1992).

[430] Chen, F. and J. Hodgkinson: Impact behaviour of composites with different fibre architecture. Proceedings of the Institution of Mechanical Engineers, Part G: Journal of Aerospace Engineering, **223** (7) 1009 (2009).

[431] Kjärstad, J. and F. Johnsson: Resources and future supply of oil. Energy Policy, **37** (2) 441-464 (2009).

[432] Farag, M.: Quantitative methods of materials substitution: application to automotive components. Materials & Design, **29** (2) 374-380 (2008).

APPENDIX A

STM mould *(all dimensions in mm)*

Female half

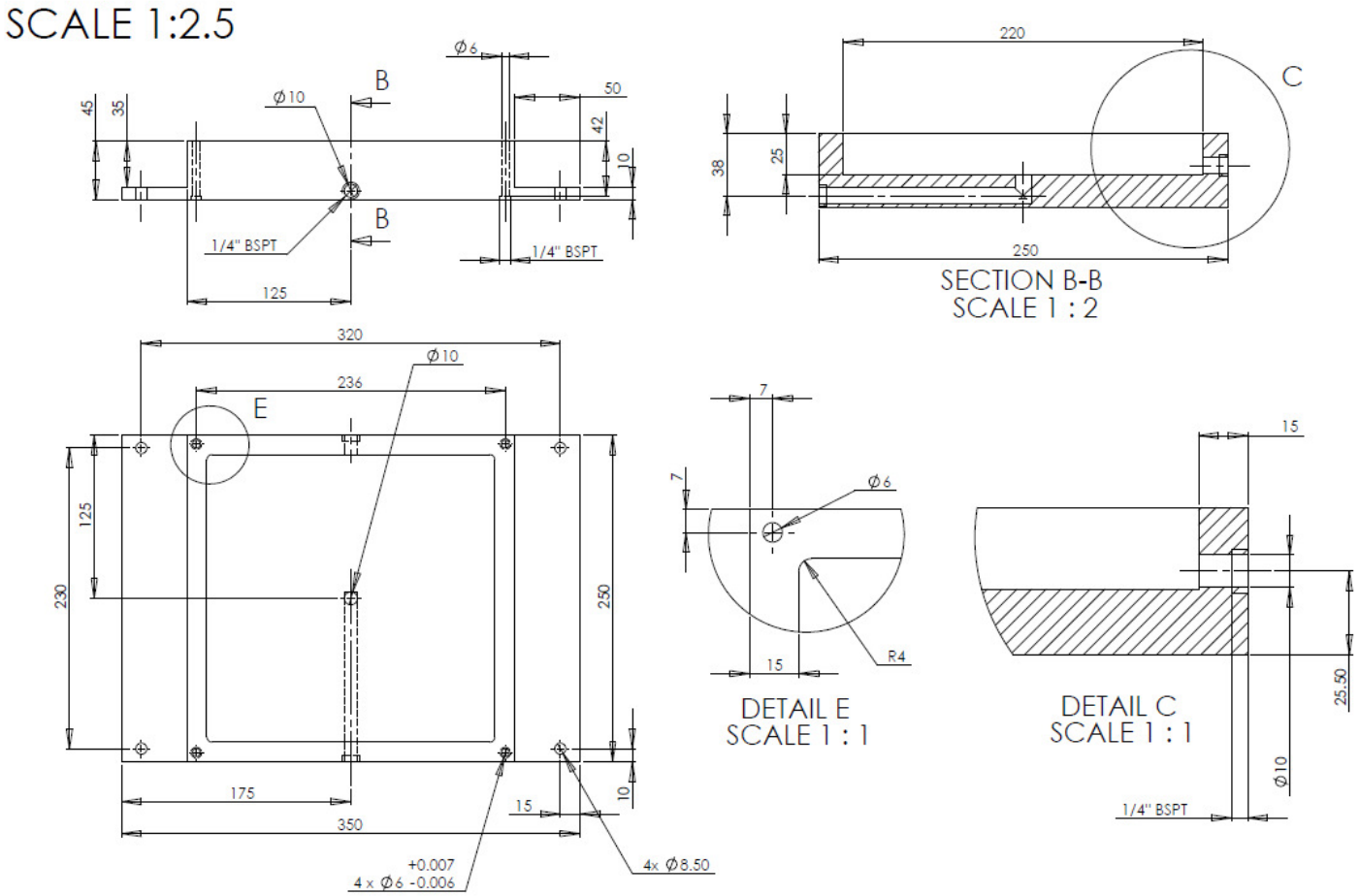

Male half

SCALE: 1:2.5

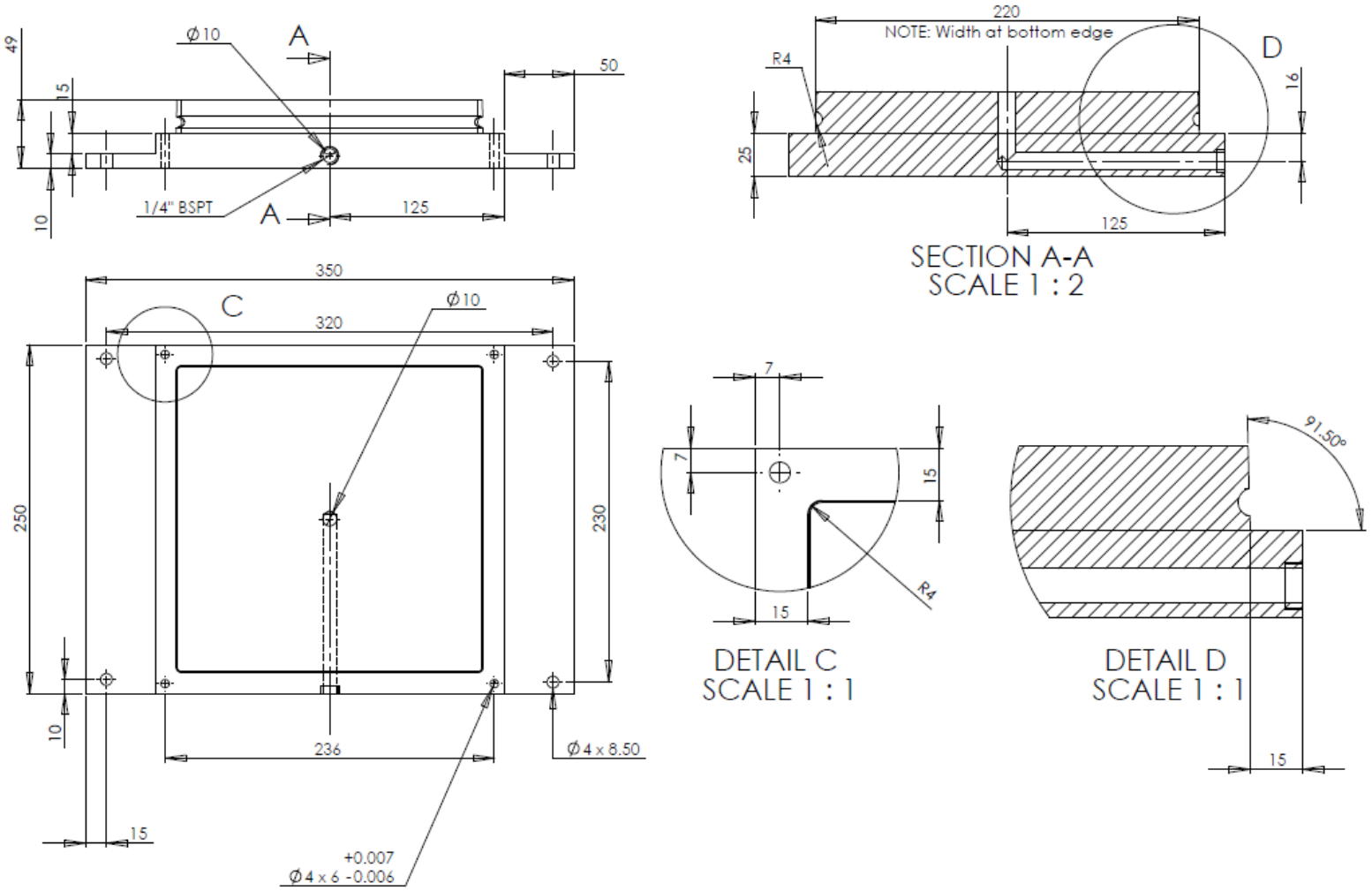

APPENDIX B

List of Journal Publications resulting from this Ph. D. Thesis:

- Huber, T., J. Müssig, O. Curnow, S. Pang, S. Bickerton, and M. Staiger: A critical review of all-cellulose composites. Journal of Materials Science, **47** (3) 1171-1186 (2012).
- Huber, T., S. Bickerton, J. Müssig, S. Pang and M. Staiger: Solvent infusion processing of all-cellulose composite materials. Carbohydrate Polymers, 90(1), 730–733 (2012)
- Huber, T., S. Pang and M. Staiger: All-cellulose composite laminates. Composites Part A, **43** (10), 1738–1745 (2012)